University of Huddersfield

Pre-clinical Evaluation of Novel Inorganic Compounds as Potential Anticancer Therapies

Samantha Louise Shepherd

A thesis submitted to the University of Huddersfield in partial fulfilment of the requirements for the degree of Doctor of Philosophy

The University of Huddersfield (in collaboration with Leeds University; Warwick University and North Eastern Hill University, Shillong, India)

January 2015 – November 2017

Copyright statement

Abstract

Background: Recent developments in our understanding of the biology of cancer has provided the opportunity to develop targeted agents with more specific pharmacological activity against cancer cells. Despite this shift toward targeted drug discovery, the much hoped-for paradigm shift in cancer treatment has not been realised. Tumour heterogeneity, plasticity and genomic instability are issues that contribute to this problem. One approach to circumvent these issues is to adopt a phenotypic based approach to drug evaluation where compounds with multiple mechanisms of action leading to a desirable phenotypic effect can be identified. The challenge with such an approach is to retain selectivity toward cancer cells as opposed to non-cancer cells.

Aims: The aim of this study is to apply a phenotype based drug evaluation program that incorporates a measure of selectivity to the preclinical evaluation of a series of novel organometallic complexes.

Methods: In this study, a series of novel inorganic complexes were evaluated against cancer and non-cancer cell lines. The primary evaluation procedures involved chemosensitivity testing with compounds being selected for further studies based upon (i) potency (ii) an *in vitro* selectivity index (SI) defined as the IC_{50} for non-cancer cells divided by the IC_{50} for cancer cells and (iii) comparable or improved properties than cisplatin, oxaliplatin and carboplatin with respect to potency and selectivity. Those compounds that met the selection criteria were evaluated further with the initial aim of characterising key pharmacological events such as cell cycle effects and induction of apoptosis.

Results and Discussion: Initial studies focused on the clinically approved platinum based with cisplatin and oxaliplatin being significantly more potent than carboplatin. Selectivity for cancer over non-cancer cells was observed with selectivity index (SI) values typically in the range of 0.85-9.71, 0.36-3.35 and 2.18-7.44 for cisplatin, oxaliplatin and carboplatin respectively. A total of 210 test compounds were evaluated in this thesis and of these, a total of 91 compounds exhibited potency values equal to or better than the platinates. In contrast however, only 64 compounds had superior SI values compared to platinates. Of these, the most promising compounds were a series of large molecular weight metallohelicates that exhibited potency (in the nM range) and SI values up to a maximum of 93 (nearly 28 times higher than the best performing platinum drug). Analysis of these compounds demonstrated that they do not induce apoptosis, but preliminary data suggests that they induce an autophagic death response.

Conclusions: The results of this study have demonstrated that a phenotypic based drug evaluation process based upon potency and selectivity *in vitro* is capable of identifying novel chemical entities with promising properties. This screen has more discriminatory power than potency alone and the concept of an '*in vitro* selectivity index' has proved valuable in identifying a series of novel metallohelicate compounds as potential anti-cancer drugs. Significant further work is required to identify their mechanism(s) of action and pharmacological properties but their potential ability to induce autophagic cell death over apoptosis is of interest.

Contents

List of Tables

List of Figures

Dedications and Acknowledgements

First and foremost, I would like to thank my 1st supervisor Professor Roger Phillips and my 2nd supervisor Dr Simon Allison to whom I am indebted and share the credit of my work with. Both supervisors are forever encouraging and supportive and I couldn't have asked for better scientists and people to have guided me. Completing this in 2 years and 10 months has been very tight and I owe a large gratitude to my ever patient, helpful and excellent brew making fiancé Frankie who has shared many sunrises with me whilst I frantically write or run another assay. My family although they think I am still at college are forever proud, no matter how little they understand what I do and never cease to cheer me up. The whole of the PGR office has been an endless source of laughter and support, but I owe particular thanks to my own and extended research family Hollie, Kartheek, Omar, Tsitsi, "Big" Scott and Suliman. I would like to take time to also thank my close friends Becky, Joanne, Kelsey and Sarah who have lifted me up more times than I can remember and have been waiting ever so patiently for a post thesis night out.

List of Publications

1. Synthesis, structural, DFT calculations and biological studies of rhodium and iridium complexes containing azine Schiff-base ligands; Sanjay Adhikari, Dipankar Sutradhar, **Samantha L. Shepherd**, Roger M. Phillips, Asit K. Chandra, K. Mohan Rao. Polyhedron, Volume 117, 15 October 2016, Pages 404–414. DOI: 10.1016/j.poly.2016.06.001.

2. Preclinical anti-cancer activity and multiple mechanisms of action of a cationic silver complex bearing N-heterocyclic carbene ligand; Simon J.Allison Maria.Sadiq EfstathiaBaronou Patricia A.Cooper ChrisDunnill Nikolaos T.Georgopoulos AyşeLatif **Samantha L. Shepherd** Steve D.Shnyder Ian J.Stratford Richard T.Wheelhouse Charlotte E.Willans Roger M.Phillips, Cancer Letters, Volume 403, 10 September 2017, Pages 98-107. DOI: 10.1016/j.canlet.2017.04.041.

3. Synthesis, Structural and Biological Studies of Some Half-Sandwich d^6-Metal Complexes with Pyrimidine-Based Ligands; Basava Punna Rao Aradhyula, Mahesh Kalidasan, Krishnakant Gangele, Debojit K. Deb, **Samanta L. Shepherd**, Roger M. Phillips, Krishna Mohan Poluri, Mohan Rao Kollipara, *Chemistry Select*, volume 2, Issue 6, February 23, 2017 Pages 2065–2076. DOI: 10.1002/slct.201601926.

4. Half-sandwich ruthenium, rhodium and iridium complexes featuring oxime ligands: Structural studies and preliminary investigation of *in vitro* and *in vivo* anti-tumour activities; Narasinga Rao Palepu, Sanjay Adhikari, Richard Premkumar J, Akalesh K. Verma, **Samantha L. Shepherd**, Roger M. Phillips, Werner Kaminsky, Mohan Rao Kollipara, *Applied Organometallic Chemistry*, volume 31, Issue 7, July 2017. DOI: 10.1002/aoc.3640.

5. Neutral and cationic half-sandwich arene ruthenium, Cp*Rh and Cp*Ir oximato and oxime complexes: Synthesis, structural, DFT and biological studies; Sanjay Adhikari, Narasinga Rao Palepu, Dipankar Sutradhar, **Samantha L. Shepherd**, Roger M. Phillips, Werner Kaminsky, Asit K. Chandra, Mohan Rao Kollipara, *Journal of Organometallic*

Chemistry, volume 820, issue 1, October 2016, pages 70–81. DOI: 10.1016/j.jorganchem.2016.08.004.

6. Anticancer metallohelices: nanomolar potency and high selectivity; Rebecca A. Kaner, Simon J. Allison , Alan D. Faulkner , Roger M. Phillips , David I. Roper , **Samantha L. Shepherd** , Daniel H. Simpson , Nicholas R. Waterfield and Peter Scott, Chemical Science, volume 7, issue, 26th October 2015, 7, pages 951-958. DOI: 10.1039/C5SC03677A.

7. Hypoxia-Sensitive Metal β-Ketoiminato Complexes Showing Induced Single-Strand DNA Breaks and Cancer Cell Death by Apoptosis; Rianne M. Lord, Andrew J. Hebden, Christopher M. Pask, Imogen R. Henderson, Simon J. Allison, **Samantha L. Shepherd**, Roger M. Phillips, and Patrick C. McGowan, *J. Med. Chem.*, 2015, volume 58, issue 12, pages 4940–4953. DOI: 10.1021/acs.jmedchem.5b00455.

Chapter 1 - Introduction

1.1 What is Cancer?

Cancer is fundamentally defined as the abnormal, uncontrolled growth of previously normal cells resulting from the accumulation of DNA alterations (genetic and epigentic) and defective cellular function. The primary characteristic of cancer is its ability to replicate uncontrollably, to defy normal restraints on cell division and an inability to undergo programmed cell death. This results in an overall increase in the number of cells and the formation of solid masses. Its second major property is its ability to invade and colonise nearby and distant tissues forming secondary tumours in territories often reserved for other cells. This property distinguishes benign from malignant tumours and the more widely a cancer spreads, the more difficult it is to eradicate (Alberts, 2002). As normal cells transform into cancer cells, they acquire a number of characteristics or 'hallmarks'.

In 2000 Hanahan and Weinberg described these hallmarks of cancer, which comprise of six biological capabilities acquired during the multistep development of human tumours (illustrated in figure 1.1A). Together these hallmarks constitute an organising principle that provides a logical framework for understanding the remarkably diverse and complex tumour microenvironment. The six initial hallmarks identified were; 1) sustaining proliferative signalling, 2) evading growth suppressors, 3) resisting cell death, 4) inducing angiogenesis, 5) enabling replicative immortality and 6) activating invasion and metastasis (Hanahan & Weinberg, 2000). In 2011, the same

authors described four additional distinct characteristics (illustrated in figure 1.1B) of the tumour cell and its environment consisting of two emerging hallmarks and two enabling hallmarks. The two emerging hallmarks outlined are believed to be important in the pathogenesis of some if not all cancers. The first is the ability of cancers to deregulate cellular energetics resulting in support for neoplastic proliferation. The second allows cancer cells to evade immunological destruction and like the first, is classed as an emerging hallmark. Additionally two enabling characteristics were identified genomic instability and tumour promoting inflammation (Hanahan & Weinberg, 2011). The importance of these articles is that they summarise the key molecular and biological events that lead to cancers and this understanding is fundamentally important in the development of new therapies for treating cancer as will be described later.
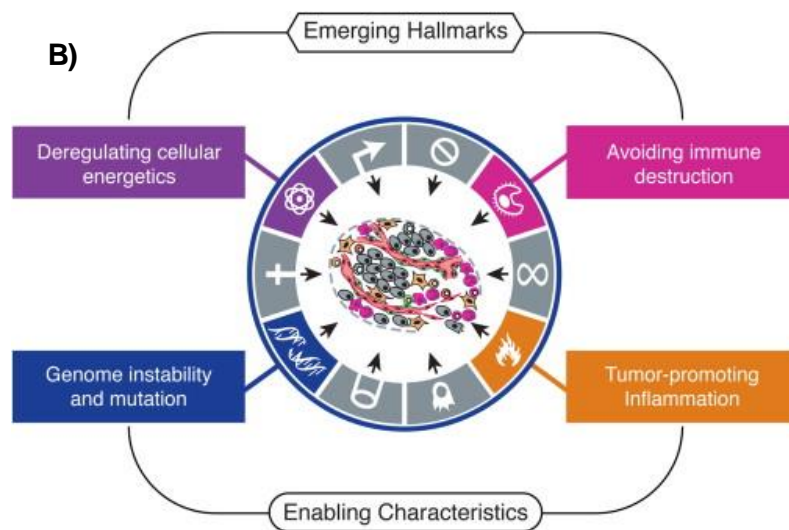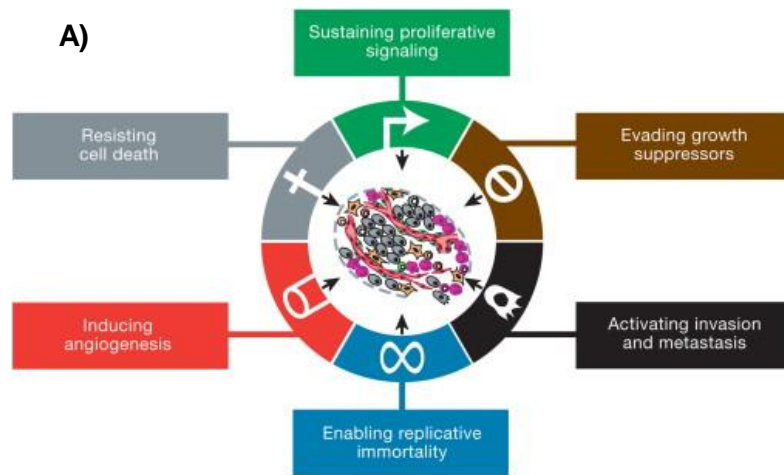
Figure 1.1: The A) Six original hallmark capabilities as proposed by Hanahan and Weinberg in 2000

(panel A), along with the emerging hallmarks and enabling characteristics as proposed in 2011 (panel B).

Both articles (Hanahan & Weinberg, 2000; Hanahan & Weinberg, 2011) represent seminal overviews of

tumour biology that directly impact upon drug discovery.

1.2 - The Cancer Problem

Despite recent advances in early detection, treatment, genetic testing and understanding of the molecular basis of cancer biology, cancer remains one of the leading causes of death worldwide. It is estimated to be responsible for one in every eight deaths (Garcia et al., 2007; Lucas et al., 2012). Globally, cancer is a massive burden both financially and socially with an estimated 1,685,210 new cases predicted for 2016 in the United States alone. Of these estimated cases, it is predicted that 595,690 people would succumb to the disease (WHO, 2015). The four most prevalent cancers in the UK and the US are breast, lung, prostate and colorectal (ACS, 2016) with pancreatic cancer being the most lethal malignancy; only 7.7% of reported cases survive 5 years (NCI, 2016). These alarming statistics for pancreatic cancer have not improved over 40 years, largely due to its typically late diagnosis, its aggressive behaviour and resistance to both chemotherapy and radiotherapy (Sclafani, Cunningham, Okines, Ratnayake, & Chau, 2017) . Therefore, improved development and design of new strategies for (i) early detection of the disease (ii) prevention via avoidance of known risk factors and (iii) better treatments including surgery, radiotherapy and chemotherapy are needed. Within the field of chemotherapy, the search for new anticancer agents has been and remains an important area of research where the ultimate aim is to increase treatment efficacy, prolong survival and improve quality of life for patients, particularly for those with advanced metastatic disease. Along with the emergence of resistant tumours and the severe side effects associated with chemotherapeutic agents, the field is observing reduced clinical efficiency of a

large variety of anticancer agents that are currently in practice (Ali et al., 2012). The aim of drug development for novel chemotherapeutic agents is therefore focused on the identification of agents which exert an adequate therapeutic index reflecting the treatments' specific effects on target cells, whilst exhibiting a lack of clinically significant effects on the hosts "healthy" cells (Sellers & Fisher, 1999). Potency and selectivity are therefore the ultimate therapeutic goal to maximise clinical outcome.

1.3 - Chemotherapy

The origins of cancer chemotherapy can be traced back to the use of mustard gas in World War One where physicians noted a drop in white cell counts in soldiers exposed to mustard gas (Nobel & Farmacológico). It was not until the pioneering work of Gilman and Goodman in the 1940s that the first chemotherapy agent was developed and used in humans. These drugs were derivative of sulphur mustard (nitrogen mustards called methyl-bis (β-chloroethyl) amine hydrochloride and tris (β-chloroethyl) amine hydrochloride) and significant effects on previously untreatable cancers such as Hodgkins lymphoma, lymphosarcoma and leukaemias were reported (Goodman et al., 1946). These compounds are alkylating agents that induce cell death by binding to DNA (cross linking). Since their discovery, a number of chemotherapy agents have been discovered, all of which typically target the process of cell replication at various stages (figure 1.2). Traditional anticancer drug development concentrated on the malignant characteristic that tumour cells replicate more rapidly than normal cells and that DNA replication is the main biochemical feature driving the cancer

process. As a result the majority of drugs routinely used in clinical practice result in DNA damage, interruption of cell division and subsequently cell death (Bailón-Moscoso, Romero-Benavides, & Ostrosky-Wegman, 2014). Most chemotherapy drugs cause damage to DNA or prevent chromosomal replication leading to programmed cell death (apoptosis)(Al-Dimassi, Abou-Antoun, & El-Sibai, 2014). These drugs can be classified into five groups and can be summarised by the stage at which they are most active in the cell cycle (figure 1.2).

Cytotoxic antibiotics:

Cell cycle non-specific, therefore tend be of use in slow growing tumours that have a low growth fraction. Include anthracyclines (doxorubicin, epirubicin), bleomycin, mitoxantrone

Antimetabolites:

Analogues of nucleic acid bases, which are converted to nucleotides and incorporated into DNA , thus acting on cells undergoing DNA synthesis, these include methotrexate, 5-fluorouracil, capecitabine and 6-mercaptopurine.

Topoisomerase inhibitors:

Active during S-phase as they interfere with the activity of enzymes functioning during DNA replication. These include Topoisomerase-I inhibitors (irinotecan, topotecan), topoisomerase-II inhibitors (etopside).

Alkylating agents:

Cell cycle phase independent agents attack both dividing and non-dividing cells include platinums (cisplatin, carboplatin), nitrogen mustard derivatives (chlorambucil) and oxazophosphorines (cyclophosphamide, ifosfamide).

Mitotic inhibitors:

Prevent formation of mitotic spindle by binding to tubulin subunits therefore acting on cells undergoing mitosis, include taxanes (paclitaxel) and vinca alkaloids (vincristine).

Figure 1.2: Summary of mechanistic and cell cycle dependency of the classical cytotoxic agents. G1, S, M, G2 and G0 refer to the stages of the cell cycle and the action of the 5 key groups of cytotoxic drugs on cells at different stages of the cell cycle is illustrated. This figure has been adapted from reference sources (Airley, 2009; Bhosle & Hall, 2009).

Although the use of classical cytotoxic agents has achieved significant success, the biochemical selectivity of these conventional cytotoxic agents is poor. Side effects are common and can be life threatening leading to dose limiting toxicity. It is well-documented that dose limiting toxicity not only reduces patient compliance, but it can also be the cause or a contributing factor towards a patient's decline in health or their mortality. Due to the agents ubiquitous targeting of DNA, selectivity between normal and cancer cells is poor as the drugs cannot distinguish between a replicating cancer cell and a replicating normal cell. Side effects of chemotherapeutic agents include nausea and vomiting, hair loss, mucositis, leukopaenia and pancytopaenia, mainly due to their non-specific targeting of proliferating cells. More severe toxicities caused by chemotherapeutic agents include cardiotoxicity, renal toxicity, neurotoxicity, extravasations and nephrotoxicity which is most commonly observed with the platinum compounds (Plenderleith, 1990).

In addition to toxicity, the emergence of a drug resistant phenotype is a further major challenge to successful chemotherapy. Over time, on-going genetic instability generates a plethora of alterations and diversity within a cancer, which can lead to the promotion of growth and survival advantages and treatment resistance (Turner & Reis-Filho, 2012). Resistance is a major limiting factor of chemotherapy treatment in solid tumours contributing to lack of response and consequently failure to adequately treat the tumour. Tumours can be either intrinsically resistant prior to treatment or can acquire resistance during treatment towards agents they were once susceptible

towards (Kerbel, Kobayashi, & Graham, 1994). The principle mechanisms of resistance to cytotoxic chemotherapy include well documented mechanisms of altered membrane transport resulting in the acceleration of drug efflux. The most studied example of this is the enhanced expression of ATP binding cassette (ABC) transporter proteins, such as P-glycoprotein (Pgp) (Gottesman, Fojo, & Bates, 2002). This increased efflux of the drug from the intracellular space leads to "multi-drug resistance" due to its ability to affect a number of chemotherapeutic agents (Wilson, Longley, & Johnston, 2006). Other mechanisms may include the alteration of target proteins such as mutated topoisomerase II, decreased drug activation and increased drug degradation due to alteration of enzyme expression related to drug metabolism. Other mechanisms of drug resistance include drug inactivation, subcellular re-distribution, drug interactions, enhanced DNA repair and failure to undergo apoptosis as a result of mutated cell cycle proteins (Luqmani, 2005).

The emerging hallmarks highlighted in figure 1.1 provide the survival mechanisms to withstand environmental stresses such as the ones induced by chemotherapy with hypoxia being a pivotal driving force of malignant progression (Al-Dimassi et al., 2014). Due to the rapid proliferation tumour cells rapidly outgrow their blood supply, leading to areas of necrosis bordered by hypoxic tissue. These adaptive molecular changes are transcriptionally regulated via hypoxia inducible factors (HIFs), which up regulate hypoxia inducible genes regulating angiogenesis, anaerobic glycolysis and cell survival genes, whilst suppressing genes associated with cell death (Semenza, 2003). For this

reason tumour hypoxia and its effects have become attractive targets for targeted anticancer agents due to their strong correlation with increased malignancy, likelihood of metastasis and treatment failure (Airley, 2009).

As indicated above recent developments in molecular biology and our greater understanding of the biology of cancer have provided researchers with the opportunity to develop novel agents that are targeted at the hallmark characteristics of the disease. As these agents target cancer biology, the hope was that these drugs would have greater pharmacological activity against cancer cells and be more selective than cytotoxic drugs. Agents in this class are designed to inhibit and/or modify a selected molecular target deemed important in cancer progression, growth and/or metastasis (Narang & Desai, 2009). These agents are designed to target specific aspects of tumour biology which although are expressed in variable degrees from patient to patient are characteristic properties with the same type of cancer. Examples of these agents are illustrated below (Figure 1.3)
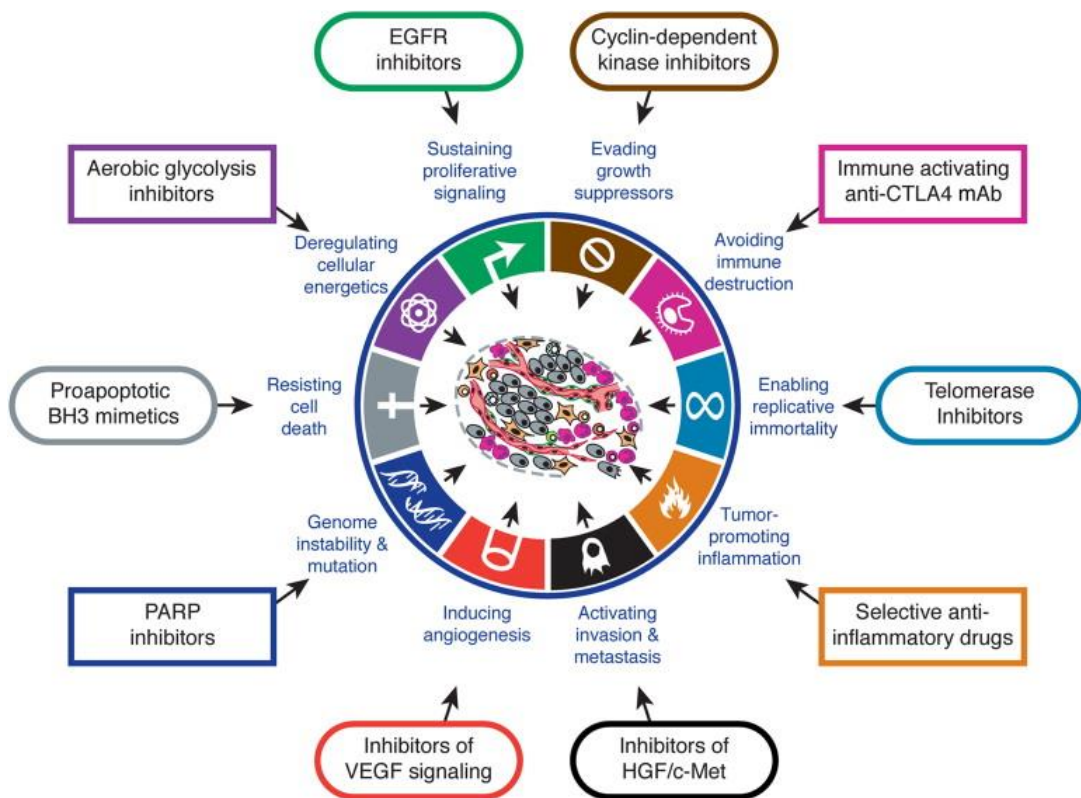
Figure 1.3: Novel drugs that target the Hallmarks of Cancer. The hallmarks of cancer as defined by Hanahan and Weinberg (2011) are presented in the inner components of the 'the wheel' and the major groups of therapeutic agents targeting these hallmarks are described on the outer part of the wheel. These agents reflect the fact that understanding the biology of the disease can provide a number of therapeutic opportunities.

These ten capabilities distinguish tumour cells from normal cells and have guided the development of novel targeted agents. Further understanding of the complex systems and molecular changes underlying cancer development have facilitated the research and development of agents that specifically target these malfunctioning genes and pathways. Targeting the 'oncogenic drivers' that lead to cancer has now

lead to the development of more effective and rationally designed cancer therapy (Sawyers, 2004).

These include Imatinib (Gleevec) which is small molecule inhibitor of the BCR-ABL tyrosine kinase, which was initially approved for use by the FDA in 2001 for the treatment of chronic myelogenous leukaemia (CML) and has since been approved in the use of a number of gastrointestinal cancers (Pray, 2008). Others in include bortezomib (Velcade) a small molecule proteasome inhibitor, rituximab (Rituxin) and trastuzumab (herceptin) which are both monoclonal antibodies, which induce cancer cell death by evoking an immune response. Sawyers (2004) discusses the mechanistic detail of such targeted therapies in much more in depth and reviews their clinical relevance in modern cancer therapy.

With the development of drugs that target specific biochemical features of cancer, it was hoped that there would be a paradigm shift in the treatment of cancer leading to reduced mortality and reduced side effects. It was also hoped that the problem of drug resistance which is a common feature of classical cytotoxic drugs would not be a problem. Whilst the discovery and development of new targeted therapies has generated effective and novel cancer therapies, significant concerns remain, and it is now apparent that the much hoped-for paradigm shift in cancer treatment has not occurred. The reasons for this apparent lack of success are gradually being unravelled but the key issues are the emergence of new resistance mechanisms (*via* mutation of

the pharmacological target for example), tumour heterogeneity and tumour plasticity, details of which are described elsewhere (Meacham & Morrison, 2013).

With regards to the emergence of drug resistance, the presence within a single tumour of multiple clones of cells with different genomic backgrounds and characteristics can lead to the positive selection of a drug resistant clone (Greaves & Maley, 2012) Furthermore, evidence has emerged demonstrating that cancer cells have the ability to switch between different phenotypical cellular states allowing them to circumvent the blockade of a specific pathway by switching to another (Aparicio et al., 2015; Meacham & Morrison, 2013). This phenomenon is referred to as plasticity and it allows cells to differentiate into other cell types that may be functionally, very far away from the original cell. This new paradigm of cellular differentiation, once viewed as a unidirectional process allows the cancer cells to create adaptive mutations in an almost Darwinian environment with the "fittest" surviving the selective pressure of the drug growing and forming a resistant state (Gravitz, 2014). This selective pressure of targeted therapy is causing cells to rewire their circuitry during treatment and may be driving tumours to become more heterogeneous (Bourzac, 2014). In some cases therefore, it could be considered that some targeted therapies are "too targeted" making the "magic bullet" theory becoming harder to achieve (ElShamy & Duhé, 2013).

In addition to resistance, selective therapy poses difficulties chemically, as it is very difficult to chemically achieve single target specificity. This is because compounds

are found to interact with multiple targets with most drug molecules interacting with an estimated six known molecular targets on average (Mestres, Gregori-Puigjané, Valverde, & Solé, 2009). This gives further support to the shift from the concept of "one drug, one target" which is the cornerstone of target based drug development (Lee & Bogyo, 2013). Furthermore it is now becoming evident that many of the most effective drugs in cancer therapy such as Gleevec act on multiple rather than single targets (Paolini, Shapland, van Hoorn, Mason, & Hopkins, 2006). This phenomenon whereby compounds hit multiple targets is known as poly-pharmacology and represents a novel avenue for novel drug discovery. Designing drugs with a specific yet multi-target profile or designing a rational combination of such is complex but it could tackle the two major causes for attrition in drug development – poor efficacy and toxicity (Hopkins, 2008).

1.4 - Phenotypic Approach to Drug Discovery and Target Deconvolution

In view of the evidence emerging demonstrating that therapeutic agents targeted at specific pathways may be ineffective in the long term, there has been a resurgence in interest in a phenotypic based approach to drug discovery. Very much along the lines of the random screening program run by the National Cancer Institute in the United States (the NCI60 screen), this approach assumes that there are compounds in existing archives that are capable of targeting multiple pathways leading to a phenotypically desirable effect (reduced angiogenesis, reduced invasion for example). The selection of the specific endpoint that identifies a desirable phenotypic effect can

be varied and this distinguishes this approach from the NCI60 screen. Once a promising compound has been identified, then the process of understanding its mechanism(s) of action can begin in a process known as target deconvolution (Lee & Bogyo, 2013). As with all drug development approaches, there are significant advantages and challenges. With regards to advantages, this approach has the potential to identify compounds capable of inducing a useful therapeutic effect *via* multiple mechanisms of action. This has the potential to reduce the problem of tumour heterogeneity by being able to target multiple clones and thereby reducing the emergence of resistant clones. Furthermore, there are significant opportunities to identify molecules that have novel chemical structures. In the years between 1998-2008 259 therapeutic agents have been approved by the FDA (Food and Drug Administration) 50 of which were small molecule first in class drugs, 28 were discovered by a phenotypic approach and 17 by target based drug discovery (Swinney & Anthony, 2011). Many drugs in use today have been discovered *via* phenotypic drug discovery including ezetimibe (cholesterol lowering drug) and linezolid (antimicrobial). The utility of phenotypic drug discovery allows for the investigation of drugs by phenotypic response allowing for the discovery of compounds which exert novel and unexpected mechanisms of action. This is particularly useful for diseases which do not have established and/or validated therapeutic targets allowing drug discovery in rarer and lesser understood conditions (Zheng, Thorne, & McKew, 2013).

The major challenge this approach faces however is the issue of selectivity for cancer cells over non-cancer cells. By identifying compounds with multiple mechanisms of action, it becomes challenging to identify compounds that selectively target cancer cell biology.

Despite the challenges of this approach to drug discovery there are significant potential advantages to a phenotypic based approach that make it an attractive alternative to targeted drug discovery pathways (Gujral, Peshkin, & Kirschner, 2014). The concept is relatively straight forward, and it relies on the identification of hit compounds with desirable properties followed by target deconvolution to identify mechanism(s) of action. It determines the mechanisms of action, identifies effective pathways, determines suitable combinations of drug targets or drugs whilst addressing any target specific or off target toxicity early in the discovery of the drug (Boran & Iyengar, 2010; Drews, 2000; Lee & Bogyo, 2013). Within this context, this thesis focuses on the evaluation of a series of novel organometallic compounds as poly-targeted anti-cancer agents using a phenotypic and target deconvolution based approach. Within this context, this thesis focuses on the evaluation of a series of novel organometallic compounds as poly-targeted anti-cancer agents using a phenotypic and target deconvolution based approach. Details of the rationale and aims of the project are described in more detail in the following sections.

1.5 - Rationale and Aims of Thesis

In recent years organometallic complexes have undergone a resurgence in interest largely because they have been shown to exert their effects *via* mechanisms that do not involve DNA alkylation (Gasser, Ott, & Metzler-Nolte, 2010). Current research is therefore shifting away from the cisplatin paradigm where DNA is the established target with a number of new and alternative metal complexes often showing innovative mechanisms of action including targeting of multiple biologically important pathways (Bruijnincx & Sadler, 2008). Their diverse chemical structures and chemical properties make this class of compounds good candidates for a phenotypic based approach to drug discovery and this thesis focuses on evaluating a series of novel organometallic complexes from a variety of collaborative laboratories.

With regards to the phenotypic evaluation strategy, the approach employed is chemosensitivity testing against cancer cell lines *in vitro* which is similar to the strategy employed by the NCI (although nowhere near as comprehensive). The steps that make this approach distinct from the NCI is the inclusion of non-cancer cell lines in the panel with the aim of establishing an *in vitro* 'selectivity index' as a key decision-making tool for selecting interesting compounds for further development. This addresses the key potential limitation of phenotype based drug discovery programs which is the issue of selectivity and how will this be achieved by compounds with multiple mechanisms of action. In addition, the *in vitro* selectivity index can be determined for the clinically

approved platinum based drugs and this information can be used as a further decision-making point. In summary therefore, the aims of this thesis are:

1. To evaluate the cytotoxic activity of platinum based anti-cancer drugs with a view to establishing a baseline selectivity index defined as the ratio of IC_{50} values in non-cancer cells to cancer cells.

2. To determine the potency and *in vitro* selectivity of a series of novel organometallic complexes and select compounds for further evaluation based upon (i) better selectivity than the platinates *in vitro* and (ii) equivalent or better potency than platinates *in vitro*.

3. For those compounds that meet the selection criteria defined above, their pharmacological properties and potential mechanism(s) of action will be explored.

4. In some cases where the chemical structures suggest that the compounds may have preferential activity in the tumour microenvironment, the ability of these compounds to selectivity kill hypoxic cells will be determined.

5. To critically appraise whether this approach to drug development is capable of leading to the selection of compounds that have anti-tumour activity *in vivo*. All *in vivo* studies were conducted by collaborators at the University of Bradford and acknowledgement to their involvement in the project is provided at the appropriate place in this thesis.

Chapter 2 – General Methods

2.1 - Materials

Unless otherwise stated, all reagents were obtained from Sigma Aldrich (Poole, Dorset) and all cell lines were obtained from either the American Tissue Culture Collection (ATCC) or European Collection of Cell Cultures (ECACC). A list of the cell lines used are presented below in table 2.1 and 2.2:

2.2 - Cell lines and Media

2.2.1 - Non-Cancerous Cell Lines

Cell line	Description	Media	Supplementation
ARPE-19	Retinal pigmented epithelium	DMEM F:12	1mM sodium pyruvate, 2mM L-glutamine, 10% FBS.
WI-38	Normal lung fibroblasts	EMEM	1mM sodium pyruvate, 2mM L-glutamine, 10% FBS.

Table 2.1: Summary of non-cancerous cell lines used throughout this investigation along with their culture media and additives, note media purchased is both L-glutamine and sodium pyruvate free.

2.2.2 - Cancerous Cell Lines

Cell line	Description	Media	Supplementation
BE	Colon carcinoma	DMEM	1mM sodium pyruvate, 2mM L-glutamine, 10% FBS.
HCT116 p53$^{+/+}$	P53 wild type colonic adenocarcinomas	DMEM	1mM sodium pyruvate, 2mM L-glutamine, 10% FBS.
HCT116 p53$^{-/-}$	P53 knock down colonic adenocarcinomas	DMEM	1mM sodium pyruvate, 2mM L-glutamine, 10% FBS.
HT29	Human colorectal adenocarcinoma	DMEM	1mM sodium pyruvate, 2mM L-glutamine, 10% FBS.
MIA-PaCa$_2$	Pancreatic carcinoma	DMEM	1mM sodium pyruvate, 2mM L-glutamine, 10% FBS.
Panc 10.05	Pancreatic adenocarcinoma	RPMI 1640	1mM sodium pyruvate, 2mM L-glutamine, 10mg/litre human insulin, 15% FBS.
PSN – 1	Epithelial like pancreatic adenocarcinoma	RPMI 1640	1mM sodium pyruvate, 2mM L-glutamine, 10% FBS heat inactivated heat inactivated FBS supplied by Fisher Life Technologies.
MDA-MB-231	Mammary gland adenocarcinoma	L-15	1mM sodium pyruvate, 2mM L-glutamine, 10% FBS.

Table 2.2: Summary of cancerous cell lines used throughout this investigation along with their culture media and additives. Note media purchased is both L-glutamine and sodium pyruvate free.

All cells were routinely maintained in antibiotic free culture media as monolayer cultures and incubated at 37°C in a humidified, CO_2 enriched (5%) atmosphere. Cancer cell lines were passaged for up to 10 passages, after which they were then discarded to reduce the risk of genetic drift affecting the reproducibility of results. Once cultures had reached passage 10, new cultures were resuscitated from stock cultures stored in the liquid nitrogen bank. Non-cancerous cells lines were maintained in culture until they showed signs of deterioration (slow growth rates and senescence) and new cultures were then established from the liquid nitrogen bank.

2.3 - Cell Culture Methods

All general cell culture was undertaken in laminar flow hoods using sterile techniques with sterile reagents ensuring sterility of cultured cells. Cells were checked daily to ensure expected growth as per specification and to avoid cells overgrowing. Prior to use all reagents are warmed in a water bath at 37°C for at least 30 minutes to prevent shock to the cells.

2.3.1 - Resuscitation of Cells from Cryo-Preservation

When cells were removed from liquid nitrogen efficiency is key to ensure the cells are removed from the freezing medium as soon as possible. Once cells are taken from the liquid nitrogen they were defrosted rapidly in a water bath at 37°C, then immediately added to at least 20ml of culture medium, ensuring the DMSO in the freezing medium is thoroughly diluted. The resulting suspension was centrifuged at 1000-1500 rpm (depending on cell line) for 3 minutes producing a cell pellet from which the media solution was carefully removed. The resulting pellet was then re-suspended in culture media and an adequate volume of cell suspension added to the desired cell culture flask.

2.3.2 - Counting Cells in a Haemocytometer

The haemocytometer was cleaned with 70% alcohol before and after use and thoroughly dried. Once dried the coverslip were fixed in place (pressed down until newton rings are visible), 10µl of cell suspension (treated with trypan blue to help distinguish viable from non-viable cells) was carefully added to the haemocytometer

being careful not to overfill the chamber. The haemocytometer was then placed on an inverted microscope using 10 x objective lens and unstained, viable cells counted in each of the four corner squares (made up of 16 smaller squares), counting only cells set within the squares and on the right and lower boundaries (see figure 2.1). The resulting cell number was divided by 4 to give an average, multiplied by the dilution of the contrast media, then further multiplied by 10^4 which gives the number of viable cells within 1ml of the cell suspension.
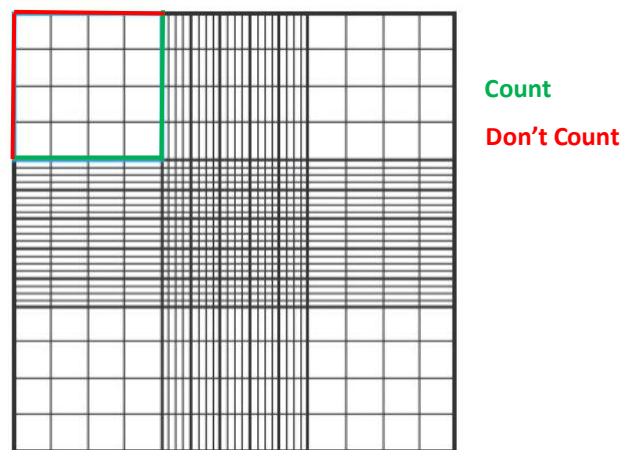
Count
Don't Count

Figure 2.1: General haemocytometer gridlines with one of the four "counting squares" highlighted.

2.3.3 - Sub-Culturing by Trypsinisation of Monolayer Cultures

Sub-culturing was undertaken either to prepare cells for specific experiments or to maintain cell cultures in exponential growth for future use. Media was removed from the flasks in which the cells are attached, the cells were then washed twice with PBS removing residual FBS, which inactivates the trypsin solution. The PBS was then

removed and replaced with a sufficient volume (depending on flask size) of trypsin 1x solution and the flask gently rolled to ensure sufficient coverage. The flasks are incubated at 37°C for between 1 to 5 minutes depending on the cell line and their confluency. Once detached, cells were immediately re-suspended in growth medium to inhibit the action of trypsin. Cells were added to a fresh, labelled flask as per recommended split ratio and the required volume of culture media is added. The cells are then incubated overnight to reattach and settle following which the media is changed to remove any residual trypsin. Each time a cell line is sub-cultured the passage number is recorded on the flask.

2.3.4 - Cryo-Preservation

Following trypsinisation as described above, cells were re-suspended in culture media containing 20% FBS and 10% DMSO and 1ml of this cell suspension placed in a pre-labelled cryo-vial. The cryo-vials were then frozen by gradient freezing using a Nalgene "Mr Frosty" system loaded with isopropyl. Once the cryo-vials are inserted into the "Mr Frosty" at room temperature, this was placed in a -80°C freezer overnight prior to transferring the cryo-vials into the liquid nitrogen storage facility. The exact location, number of vials, date and cell line details were then entered into the liquid nitrogen storage logging system.

2.4 - Validation of the Clonogenic Assay

To validate the clonogenic assay for use in chemo-sensitivity testing, the relationship between the number of cells seeded and the number of colonies formed

was determined. Each cell line was seeded into six well plates at seeding densities ranging from 500 cells to 3500 cells per well. Each of the seeding densities were replicated three times and cells were incubated at 37°C in a humidified, CO_2 enriched (5%) atmosphere. The plates were visually monitored (to determine when distinct colonies of >50 cells had formed) on days 2,3,4,8 and 9 with media changes made on days 4 and 8. The plates were quartered with each quadrant monitored for colony formation and overlapping colonies. If cell colonies in a single quadrant started to exceed 25 colonies or overlapping occurred, it was documented as these factors suggest overcrowding and this affects the ability to count the colonies accurately. Once colonies had formed (usually after 10 days incubation) viable colonies were stained (as described in 2.4.1 below) and counted using an Oxford Optronix Gel Count (Colony Counter). The software accurately counts all viable colonies along with providing mean colony diameter readings.

2.4.1 - Viable Colony Staining Protocol

Medium was removed, and cells were washed twice with PBS. After removal of PBS, 2-3 ml per well of fixation solution (acetic acid: methanol 1:7) was added and left at room temperature (RT) for 5 min. After 5 minutes, the fixative solution was removed and plates were dried at RT for 15 minutes. Once dried, 0.5% crystal violet solution was added to each well and incubated at 37°C for 2 hours. After removal of the crystal violet, the dishes/plates were carefully immersed in tap water to rinse off the crystal violet taking care not to remove any colonies. The dishes/plates were then

air-dried at RT for two days after which they were then processed by the Optronix Gel Count (Colony Counter), which uses high resolution imaging to accurately count and size colonies and spheroids.

2.5 - The MTT Assay

2.5.1 - Validation of the MTT Assay

A single cell suspension was prepared at 5×10^4 cells per ml. A 96 well plate was then seeded with varying volumes of cell suspension (ranging from 200 µl to 0 µl, decreasing in 20 µl aliquots) and medium added to make the final volume in each well up to 200 µl. The first lane contained 200 µl of media only to serve as a blank for the spectrophotometric readings and each condition was repeated 8 times (i.e. rows A-H on the 96 well plate). Immediately after plating the cells, 20µl of 3-(4,5-dimethylthiazol-2-yl)-2,5-diphenyltetrazolium bromide (MTT, 5mg/ml) was added to each well and cells were incubated at 37°C for 4 hours. Following incubation, the media/MTT solution was removed from each well taking care not to remove any of the formazan crystals. After removal of the media, 150µl of dimethyl sulfoxide (DMSO) was added to each well and mixed with a micro spatula to ensure the formazan crystals have fully dissolved. The plates were then immediately read by a Tecan microplate photometer set at 540nm. The mean true absorbance was calculated (mean absorbance of wells containing cells minus the mean of the blank) for each lane and plotted against cell number.

2.5.2 - Determination of Optimum Seeding Densities for Use in the MTT Assay

Previous studies in the laboratory had established the optimum seeding density for most cell lines used in this thesis except for PSN-1 and Panc-10.05 cell lines. To ensure that cells remain in exponential growth at the end of the chemosensitivity assay, PSN-1 and Panc-10.05 cells were seeded into 96 well plates at increasing cell densities per row ranging from 100-2000 cells per well then incubated at 37° for five days to mimic the total time cells are cultured in chemosensitivity assays). After five days, the medium was removed from each well and 200μl of fresh medium added along with 20μl of MTT (5 mg/ml). The MTT assay was conducted as described above and cell number plated against absorbance determined. The cell seeding density that gave results within the linear portion of the results obtained was selected for use in chemosensitivity studies.

2.5.3 - Chemosensitivity Studies Under Aerobic Conditions

Culture plates (96 well) were seeded as per the optimum initial seeding density established above and left overnight in the incubator at 37°C in a CO_2 enriched atmosphere (5%) for cells to adhere to the plates. Test compounds were dissolved in either water based solutions i.e. medium or DMSO (details provided in each subsequent chapter) and a range of drug concentrations prepared by serial dilution. For compound's not soluble in water/media the final concentration of DMSO was 0.1% (v/v) which is not known to be toxic to cells. Within each 96 well plate, blanks, controls and five compounds at eight different concentrations repeated twice were evaluated

on each plate as illustrated in figure 2.2. For each compound, an initial run was completed with a wide concentration range from 0.00128μM-100μM. Cells were exposed to compounds for 96 hours before cell survival was determined using the MTT assay as described above.

2.5.4 - Determination of the IC_{50} Value

The IC_{50} (inhibitory concentration at 50%) values were calculated by firstly subtracting the average absorbance of the blank column from all the average absorbance values to obtain the true absorbance. The percentage cell survival was then calculated using the true absorbance value as 100% cell survival. The IC_{50} value was calculated by plotting the percentage cell survival on a scatter graph, performing linear regression analysis and then using the equation Y=MX+C where Y=50 (50%) and M and C are calculated from the line plotted on the scatter graph X (the concentration). Once an approximate IC_{50} was established, experiments were then repeated using a much narrower concentration range to determine an accurate IC_{50}. All experiments were performed in triplicate on separate days to achieve a mean IC_{50}. In addition to the novel organometallics, a platinum panel was also run as a benchmark for the novel compounds (see chapter 3).

	A	B	C	D	E	F	G	H	I	J	K	L
1	Blank	Control	Drug 1		Drug 2		Drug 3		Drug 4		Drug 5	
2	Blank	Control										
3	Blank	Control			Increasing drug concentration							
4	Blank	Control										
5	Blank	Control										
6	Blank	Control										
7	Blank	Control										
8	Blank	Control										

Figure 2.2: Typical MTT plate setup used to test allowing 5 compounds to be tested per 96 well plate.

2.5.5 - Chemosensitivity Studies Under Hypoxic Conditions

Culture plates (96 well) were seeded using the optimum density determined above and left overnight in the incubator at 37°C for cells to adhere to the plates. The plates were then transferred to the Don Whitley H35 hypoxia workstation set at 0.1% O_2, 94% N_2, 5% CO_2 and 37°C. Along with the corresponding medium for the specific cell type, the plate(s) and the medium are then left for a further 24 hours in order for the oxygen to be purged and cells to adapt to hypoxic conditions. Cells were then exposed to drugs as described above in the hypoxia cabinet for a further for 96 hours. After 96 hours the medium was removed from each well and 20µl of MTT (5 mg/ml) was added to each well. The plates were then incubated in the hypoxia cabinet for 4 hours. After 4 hours, the media/MTT solution was then carefully removed from each well taking care not to remove any of the formazan crystals. After removal of the medium, 150µl of dimethyl sulfoxide (DMSO) was added to each well and mixed with a micro-spatula to ensure the formazan crystals have fully dissolved. The plates were then immediately read by a Tecan reader set at 540nm. IC_{50} values were calculated as

described above. As per previous protocols, all experiments were performed in triplicate to achieve a mean IC_{50} ± standard deviation.

2.5.6 - Pseudo-Hypoxic Conditions

Culture plates (96 well) were seeded at the optimum cell density as described above and left overnight in the incubator at 37°C for cells to adhere to the plates. After 24 hours, the medium on all plates in all wells was then replaced with medium containing cobalt (II) chloride hexahydrate at a concentration of 150µM for an additional 24 hours. After 24 hours the cobalt medium is removed, washed with PBS and replaced with fresh cobalt chloride (150 µM) supplemented medium containing drug solutions covering a range of concentration. Following a 96-hour drug exposure under aerobic conditions, cell survival was determined using the MTT assay as described above. Each experiment was repeated in triplicate and the results presented are the mean ± standard deviation.

2.6 - Analysis of Drug Induced Cell Cycle Arrest and Apoptosis Induction Using the NucleoCounter (NC-3000) Cytometer

The NucleoCounter 3000 or NC3000 is an advanced cytometer which uses fluorescence imaging to characterise cell properties. Compounds which were selected as being lead compounds based on their potency and/or selectivity index relative to that of the platinum standards were assessed for cell cycle arrest and apoptosis induction.

2.6 1 - 96-Hour Investigations

For each of the compounds selected for further analysis, three T-25 flasks with 1.66×10^5 cells and left overnight in the incubator at 37°C to allow the cells to adhere to the flasks. A further flask was also seeded at the same cell density to serve as a control. The seeding density reflects the seeding density used for the MTT assays multiplied by the ratio of the area of a T25 flask to that of a single 96 well (i.e. the number of cells per cm^2 is the same in both cases). Cells were exposed to corresponding IC_{50} values of compounds and in cases where organic solvents such as DMSO were used to dissolve compounds, a final concentration of 0.1% v/v DMSO was maintained in both treated and control flasks. As per previous MTT protocols the flasks were then incubated at 37°C for 96 hours. After drug exposure, images were taken (Evos XL digital microscope) of each flask for visual comparison prior to trypsinisation to obtain a cell suspension. Cells were then analysed using the NC3000 and the following tests were performed: (i) a viability assay (ii) measurement of apoptosis induction and (iii) cell cycle analysis. For all these assays, the original medium was always kept and re-added prior to centrifugation to create a cell suspension with all living, apoptotic and necrotic populations present.

2.6.2 - Varied Time Point Investigations

For some compounds, timed drug exposures were employed and in these cases, a higher seeding density (7×10^5 cells/T25) was used. Cells were exposed to test compounds (at the IC_{50} concentration) for time points ranging from 1 to 72 hours,

following which cells were washed twice with PBS and trypsinised to generate a single cell suspension as described above.

2.6.3 - Viability Assay

Following the preparation of a single cell suspension, cells were drawn into the Via1-cassette by inserting the tip of the cassette into the cell suspension and pressing the piston. The Via1-cassettes are pre-loaded with Acridine orange, which stains the entire population and DAPI which stains the non-viable cells only. The cassettes were then immediately placed into the NC-3000 for analysing. The cell suspension should be in the range of 5×10^4 cells/ml to 5×10^6 cells/ml to assure reliable results in the viability assay and ensuring manageable cell densities for subsequent assays. The viability assay not only determines the viability of a cell suspension but provides and accurate cell count which facilitates the use of consistent cell numbers throughout subsequent assays.

2.6.4 - Mitochondrial Potential Assay

To determine whether compounds induced apoptosis, a mitochondrial membrane potential assay was performed. A suspension of 1×10^6 cells/ml was prepared in PBS to 12.5µl of 200µg/ml JC-1 was added. The resulting suspension was then incubated for 10 minutes at 37°C before being centrifuged at 400g for 5 minutes. The supernatant was then removed *via* careful pipetting to avoid disturbing the pellet. The pellet was then washed twice with PBS to remove JC-1 dye and prevent unspecific binding then vortexed to reduce the occurrence of aggregates. The supernatant was then carefully

removed and the pellet re-suspended in 250µl of 1µg/ml DAPI in PBS then analysed immediately on an A8 or A2 slide (Chemometec) depending on the number of samples. These are plain glass slides with no impregnated stains or dyes and the number corresponds to the number of samples that can be analysed on them. The rationale behind the assay is that it automates detection of cells with collapsed mitochondrial membrane potential (de-polarised), which is known to precede apoptosis. The cells are dyed with JC-1 which in negatively charged, healthy cells stain fluorescent red as it accumulates and aggregates in the mitochondrial matrix. In apoptotic cells the mitochondrial potential collapses and the JC-1 localises in the cytosol in its fluorescent green form. Late apoptotic and necrotic cells are stained blue by DAPI. Non-viable/necrotic cells with a high DAPI signal were discounted from the results to reduce the inclusion of naturally occurring cell death. The degree of apoptosis is measured using a scatter plot of JC-1 red fluorescence vs JC-1 green fluorescence, therefore apoptotic cells present with a reduction in red/green fluorescence ratio.

2.6.5 - Annexin V Assay

As no single assay is exclusively selective for apoptosis induction, an additional apoptotic assay (the Annexin V assay) was also performed. From the viability assay a cell suspension at $2\text{-}4\text{x}10^5$ cells/ml was prepared in PBS. The cells were washed twice in PBS before re-suspending the cell pellet in 100µl of Annexin V binding buffer (BD Biosciences). Annexin V-CF488A conjugate (2µl) (Santa Cruz Biotechnology) and Hoechst 33342 (final concentration 10µg/ml) (Thermo-Scientific) was then added and

the resulting suspension mixed thoroughly and incubated at 37°C for 15 minutes. After

incubation, the suspension was centrifuged for 5 minutes at 400g and the cell pellet

was re-suspended in 300µl of Annexin V binding buffer and mixed thoroughly. The

suspension was again centrifuged, the supernatant removed, and the resulting pellet

re-suspended in 100µl of Annexin V binding buffer and 10µg/ml Propidium Iodide (PI).

This cell suspension was analysed immediately by adding 30µl to an A2 slide. The

whole cell population will be stained by Hoechst 33342 emitting violet light with

Annexin V-CF488A conjugate staining apoptotic cells a fluorescent green light. Non-

viable/late apoptotic cells will be stained with both Hoechst and PI emitting violet and

red light respectively, with late apoptotic population also emitting green fluorescence

(Annexin V CF488A). The fluorescence intensity of Annexin V-CF488A vs the

fluorescence intensity of PI is displayed in a scatter plot with only cells with nuclei

(Hoechst 33342 stained) being displayed on the scatter plot. This assay therefore

quantifies healthy, early apoptotic, late apoptotic and non-viable cells.

2.6.6 - Cell Cycle Assay

To determine whether, or not, selected compounds induced cell cycle arrest, a cell

suspension at 1×10^6 cells/ml was prepared. Cells were washed twice in PBS prior to

the addition of 250µl of Solution 10 (lysis buffer, Chemometec) supplemented with

10µg/ml DAPI. The cell suspension was then incubated for 5 minutes at 37°C followed

by the addition of 250µl of solution 11 (stabilisation buffer, Chemometec). The

resulting sample was then immediately analysed again using A2 or A8 slides dependent

on the number of samples. The principle of the assay is that DNA content of cells is quantified based on DNA staining with DAPI. In a single population, cells are distributed among three major phases; G_1/G_0 with one set of paired chromosomes per cell, S phase where DNA is synthesised thus resulting in variable DNA content, and G_2/M phase where there are two sets of paired chromosomes per cell. Sub G_1 populations are classed as apoptotic with populations with higher fluorescent intensities than G_2/M phase being classed as polyploid. DAPI intensity vs cell population is plotted on a histogram which is used to quantify the percentage of the cell population in the various cell cycle stages based on DAPI intensity which directly relates to DNA content.

2.6.7 Statistical analysis

In order to determine if variances in two populations i.e. activity of specific compounds in non-cancerous opposed to cancerous cell lines are statistically significant paired t-test were completed. This statistical analysis of two means tests the hypothesis that the use of different cell lines, isogenic clones or alterations in oxygen tension results in significant differences in the activity of both our platinum standards and novel compounds. This statistical formula results in a P-value or probability value which when below 0.05 established statistical significance between two populations.

Chapter 3 - Response of Human Tumour Cells and Non-Cancer Cells to Clinically Approved Platinum Based Anti-Cancer Drugs

3.1 - Introduction

This chapter concentrates on the validation and optimisation of chemosensitivity assays methodologies and the characterisation of cellular response to clinically approved platinum based anti-cancer drugs. The purpose of this is to establish a 'baseline' or 'yardstick' against which the relative merits of novel organometallic compounds can be measured with regards to (i) potency and (ii) selectivity for cancer as opposed to non-cancer cell lines. In effect, compounds will be selected for further evaluation if they demonstrate superior activity profiles compared to established metal containing anti-cancer drugs. The following information reviews the current literature with regards to platinum based anti-cancer drugs with respect to their pharmacology.

As described earlier in this thesis, cisplatin remains one of the leading drugs in cancer therapy and is used for the treatment of a variety of cancers including ovarian, testicular, lung and bladder cancers. Cisplatin is present in 32 of 78 treatment regimens listed in the Martindale (Press, 2017) and is utilised not only as a mono-therapeutic agent but also its use in combination therapy (Sweetman, 2009). *Cis*-diamminedichloroplatinum (II) better known as cisplatin is a metal co-ordination compound which was approved for clinical use in testicular cancer in 1978 (Loehrer &

Einhorn, 1984) and remains one of the most potent anti-tumour agents known. It's clinically considered one of the most effective chemotherapeutic agent and is used to treat 50% of all cancers including testicular, ovarian, head and neck, colorectal, bladder and lung cancer (Galanski, Jakupec, & Keppler, 2005). Its anti-tumour effect remains a benchmark for novel metal-based anti-cancer agents. It is thought cisplatin enters the cell by three modes of action passive diffusion, copper transporter proteins and/ or organic cation transporters (Puckett, Ernst, & Barton, 2010). Cisplatin exerts its anticancer effects by multiple modes of action, yet most prominently via the formation of DNA lesions *via* covalent bonding to Guanine and to a lesser extent adenine, resulting in intra and inter-strand adducts (demonstrated in figure 3a). These adducts cause bending and unwinding of the DNA culminating in the induction of mitochondrial dysfunction (Galluzzi et al., 2012). This mitochondrial dysfunction has been shown to precede apoptosis and the loss of mitochondrial membrane potential is thought to take a central role in apoptosis causing the release of apoptogenic factors and the loss of oxidative phosphorylation (Ly, Grubb, & Lawen, 2003).
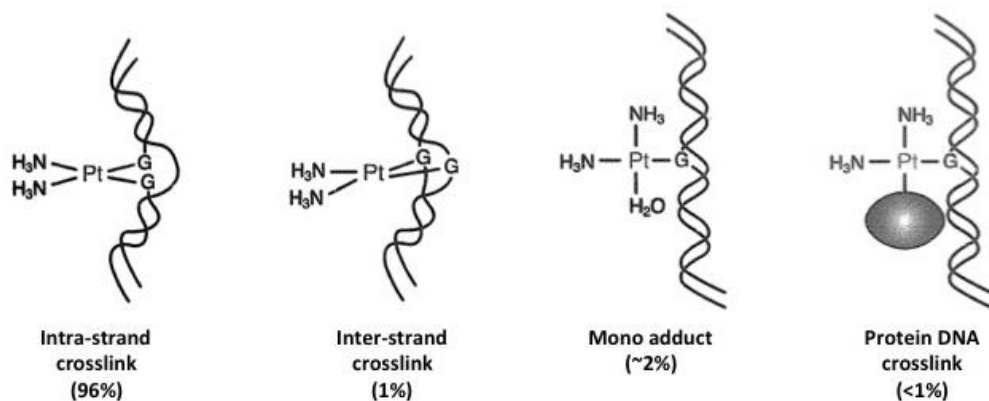
Figure 3a: Main DNA lesions formed upon cisplatin binding to DNA, adapted from (Cepeda et al., 2007; Conconi, 2013).

In the 40 years since its discovery, the success of cisplatin has motivated the synthesis of several hundred platinum derivatives. Yet of the vast number of novel platinate compounds synthesised, only 23 other platinum based drug have entered clinical trial and of these, only two have gained international marketing approval (Wheate, Walker, Craig, & Oun, 2010). This lack of success is due largely to limitations associated with dose limiting toxicity and ever-increasing resistance towards platinum therapy.

Resistance towards cisplatin treatment has been studied extensively and as previously discussed has been attributed to two broad mechanisms. The first mechanism involves the reduction of DNA damage induction either by reduced drug uptake or drug inactivation by thiol containing species (Kelland, 2000, 2007). The second mechanism involves a failure to achieve cell death after platinum DNA adduct formation, mainly because of upregulation of DNA repair (Al-Dimassi et al., 2014). Of

the five recognised DNA repair pathways that repair DNA following damage (nucleotide excision repair, mismatch repair, double strand break repair, base excision repair and direct repair (Giaccone, 2000), two have been identified as the mechanism behind increased tolerance to platinum induced DNA damage. These two pathways are upregulation of nucleotide excision repair and loss of function of the mismatch repair pathway which ordinarily triggers an apoptotic response (Galluzzi et al., 2012).

In addition to direct resistance to DNA damage, platinum resistance may also be mediated through alterations to downstream proteins involved in apoptosis such as P53 and the BCL_2 family (Kelland, 2000). As previously discussed, cisplatin therapy is known to bind with DNA resulting in distortion in the DNA including unwinding and bending. These DNA adducts can impede key cellular processes such as DNA replication and transcription leading to a cellular stress response and commonly the induction of apoptotic cell death. The phenotypic effects of these adducts can also include prolonged G2 cell cycle arrest, altered growth *via* signal transduction pathways, or differentiation (Kelland, 2007) Tumours can acquire resistance to apoptosis by the increased expression of anti-apoptotic proteins or by the downregulation or mutation of pro-apoptotic proteins (Igney & Krammer, 2002). Resistance caused by mutations in P53 and the DNA repair pathways are a major limitation to platinum therapy and therefore, novel approaches are needed to circumvent this major therapeutic problem.

Carboplatin was the first of the two novel platinum agents to gain global approval and it is now the drug of choice for treatment of ovarian cancer (Ai, Lu, Qiu, & Fan, 2016; Piccart, Lamb, & Vermorken, 2001). Carboplatin is often referred to as a cisplatin pro-drug as it requires conversion to its reactive species and the rate of conversion is much slower than that of cisplatin. This reduction in conversion rates significantly diminishes the nephrotoxic effects seen with cisplatin (Kostova, 2006). This is a result of replacing dichloride ligands with 1,1-cyclobutanedicarboxylate (see table 1 for compound structures) which aquates much slower. Platinum toxicity is directly related to the ease at which these leaving groups are aquated (i.e. how easily they are displaced by water). Therefore, by manipulating these leaving groups, carboplatin is converted to its reactive species much slower which significantly reduces the dose limiting nephrotoxic effects observed with cisplatin (Wheate et al., 2010). Unfortunately, carboplatin does carry its own side effects including myelosuppression and thrombocytopenia, which can be managed with adjuvant treatments such as the granulocyte-stimulating growth factors, filgrastim and pegfilgrastim alongside regular monitoring of bloods. These side effects, although dose limiting, can be managed unlike the potentially life-threatening nephrotoxicity observed with cisplatin. This therefore enables the administration of higher doses and much more prolonged administration of carboplatin to patients compared to cisplatin. Despite its altered toxicity profile, carboplatin's mechanism of action mirrors that of cisplatin forming the same adducts as cisplatin resulting in cross resistance. This therefore reduces the clinical application of carboplatin especially in colorectal and pancreatic tumours to

which cisplatin resistance is already well established (Weiss & Christian, 1993)(Weiss & Christian, 1993).

The limitations of cisplatin and carboplatin ultimately led to the development and subsequent approval of the second platinum agent, oxaliplatin. This compound showed both a reduced toxicity profile and the ability to overcome cisplatin resistance (Misset, Bleiberg, Sutherland, Bekradda, & Cvitkovic, 2000). Oxaliplatin as a single agent and as part of combinational therapy shows little cross-resistance with cisplatin or carboplatin.

Although oxaliplatin targets the same DNA site as cisplatin and carboplatin, the resulting DNA adducts formed differ in structure. The two amine ligands presented on cisplatin are substituted for single bidentate ligands with 1,2-diaminocyclohexane (DACH) carrier ligands. These DACH ligands form much bulkier, hydrophobic adducts which point into the DNA major groove preventing the binding of DNA repair proteins (Misset, Bleiberg, Sutherland, Bekradda, & Cvitkovic, 2000; Raymond, Chaney, Taamma, & Cvitkovic, 1998). It is also these oxalate ligands, which reduce the toxicity profile of oxaliplatin. Its potential was initially overlooked for a decade due to dose limiting neuropathy although this was subsequently found to be avoidable with the addition of calcium and magnesium solutions (Cersosimo, 2005). As a single agent, oxaliplatin has limited but consistent activity but as a combinational therapy, it holds much promise. It shows remarkable synergistic activity with fluoropyrimidines such as 5-fluorouracil/folic acid for which it is clinically licensed as a combinational therapy for

metastatic colorectal cancer (FOLFOX regimen) and locally advanced and metastasised pancreatic cancer (FOLFORINOX regimen) (Conroy et al., 2011; Raymond, Chaney, Taamma, & Cvitkovic, 1998). Its synergistic potential as a combinational therapy has more recently been investigated in platinum resistant ovarian cancers as both an active regimen with topotecan (topoisomerase-I inhibitor) and as a moderately effective multi-drug regimen with gemcitabine (Elshebeiny & Almorsy, 2016; Stein et al., 2013).

As stated earlier, this thesis is designed to evaluate a series of chemically diverse organometallic complexes in the hope of identifying lead compounds that can be evaluated further. To select these novel compounds for further evaluation, the potency and selectivity of platinum based complexes under aerobic and hypoxic conditions will be determined as this serves as a benchmark against which the relative merits of novel compounds can be judged. In essence, if novel compounds perform as well as or better than platinum based compounds in initial experimental chemosensitivity studies, they will be selected as potential 'hit' compounds for further evaluation. The purpose of this chapter therefore is to characterise the response of cell lines to cisplatin, carboplatin and oxaliplatin under various experimental conditions.

3.2 - Methods

3.2.1 - Chemosensitivity Studies

All compounds were obtained from Sigma Aldrich (Dorset, UK) and stock solutions were prepared as described in table 3. All stock solutions of drugs were aliquoted into 2µl batches and stored at -20°C until required for chemosensitivity studies. Stock solutions were not subjected to repeated freeze thaw conditions and all stocks were disposed of 3 months after preparation. All results represent the mean ± standard deviation of three independent experiments. The selectivity index is defined as the mean IC_{50} of non-cancer cells divided by the IC_{50} for tumour cells; values >1 indicate selectivity for tumour cells *in vitro*.

Compound	MW	Diluent	Solubility	Molar concentration (mM)	Compound structure
Carboplatin	371.25	PBS	10mg/ml	20mM	
Cisplatin	300.05	PBS	2.5mg/ml	1mM	
Oxaliplatin	397.29	PBS	5mg/ml	10mM	
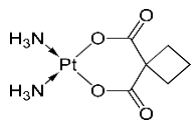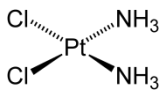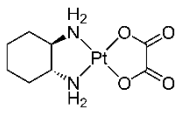
Table 3.1: Preparation of stock solutions for platinum compounds.

3.2.2 - NucleoCounter 3000 Studies

Cisplatin is known to induce apoptosis and G_2/M cell cycle arrest and it is therefore an ideal positive control to compare with the novel compounds tested. The NC3000 studies were completed as per sections 2.6.2, 2.6.3, 2.6.4, 2.6.5 and 2.6.6 with all compounds sourced and prepared as per section 2.2.1. In all cases, cisplatin was used at a concentration of 30µM which is known to induce apoptosis and cell cycle arrest (Berndtsson et al., 2007; Zaffaroni et al., 1998).

3.3 - Results

3.3.1 - Validation of the Clonogenic Assay as an Endpoint for Chemosensitivity Testing

The clonogenic assay was performed as described in section 2.3 where the initial objective was to determine the relationship between the number of cells plated and the number of colonies formed. Initial studies were conducted using the pancreatic cancer cell line Panc 10.05 and significant problems were encountered. These are illustrated in figure 2.1 where large 'super colonies' formed in the centre of each 6 well plate, particularly at initial seeding densities of 1000 cells per well or greater. This result was reproducible and despite several attempts to improve the situation, it was not possible to determine the relationship between cell number and number of colonies formed in this cell line.
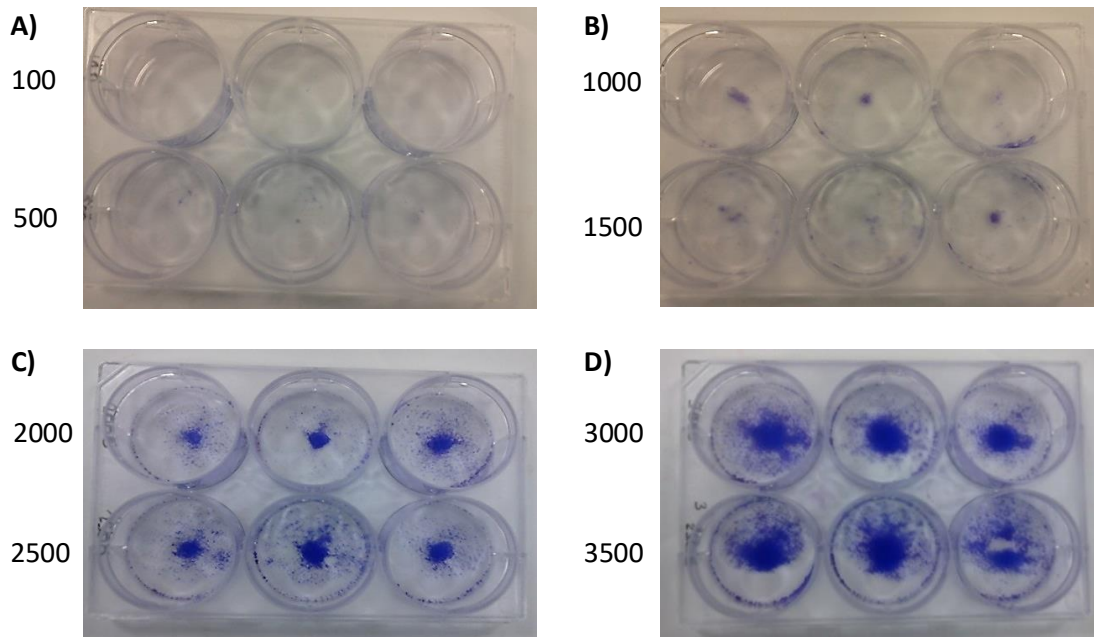
Figure 3.1: Validation of the clonogenic assay using Panc10.05 cells. These experiments were conducted in 6 well plates using a range of initial seeding densities (as indicated on the left-hand side of each plate). Cells were cultured for up to 10 days to allow colonies to form and colonies were stained with methylene blue. The results demonstrate that the majority of colonies formed in the centre of each well making it impossible to assess colony formation accurately.

To reduce the possible clustering of cells at the time of seeding, a number of dispersion and agitation techniques were used. Firstly, when the cell suspension was added to each well whilst seeding, it was added at four points North, East, South and West. Then every 20 minutes for 1 hour the plates were agitated by again moving the plates North, East, South and West as Panc10.05 cells start to adhere after 10-15 minutes with around 40% of the cells being attached after 30 minutes. The results displayed in figure 2.2 demonstrate that better colony dispersion occurred although

clustering in the centre of the well was still apparent. Furthermore, cells also formed colonies at the edge of each well. Even with careful agitation, it was not possible to determine the relationship between cells number and colony formation in the Panc10.05 cell line.
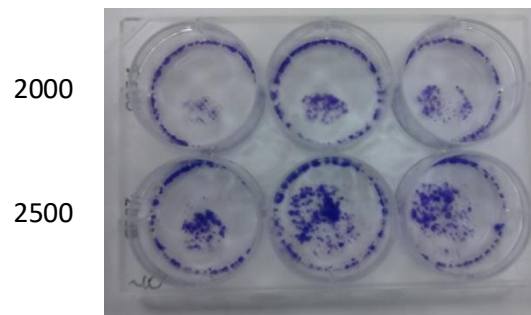
Figure 3.2: Colony formation by Panc10.05 cells following agitation. Ranges of cell numbers were seeded across the 6 well plates and whilst greater colony dispersion occurred, a strong rim of colonies formed at the edge of each well.

To determine whether the results obtained above were unique to Panc10.05 cells, further clonogenic assays were also performed using an additional cell line. MDA-MB - 231 the mammary gland breast adenocarcinoma was used but as illustrated in figure 2.3, the same issues with central clumping and overlapping was observed. Because of these technical issues encountered, the clonogenic assay was not used as the endpoint for chemosensitivity testing in this thesis.
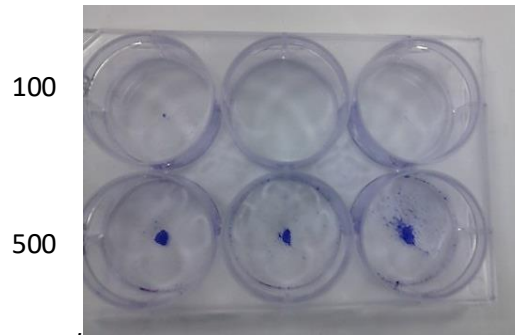
Figure 3.3: Colony formation of MDA-MB-231 cells plated at 100 and 500 cells per well. Central clumping was still apparent regardless of change in cell line.

3.3.2 - Validation of the MTT Assay for use as an Endpoint for Chemosensitivity Testing

Validation assays designed to determine the relationship between cell number and absorbance at 540nm were performed as described in section 2.4.1. The results for MIA-PaCa$_2$ and ARPE-19 cells are presented in figures 2.4 and 2.5 respectively. The results demonstrate that a linear relationship between cell number and absorbance was obtained in both tumour (MIA-PaCa$_2$) and non-cancer (ARPE-19) cells. The MTT assay was therefore considered a valid endpoint for chemosensitivity testing.
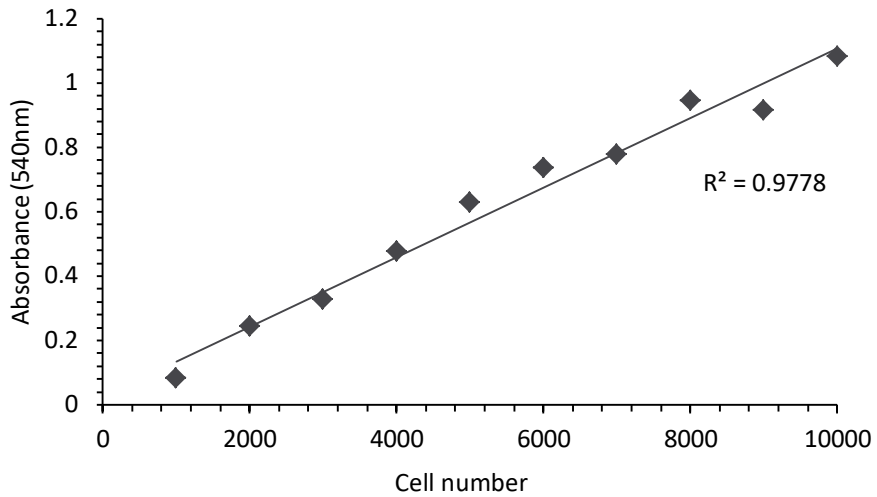
Figure 3.4: Relationship between cell number (MIA-PaCa$_2$) and absorbance generated using the MTT assay. The results are for one experiment only (n=1 with 8 replicates) and R2 represents the regression coefficient obtained following linear regression analysis (the solid line).
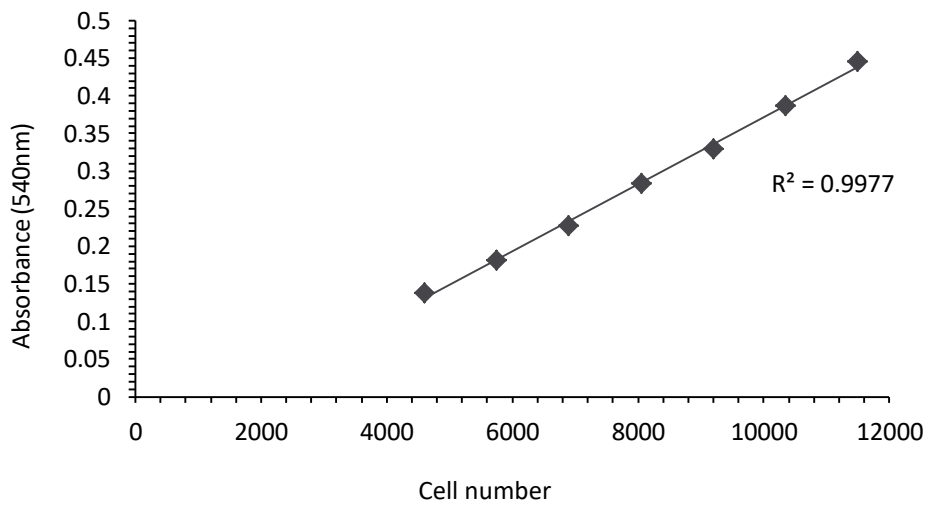
Figure 3.5: Relationship between cell number (ARPE-19) and absorbance generated using the MTT assay. The results are for one experiment only (n=1 with 8 replicates) and R2 represents the regression coefficient obtained following linear regression analysis (the solid line).

3.3.3 - Determination of the Optimum Seeding Density for the MTT Assay

In all assays such as the MTT assay it is essential that the controls (untreated) remain in exponential growth at the end of the 96-hour drug exposure period otherwise erroneous results can be obtained. This is clearly a function of how many cells you add to each well and the duration of the culture period. To establish the initial seeding density, a range of cell numbers were plated into 96 well plates and cultured for 96 hours before conducting the MTT assay. The results are presented in figures 3.6 and 3.7. The results for Panc10.05 cells (figure 3.6) demonstrate that as the initial cell seeding density increases, the absorbance values post incubation increase linearly up to a maximum of 1.08. Initial seeding densities between 1000 and 1500 gave good results in terms of the absorbance generated and viability at the end of the 96-hour exposure period. In contrast, similar studies using the non-cancer PSN-1 cell line demonstrated significantly different results (figure 3.7). In this case, initial cell seeding densities above 1500 cells generated reduced absorbance values suggesting that cultures were entering the 'death' phase of the growth curve after 96-hour incubation. A seeding density of 1000 cells per well was chosen in this case. Similar studies were conducted for all the cell lines employed in this thesis and the results are summarised in table 3.2.
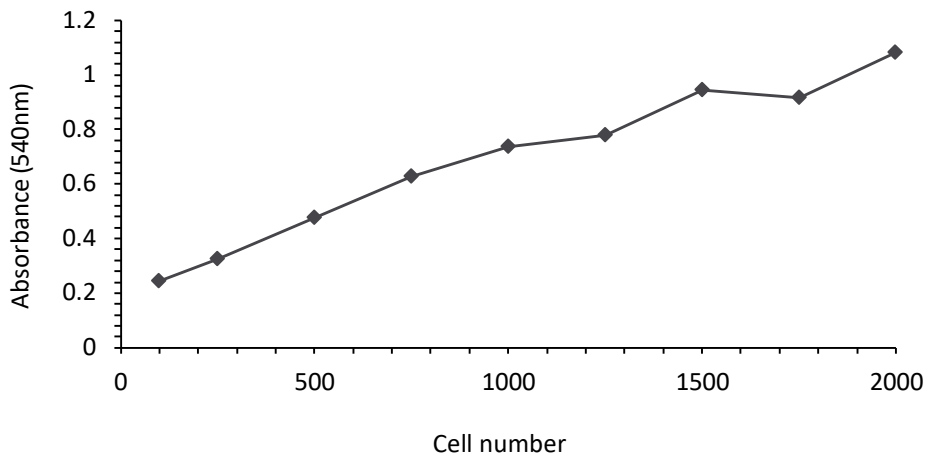
Figure 3.6: Relationship between cell number and absorbance generated using the MTT assay. This experiment was run once (n=1 with 8 replicates) to obtain an optimal seeding density for the Panc10.05 cell line.
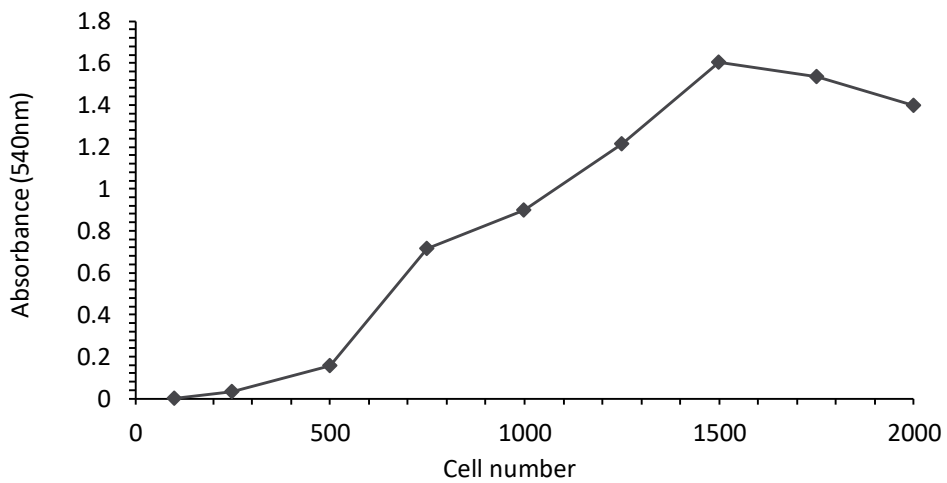
Figure 3.7: Relationship between cell number and absorbance generated using the MTT assay. This experiment was run once(n=1 with 8 replicates) to obtain an optimal seeding density for the PSN-1 cell line.

Cell line	Description	Optimal seeding density
ARPE-19	Retinal pigmented epithelium	2000
W1-38	Normal lung fibroblasts	3000
BE	Colon carcinoma	2000
HCT116 p53$^{+/+}$	P53 up-regulated colonic adenocarcinomas	2000
HCT116 p53$^{-/-}$	P53 knock down colonic adenocarcinomas	2000
HT29	Human colorectal adenocarcinoma	2000
MIA-PaCa$_2$	Pancreatic carcinoma	2000
Panc 10.05	Pancreatic adenocarcinoma	2000
PSN − 1	Epithelial like pancreatic adenocarcinoma	1000

Table 3.2: Summary of optimal seeding densities for the different cell lines used in chemosensitivity testing**.**

3.3.4 - Response of Cancer and Non-Cancer Cell Lines to Cisplatin, Carboplatin and Oxaliplatin

3.3.4.1 - Aerobic Conditions

The response of a panel of cancer and non-cancer cell lines to 96 hours of continuous exposure to cisplatin, carboplatin or oxaliplatin under aerobic conditions is presented in figure 3.8 (dose response for HCT116 cancer cells) with IC$_{50}$ values for all cell lines presented in figure 3.9. In general terms, carboplatin was the least active compound against all cell lines tested with IC$_{50}$ values ranging from 10.45 ± 3.15 to 77.73 ± 10.52µM (Figure 3.9). Cisplatin and oxaliplatin were significantly more active *in vitro* with some cell lines being very sensitive (sub µM IC$_{50}$) to cisplatin (BE and HT-29) and oxaliplatin (HCT116 p53$^{+/+}$).
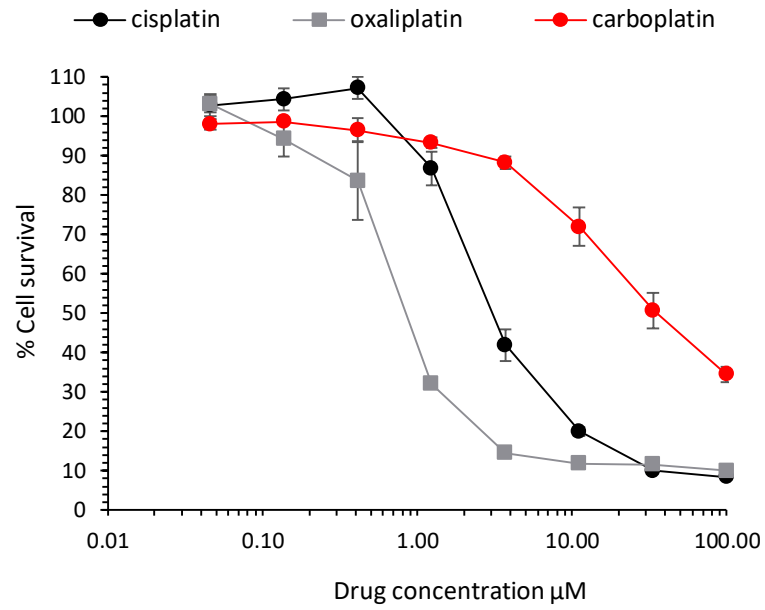
Figure 3.8 Percentage cell survival of HCT116 p53$^{+/+}$ cell line in response to increasing doses of the three

platinate standards cisplatin, carboplatin and oxaliplatin. Data are from three independent MTT assays

n=3 (each individual experiment replicated twice) and are represented by the mean ± SE. The

percentage cell survival values are expressed as a percentage of viable cells compared with untreated

controls.
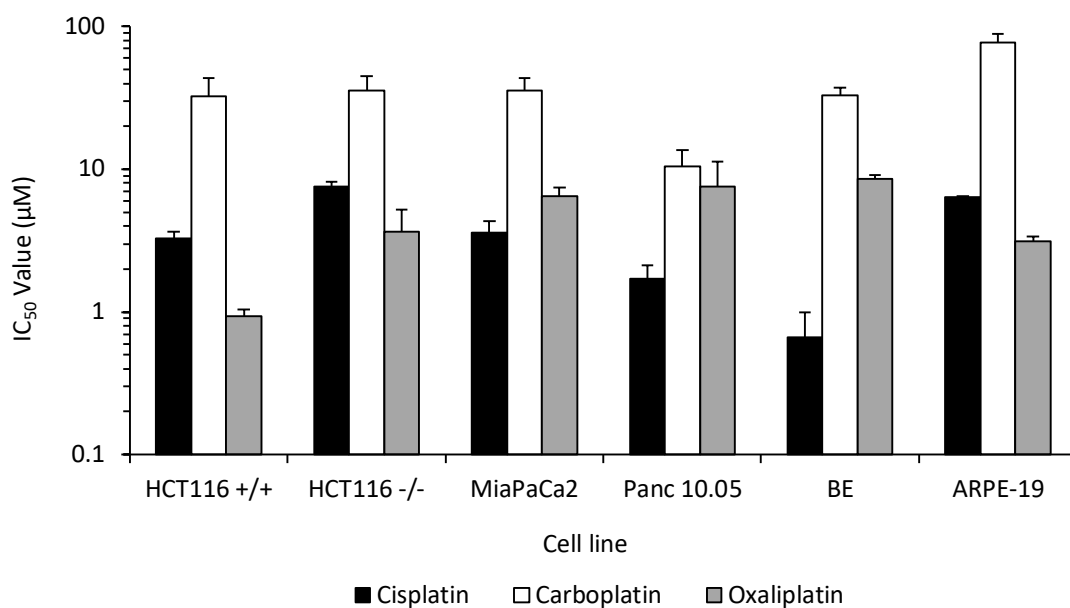
	Average IC$_{50}$ ± standard deviation (µM)							
Compound	**BE**	**MIA-PaCa$_2$**	**HCT116 p53$^{+/+}$**	**HCT116 p53$^{-/-}$**	**PANC10.05**	**HT-29**	**ARPE-19**	**WI-38**
Cisplatin	0.66 ±0.33	3.62 ±0.74	3.26 ±0.38	7.52 ±0.65	1.71 ±0.41	0.25 ±0.11	6.41 ± 0.95	2.18 ±0.74
Carboplatin	32.72 ±4.64	35.59 ±7.91	32.37 ±11.14	35.7 ±9.06	10.45 ±3.15	-	77.73 ±10.52	-
Oxaliplatin	8.56 ±0.48	6.44 ±1.05	0.93 ±0.11	6.44 ±1.05	7.54 ±3.85	-	3.12 ±0.28	-

Figure 3.9: Response of a panel of cell lines to oxaliplatin, cisplatin and carboplatin. The results presented are the mean IC$_{50}$ values ± SD for three independent experiments n=3 (each individual experiment replicated twice).

3.3.4.2 - Selectivity Indices *In Vitro*

The relative activity of cisplatin, oxaliplatin and carboplatin against tumour and non-cancer cells (ARPE-19) is presented and illustrated graphically in figure 3.10. The selectivity index (SI) is defined as the IC_{50} for non-cancer cells divided by the IC_{50} for cancer cells with values greater than 1 indicating selectivity for cancer as opposed to non-cancer cells. In the case of ARPE19 cells, carboplatin was selectively toxic to all cancer cells with SI values ranging from 2.18 to 7.44 resulting in statistically significant (p-value = less than 0.05) reductions in potency toward the none cancerous cell line investigated. Similarly, with cisplatin, SI values ranged from 1.77 to 9.71 in all cancer cells except for HCT116 p53$^{-/-}$ cells where an SI of 0.85 was obtained (*p*-value 0.32). Oxaliplatin on the other hand was generally less toxic towards the cancer cells resulting in statistically significant (p-value = less than 0.05) decreases in potency towards 3 out of the 5 cancer cell lines investigated.
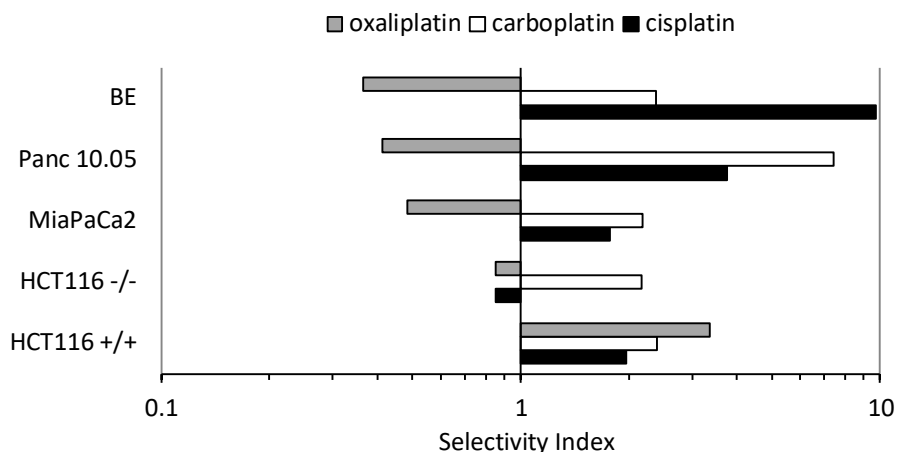
Compound	BE		MIA-PaCa$_2$		HCT116 p53$^{+/+}$		HCT116 p53$^{-/-}$		PANC10.05	
	SI	*p*-value	SI	*p*-value	SI	*p*-value	SI	*p*-value	SI	*p*-value
Cisplatin	9.71	0.0043	1.77	0.10	1.97	0.033	0.85	0.32	3.75	0.025
Carboplatin	2.38	0.029	2.18	0.031	2.40	0.023	2.18	0.014	7.44	0.0089
Oxaliplatin	0.36	0.0064	0.48	0.020	3.35	0.010	0.85	0.65	0.41	0.047

Figure 3.10: Selectivity index of three platinum compounds on a range of cancerous cell lines. The selectivity index is defined as the ratio of the mean IC$_{50}$ in non-cancerous cells to the mean IC$_{50}$ in cancerous cells. As mean values are used to calculate the SI, no error bars are present in this data set. Statistical analysis was performed using a student's t-test where values <0.05 indicates a statistically significant difference between IC$_{50}$ values in cancerous and none cancerous cell lines.

3.3.4.3 - Response of HCT116 Cells to Cisplatin, Carboplatin and Oxaliplatin: P53 Dependency

The HCT116 p53$^{+/+}$ and HCT116 p53$^{-/-}$ cells are isogenic colorectal carcinoma cells that differ only with regards to their p53 status. The relationship between p53 status and the response of cells to platinum based anti-cancer drugs is presented in figure 3.11. Whilst no significant difference exists in the response of HCT116 p53$^{+/+}$ and HCT116 p53$^{-/-}$ cells to carboplatin (p=0.2461) and oxaliplatin (p=0.0862) the p53 null cell line HCT116 p53$^{-/-}$ was significantly more resistant to cisplatin (p = 0.0035). In the search for novel anti-cancer drugs with activity against p53 null tumours, this baseline information will also be used to characterise the activity of novel compounds tested in this thesis.
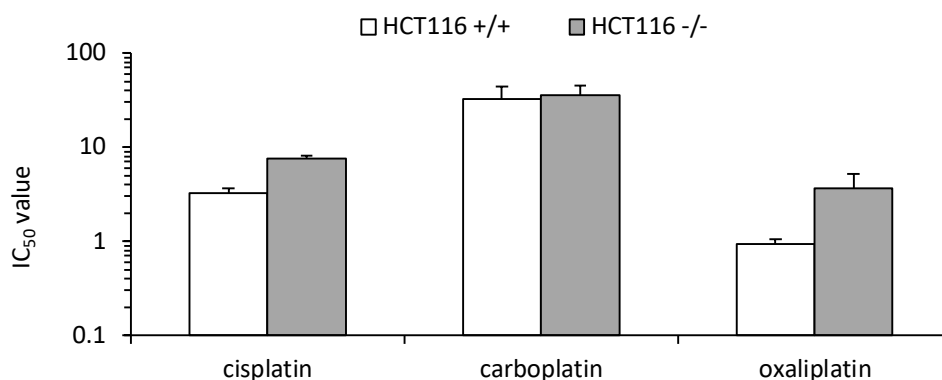
	Average IC$_{50}$ ± standard deviation (μM)		
	Cisplatin	**Carboplatin**	**Oxaliplatin**
HCT116 p53$^{+/+}$	3.26±0.38	32.37±11.14	0.93±0.11
HCT116 p53$^{-/-}$	7.52±0.65	35.7±9.06	6.44±1.05
***p*-value**	0.0035	0.2461	0.0862

Figure 3.11: Comparison of IC$_{50}$ values ± SD of platinum compounds towards HCT116 p53$^{+/+}$ and p53$^{-/-}$ isogenic clones. Data generated by triplicated MTT assays completed on consecutive days n=3 (each individual experiment replicated twice). Statistical analysis was performed using a student's t-test where values <0.05 indicates a statistically significant difference between IC$_{50}$ values HCT116 p53$^{+/+}$ and HCT116 p53$^{-/-}$ cell lines.

3.3.4.4 - Response of Cancer Cells Following Continuous Exposure to Cisplatin, Carboplatin and Oxaliplatin Under Hypoxic Conditions

A comparison of the dose response of HCT116 p53$^{+/+}$ and MIA-PaCa$_2$ cells to platinum based anti-cancer drugs under aerobic and hypoxic conditions (0.1% O_2) is presented in figures 3.12 to 3.14 (IC$_{50}$ values summarised in table 3.3). The results demonstrate that hypoxia (0.1% O_2) significantly reduces the activity of cisplatin, carboplatin and oxaliplatin (all supported by *p*-values <0.05). Oxaliplatin was the most active of the platinates against the MiaPac$_2$ pancreatic cancer cell line under hypoxia IC$_{50}$ 87.72 ± 7.29µM), As with aerobic investigations carboplatin appeared the least active under hypoxic conditions with an IC$_{50}$ value unattainable in both cell lines with drug concentrations up to 100µM.

3.3.4.4.1 - Cisplatin
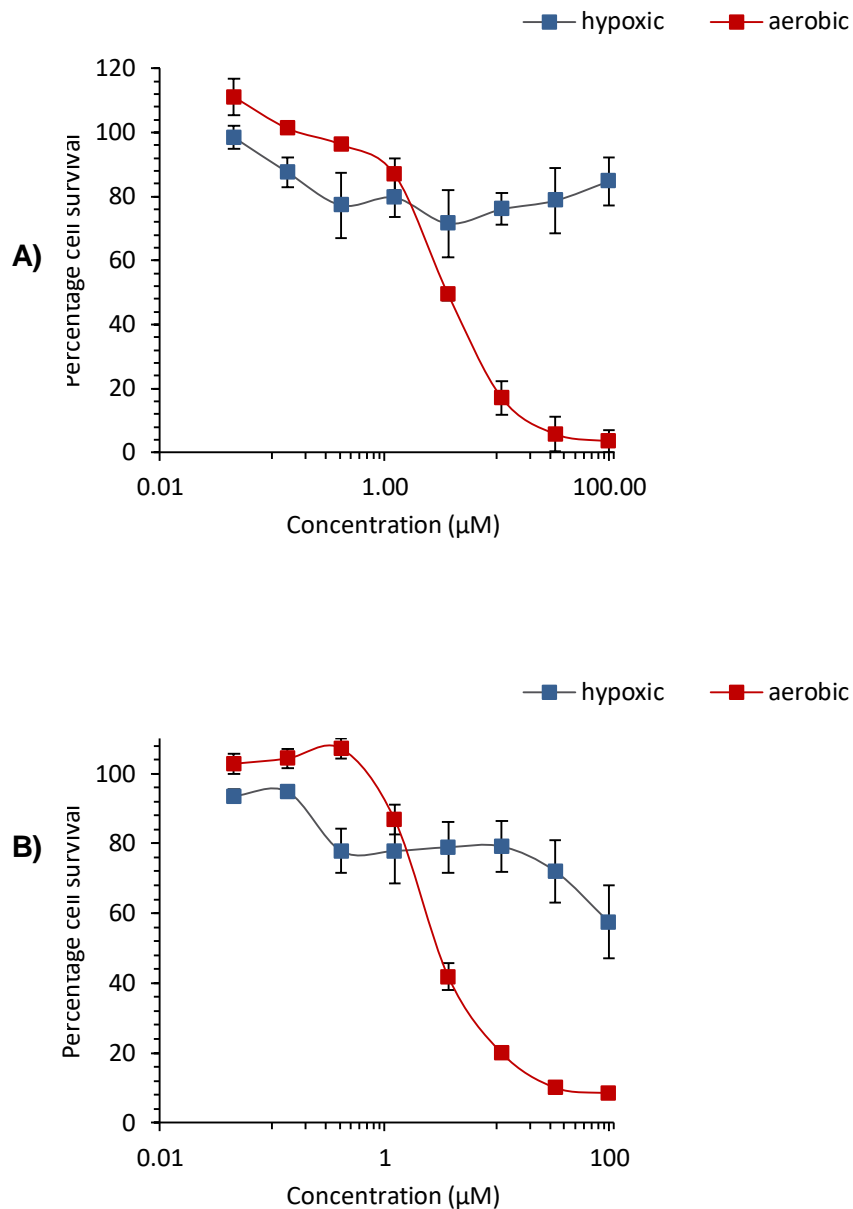
Figure 3.12: Dose response curves of cisplatin towards A) MIA-PaCa$_2$ and B) HCT116 p53$^{+/+}$ cell lines in both hypoxic and aerobic conditions. Data from three independent MTT assays n=3 (each individual experiment replicated twice) and are represented by the mean ± SE. The percentage cell survival values are expressed as a percentage of viable cells compared with untreated controls.

3.3.4.4.2 - Carboplatin
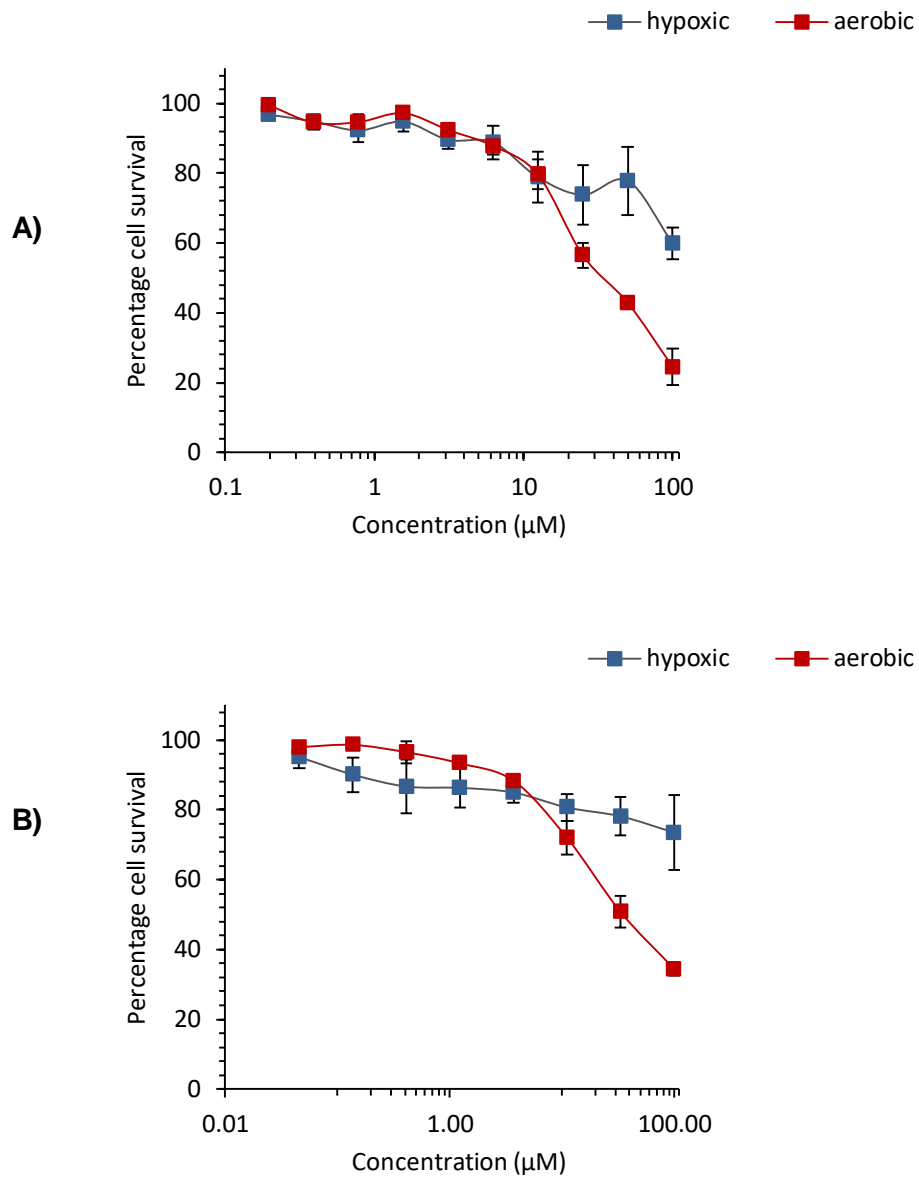
Figure 3.13: Dose response curves of carboplatin towards A) MIA-PaCa$_2$ and B) HCT116 p53$^{+/+}$ cell lines in both hypoxic and aerobic conditions. Data from three independent MTT assays n=3 (each individual experiment replicated twice) and are represented by the mean ± SE. The percentage cell survival values are expressed as a percentage of viable cells compared with untreated controls.

3.3.4.4.3 - Oxaliplatin

A)

B)
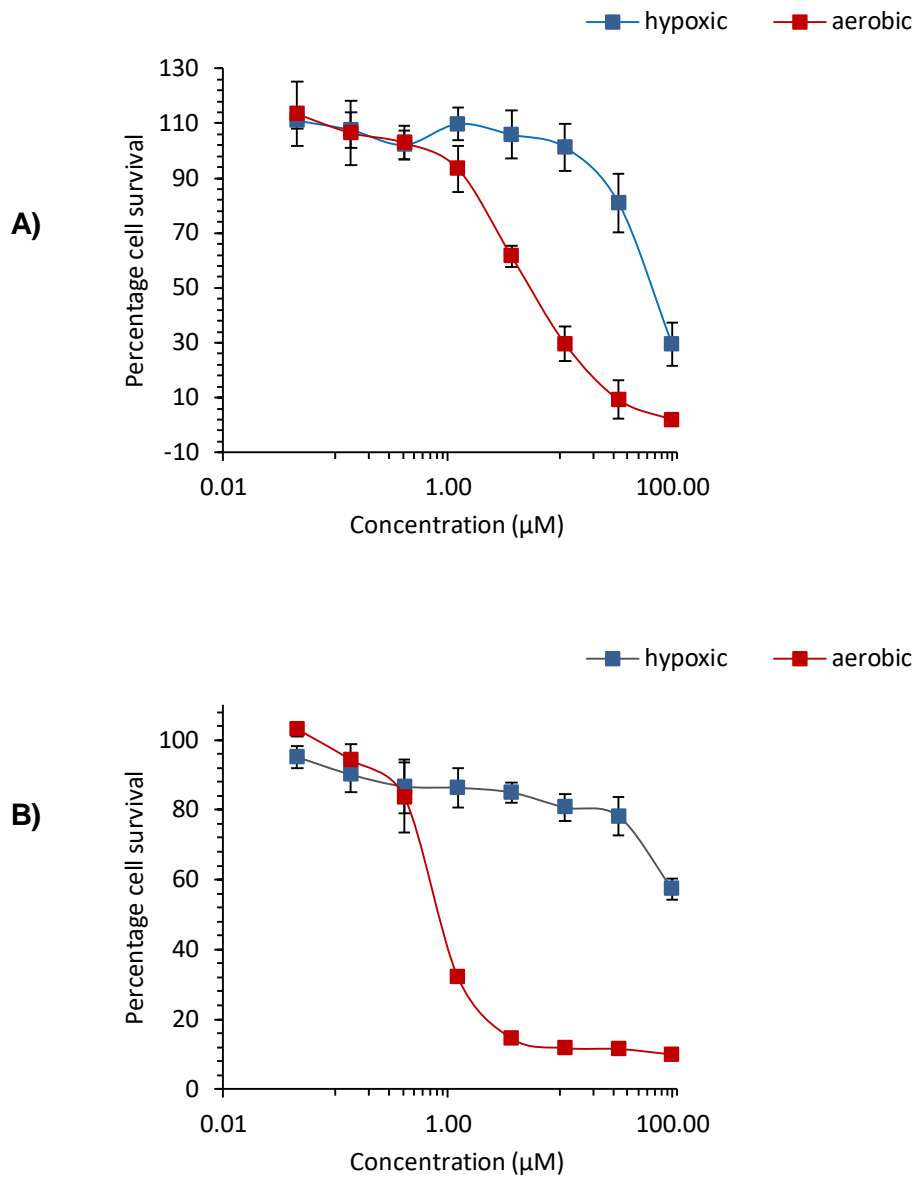
Figure 3.14: Dose response curves of oxaliplatin towards A) MIA-PaCa$_2$ and B) HCT116 p53$^{+/+}$ cell lines in both hypoxic and aerobic conditions. Data from three independent MTT assays n=3 (each individual experiment replicated twice) and are represented by the mean ± SE. The percentage cell survival values are expressed as a percentage of viable cells compared with untreated controls.

Average IC$_{50}$ ± standard deviation (μM)								
	Cisplatin			**Carboplatin**			**Oxaliplatin**		
	Aerobic	**Hypoxic**	**_p_-value**	**Aerobic**	**Hypoxic**	**_p_-value**	**Aerobic**	**Hypoxic**	**_p_-value**
HCT116 p53$^{+/+}$	3.26±0.38	95.49±3.92	0.00071	32.37±11.14	>100	0.0089	0.93±0.11	>100	0.00000041
MIA-PaCa$_2$	3.62±0.74	>100	0.00002	35.59±7.91	>100	0.0050	6.44±1.05	87.72±7.29	0.0021

Table 3.3: Summary of IC$_{50}$ values of three platinum compounds towards HCT116 p53$^{+/+}$ and MIA-PaCa$_2$ cell lines under hypoxic and aerobic conditions. Data from three independent MTT assays n=3 (each individual experiment replicated twice) and are represented by the mean ± SD. Statistical analysis was performed using a student's t-test where values <0.05 indicates a statistically significant difference between IC$_{50}$ values in hypoxic and aerobic conditions in two cancerous cell lines.

3.3.4.5 - Response of HCT116 p53$^{+/+}$ and MIA PaCa$_2$ Cells to Platinates Under Pseudo-Hypoxic Conditions

The response of HCT116 p53$^{+/+}$ and MIA-PaCa$_2$ cells to platinum based anti-cancer drugs under aerobic and pseudo-hypoxic conditions is presented in figures 3.15 to 3.17 and summarised in table 3.4. The results demonstrate that under pseudo-hypoxic conditions, all cells are more resistant to platinum-based drugs compared to aerobic conditions with cisplatin and carboplatin displaying significantly reduced potency (_p_-values <0.05). The magnitude of the change in sensitivity varies but is typically a 2 to 3-fold increase in resistance.

3.3.4.5.1 - Cisplatin
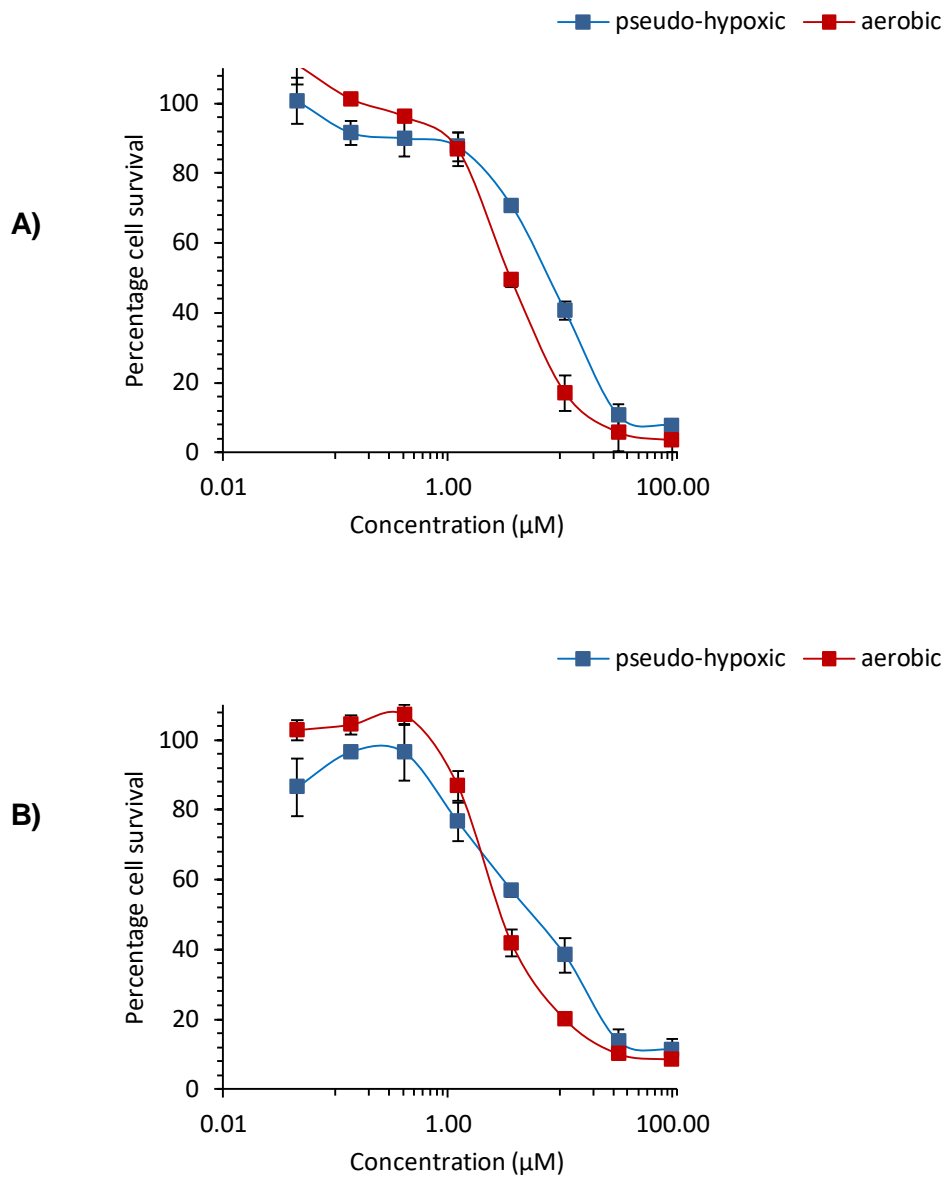
Figure 3.15: Dose response curves of cisplatin towards A) MIA-PaCa$_2$ and B) HCT116 p53$^{+/+}$ cell lines in both pseudo-hypoxic and aerobic conditions. Data from three independent MTT assays n=3 (each individual experiment replicated twice) and are represented by the mean ± SE. The percentage cell survival values are expressed as a percentage of viable cells compared with untreated controls.

3.3.4.5.2 - Carboplatin
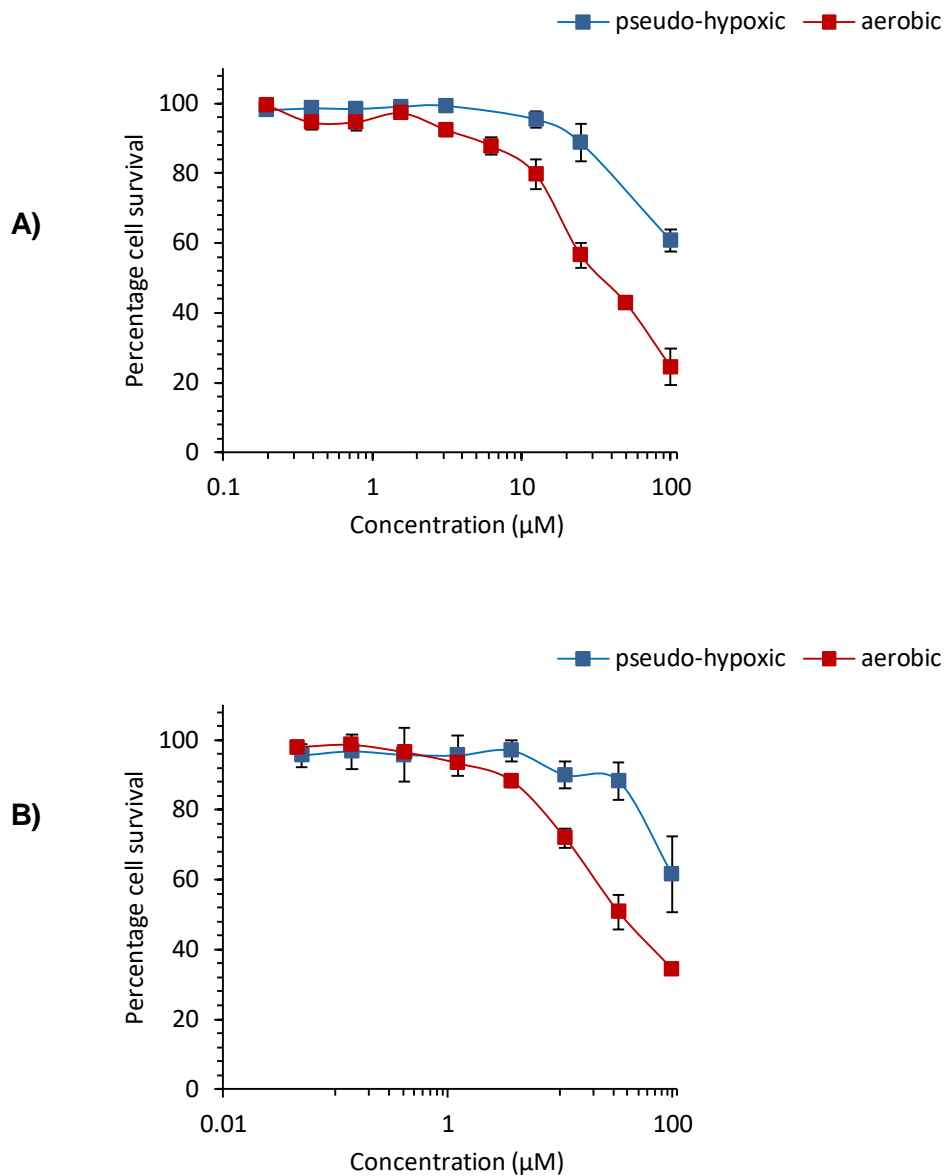
Figure 3.16: Dose response curves of carboplatin towards A) MIA-PaCa$_2$ and B) HCT116+/+ cell lines in both pseudo-hypoxic and aerobic conditions. Data from three independent MTT assays n=3 (each individual experiment replicated twice) and are represented by the mean ± SE. The percentage cell survival values are expressed as a percentage of viable cells compared with untreated controls.

3.3.4.5.3 - Oxaliplatin
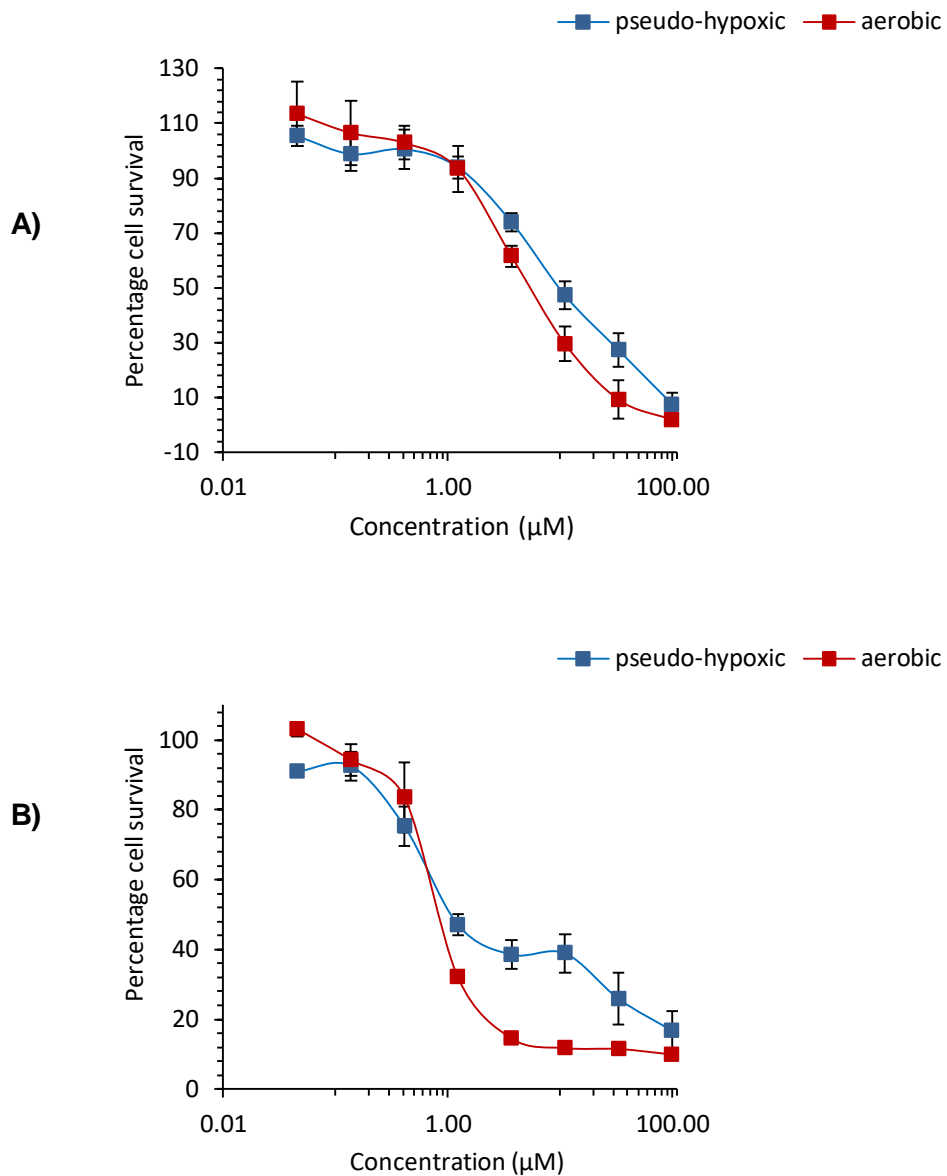
Figure 3.17: Dose response curves of oxaliplatin towards A) MIA-PaCa$_2$ and B) HCT116 p53$^{+/+}$ cell lines in both pseudo-hypoxic and aerobic conditions. Data from three independent MTT assays n=3 (each individual experiment replicated twice) and are represented by the mean ± SE. The percentage cell survival values are expressed as a percentage of viable cells compared with untreated controls.

	Average IC$_{50}$ ± standard deviation (µM)								
	Cisplatin			Carboplatin			Oxaliplatin		
	Aerobic	Pseudo-Hypoxic	*p*-value	Aerobic	Pseudo-Hypoxic	*p*-value	Aerobic	Pseudo-Hypoxic	*p*-value
HCT116 p53$^{+/+}$	3.26±0.38	6.83±2.12	0.095	32.37± 11.14	>100	0.0089	0.93±0.11	1.53±0.52	0.14
MIA-PaCa$_2$	3.62±0.74	8.78±0.89	0.0017	35.59± 7.91	>100	0.0050	6.44±1.05	12.09±4.84	0.24

Table 3.4: Summary of IC$_{50}$ values of three platinum compounds towards both colorectal and pancreatic cancerous cell lines HCT116 p53$^{+/+}$ and MIA-PaCa$_2$ in pseudo-hypoxic and aerobic conditions. Data from three independent MTT assays n=3 (each individual experiment replicated twice) and are represented by the mean ± SD. Statistical analysis was performed using a student's t-test where values <0.05 indicates a statistically significant difference between IC$_{50}$ values in pseudo-hypoxic and aerobic conditions in two cancerous cell lines.

3.3.5 - Analysis of Cisplatin Induced Apoptosis and Cell Cycle Arrest

To create a baseline set of parameters by which the activity of novel test compounds can be compared, the ability of cisplatin to induce cell cycle arrest and apoptosis was determined. The assays were conducted on both HCT116$^{+/+}$ and ARPE-19 cell lines to establish any differences between the response of cancerous and non-cancerous cell lines, which will be of particular interest with our novel "hit" compounds. The time points at which the assays were completed were 2, 8, 24, 48 and 72 hours, with an untreated control sample for each time point.

3.3.5.1 - Viability Assay

The results of viability assays completed on both untreated and treated (cisplatin 30µM) samples over a 72-hour period are summarised in tables 3.5 and 3.6 and

displayed in figures 24 and 25. In the case of HCT 116 p53$^{+/+}$ cells, whilst control cultures grew consistently over the 96 hour period, cultures treated with cisplatin remained at a constant cell number. In contrast, a significant decrease in viable cell number was observed in ARPE-19 cells treated with cisplatin.

	2 hours		8 hours		24 hours	
	Control	Cisplatin	Control	Cisplatin	Control	Cisplatin
Viability (%)	96.5	96.3	96.5	97.1	95.4	82.4
Cell count	1.22×10^6	1.26×10^6	1.22×10^6	1.23×10^6	3.02×10^6	1.52×10^6

	48 hours		72 hours	
	Control	Cisplatin	Control	Cisplatin
Viability (%)	93.9	85.1	95.6	91.6
Cell count	5.35×10^6	1.40×10^6	5.57×10^6	1.26×10^6
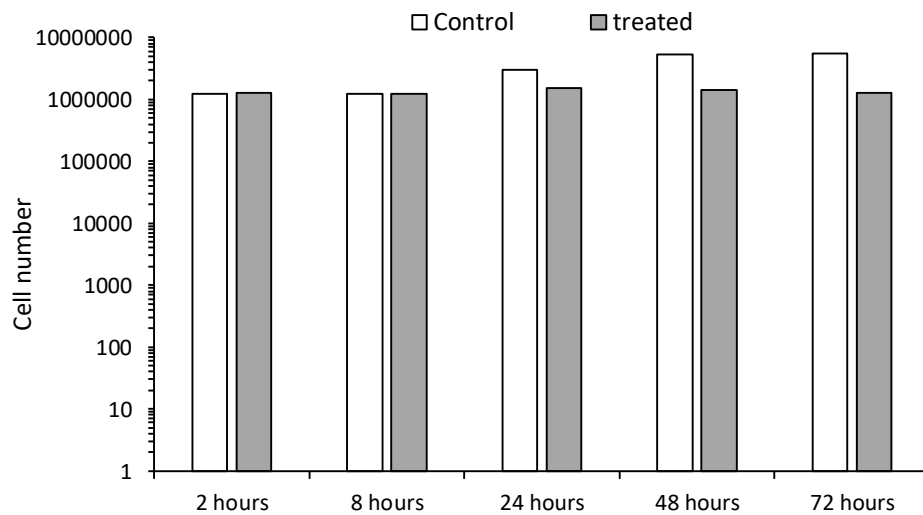
Figure 3.18: Viability assay data of both cisplatin (30µM) and untreated controls on human colorectal adenocarcinoma HCT116 p53$^{+/+}$ cells at various time points over a 72-hour exposure. The viability is presented as a percentage and an accurate cell count calculated based on the entire population which is stained with Acridine Orange and non-viable cells stained by 4',6-diamidino-2-phenylindole (DAPI) (n=1).
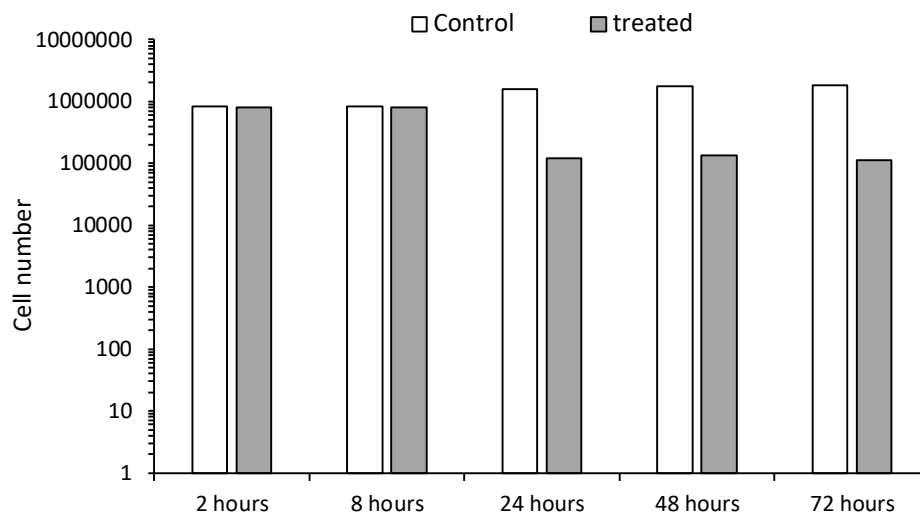
	2 hours		8 hours		24 hours	
	Control	Cisplatin	Control	Cisplatin	Control	Cisplatin
Viability (%)	96.9	92.9	92.4	92.9	93.7	81.8
Cell count	8.41×10^5	8.08×10^5	8.31×10^5	8.08×10^5	1.57×10^6	1.19×10^5

	48 hours		72 hours	
	Control	Cisplatin	Control	Cisplatin
Viability (%)	96.1	64.3	96.9	66.0
Cell count	1.74×10^6	1.35×10^5	1.82×10^6	1.13×10^5

Figure 3.19: Viability assay data of both cisplatin (30µM) and untreated controls on non-cancerous retinal epithelial ARPE-19 cells at various time points over a 72-hour exposure. The viability is presented as a percentage and an accurate cell count calculated based on the entire population which is stained with Acridine Orange and non-viable cells stained by 4',6-diamidino-2-phenylindole (DAPI) (n=1).

3.3.5.2 - Annexin V Assay

The annexin V assay as illustrated in figure 3.20 detects both early and late phase apoptosis/ or necrosis with an increase in annexin V staining being representative of early apoptosis and an increase in propidium iodide staining being representative of late apoptosis. For both the cancerous HCT116$^{+/+}$ and non-cancerous ARPE-19 cell lines there is a definitive increase in induction of apoptosis with increasing exposure time to cisplatin (tables 3.5 to 3.6). The induction of apoptosis is more profound in the non-cancerous ARPE-19 cells (observed after 2 hours exposure as opposed to 24 hours in HCT116$^{+/+}$).

Untreated control

A) **B)** **C)**
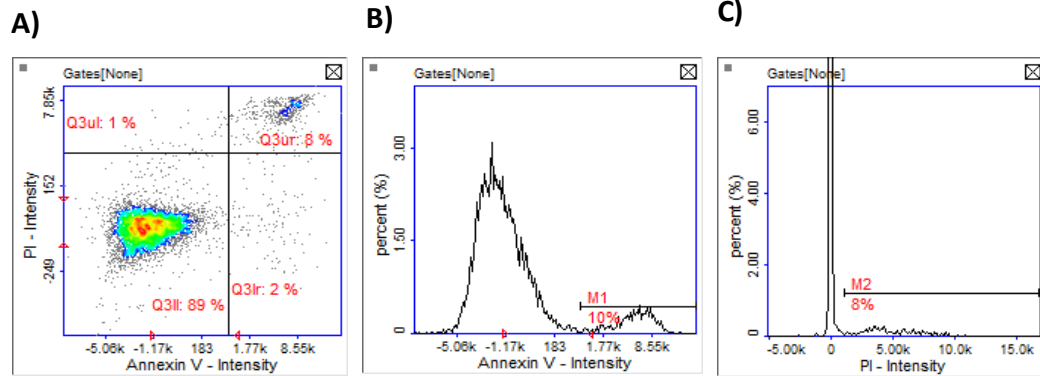
Cisplatin treated
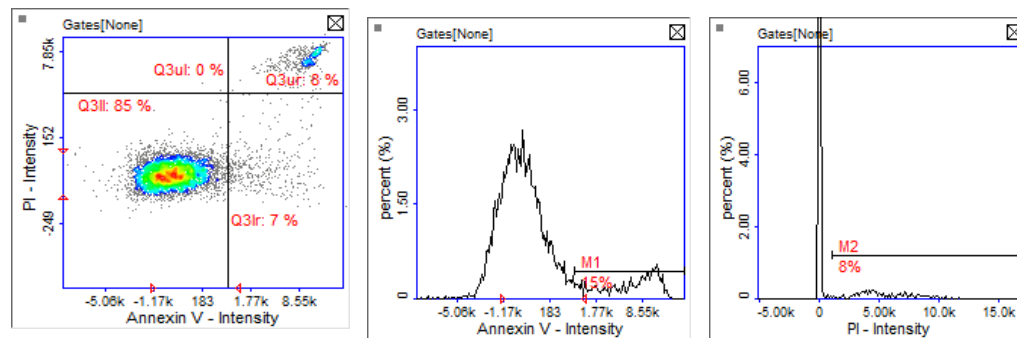
Figure 3.20: Representative example of data generated by the Annexin V assay. Annexin V assay after 2-hour cisplatin (30µM) exposure on colorectal adenocarcinoma HCT116$^{+/+}$ cells. The quadrant on scatter plot A is determined by firstly gating the entire population expressing Propidium Iodide (PI) in histogram C this sets the parameter for the upper quadrants (Q3ur) late apoptotic –necrotic and none viable (Q3ul) portions of the cell population. The maximum intensity peak (histogram B - annexin V intensity) is then gated, this determines the apoptotic portion of the cell population (right side of the quadrant late Q3ur and early Q3lr). Any cells therefore gated in the lower left quadrant within the plot (Hoechst 33342 positive, PI negative and little to no annexin V expression) are healthy (n=1).

	2 hours		8 hours		24 hours	
	Control	**Cisplatin**	**Control**	**Cisplatin**	**Control**	**Cisplatin**
Healthy	89	85	83	75	80	62
Apoptotic	2	7	4	5	6	16
Late apoptotic/ necrotic	8	8	11	17	13	19
None viable	1	0	2	3	1	3

	48 hours		72 hours	
	Control	**Cisplatin**	**Control**	**Cisplatin**
Healthy	88	64	85	55
Apoptotic	3	11	4	36
Late apoptotic/ necrotic	7	22	10	9
None viable	4	3	1	0

Table 3.5: Summary of annexin V data on colorectal adenocarcinoma HCT116 p53$^{+/+}$ cells after exposure to cisplatin (30µM) at varying time points. Data displayed as percentage values of total cell population (n=1).

	2 hours		8 hours		24 hours	
	Control	Cisplatin	Control	Cisplatin	Control	Cisplatin
Healthy	75	46	75	43	82	49
Apoptotic	14	43	10	32	14	27
Late apoptotic/ necrotic	11	11	15	19	10	23
None viable	0	0	0	6	1	1

	48 hours		72 hours	
	Control	Cisplatin	Control	Cisplatin
Healthy	95	15	84	10
Apoptotic	1	7	5	24
Late apoptotic/ necrotic	3	67	10	58
None viable	1	11	1	8

Table 3.6: Summary of annexin V data on non-cancerous retinal epithelial cells after exposure to cisplatin (30µM) at varying time points. Data displayed as percentage values of total cell population (n=1).
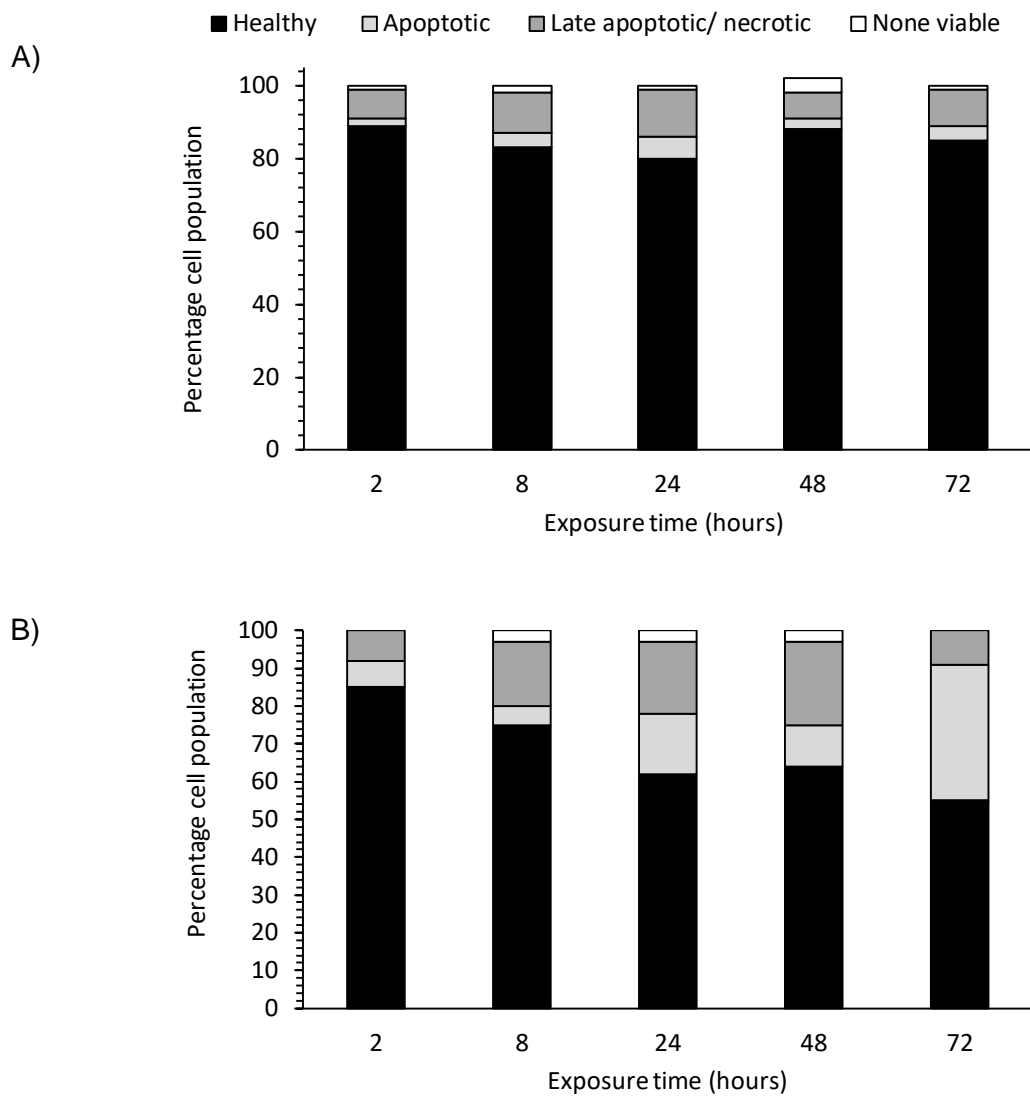
Figure 3.21: Summary of annexin V data on A) untreated and B) cisplatin (30μM) treated colorectal

adenocarcinoma HCT116+/+ cells over 72 hours (n=1).
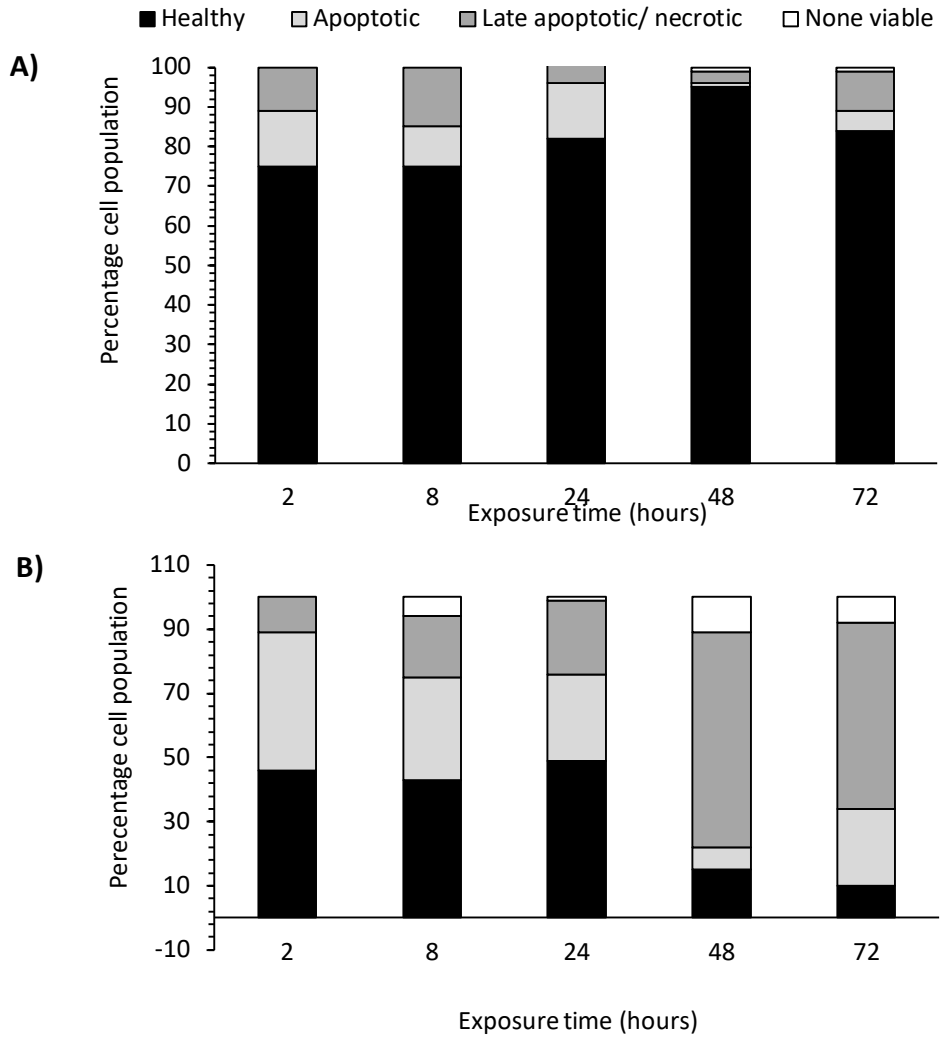
Figure 3.22: Summary of annexin V data on A) untreated and B) cisplatin (30μM) treated non-cancerous

retinal epithelial ARPE-19 cells over 72 hours (n=1).

3.3.5.3 - Mitochondrial Potential Assay

The analysis of the mitochondrial potential assay on both treated (cisplatin 30μM) and untreated samples over a 72-hour period is explained in figure 3.23 with the processed data summarised in tables 3.7 and 3.8. The processed data is also further illustrated in figures 3.24 and 3.25 with both cancerous and non-cancerous cells demonstrating increased induction of apoptosis with increased exposure time. Increased induction of apoptosis can be observed after just 2 hours exposure with the ARPE-19 cells and after 8 hours with the HCT116$^{+/+}$ cells.

Untreated control
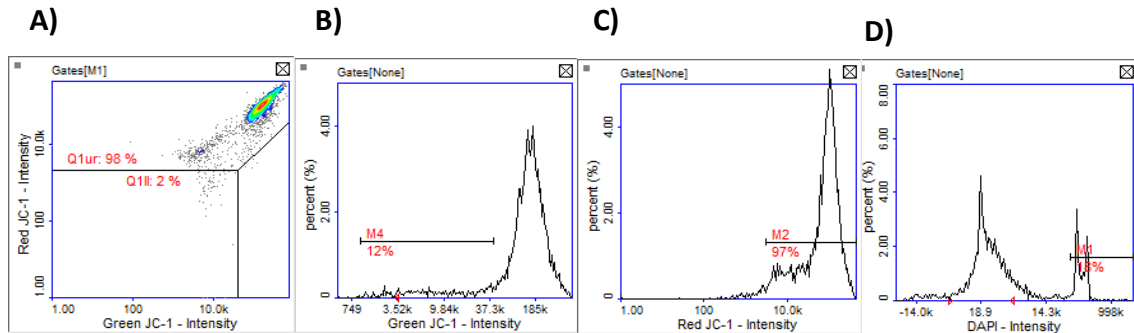
Cisplatin treated
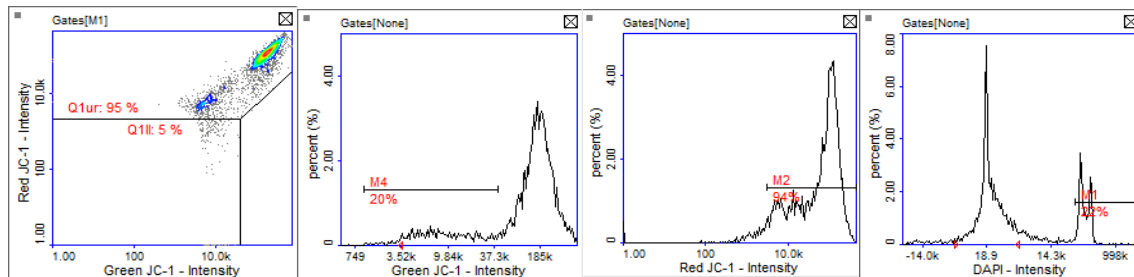
Figure 3.23: Mitochondrial potential assay after 2-hour cisplatin (30µM) exposure on colorectal adenocarcinoma HCT116$^{+/+}$ cells. The quadrant on scatter plot A is determined by firstly gating the high intensity DAPI peak (histogram D) and excluding them from scatter plot A as these are necrotic cells. The high intensity red JC-1 peak (histogram C) and the entire population excluding the high intensity JC-1 green peak (histogram B) are used to define the healthy population and thus plot the boundaries on scatter plot A, populations above the boundary are deemed healthy and anything below are apoptotic, the high intensity DAPI stained population is the necrotic portion.

	2 hours		8 hours		24 hours	
	Control	Cisplatin	Control	Cisplatin	Control	Cisplatin
Healthy	80	74	78	63	80	51
Apoptotic	2	4	6	19	5	38
Necrotic	18	22	16	18	15	11

	48 hours		72 hours	
	Control	Cisplatin	Control	Cisplatin
Healthy	74	37	68	33
Apoptotic	13	56	23	62
Necrotic	13	7	9	5

Table 3.7: Summary of mitochondrial potential data on colorectal adenocarcinoma HCT116 p53$^{+/+}$ cells after exposure to cisplatin (30μM) at varying time points. Data displayed as percentage values of total cell population (n=1).

	2 hours		8 hours		24 hours	
	Control	Cisplatin	Control	Cisplatin	Control	Cisplatin
Healthy	82	65	74	66	82	65
Apoptotic	11	30	14	28	8	33
Necrotic	7	5	12	6	10	2

	48 hours		72 hours	
	Control	Cisplatin	Control	Cisplatin
Healthy	87	29	79	48
Apoptotic	8	67	12	42
Necrotic	5	4	9	9

Table 3.8: Summary of mitochondrial potential data on non-cancerous retinal epithelial cells after exposure to cisplatin (30μM) at varying time points. Data displayed as percentage values of total cell population (n=1).
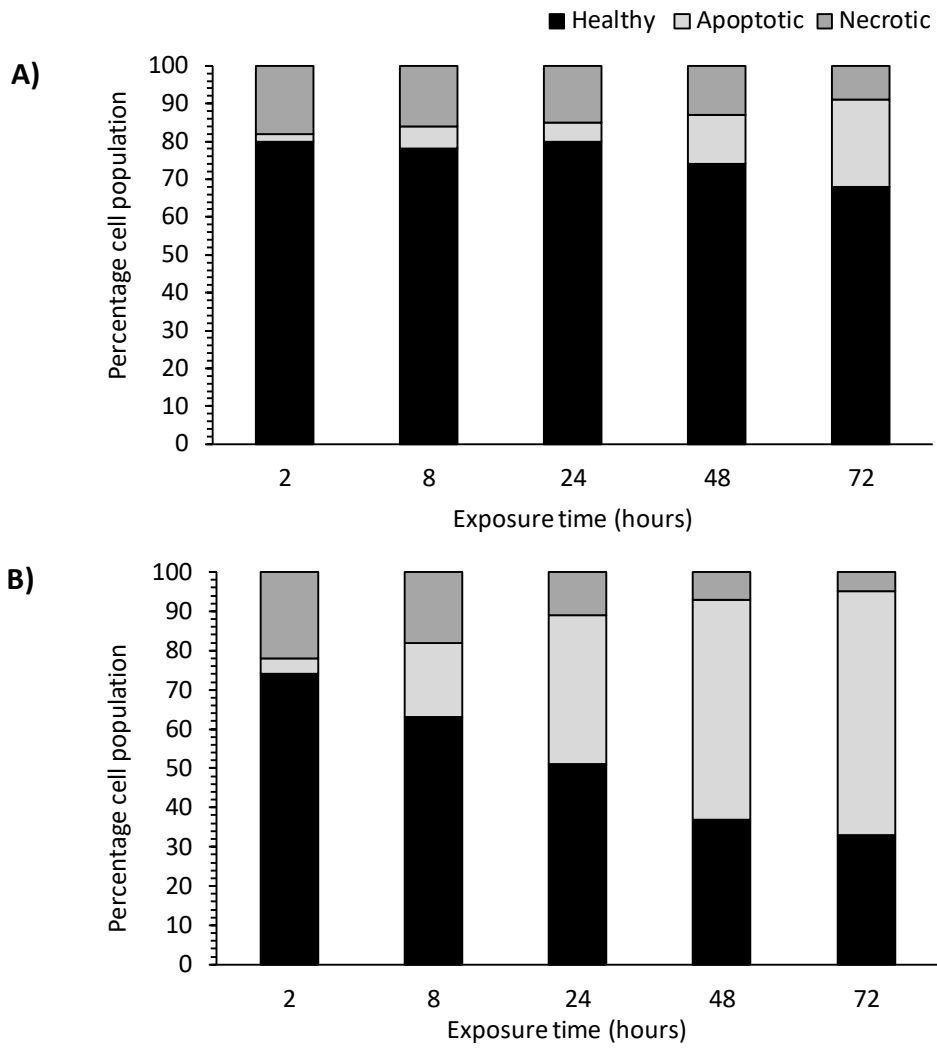
Figure 3.24: Summary of mitochondrial potential assay on A) untreated and B) cisplatin (30µM) treated colorectal adenocarcinoma HCT116 p53$^{+/+}$ cells over 72 hours (n=1).
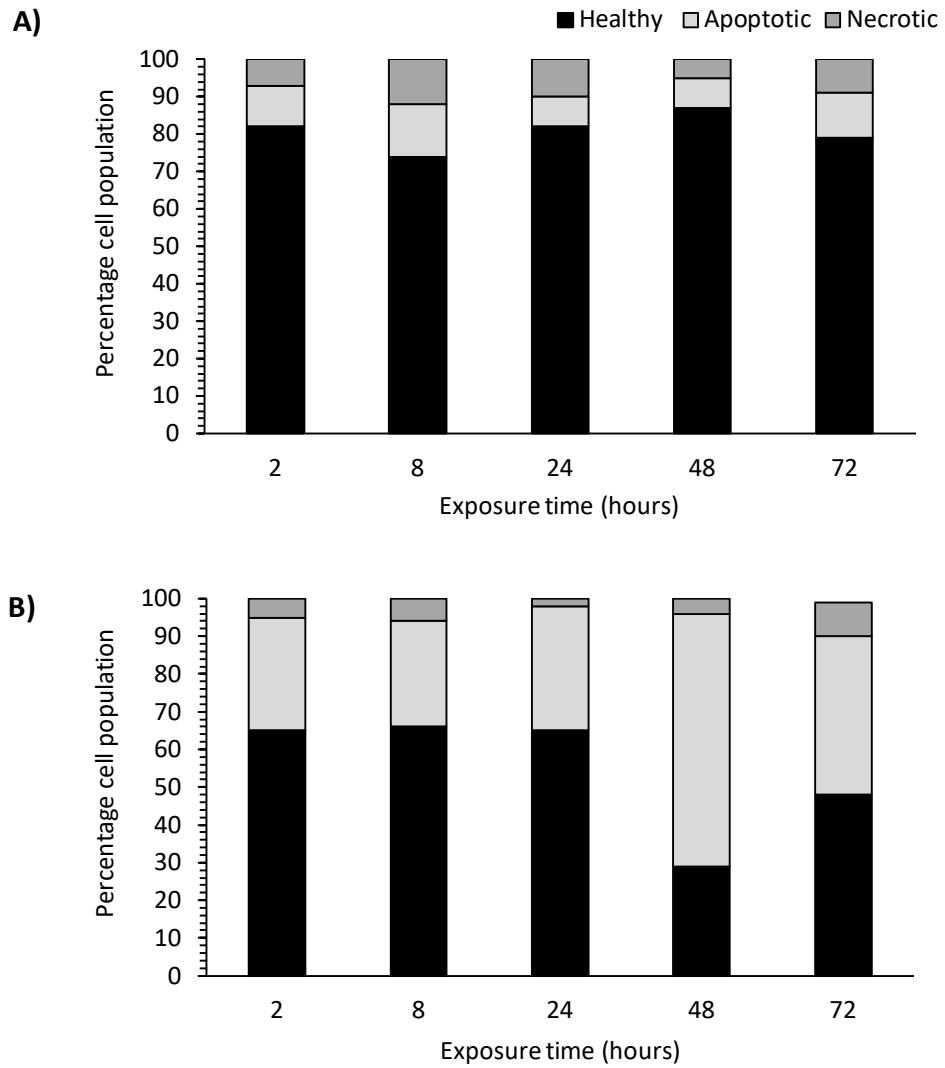
Figure 3.25: Summary of mitochondrial potential assay on A) untreated and B) cisplatin (30µM) treated non-cancerous retinal epithelial ARPE-19 cells over 72 hours (n=1).

3.3.5.4 - Cell Cycle Assay

Figure 3.26 demonstrates the process by which the cell cycle data is processed with tables 3.9 and 3.10 displaying the processed data of untreated and treated (cisplatin 30µM) samples for both the cancerous and non-cancerous cell lines over a 72-hour period. In both the cancerous and non-cancerous cell lines, the untreated samples display increased cell populations within the G0/G1 phase with increased exposure time. The treated samples begin to display notable cell cycle disruption after 24 hours exposure in HCT116 P53$^{+/+}$ cells with a significant increase of cells in the G2/M phase. In ARPE-19 cells however, there was a significant increase in cells in the sub G0 phase which were deemed apoptotic.

Untreated control   **Cisplatin treated**
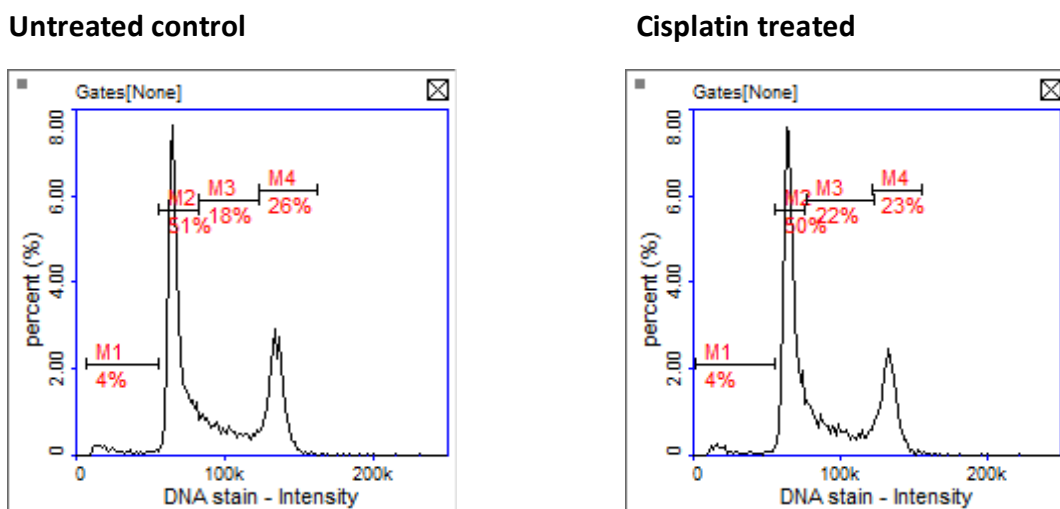
Figure 3.26: Cell cycle assay after 2-hour cisplatin (30µM) exposure on colorectal adenocarcinoma HCT116 p53$^{+/+}$ cells. The intensity of signal dictates the cell cycle stage as explained in section 1.6.6. The M2 gate represents G0/G1 phase, M3 represents S phase and M4 represents G2/M phase. Sub G0 phase represented by the M1 gate are deemed the apoptotic population of cells and cells with an intensity higher than G2/M phase are either binucleated or aggregated cells.

	2 hours		8 hours		24 hours	
	Control	Cisplatin	Control	Cisplatin	Control	Cisplatin
Sub G_0/apoptotic	4	4	2	2	2	6
G_0/G_1	51	50	55	57	63	26
S phase	18	22	23	23	16	30
G_2/M	26	23	19	17	16	35

	48 hours		72 hours	
	Control	Cisplatin	Control	Cisplatin
Sub G_0/apoptotic	2	6	2	4
G_0/G_1	69	27	87	25
S phase	14	9	4	7
G_2/M	12	55	6	61

Table 3.9: Summary of cell cycle data on colorectal adenocarcinoma HCT116 p53$^{+/+}$ cells after exposure to cisplatin (30μM) at varying time points. Data displayed as percentage values of total cell population (n=1).

	2 hours		8 hours		24 hours	
	Control	Cisplatin	Control	Cisplatin	Control	Cisplatin
Sub G_0/apoptotic	2	2	3	3	3	12
G_0/G_1	57	57	58	58	82	48
S phase	19	20	19	19	4	22
G_2/M	17	17	16	17	10	15

	48 hours		72 hours	
	Control	Cisplatin	Control	Cisplatin
Sub G_0/apoptotic	3	41	3	50
G_0/G_1	81	28	80	20
S phase	5	17	5	19
G_2/M	11	12	12	8

Table 3.10: Summary of mitochondrial potential data on non-cancerous retinal epithelial cells after exposure to cisplatin (30μM) at varying time points. Data displayed as percentage values of total cell population (n=1).
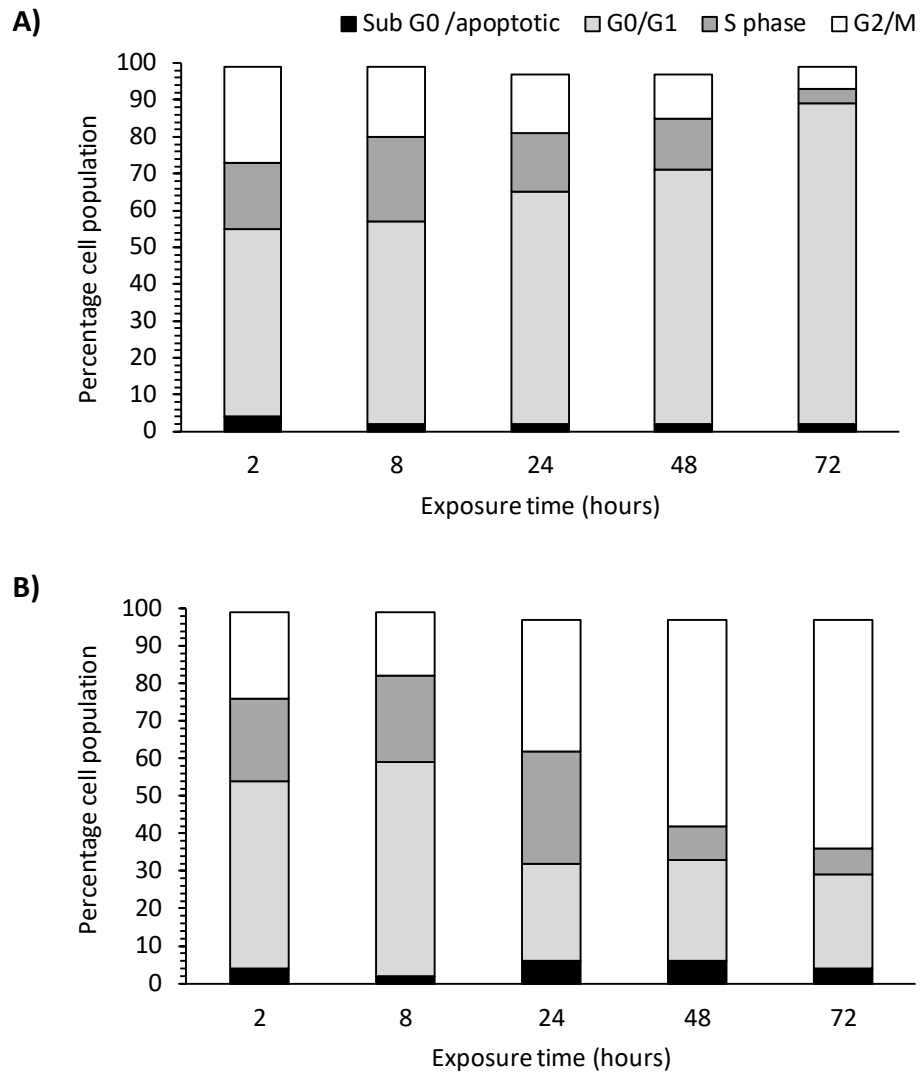
Figure 3.27: Summary of cell cycle assay on A) untreated and B) cisplatin (30µM) treated colorectal adenocarcinoma HCT116 p53$^{+/+}$ cells over 72 hours (n=1).
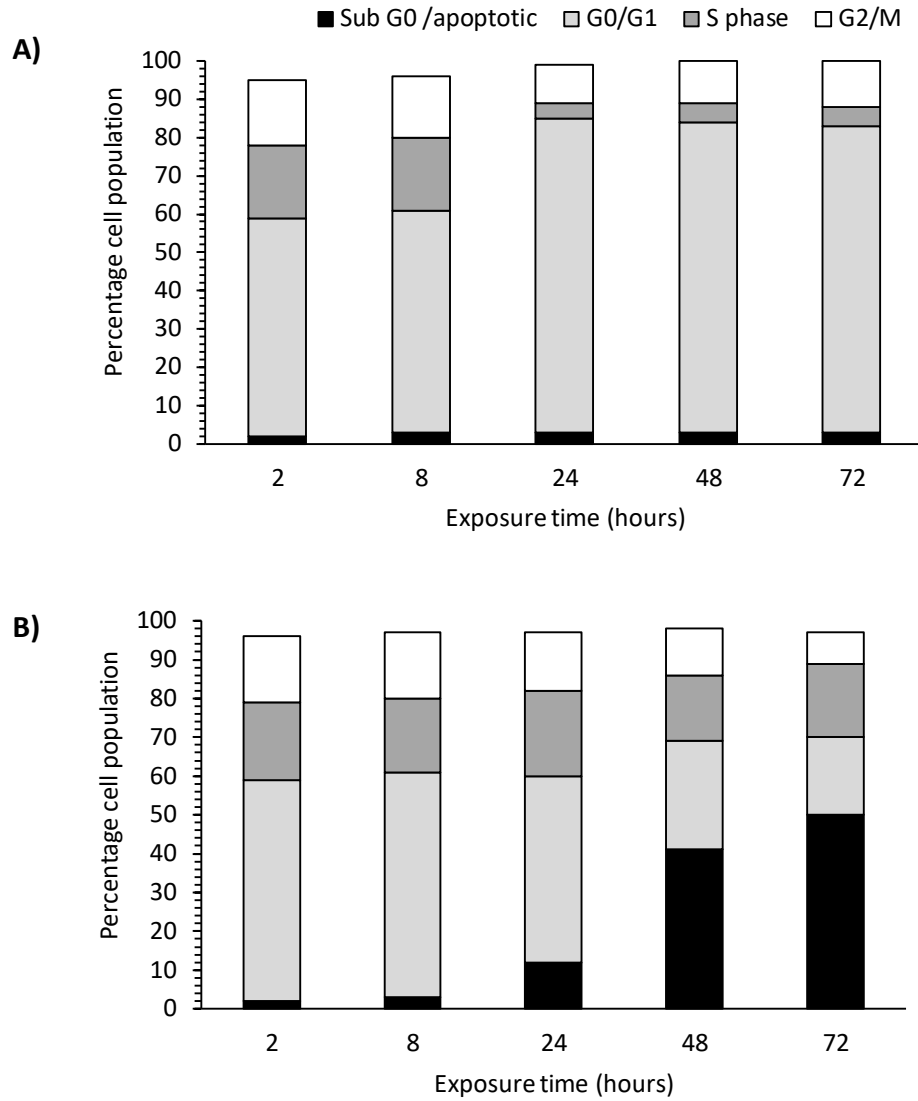
Figure 3.28: Summary of cell cycle assay on A) untreated and B) cisplatin (30µM) treated non-cancerous retinal epithelial ARPE-19 cells over 72 hours (n=1).

3.4 - Discussion

3.4.1 - Clonogenic Assays and Validation of the MTT Assay

The clonogenic assay is an established endpoint for measuring chemosensitivity and this method was initially explored for use in this project. As demonstrated in the results section, initial validation studies designed to assess the relationship between the number of colonies formed and the cell number seeded proved challenging due to the 'clumping' and merging of colonies in the centre of each well. This phenomenon occurred at various cell-seeding densities and was not significantly improved by making sure cells were well dispersed at the time of seeding. This effect was observed in two cell lines and at this stage, the clonogenic assay was abandoned and it was decided that the MTT assay endpoint would be used as the primary endpoint for assessing chemo sensitivity.

The reasons why the clonogenic assay did not generate usable results are not clear, especially as this is an established methodology. Cancer cells are highly mobile, and it is likely that the clumping/merging of colonies is due to cell migration over the course of the assay. One way of solving this is to use semi-solid matrices (such as soft agarose) as these restrict the movement of cells. This however adds to the complexity of the assay procedures and is not applicable to testing potentially large numbers of compounds. The MTT assay however proved reliable and a good correlation between cell number and absorbance was obtained. This assay is suitable for moderate to large-

scale screening and therefore it was adopted as the assay of choice in the first phase of the project. To avoid potential problems caused by test compounds interfering with the metabolic conversion of MTT to formazan, all plates were visualised prior to the addition of MTT to determine approximately where the IC_{50} resides. If results different significantly from the observed range of IC_{50} values, then further studies would be required using a different assay endpoint.

3.4.2 - Chemosensitivity Investigations of Platinum Compounds

For chemosensitivity studies to work, the drug or test compound must be soluble in biologically compatible solvents. Frequently DMSO is used to dissolve compounds but in the case of cisplatin, this is can cause significant problems. An investigation into the effects of DMSO as a solvent for platinum compounds by Hall et al. (2014) determined that platinum cytotoxicity was greatly diminished compared to cisplatin dissolved in aqueous media. The study also demonstrated using mass spectrometry that solvation in DMSO results in ligand displacement and dramatic alterations to the structure of the platinum compounds. All the platinum based drugs used in this chapter and throughout the thesis were therefore dissolved in PBS to avoid this potential source of error.

Cisplatin displays the greatest cytotoxicity throughout the cancerous cell line panel with the exception of the HCT116 cell lines. Oxaliplatin as previously discussed is the most widely used chemotherapy agent for the treatment of advanced stages of colorectal cancers in the clinic, with these tumours showing much greater resistance to

cisplatin than oxaliplatin (Park, 2014). This shift in potency could be attributed to the differing mechanism of the dach-platinum complex formed by oxaliplatin compared to that of cis-diammine platinum complexes generated by cisplatin and carboplatin. Although not fully defined, in humans at least six MMR proteins are required for mismatch recognition, these proteins form a number of heterodimer combinations, it is these complexes which then recognise mispaired bases or insertions/deletions in DNA and coordinate communication between mismatch recognition complexes and additional proteins required for MMR (Peltomäki, 2001). The aforementioned study by Vaisman et al. (1998) identified HCT116 cell lines lack the protein MLH1 which results in the loss of mismatch repair activity due to the subsequent defects in the hMutLα mismatch recognition complex. Where cisplatin and carboplatin rely on mismatch recognition to exert their action and are greatly affected by this bypass of platinum adducts, the bulkier dach adducts formed by oxaliplatin are not recognised by the mismatch recognition complexes thus not dependent on mismatch repair systems (Drummond, Anthoney, Brown, & Modrich, 1996). Tumours with defects in mismatch repair will therefore respond better to oxaliplatin opposed to cisplatin and carboplatin, which is reflected by the chemosensitivity data. These results are further validated by the chemosensitivity data collected by Vaisman et al. (1998) whom found oxaliplatin to be more potent in a number of isogenic clones of the HCT116 cell line compared to cisplatin.

In addition to increased sensitivity of HCT116 cell lines toward carboplatin it is pertinent to discuss the difference between sensitivity toward platinum compounds and p53 expression. Across the three platinum compounds chemo-sensitivity is reduced by a lack in p53 expression. p53 an established clinical barrier for conventional cancer therapy with the tumour suppressor gene is the most frequently mutated gene in human cancers and thought to be involved in the maintenance of the genome integrity (Hollstein et al., 1999). It has been extensively documented that cisplatin and its' recognised platinum derivatives induce apoptosis in cells with functional p53 with recent studies in HCT116 cell lines establishing p53 deficient cells are much less sensitive to apoptosis by cisplatin (Bragado, Armesilla, Silva, & Porras, 2007). It is therefore expected the HCT116 p53$^{-/-}$ cell line will be more resistant to platinum therapy as displayed by the data in figure 13.

A central cornerstone of the hypothesis being tested in this thesis is that determination of the selectivity index *in vitro* could help identify compounds for further evaluation in the context of phenotypic based drug discovery programs. In this context, the platinum based compounds were evaluated against non-cancer cell lines thereby enabling a selectivity index *in vitro* to be created. This was defined as the IC$_{50}$ in non-cancer cells divided by the IC$_{50}$ in cancer cells and all values above 1 indicate selectivity towards cancerous cells over non-cancerous cells. From clinical experience it is well established the platinum agents carry debilitating side effects with cisplatin presenting as the least selective with resulting side effects that are irreversible and

often chronic. Figure 3.10 displays the relative selectivity's of the cell line panel used in this investigation compared to ARPE-19 cell line. Overall, oxaliplatin displays the poorest selectivity with only one cell line displaying a selectivity index over one (HCT116 p53$^{+/+}$). This is due to its potency towards the ARPE-19 (IC$_{50}$ = 3.12 ± 0.28µM, figure 3.9) making it the most potent platinum agent in this particular non-cancerous cell line. Carboplatin on the other hand is not very active against the ARPE-19 cell line (IC$_{50}$ = 77.73 ± 10.52µM, figure 3.9) which results in the highest selectivity overall; selectivity indices were all at two or above (figure 3.10). This reflects the rationale behind the synthesis of carboplatin and its mores stable leaving group, which lowers its toxicity profile. Although more selective, this poor activity on the non-cancerous cell line is also reflected in its lack of potency on the cancerous cell lines, which as discussed above is estimated to be 20-40 times lower than that of cisplatin. Cisplatin although fairly potent towards the non-cancerous cell line (IC$_{50}$ = 6.41 ± 0.95µM, figure 3.9) does display one of the highest selectivity indexes within this panel on the colorectal BE cell line. Overall only one cell line (HCT116 p53$^{+/+}$) has a selectivity index lower than one therefore suggesting cisplatin is the most desirable compound of the three platinum compounds investigated displaying both selectivity and potency.

Hypoxia is a significant barrier to effective chemotherapy with hypoxic cells being more resistant to a wide range of anti-cancer therapy (Teicher, 1994) , which will be discussed in more detail in chapter 6. It is well-documented that platinum chemotherapy agents are much more resistant to cells with hypoxic profiles and the

results presented in this study (figures 3.12-3.14) are consistent with these findings. In this study, all the compounds had significantly increased IC_{50} and in many cases IC_{50} values could not be determined (above the highest drug concentration tested). To investigate the potential effects of HIF-1 on the cytotoxic properties of platinum based drugs, a pseudo-hypoxic state was induced by conditioning the cells with cobalt chloride, a known HIF-1 inducer (Pourpirali et al., 2015). From the results presented in figures 3.15-3.17, the addition of cobalt chloride reduces the potency of platinum based chemotherapy drugs suggesting a role for HIF1 in resistance of cells to platinum based drugs. Although enhanced, the chemoresistance observed is much less than that seen in true hypoxic conditions suggesting that even in a mono-layered cell culture environment, hypoxia may contribute to resistance *via* additional mechanisms other than HIF-1 induction alone.

3.4.3 - Cisplatin Induced Apoptosis and Cell Cycle Disruption

Both annexin V assays and mitochondrial potential assays were completed to detect cisplatin induced apoptosis (figures 3.21-3.22 and 3.24-3.25). These assays were compared on both the cancerous HCT116 p53$^{+/+}$ cell line and non-cancerous ARPE-19 cell line for exposure times up to 72 hours. Both the apoptotic assays showed an increase in apoptotic induction with increasing exposure time with apoptosis being induced as early as 2-hour exposures in the ARPE-19 cell line.

Cisplatin known to induce G_2/M phase arrest was used as a positive control to help define an appropriate exposure time for novel compounds with unknown mechanism.

As with the apoptotic assays a time dependent dose response was observed with G_2/M phase arrest observed after 24 hours.

3.5 - Conclusion

The aim of this chapter was to define parameters by which the relative merits of novel compounds can be measured as part of a strategy to identify "hit" compounds which possess improved properties in terms of (i) selectivity *in vitro* (ii) potency (iii) activity against p53 null and (iv) hypoxic cells. Quantitative data has been collected in the form of chemosensitivity data which acts as a direct comparative parameter for our novel compounds. Another aim of the chapter was to aid the mechanistic profiling of our novel compounds in terms of establishing exposure time parameters for the analysis of apoptotic induction and cell cycle disruption. These studies demonstrated that induction of apoptosis and cell cycle disruption can be detected after exposure times of 24 hours and above. The parameters established in this chapter therefore provide a 'yardstick' for potency, selectivity for cancer cells *in vitro*, the effect of hypoxia (and pseudo-hypoxia) on cellular response, induction of apoptosis and effects on cell cycle kinetics against which the relative merits of test compounds can be measured.

Chapter 4 - Cobalt Complexes as Anti-Cancer Agents

4.1 - Introduction

The evolution of resistance and the toxic side effects associated with classical platinum-based anti-cancer drugs has stimulated the search for novel organometallic complexes with improved anti-cancer properties. Initial studies were predominantly focused on platinum based compounds but over recent years, studies have demonstrated that other metal containing compounds have anti-cancer effects that are not caused by inducing DNA damage (Gasser et al., 2010). Due to the biological importance of metals in many metabolic processes, metals such as cobalt have been extensively studied over the past three decades for their anti-microbial, anti-viral and anti-cancer properties (Munteanu & Suntharalingam, 2015).

Cobalt is a trace element naturally occurring in all animals, predominantly in the form of cobalamin (Vitamin B12). Cobalt plays a crucial role in several biological processes such as red blood cell formation and DNA synthesis and it possesses an array of properties which can be manipulated to yield promising drug candidates (Sigel, Sigel, & Sigel, 2013). Given its prominent biological role, the body already possesses the ability to naturally overcome cobalt overload thereby offering the potential for reduced toxicity profiles unlike many non-essential metals (Elvers, Hawkins, & Schultz, 1992). Cobalt is a trace element naturally occurring in all animals, predominantly in the form of cobalamin (Vitamin B12). Cobalt plays a crucial role in several biological

processes such as red blood cell formation and DNA synthesis and it possesses an array of properties which can be manipulated to yield promising drug candidates (Sigel et al., 2013). Given its prominent biological role, the body already possesses the ability to naturally overcome cobalt overload thereby offering the potential for reduced toxicity profiles unlike many non-essential metals (Elvers et al., 1992). A variety of cobalt based complexes have been synthesised and evaluated as potential anti-cancer agents with their novel and varied mechanisms of action contributing to their appeal. These mechanisms have been extensively reviewed elsewhere (Munteanu & Suntharalingam, 2015) and they include the ability to target hypoxic cells. Hypoxia in tumours is caused by a poor and inefficient vascular supply to tumours and is widely regarded as a major contributing factor to drug resistance, resistance to radiotherapy and the evolution of an aggressive phenotype (Unruh et al., 2000). There has been considerable interest in the development of hypoxia activated prodrugs (Phillips, 2016) and this includes cobalt based compounds.

Their ability to serve as potential hypoxia activated prodrugs stems from their redox properties with the reduction of Co(III) to Co(II) being favoured under hypoxic conditions (Baran & Konopleva, 2017; de Souza et al., 2016). Various mechanisms have been described including the release of ligands such as EGFR inhibitors following reduction of Co(III) to Co(II) (Karnthaler-Benbakka et al., 2014). Although its mechanism is widely unknown, bioactive cobalt complexes exert their mode of action in three proposed classes complexes reactive to ligand exchange and the

aforementioned complexes with bioactive ligands and bio-reductively activated cobalt

complexes all of which are summarised in figure 4a.
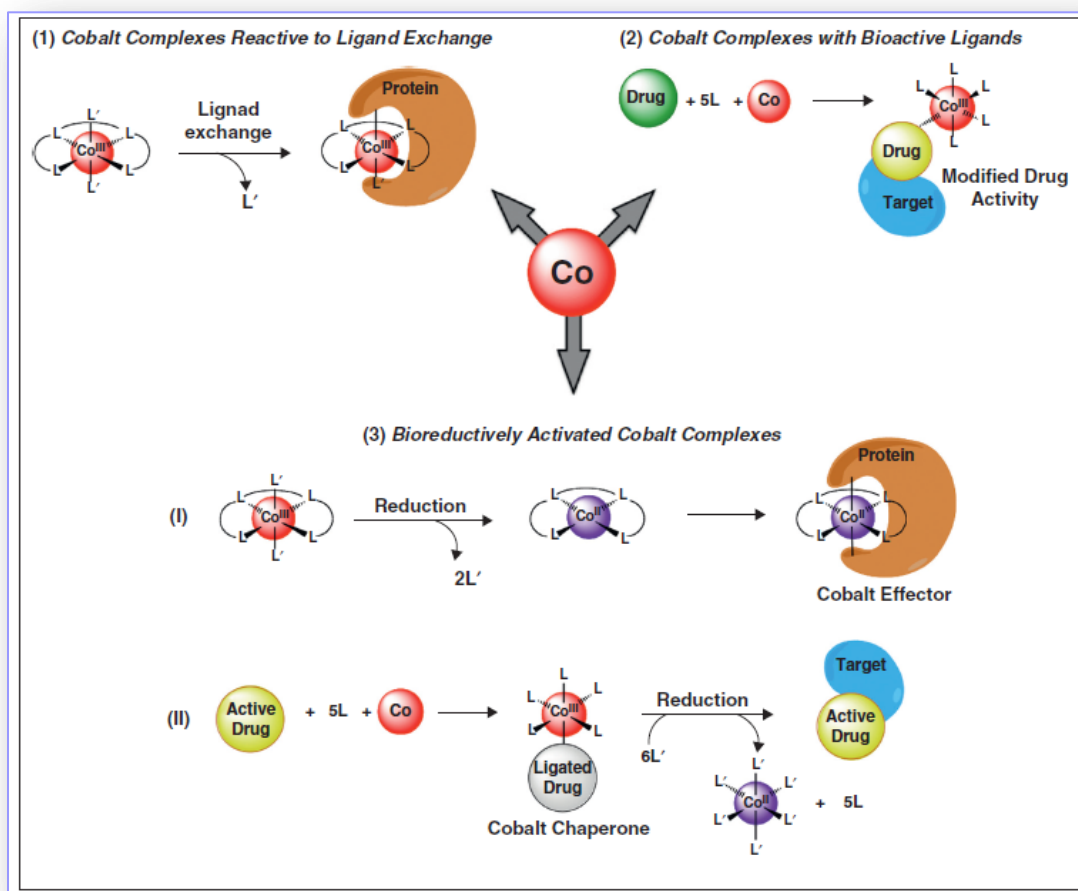
Figure 4a: Summary of the modes of action of bioactive cobalt complexes. Adapted from (Heffern,

Yamamoto, Holbrook, Eckermann, & Meade, 2013)

In a collaboration with Professor Patrick McGowan at the University of Leeds, a series of cobalt compounds conjugated to various ligands including the biologically active ligand picolinamide. Picolinamide is known to inhibit poly(ADP-ribose) polymerases (PARP) (Piskunova, Iurova, Zabezhinskiǐ, & Anisimov, 2007; Yamamoto & Okamoto, 1980) and it is widely regarded as attractive target in cancer therapy. It has an established role in the DNA repair process and its inhibition has been explored as a mechanism of (i) sensitising cancer cells to DNA damaging agents and (ii) directly inducing cell death *via* the process of synthetic lethality (Bryant et al., 2005; Farmer et al., 2005). Synthetic lethality is based on the hypothesis that a combination of deficiencies in the expression two or more genes results in increased cell death where either deficiency alone does not (Iglehart & Silver, 2009) . PARP and BRCA genes are involved in cellular DNA repair therefore the mutation of either one still allows for DNA repair by the alternative pathway. The exploitation of synthetic lethality is based on the treatment of BRCA mutated cancers with PARP inhibitors resulting in increased sensitivity and ultimately increased cell death, summarised in figure 4b (Lord, Tutt, & Ashworth, 2015).
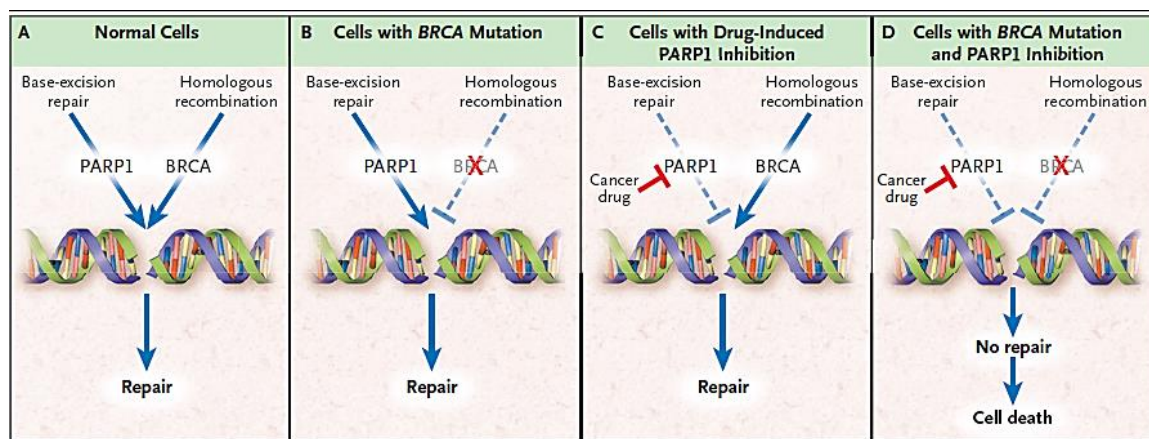
Figure 4b: Mechanism of cell death by exploitation of synthetic lethality with the use of PARP-1 inhibitors in BRCA mutated malignancies. Taken from Inglehart and Silver (2009).

A series of compounds were provided in either the active cobalt (II) form or as a prodrug in the form of cobalt (III). The aim of the research presented in this chapter was to evaluate the potency and selectivity of these compounds under aerobic conditions together with the evaluation of Co(III) derivatives conducted under both aerobic and hypoxic conditions.

4.2 - Methods

A series of compounds were obtained from Professor McGowan's research group and these were organised into Classes (1 to 3) with class 1 compounds split into 2 sets based on structural criteria. The chemical structures and preparation of stock solutions are presented below.

4.2.1 - Chemical Structures and Preparation of Drug Stock Solution

Red form	Brown form
Class 1 Set 1	
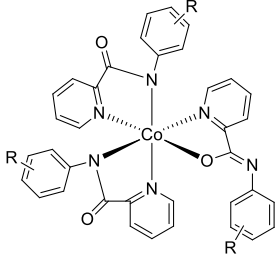
Compound	MW	Weight (mg)	Diluent	Diluent volume (μl)	Molar concentration (mM)	R substituent
Cobalt (III) tris-picolinamide red form						
LG097-2	650.57	0.65	DMSO	9.99	100	H
LG156	704.54	1.98	DMSO	28.1	100	2-F
LG155	704.54	3.70	DMSO	52.6	100	3-F
LG154	704.54	3.40	DMSO	48.3	100	4-F
LG157	758.51	1.96	DMSO	25.8	100	2,4-diF
LG158	758.51	3.52	DMSO	46.4	100	2,5-diF
LG164	753.91	1.87	DMSO	24.8	100	3-Cl
LG163	753.91	3.83	DMSO	50.8	100	4-Cl
LG169	887.26	2.18	DMSO	24.6	100	3-Br
LG167	887.26	3.11	DMSO	42.9	100	4-Br
LG103-2	854.57	1.33	DMSO	15.6	100	3-CF$_3$
LG104-2	854.57	1.66	DMSO	19.4	100	4-CF$_3$
LG101-2	1058.56	3.63	DMSO	34.3	100	3,5-diCF$_3$
LG153	692.65	1.48	DMSO	21.4	100	3-Me
LG145	692.65	1.78	DMSO	25.7	100	4-Me
LG121	734.73	12.12	DMSO	165	100	3,5-diMe
Cobalt (III) tris-picolinamide brown form						
LG097-1	650.57	1.43	DMSO	22	100	H
LG152-1	692.65	1.31	DMSO	18.9	100	3-Me
LG144-1	692.65	1.32	DMSO	19.1	100	4-Me
LG100A	734.73	2.21	DMSO	30.1	100	3,5-diMe

Table 4.1: Class 1, set 1 cobalt (III) tris-picolinamide complexes structure and stock solution preparation.

Red form	Brown form

Class 1
Set 2

Compound	MW	Weight (mg)	Diluent	Diluent volume (μl)	Molar concentration (mM)	R substituent
Cobalt (III) tris-picolinamide red form						
LG290-2	830.73	3.07	DMSO	36.96	100	3,5-diOMe
LG293-2	740.65	2.45	DMSO	33.08	100	4-OMe
Cobalt (III) tris-picolinamide brown form						
LG290-1	830.73	3.29	DMSO	39.60	100	3,5-diOMe
LG293-1	740.65	3.00	DMSO	40.50	100	4-OMe

Table 4.2: Class 1, set 2 cobalt (III) tris-picolinamide complexes structure and stock solution preparation.

	SCN	Cl	H₂O (I⁻ counterion)

Class 2

Compound	MW	Weight (mg)	Diluent	Diluent volume (μl)	Molar concentration (mM)	R substituent
Cobalt (II) bis-picolinamide-SCN						
LG116	571.54	4.87	DMSO	85.21	100	H
LG175	599.59	2.16	DMSO	36.02	100	2-Me
LG174	599.59	2.73	DMSO	45.53	100	3-Me
LG173	599.59	2.04	DMSO	34.02	100	4-Me
LG176	627.65	5.07	DMSO	80.78	100	2,3-diMe
LG137	627.65	5.28	DMSO	84.12	100	3,5-diMe
LG297	631.59	2.13	DMSO	33.72	100	4-OMe
LG298	691.64	3.34	DMSO	48.29	100	3,5-diOMe
Cobalt (II) bis-picolinamide-Cl						
LG107	526.28	2.38	DMSO	45.22	100	H
Cobalt (II) bis-picolinamide-H₂O (I⁻ counterion)						
LG113	745.21	7.52	DMSO	100.91	100	H

Table 4.3: Class 2 cobalt (II) bis-picolinamide complexes structure and stock solution preparation

	Simple acac			Ferrocene acac		
Class 3						

Compound	MW	Weight (mg)	Diluent	Diluent volume (μl)	Molar concentration (mM)	R substituent
Cobalt (II) bis-picolinamide$_2$(acac) with simple acac						
LG300	824.46	2.22	DMSO	26.92	100	CH_3
LG275	886.53	2.64	DMSO	29.78	100	Ph
LG268	948.60	2.02	DMSO	21.29	100	Ph & Ph
LG276	904.52	2.46	DMSO	27.19	100	3-F Ph
LG277	904.52	3.64	DMSO	40.24	100	4-F Ph
LG278	900.55	2.11	DMSO	23.43	100	3-Me Ph
LG279	900.55	4.15	DMSO	46.08	100	4-Me Ph
LG280	916.55	3.85	DMSO	42.00	100	4-OMe Ph
LG296	954.53	5.15	DMSO	53.95	100	$4-CF_3$ Ph
Cobalt (II) bis-picolinamide$_2$(acac) with ferrocene acac						
LG263	994.45	1.90	DMSO	19.10	100	CH_3
LG264	1048.42	2.44	DMSO	23.27	100	CF_3
LG274	1030.43	4.22	DMSO	40.95	100	CF_2
LG266	1056.52	3.30	DMSO	31.23	100	Ph
LG271	1074.51	2.33	DMSO	21.58	100	3-F Ph
LG269	1074.51	4.50	DMSO	41.88	100	4-F Ph
LG272	1092.50	1.54	DMSO	14.09	100	3,5-diF Ph
LG289	1070.54	7.71	DMSO	72.02	100	3-Me Ph
LG265	1070.54	2.83	DMSO	26.43	100	4-Me Ph
LG273	1084.57	7.54	DMSO	69.52	100	3,5-diMe Ph

Table 4.4: Class 3 cobalt (II) bis-picolinamide complexes with acetylacetone (acac) ligands, structure and stock solution preparation.

Compounds LG300/265/273 (highlighted) were not fully soluble therefore were withdrawn.

All drug stock solutions were stored at -20°C in individual 2µl aliquots to prevent any potential degradation of the compounds caused by repeat freeze thawing cycles. All stock solutions were discarded after 3 months of storage.

4.2.2 - Chemo-Sensitivity Testing, Analysis of Cell Viability and Cell Cycle Inhibition

The response of cell lines following continuous 96-hour exposures to test compounds under aerobic and hypoxic conditions was determined using the MTT assay, details of which have been described elsewhere in this thesis (see 1.5). Analysis of cell viability and cell cycle parameters was determined using the NC3000 cytometer, details of which have been described elsewhere (see 1.6). For these experiments, drug exposure concentrations ranged from 5µM to 20µM; duration of drug exposures was set at 96 hours to replicate the conditions used in the MTT assays.

4.3 - Results

4.3.1 - Chemosensitivity Studies in Aerobic Conditions

The response of cell lines to various test LG compounds are presented in table 3.1. A significant number of compounds were inactive against all cell lines with IC_{50} values greater than the highest dose tested which was typically 100µM. Some compounds

showed only modest activity against one or two cell lines (e.g. LG169) but of the compounds tested, only LG101-2 and LG100A showed significant activity *in vitro*.

4.3.1.1 - Response of MIA-PaCa$_2$, BE and ARPE-19 Cells to Test Compounds Under Aerobic Conditions

Compound	IC$_{50}$ value ± standard deviation		
	MIA-PaCa$_2$	BE	ARPE-19
LG097-2	>100	>100	>100
LG156	>100	>100	>100
LG155	>100	>100	>100
LG154	>100	>100	>100
LG157	>100	>100	>100
LG158	>97.46	>100	>100
LG164	>86.38	>100	>65.5
LG163	>100	>93.21	>100
LG169	68.46±13.51	>100	>100
LG167	37.40±18.89	>74.87	>65.42
LG103-2	>62.33	>100	>100
LG104-2	>100	>100	>100
LG101-2	37.43±8.69	3.77±1.98	7.57±3.92
LG153	>100	>100	>100
LG145	>100	>100	>100
LG121	>98.06	>100	>100
LG097-1	>66.99	>100	>82.42
LG152-1	45.54±2.80	52.61±6.99	37.89±18.12
LG144-1	55.82±1.63	37.45±13.04	30.20±5.23
LG100A	7.38±2.17	19.31±1.38	9.63±6.88
LG290-2	>100	-	>100
LG293-2	>100	-	>100
LG290-1	>100	-	>100
LG293-1	>100	-	>100
LG116	>100	-	>100

Table 4.5: Response of pancreatic carcinoma cell line MIA-PaCa$_2$, colorectal carcinoma cell line BE and the non-cancerous retinal epithelial cell line ARPE-19 following continuous 96-hour exposure to LG cobalt based compounds. The results presented are the mean IC$_{50}$ values ± standard deviations for three independent experiments n=3 (each individual experiment replicated twice). The most promising results in terms of potency are highlighted in red. The ">" symbol represents the highest dose tested *in vitro*.

	IC$_{50}$ value ± standard deviation		
Compound	**MIA-PaCa$_2$**	**BE**	**ARPE-19**
LG175	>100	-	>100
LG174	>100	-	>100
LG173	>100	-	93.44
LG176	>100	-	82.5
LG137	>100	-	>100
LG297	>100	-	>100
LG298	>100	-	>100
LG107	>100	-	>100
LG113	>100	-	>100
LG275	>100	-	>100
LG268	>100	-	>100
LG276	>100	-	>100
LG277	>100	-	>100
LG278	>100	-	>100
LG279	>100	-	>100
LG280	>100	-	>100
LG296	92.04±13.79	-	>100
LG263	>100	-	>100
LG264	>100	-	>100
LG274	32.85±6.82	-	>100
LG266	>100	-	>100
LG271	>100	-	>100
LG269	>100	-	>100
LG272	>100	-	>100
LG289	>100	-	>100
Cisplatin	3.62 ± 0.74	0.66 ± 0.33	6.41 ± 0.95
Carboplatin	35.59 ± 7.91	32.72 ± 4.64	77.73 ± 10.52
Oxaliplatin	6.44 ± 1.05	8.56 ± 0.48	3.12 ± 0.28

Table 4.5 (continued): Response of pancreatic carcinoma cell line MIA-PaCa$_2$, colorectal carcinoma cell line BE and the non-cancerous retinal epithelial cell line ARPE-19 following continuous 96-hour exposure to LG cobalt based compounds. The results presented are the mean IC$_{50}$ values ± standard deviations for three independent experiments n=3 (each individual experiment replicated twice). The most promising results in terms of potency are highlighted in red. The ">" symbol represents the highest dose tested *in vitro*. Platinum standards included as a reference of activity.

4.3.2 - Comparison of LG101-2 and LG100A with Platinum Based Anti-Cancer Drugs

The performance of LG101-2 and LG100A in terms of (i) potency and (ii) selectivity compared to platinum based anti-cancer drugs is presented in figures 4.6 and 4.7 respectively. With regards to potency against the two cancer cell lines tested, both LG101-2 and LG100A were less active than cisplatin and oxaliplatin. Compared to carboplatin, LG100A was significantly more potent against MIA-PaCa$_2$ cells but only marginally more active against BE cells. LG101-2 was approximately 8-fold more active than carboplatin against BE cells (IC$_{50}$ of 3.77uM versus 32.72uM) but the response of MIA-PaCa$_2$ cells was comparable to carboplatin. Both LG compounds were more active against the ARPE-19 non-cancer cell line than carboplatin. In contrast, LG100A was less active against ARPE-19 cells than oxaliplatin and cisplatin.

With regards to selectivity for cancer as opposed to non-cancer cells (figure 4.7), both LG compounds had lower selectivity indices compared to cisplatin and carboplatin. Compared to oxaliplatin there was some evidence of improved selectivity in MIA-PaCa$_2$ (LG100A only) and BE (LG101-2 only) cells but overall, there was no significant improvement in selectivity. None of the compounds display statistically significant reductions in activity toward none cancerous cell opposed to cancerous cell lines.
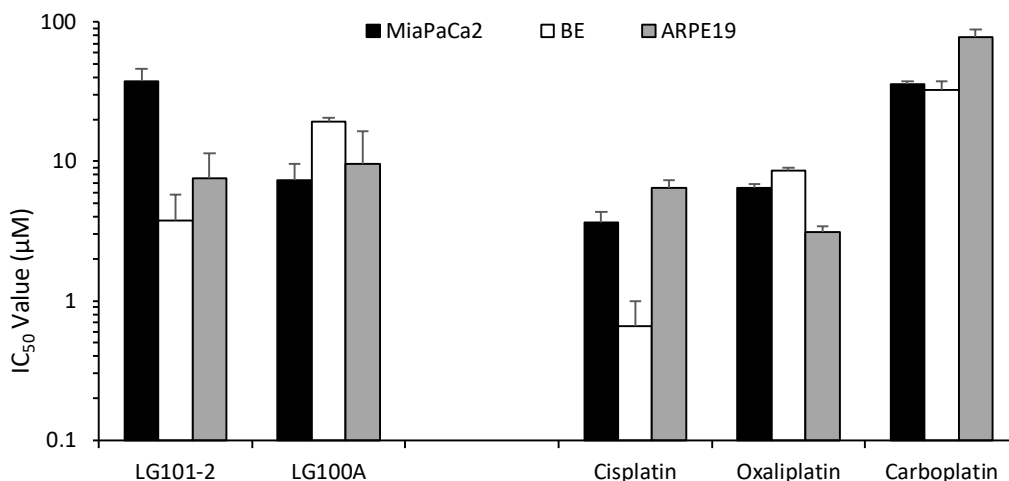
Compound	MIA-PaCa$_2$	BE	ARPE-19
LG100A	7.38 ± 2.17	19.31 ± 1.38	9.63 ± 6.88
LG101-2	37.43 ± 8.69	3.77 ± 1.98	7.57 ± 3.92
Cisplatin	3.62 ± 0.74	0.66 ± 0.33	6.41 ± 0.95
Carboplatin	35.59 ± 7.91	32.72 ± 4.64	77.73 ± 10.52
Oxaliplatin	6.44 ± 1.05	8.56 ± 0.48	3.12 ± 0.28

Figure **4.1**: Comparison of the potency of LG101-2 and LG100A to cisplatin, oxaliplatin and carboplatin on MIA-PaCa$_2$, BE and ARPE-19 cells. The values presented are the mean IC$_{50}$ values ± standard deviation of three independent experiments n=3 (each individual experiment replicated twice).
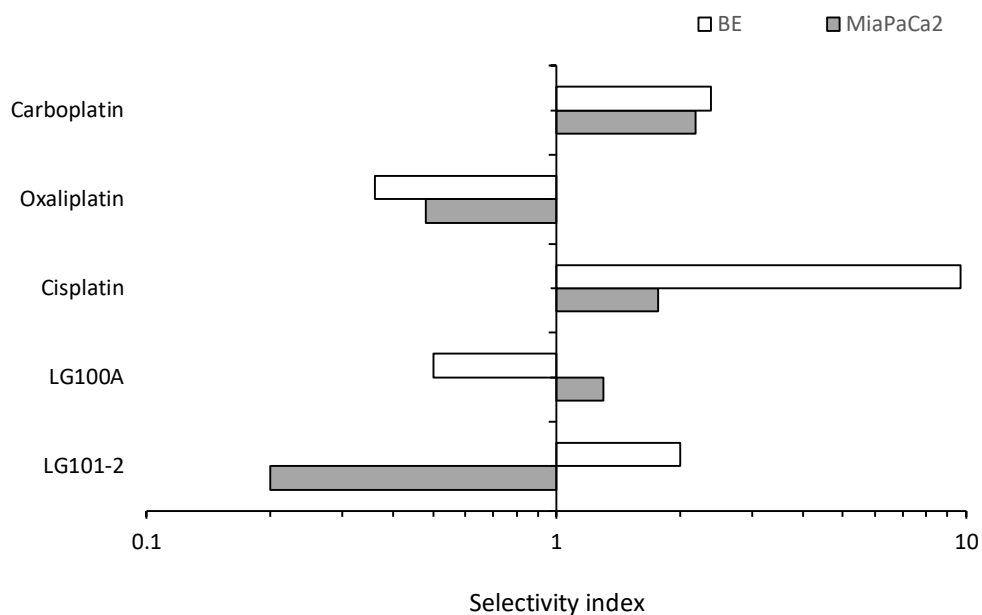
Compound	MIA-PaCa$_2$	*p*-value	BE	*p*-value
LG100A	1.3	0.71	0.5	0.18
LG101-2	0.2	0.054	2	0.35
Cisplatin	1.77	0.10	9.71	0.0043
Carboplatin	2.18	0.031	2.38	0.029
Oxaliplatin	0.48	0.020	0.36	0.0064

Figure 4.2: Comparison of the selectivity index of LG101-2 and LG100A to cisplatin, oxaliplatin and carboplatin. The selectivity index is defined as the mean IC$_{50}$ for non-cancerous cells divided by the IC$_{50}$ of cancerous cells. Values greater than 1 indicate that compounds have selectivity for cancer cells as opposed to non-cancer cells. As the mean IC$_{50}$ values are used to calculate selectivity indices, no error bars are included on the graphs. Statistical analysis was performed using a student's t-test where values <0.05 indicates a statistically significant difference between IC$_{50}$ values in cancerous and none cancerous cell lines**.**

4.3.3 - Chemosensitivity Investigations in Hypoxic Conditions

The response of cell lines to various test LG compounds in hypoxic conditions are presented in table 4.6. These compounds (Class 1, set 1; table 4.1) were selected as the cobalt in these compounds exists as Co(III) which has the potential to be reduced in a hypoxic environment to Co(II). All of the compounds tested showed either reduced activity under hypoxic conditions or the IC_{50} remained >100uM as under aerobic conditions (Table 4.6). Only two compounds (LG100A and LG152-1) have an IC_{50} value less than the highest dose tested (100μM).

4.3.3.1 - Response of MIA-PaCa$_2$ Cells to Co(III) Compounds Under Aerobic and Hypoxic Conditions

Compound	MIA-PaCa$_2$ aerobic	MIA-PaCa$_2$ hypoxia
LG097-2	>100	>100
LG156	>100	>100
LG155	>100	>100
LG154	>100	>100
LG157	>100	>100
LG158	>97.46	>100
LG164	>86.38	>100
LG163	>100	>100
LG169	68.46±13.51	>100
LG167	37.40±18.89	>100
LG103-2	>62.33	>100
LG104-2	>100	>100
LG101-2	37.43±8.69	>100
LG153	>100	>100
LG145	>100	>100
LG121	>98.06	>100
LG097-1	>66.99	>100
LG152-1	45.54±2.80	74.25±3.68
LG144-1	55.82±1.63	>100
LG100	7.38±2.17	29.68±2.18

Table 4.6: Response of MIA-PaCa$_2$ and Panc10.05 cell lines following continuous 96-hour exposure to set 1 class 1 LG cobalt compounds in hypoxic conditions. The results presented are the mean IC$_{50}$ values ± standard deviations for three independent experiments n=3 (each individual experiment replicated twice) .The most promising compounds in terms of potency LG100A and LG152-1 are highlighted in red. The ">" symbol represents the highest dose tested *in vitro*. For comparative purposes the response of the same cell line in aerobic conditions is presented within the data set.

4.3.4 - Comparison of LG100A and LG152-1 With Platinum Based Anti-Cancer Drugs

The performance of LG100A and LG152-1 in terms of potency under hypoxic conditions compared to platinum based anti-cancer drugs is presented in table 4.7. With regards to potency against cancer cell lines in hypoxia, both LG100A and LG152-1 are more active than all three platinum compounds. The hypoxic cytotoxicity ratios were all below 1 indicating resistance under hypoxia compared to aerobic conditions. In comparison to the platinates however, the level of resistance under hypoxia is significantly less with LG152-1 being only marginally more resistant under hypoxic conditions (HCR = 0.61).

Compound	MIA-PaCa$_2$ aerobic	MIA-PaCa$_2$ hypoxia	p-value	Hypoxic Cytotoxicity Ratio
LG152-1	45.54±2.80	74.25±3.68	0.00027	0.61
LG100A	7.38±2.17	29.68±2.18	0.0011	0.25
Cisplatin	3.62±0.74	>100	0.00002	>0.036
Carboplatin	35.59±7.91	>100	0.0050	>0.35
Oxaliplatin	6.44±1.05	87.72±7.29	0.0021	0.073

Table 4.7: Response of MIA-PaCa$_2$ cells following continuous 96-hour exposure to LG cobalt compounds and platinate standards in hypoxic and aerobic conditions**.** The results presented are the mean IC$_{50}$ values ± standard deviations for three independent experiments n=3 (each individual experiment replicated twice). The hypoxic cytotoxicity ratio (HCR) is defined as the ratio of IC$_{50}$ values under aerobic divided by the IC50 under hypoxic conditions. Values > 1 demonstrates that the compound has selective activity against hypoxic cells. The ">" symbol represents the highest dose tested *in vitro*. Statistical analysis was performed using a student's t-test where values <0.05 indicates a statistically significant difference between IC$_{50}$ values in hypoxic and aerobic conditions.

4.3.5 - Analysis of Cell Viability and Cell Cycle Parameters of LG101-2 and LG100A

As the most promising of the cobalt complexes in terms of potency, selectivity and activity under hypoxia, LG101-2 and LG100A were selected for further investigation. MIA-PaCa$_2$ cells were exposed to these two "hit" compounds for 96h under conditions paralleling those used for the MTT studies and analysed for any effects on cell viability and/or the cell cycle. Although LG100A was~6-fold more active than LG101-2 against MIA-PaCa$_2$ cells in the MTT chemosensitivity assays, both compounds caused a similar dose-dependent reduction in total cell number in these 96 hours experiments (Figure 4.8, Figure 4.11). The percentage cell viability for both LG101-2 and LG100A on the

other hand remained stable over the range of concentrations tested (figures 4.8 and 4.11 respectively) suggesting although cell number is reduced, the remaining cells are viable. Figures 4.10 and 4.13 demonstrate the effects of these "hit" compounds on the percentage of the cell population at specific stages of the cell cycle. For both compounds the proportion of sub-G1 cells remained stable with increasing drug concentration whilst the proportion of cells within the G_2/M and S phase increased slightly with no profound difference between the two compounds.

4.3.5.1 - LG101-2
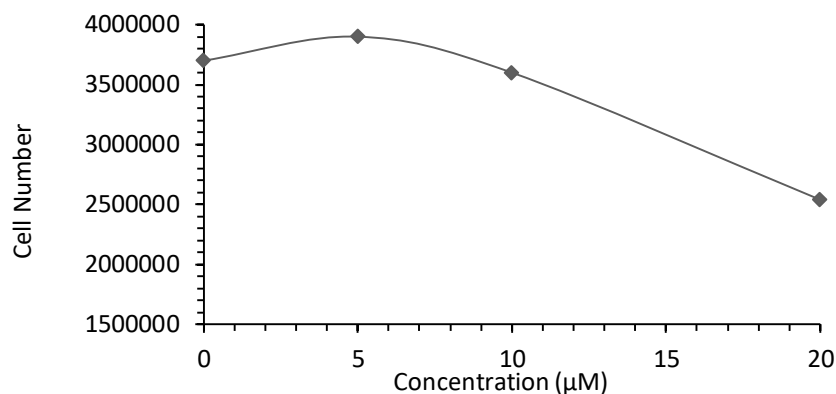
	Control	5μM	10μM	20μM
Total cells in sample	3.7×10^6	3.9×10^6	3.6×10^6	2.54×10^6
Percentage cell viability	81.8	79.5	85.4	85

Figure 4.3: Effect of increasing doses of LG101-2 on the cell number of pancreatic adenocarcinoma cell line MIA-PaCa$_2$ after 96-hour exposure. "0" denotes the control sample with concentrations of 5μM, 10μM and 20μM being tested. Cell viability is expressed as a percentage based on acridine Orange staining the entire population and DAPI which stains non-viable cells (n=1).

Control   **5μM**   **10μM**   **20μM**
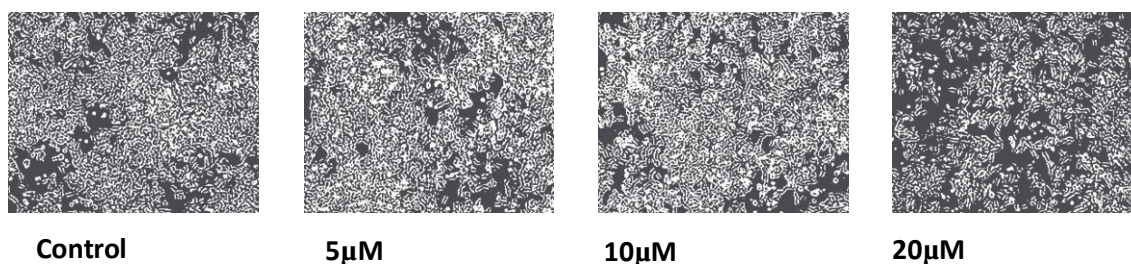
Figure 4.4: Microscope images of pancreatic adenocarcinoma cell line MIA-PaCa$_2$ exposed to increasing doses of LG101-2 over a 96- hour exposure time.
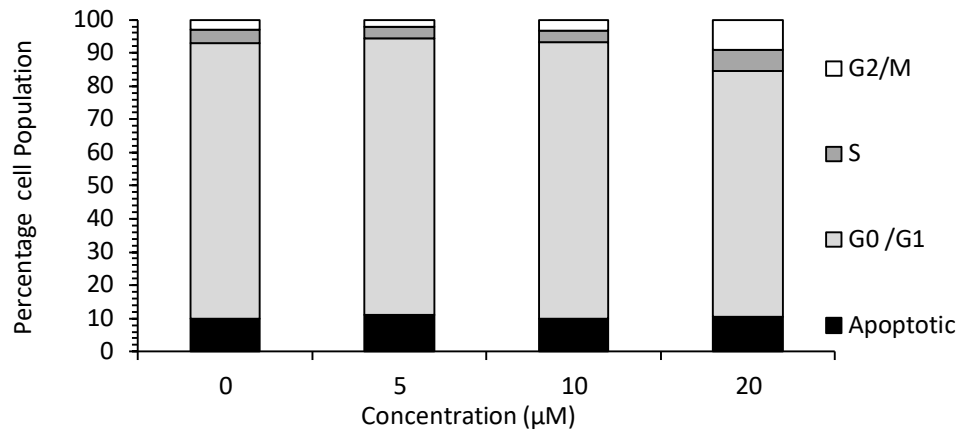
Cell cycle phase	Percentage of cell population			
	Control	5μM	10μM	20μM
Apoptotic	10	11	10	10
G_0/G_1	83	83	83	74
S	4	3	3	6
G_2/M	3	2	3	9

Figure 4.5: Cell cycle response of pancreatic adenocarcinoma cell line MIA-PaCa$_2$ to increasing doses of LG101-2 after 96-hour exposure time. "0" denotes the control sample and the percentage of the cell population within each cycle stage is determined by the cell's DNA content with nuclear stain DAPI (n=1).

4.3.5.2 - LG100A
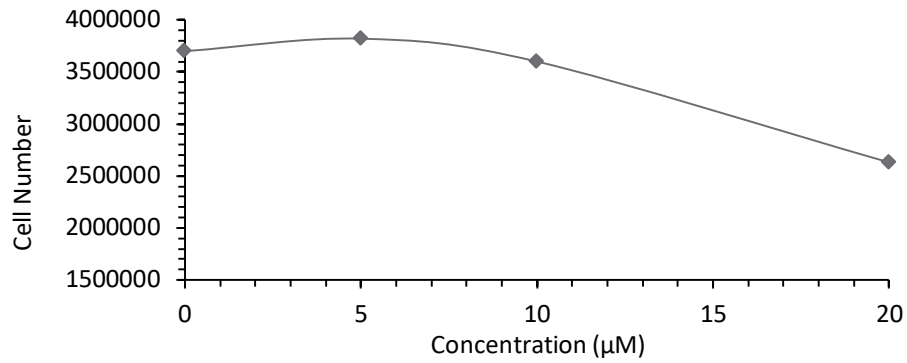
	Control	5µM	10µM	20µM
Total cells in sample	3.7×10^6	3.82×10^6	3.6×10^6	2.63×10^6
Percentage cell viability	81.8	76	76	86

Figure 4.6: Effect of increasing doses of LG100A on the cell number of pancreatic adenocarcinoma cell line MIA-PaCa$_2$ after 96-hour exposure. "0" denotes the control sample with concentrations of 5µM, 10µM and 20µM being tested. Cell viability is expressed as a percentage based on acridine Orange staining the entire population and DAPI which stains non-viable cells (n=1).

Control   **5µM**   **10µM**   **20µM**
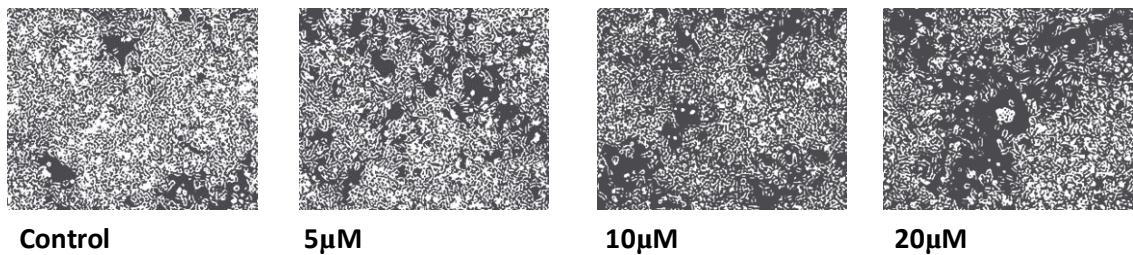
Figure 4.7: Microscope images of pancreatic adenocarcinoma cell line MIA-PaCa$_2$ exposed to increasing doses of LG100A over a 96- hour exposure time.
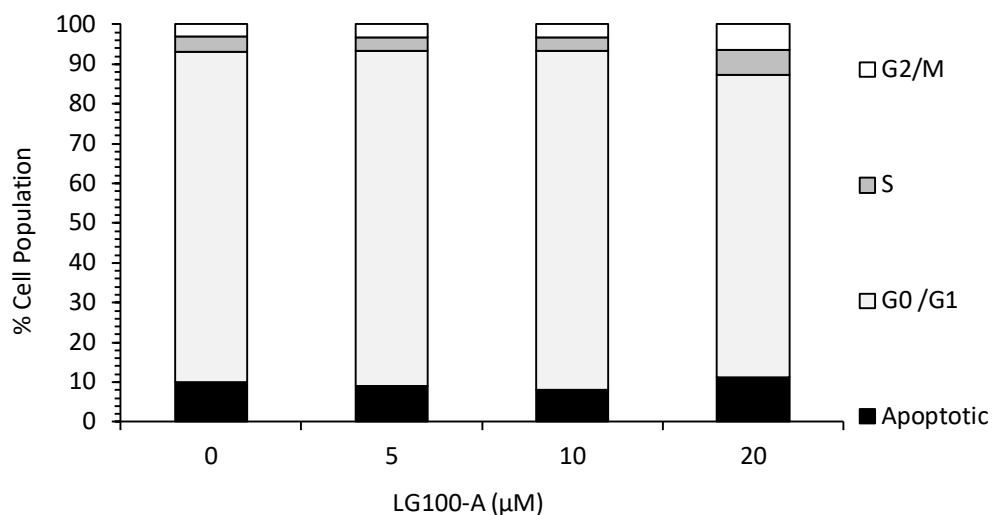
Cell cycle phase	Percentage of cell population			
	Control	5µM	10µM	20µM
Apoptotic	10	9	8	11
G_0 /G_1	83	84	85	76
S	4	3	3	6
G_2/M	3	3	3	6

Figure 4.8: Cell cycle response of pancreatic adenocarcinoma cell line MIA-PaCa$_2$ to increasing doses of

LG100A after 96-hour exposure time. "0" denotes the control sample and the percentage of the cell

population within each cycle stage is determined by the cell's DNA content with nuclear stain DAPI

(n=1).

4.4 - Discussion

From the IC_{50} values, two compounds from class 1 showed promising potency towards the three cancer cell lines tested. Although displaying poorer activity than the platinate gold standard cisplatin, these novel cobalt based compounds do display comparable and in some cases superior potency to that of carboplatin with LG101-2 also demonstrating superior potency towards the colonic adenocarcinoma cell line BE than oxaliplatin (IC_{50} = 3.7 ± 1.98µM and 8.56 ± 0.48µM respectively, table 4.5). Although potency data is initially promising the selectivity of these agents is much less impressive with none of the compounds displaying selectivity that is superior to the established platinate standards (figure 4.7).

As a number of these novel cobalt compounds exist in the form of Cobalt (III), their cytotoxic activity was also investigated in hypoxic conditions. As described in chapter 2, hypoxia significantly reduces the chemosensitivity of cells to platinum agents and hypoxic cytotoxicity ratios (HCR) are significantly below 1 in all cases. The results of HCR studies are presented in table 4.7 and these demonstrate that the novel cobalt (III) compounds are not selectively toxic to hypoxic MIA-PaCa$_2$ cells (table 4.6). Although these compounds display reduced activity in hypoxic conditions, their use in such environments should not be disregarded as LG152-1 is not as adversely affected by hypoxia (HCR = 0.61) as cisplatin (HCR = 0.036), oxaliplatin (HCR < 0.073) and carboplatin (HCR < 0.35) (table 4.6). It could therefore be argued that this improved activity in hypoxic conditions compared to the platinum standards (albeit poor in

comparison to other hypoxia activated prodrugs) is a platform on which the compounds can be developed with a view to enhancing activity under hypoxia.

Additional issues that need to be considered if these compounds are to be developed further is their solubility and stability. The compounds tested are not soluble in water/aqueous buffers and in some cases, a noticeable precipitate formed following the addition of compounds to cell culture media. This could account for the lack of activity observed in many of the compounds investigated in this study. Furthermore, initial studies demonstrated that reproducible data was difficult to obtain with some compounds suggesting that stability issues during storage maybe problematical.

Although the compounds possess many unfavourable properties two, of the compounds do possess a degree of cytotoxic activity that is comparable to platinates. With the mechanism of action of these cobalt complexes being unknown, preliminary mechanistic investigations were completed in the form of their effects on cell cycle kinetics and viability assays after a 96-hour exposure. The results of this study demonstrate that for both LG101-2 and LG100-A, there is a slight increase (just over 2%) in the population of cells within the S phase. The biggest effect on the cell cycle after exposure to the cobalt complexes is the percentage of cells in the G_2/M phase, which has more than doubled from the control to the highest concentration. This could therefore suggest the cobalt compounds initiate a level of M phase arrest; this is also reflected by the reduction of cells in the G_0/G_1 phase. The M phase or mitosis

phase is when molecular motors draw chromosomes apart and the cell divides. Many drugs such as Taxol and (as seen in chapter 2) cisplatin target this cell cycle phase freezing the process thus reducing the number of cells entering the G_1 phase resulting in reduced cell synthesis (Hartwell & Kastan, 1994). As the margins are small it is hard to fully determine if this is the case and further investigations at higher concentrations could be more informative. On reflection, the choice of a 96-hour exposure to compounds before assessing cell cycle parameters could mask any larger shifts in cell cycle kinetics that occurred before cell death. In addition to the cell cycle assay a viability assay was performed not only to help maintain a consistent cell number for the cell cycle assay but also show the effects of the drug toward cell viability and cell number. For both compounds the viability of the cells remains consistent between 70-80% yet it can be observed the cell number dramatically reduces at 20μM (figures 4.8 and 4.11) further suggesting that the compounds initiate some form of cell cycle arrest reducing cell replication thus reducing cell number without effecting viability. This could also be a manifestation of the long exposure times used in these experiments as described above. Furthermore, the preliminary mechanistic studies whilst indicating possible effects on the cell cycle does not reveal the basis of the differential activity of the two hit compounds in the chemosensitivity screens indicating the need for further investigations of this.

In conclusion, the majority of compounds evaluated here were largely inactive *in vitro* with the exception of LG101-2 and LG100-A. Both compounds showed a level of

potency that was comparable to the platinates (particularly carboplatin) but failed to show any significant improvement in the *in vitro* selectivity index compared to the platinates. In the context of drug evaluation procedures, the screen has identified compounds that are as potent as the platinates *in vitro* but fail to show any significant improvement in selectivity for cancer as opposed to non-cancer cells. On this basis, they are not promising compounds for future development. In addition to studies conducted under aerobic conditions, several Co(III) based compounds were also examined under hypoxic conditions. These studies demonstrated that whilst they do not selectively kill hypoxic cells *in vitro*, the level of resistance under hypoxia is less than that observed with the platinates. Whilst this could be viewed as an interesting result, the reality is that it does not improve the *in vitro* selectivity index and therefore these compounds are not good candidates for future development.

Chapter 5 - Ruthenium and Iridium β-Ketoiminate Compounds as Anti-Cancer Agents

5.1 - Introduction

5.1.1 - Ruthenium Compounds

Ruthenium complexes have become one of the most popular metals in drug discovery due in part to their similarities in ligand exchange kinetics to cisplatin complexes. Furthermore, their unique characteristics such as easily accessible oxidation states and its ability to mimic iron in binding to certain biological molecules make them good 'platforms' for drug development (Allardyce & Dyson, 2001). Another benefit of ruthenium complexes is that they have a tendency to adopt octahedral coordination geometries as opposed to the square planar geometries of platinum (figure 5.1). This is believed to favour the formation of inter-strand cross-links between DNA strands and this differs from the intra-strand cross link formation favoured by cisplatin. As a consequence, cell lines that have developed resistance to cisplatin via accelerated repair of the intra-strand crosslinks are still susceptible to ruthenium (Frühauf & Zeller, 1991).
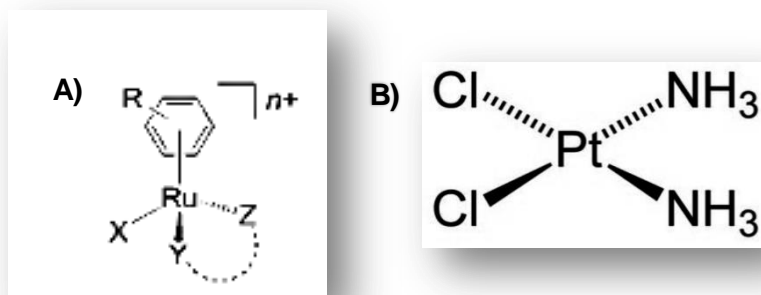
Figure 5.1: A) General chemical structure of ruthenium (II) arene "piano stool" complexes B) cisplatin's square planar geometry. Adapted from Sadler and Peacock (2008).

This co-ordination environment also plays an important role in the stabilisation of the complexes in varying oxidation states, thus dictating the redox properties of the central metal ion (Antonarakis & Emadi, 2010; Baitalik & Adhikary, 1997; Chakravarty & Bhattacharya, 1996). An additional advantage to this differing ligand geometry is the ability to fine tune ligand affinities, substitution rates and redox potential (Amin & Buratovich, 2009). This increases the specificity of the agents towards cancerous cells as the majority of the drug will be deposited in the cancer cells, which, in turn increases the therapeutic activity of the drug. These properties are summarised in figure 5.2.
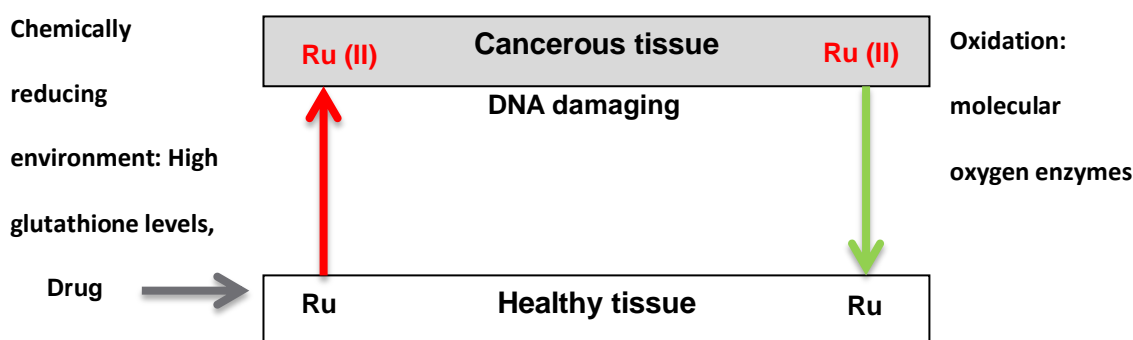
Figure 5.2: Oxidation states of ruthenium, adapted from (Allardyce & Dyson, 2001). A unique property of ruthenium is its easily accessible oxidation states existing as its inert state Ru(III), and biologically active state Ru(II). Ru(III) can therefore be administered as a pro-drug which is converted to its active state in reducing environment improving selectivity and bioavailability of the drug (Antonarakis & Emadi, 2010).

Ruthenium compounds have an array of clinical applications including use as immunosuppressant's and antimicrobials, and now Novel Anti-Tumour Metastasis Inhibitor A (NAMI-A) is the first representation of a ruthenium complex (III) complex to undergo clinical trials. NAMI-A has entered phase II clinical trials as an anti-metastatic agent and is demonstrating potential importance to the treatment of cancer (Büchel et al., 2017). The proposed mechanism(s) of action of NAMI-A include its direct effect on tumour cell DNA via coordination binding to nucleic acids, transient cell cycle arrest of tumour cells in the pre-mitotic G_2/M phase and the inhibition of matrix metalloproteinases which play a critical role in angiogenesis and the invasion and metastatic process (Antonarakis & Emadi, 2010; A Bergamo et al., 1999; Pluim, van Waardenburg, Beijnen, & Schellens, 2004; Vacca et al., 2002; Zorzet et al., 2000). These

anti-angiogenic and anti-invasive properties allow NAMI-A to specifically target tumour metastases, preventing both the formation of metastases but also their growth once established (Leijen et al., 2015). Not only has NAMI-A showed selectivity to solid tumours as a mono-therapy chemotherapeutic agent but has recently completed a phase I/II study in combination with gemcitabine as a second line treatment for non-small cell lung cancer (Alberta Bergamo, Riedel, Dyson, & Sava, 2015).

5.1.2 - Iridium Compounds

In contrast to ruthenium complexes, Iridium complexes have received much less attention as potential anti-cancer agents. This previous lack of interest is due to them being considered unlikely candidates owing to the kinetic inertness of iridium as a transitional metal centre (Geldmacher, Oleszak, & Sheldrick, 2012). Although known for being inert, iridium with the addition of pentamethylcyclopentadienyl (CP) forming the half sandwich fragment CP*Ir[III] has exhibited cytotoxic activity towards the A2780 human ovarian cell line. The investigation by Liu et al (2011) summarised that the chemical reactivity and cytotoxic activity of CP*Ir[III] complexes can be controlled by variation of the chelating ligands. Therefore, the optimisation of the ligands surrounding these iridium complexes is of importance in producing chemotherapeutic iridium complexes.

Investigations by Lord et al (2015) concluded that iridium complexes with a β-ketoiminato ligand generated promising IC_{50} values. In addition, it was observed that almost all the β-ketoiminato complexes were slightly more active than cisplatin with

activity against cisplatin resistant A2780cis cells. The same β-ketoiminato complexes were also more active under hypoxic conditions suggesting they are hypoxia sensitive and as described in the previous chapter, this characteristic property is of particular interest in the field of anti-cancer drug development. This data is therefore very encouraging as it could suggest iridium complexes target both aerobic and hypoxic cells in solid tumours with a higher affinity for cancer specific hypoxic environments.

5.1.3 - Aims and Objectives

In a collaboration with Dr Rianne Lord and Professor Patrick McGowan at the University of Leeds, a series of ruthenium and iridium complexes bearing β-ketoiminate ligands were synthesised and previous studies conducted by Dr Lord evaluated their activity against a panel of cell lines *in vitro*. These were all cancer cell lines and the results showed that a number of these compounds have potent cytotoxic profiles (comparable to platinates) and are not adversely affected by hypoxic conditions (R. M. Lord et al., 2015). In the context of this thesis, the purpose of this chapter was to determine the activity of these complexes against the non-cancerous ARPE-19 cell line with the aim of establishing the *in vitro* selectivity index and exploring its value as a decision-making tool compared to just potency alone.

5.2 - Methods

5.2.1 - Preparation of Drug Stock Solution

A series of iridium and ruthenium based compounds were obtained from Professor McGowan's research group, their chemical structures and the preparation of stock solutions are presented below.

Compound (as cited in paper) Metal	Molecular Weight	Weight (mg)	Volume DMSO (µl)	Stock solution (mM)	Structure
RML075 (1) Ruthenium	525.03	5.4	102.8	100	
RML100 (7) Ruthenium	585.93	8.7	148.48	100	
RML102 (8) Ruthenium	585.93	9.5	162.14	100	
RML368 (9) Ruthenium	632.99	10.2	161.14	100	
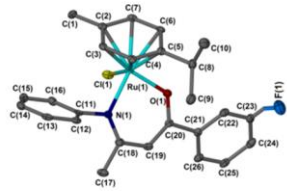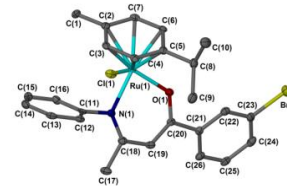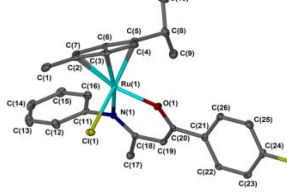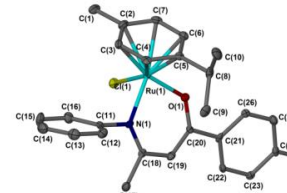
Table 5.1: Ruthenium and Iridium β-ketoiminate compounds structure and stock solution preparation.

Compound (as cited in paper) Metal	Molecular Weight	Weight (mg)	Volume DMSO (µl)	Stock solution (mM)	Structure
RML249 (11) Ruthenium	521.06	7.6	145.85	100	
RML265 (12) Ruthenium	557.10	8.6	154.37	100	
RML113 (13) Ruthenium	561.06	6.7	119.42	100	
RML363 (14) Ruthenium	430.94	10.7	248.29	100	
RML107 (15) Ruthenium	449.91	12	226.7	100	
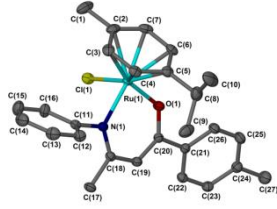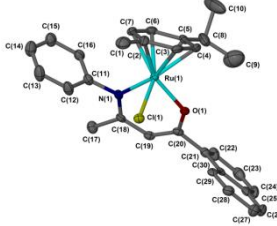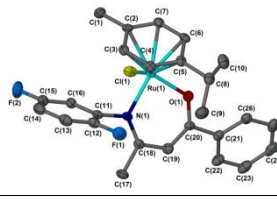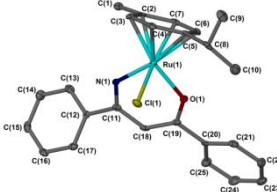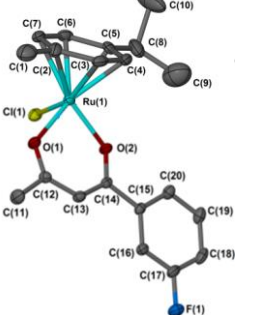
Table 5.1 (continued): Ruthenium and Iridium β-ketoiminate compounds structure and stock solution preparation.

Compound (as cited in paper) Metal	Molecular Weight	Weight (mg)	Volume DMSO (µl)	Stock solution (mM)	Structure
RML247 (18) Iridium	542.0	7.6	140.22	100	

Table 5.1 (continued): Ruthenium and Iridium β-ketoiminate compounds structure and stock solution preparation.

5.2.2 - Chemo-Sensitivity Testing

The response of HT-29 (human colon adenocarcinoma), MCF7 (human breast adenocarcinoma), A2780 (human ovarian carcinoma) and A2780cis (cisplatin resistant human ovarian carcinoma) was previously completed and published by Lord et al (2015) and these details are presented below (table 12.1 in the appendix). In this study, the activity of these compounds against the non-cancerous retinal epithelial cell line ARPE-19 was determined under aerobic conditions following continuous 96-hour exposures using the MTT assay, details of which have been described elsewhere in this thesis (see 2.5).

5.3 - Results

5.3.1 - Chemosensitivity Studies in Aerobic Conditions

The response of ARPE-19 cell line to various test RML compounds are presented in table 5.2. A broad range of IC_{50} values were obtained ranging from inactive ($IC_{50} > 100$ μM, RML247), moderately active ($IC_{50} = 51.55 \pm 5.14$μM, RML107) to active ($IC_{50} = 4.48 \pm 0.07$μM, RML075). The IC_{50} values in ARPE-19 cells were compared to those of HT-29 cells and these are presented in figure 5.2. With regards to potency, all of the novel RML compounds are less potent than cisplatin against the HT-29 cell line. In contrast, the potency of RML compounds against ARPE-19 cells is broadly similar to that of cisplatin with the exception of compounds 14 (RML107) and 15 (RML247) which were significantly less active. With regards to selectivity indices, the results presented in figure 5.4 demonstrate that none of the test compounds have selectivity indices that are greater than cisplatin. The only possible exception to this is RML247 which is inactive against ARPE-19 cells at the highest dose tested.

5.3.1.1 - Response of ARPE19 Cells to Ruthenium and Iridium Complexes Under Aerobic Conditions

Compound	Compound number as cited in Lord et al (2015)	IC$_{50}$ value (µM) ± SD
		ARPE-19
RML075	1	4.48 ± 0.07
RML100	7	7.76 ± 0.07
RML102	8	14.59 ± 0.41
RML368	9	12.0 ± 1.48
RML249	11	9.17 ± 2.36
RML265	12	7.17 ± 0.93
RML113	13	3.62 ± 0.03
RML363	14	32.03 ± 9.23
RML107	15	51.55 ± 5.14
RML247	18	>100
Cisplatin	-	6.41 ± 0.95

Table 5.2: Response of the non-cancerous retinal epithelial cell line ARPE-19 following continuous 96-hour exposure to novel RML Ruthenium and Iridium β-ketoiminate based compounds. The results presented are the mean IC50 values ± standard deviations for three independent experiments n=3 (each individual experiment replicated twice). The ">" symbol represents the highest dose tested *in vitro*.

5.3.1.2 - Comparison of RML Compounds with Platinum Based Anti-Cancer Drugs Chemosensitivity Data *In Vitro*
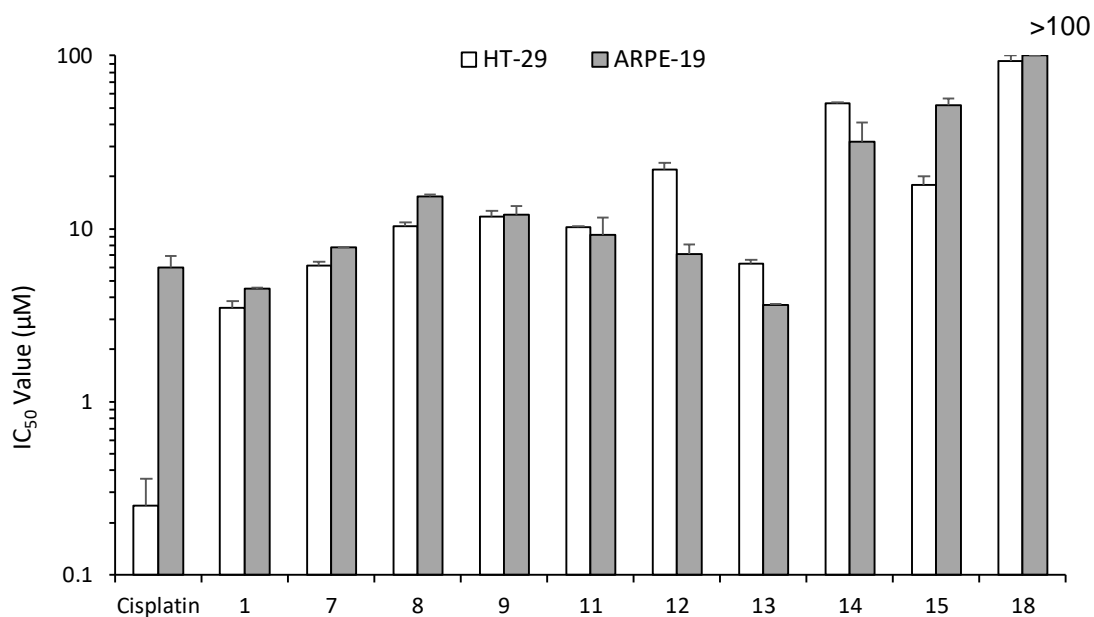
Figure 5.3: Comparison of the potency of novel RML Ruthenium and Iridium β-ketoiminate based compounds to cisplatin on HT-29 and ARPE-19 cells. The values presented are the mean IC_{50} values ± standard deviation of three independent experiments n=3 (each individual experiment replicated twice). RML247 (18) IC_{50} value on ARPE-19 cell line was displayed as 100μM but as it's IC_{50} value is higher than the maximum concentration tested (100μM) no SD is available.
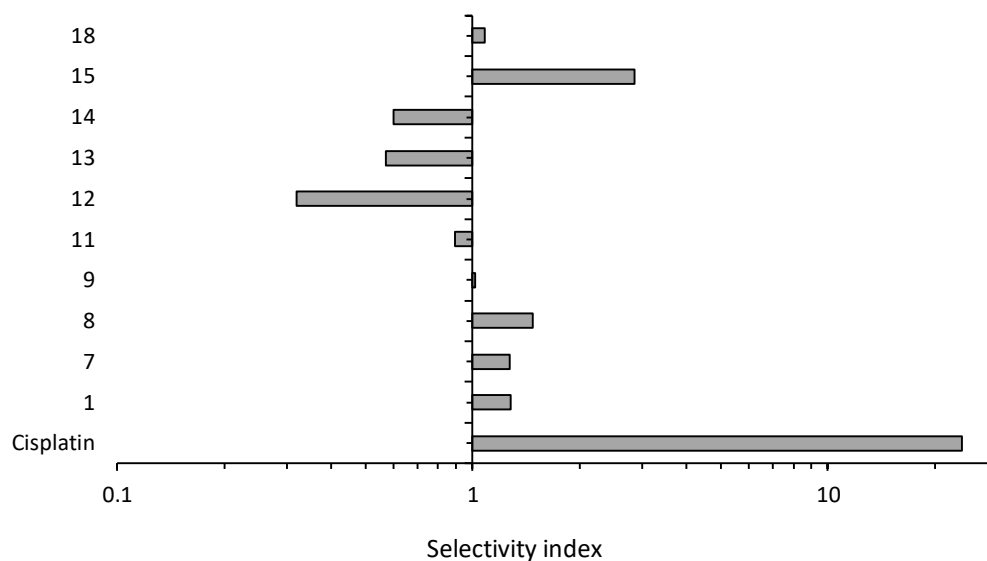
Compound	HT-29
1	1.28
7	1.27
8	1.48
9	1.02
11	0.89
12	0.32
13	0.57
14	0.6
15	2.86
18	1.08
Cisplatin	23.88

Figure 5.4: Comparison of the selectivity of novel RML Ruthenium and Iridium β-ketoiminate based compounds to cisplatin. The selectivity index is defined as the mean IC_{50} for non-cancerous cells divided by the IC_{50} of cancer cells. Values greater than 1 indicate that compounds have selectivity for cancer cells as opposed to non-cancer cells. As the mean IC_{50} values are used to calculate selectivity indices, no error bars are included on the graphs. RML247 (18) IC_{50} value on ARPE-19 cell line was displayed as 1.08 (IC_{50} value set at 100μM in ARPE-19 cell line therefore SI= >1.08).

5.4 - Discussion

Initially, the testing against cancer cells on this class of compounds was conducted by the McGowan research group and my study focused on providing additional data investigating the response of non-cancerous ARPE-19 retinal epithelial cells to the same set of compounds. This nevertheless played a key role in getting the work published (R. M. Lord et al., 2015). This discussion essentially focuses on the ARPE-19 data generated in this thesis in the context of using potency and selectivity indices to make decisions about progression of compounds for further testing.

The response of a panel of four cancer cell lines (i) HT-29 (colon adenocarcinoma), (ii) MCF-7(breast ductal carcinoma), (iii) A2780 (ovarian carcinoma) and (iv) A2780*cis* (cisplatin resistant ovarian carcinoma) was determined alongside the response of ARPE-19 cells as described above. With regards to potency, RML075 (compound 1) was the most active compound against all four cancer lines and was ~ 3-fold more active towards the cisplatin resistant A2780*cis* than cisplatin. It also showed evidence of selectivity in all cell lines with a selectivity index ranging from 1.28 to 2.35. Although this data initially presents compound 1 as a positive lead, it does not have a superior *in vitro* selectivity index compared to cisplatin with the exception of the cisplatin resistant A2780cis cell line where the *in vitro* selectivity index was 0.57. This data suggests compound 1 is likely to be inferior to cisplatin but on the other hand, its improved activity and selectivity against the cisplatin resistant cell lines suggests an alternative mechanism of action to cisplatin and this therefore warranted further

investigation of RML075. Other compounds were selected for further analysis and further details can be found in Lord et al (2015) and additional studies included analysis of the effect of hypoxia on cytotoxicity, inhibition of thioredoxin reductase and DNA damage induction. These studies demonstrated that these compounds have very different mechanisms of action than cisplatin and they were therefore of interest as potentially interesting form a mechanistic standpoint. In the context of the overall aim of this thesis, the key issue is whether or not analysis of potency and the *in vitro* selectivity index provides sufficient evidence to take compounds forward to *in vivo* testing. Whilst mechanistically interesting as described in Lord et al (2015), the experimental data suggests that the *in vitro* selectivity index is not sufficiently better than cisplatin to warrant taking these specific compounds forward for *in vivo* testing. It is unlikely that these compounds will have a better therapeutic index *in vivo* than cisplatin and on this basis, they were not selected for *in vivo* studies. As stated above however, they remain of interest from a mechanistic point of view and further studies at the University of Leeds are ongoing.

Chapter 6 -Iridium Complexes as Anti-Cancer Therapies

6.1 - Introduction

As previously discussed in chapter 5, iridium complexes in contrast to other organometallic complexes have received little interest in terms of their use as potential anti-cancer agents. This lack of interest is due to them being considered unlikely candidates owing to the kinetic inertness of iridium as a transitional metal centre (Geldmacher et al., 2012). Although previously known for their inert nature, an investigation by Lord et al. (2015) concluded that iridium complexes with a β-ketoiminato ligand exerted promising anti-cancer activity toward a number of cancerous cell lines. In addition, it was observed that almost all the β-ketoiminato complexes were slightly more active than cisplatin towards the cisplatin resistant cell line A2780cis.

Dr Gemma Sweeney of the Innovative Physical Organic Solutions (IPOS) at The University of Huddersfield has synthesised a series of iridium complexes and the fact that these were 'home grown' compounds that were novel made them worth including in this program of work. In addition, it potentially builds on the success of the iridium complexes synthesised by Patrick McGowans research group and extends the studies on this metal based complex. The aim of this study was therefore to evaluate these

against cancer cell lines initially to establish if any of these compounds had cytotoxic activity.

6.2 - Methods

6.2.1 - Preparation of Drug Stock Solution

A series of iridium based compounds were obtained from Dr Gemma Sweeny's research group, their chemical structures and the preparation of stock solutions are presented below.

Compound name	MW	Weight (mg)	Diluent	Volume (µl)	Concentration (mM)	Structure
GMSI-1	796.70	4	DMSO	50.21	100	
GMSI-3	1162.50	5.1	DMSO	43.90	100	
GMSII-1	1000.29	2.4	DMSO	24	100	
GMSII-8	1784.22	6.8	DMSO	38.11	100	
GMSII-32	492.67	9.7	DMSO	196	79.13	
GMSII-33	1276.61	5.7	DMSO	44.65	64.61	
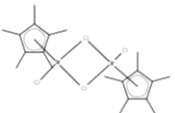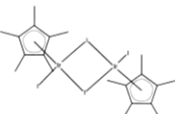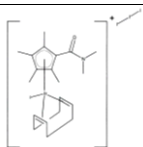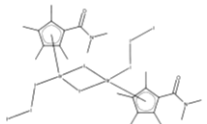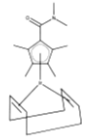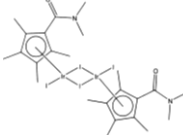
Table 6.1: Novel iridium compounds structure and stock solution preparation.

6.2.2 - Chemosensitivity Testing

The response of HT-29 (human colon adenocarcinoma), BE (human colonic carcinoma) and ARPE-19 (non-cancerous retinal epithelial) cell lines was determined under aerobic conditions following continuous 96-hour exposures to test compounds using the MTT assay, details of which have been described elsewhere in this thesis (see 2.5).

6.3 - Results

6.3.1 - Chemosensitivity Studies in Aerobic Conditions

The response of cell lines to the various GMS compounds are presented in table 6.2. The majority of these compounds proved to be inactive against the panel of cell lines with only two compounds showing activity below the highest dose tested. The lowest IC_{50} value was 62.51±22.90µM (GMSII-32) against the colorectal adenocarcinoma cell line HT-29. In regard to selectivity indices the majority of the compounds had IC_{50} values higher than the maximum concentration tested (100µM) except GMSII-1 on the colorectal carcinoma cell line BE (74.63 ± 11.19µM) and the aforementioned GMSII-32 on HT-29, which are both inactive against the non-cancerous retinal epithelial cell line ARPE-19.

	IC$_{50}$ value µM (S.D)		
Compound	BE	HT-29	ARPE-19
GMSI-1	>100	>100	>100
GMSI-3	>100	>100	>100
GMSII-1	74.63 ± 11.19	>100	>100
GMSII-8	>100	>100	>100
GMSII-32	>100	62.51 ± 22.90	>100
GMSII-33	>100	>100	>100
Cisplatin	0.66 ± 0.33	0.25 ± 0.11	6.41 ± 0.95

Table 6.2: Response of colorectal adenocarcinoma HT-29, colorectal carcinoma BE and the non-cancerous retinal epithelial cell line ARPE-19 following continuous 96-hour exposure to novel GMS iridium based compounds. The results presented are the mean IC$_{50}$ values ± standard deviations for three independent experiments n=3 (each individual experiment replicated twice). The ">" symbol represents the highest dose tested.

6.4 - Discussion

From these initial chemo-sensitivity investigations, it is very clear that these compounds do not display any cytotoxic activity towards cancerous cells. The most potent compound in this series was 250 times less potent than the gold standard cisplatin in the HT29 colorectal cell line. Only two compounds display potential selectivity toward the cancerous cell lines due to their inactivity on the non-cancerous cell line ARPE-19 but their poor potency on HT-29 cells and BE cells (IC$_{50}$ for GMSII-32 = 62.51 ± 22.90µM and IC$_{50}$ for GMSII-1 = 74.63 ± 11.19µM) make them unlikely candidates for further biological investigation. Whilst these results are disappointing, the identification of inactive compounds is still of value in the context of phenotypic screening programs. Although there is no on-going research with this research group

previous collaborations pave the way for future pre-clinical testing on any additional

compounds synthesised by IPOS.

Chapter 7 – Metal N-Heterocyclic Compounds as Anti-Cancer Agents

7.1 - Introduction

Transition metal N-heterocyclic carbene (metal-NHC) complexes are organometallic compounds consisting of a divalent organic ligand co-ordinated to the metal centre (figure 7.1) (Gasser et al., 2010). Free carbenes are characteristically unstable but once joined to a metal centre, they become stabilised and this has seen them become the most popular ligands for multiple applications including catalysis (Herrmann, 2002). Metal-NHC complexes have gained significant attention as potential anti-cancer agents due to their practical suitability for efficient drug design, fast optimisation (Liu & Gust, 2013), high degree of stability and their ease of development. NHCs bind strongly to transition metals such as gold, silver, platinum and ruthenium and several studies have demonstrated that they have anti-microbial and anti-cancer properties. Mechanistically all these metals interfere with multiple pathways, several of which play key roles in cancer biology (Oehninger, Rubbiani, & Ott, 2013).
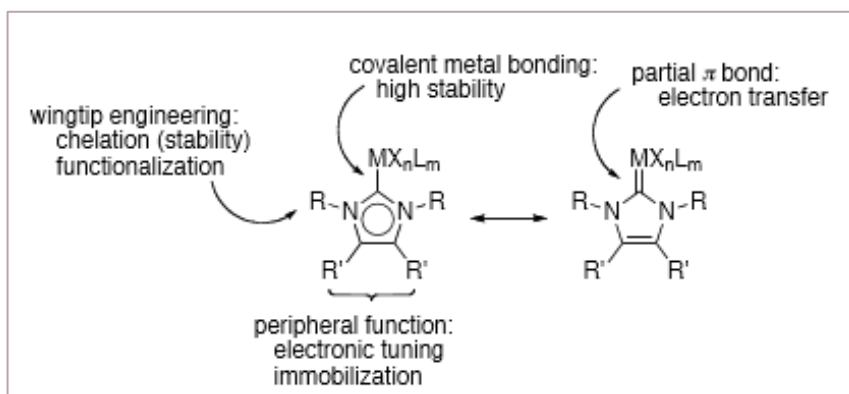
Figure 7.1: Structure of NHCs and the principles forming the basis of their appealing properties. Taken from Mercs and Albrecht (2010).

To exemplify this, a recent study published with collaborators at the University of Leeds (Dr Charlotte Willans) demonstrated that a silver NHC complex known as Ag8 (table 7.1) induced its cytotoxic effects *via* multiple mechanisms of action that did not involve alkylation to DNA. These mechanisms included (i) inhibition of topoisomerases I and II leading to single and double strand breaks in DNA (ii) inhibition of thioredoxin reductase (iii) inhibition of poly (ADP Ribose) polymerase (PARP) and (iv) inhibition of glycolysis (Allison et al., 2017). This study demonstrates that silver NHC complexes induce their cytotoxic effects *in vitro via* multiple mechanisms that are distinct from the platinates and they are therefore of considerable interest in the field of anti-cancer drug discovery.

Previous research regarding silver-NHCs has ubiquitously been in the antimicrobial field and their incorporation in various applications including wound dressing, creams and deodorants. The unparalleled structural diversity of NHCs offers high synthetic

flexibility, which alongside their strong σ donor capabilities (strong ability to bind to the metal ions) facilitates the modification of release rates making silver a promising NHC candidate (Johnson, Southerland, & Youngs, 2017; Mercs & Albrecht, 2010). In addition to its already established antimicrobial properties a number of studies have investigated silver NHCs as potential anti-cancer complexes (Mohamed, Lake, Laing, Phillips, & Willans, 2015). As silver is believed to have relatively low toxicity and is ubiquitously used in biomedical fields, it is an attractive choice as a potential anti-cancer compound. While silver is one of the most widely studied metals for anti-infective applications, a relatively small amount of research has been devoted to the metal for its anticancer properties (Wagers, Shelton, Panzner, Tessier, & Youngs, 2014). Its mechanism of action in regard to solid tumours is therefore not fully understood. It is therefore of great importance not only cytotoxic studies are completed on such complexes, but also comprehensive mechanistic studies would be of great importance to the organometallic anti-cancer therapeutic field.

Although silver NHCs exert promising activity *in vitro* their activity does not usually translate into comparable *in vivo* activity attributed to their lack of targeting and modification in metal species upon entering a biological environment (Allison et al., 2017). It is therefore of great interest to develop targeted drug delivery systems which allow the delivery and release of drug to specific sites.

In this chapter, a series of metal NHC complexes synthesised by Dr Charlotte Willans research group were evaluated *in vitro*. As in previous chapters, the aim of this

study was to characterise the activity of these compounds with regards to potency and selectivity to cancer cells *in vitro*. Compounds with superior properties than the platinates were selected and preliminary mechanistic studies conducted.

7.2 - Methods

7.2.1 - Chemical Structures and Preparation of Drug Stock Solution

All compounds for the exception HA236 (water soluble) were solubilised in DMSO. Compounds HA222 and HA223 appeared to initially dissolve in DMSO forming a homogenous solution but on recovery from storage at -20°C, precipitation occurred, and these compounds were therefore prepared fresh for each experiment. The chemical structures and preparation of stock solutions are presented below.

Compound name (description)	Molecular Weight	Weight (mg)	Volume (µl)	Concentration (mM)	Structure
Ag8 (Silver xanthine derivative)	717.89	9.1	126.76	100	
HA150 (Silver hydroxylated ligands)	395.6	7	176.94	100	
HA163 (Silver hydroxylated ligands)	609.6	8.3	136.15	100	
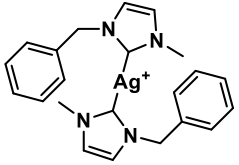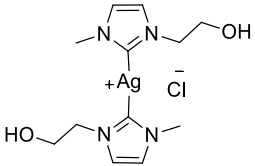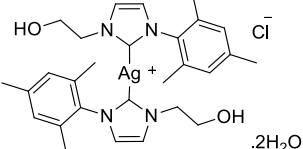
Table 7.1: Metal N-Heterocyclic compound structures, stock solution concentrations.

Compound name (description)	Molecular Weight	Weight (mg)	Volume (µl)	Concentration (mM)	Structure
NL-17 (Silver hydroxylated ligands)	455.7	6	131.66	100	
NL-21 (Silver hydroxylated ligands)	501.3	1.9	37.90	100	
NL-26 (Silver hydroxylated ligands)	547.8	2	36.51	100	
HA240 (Silver amino acid based ligand)	562.1	5	88.95	100	
HA222 (Silver polymer ligand)	490.8	7.4	150.77	100	
HA223 (Silver polymer ligand)	566.9	6.6	116.42	100	

Table 7.1 (continued): Metal N-Heterocyclic compound structures, stock solution concentrations.

Compound name (description)	Molecular Weight	Weight (mg)	Volume (µl)	Concentration (mM)	Structure
HA221 (Silver poly-L-glutamic acid)	608.5	12.5	205.42	100	
NL-37 (Silver hydroxylated ligands)	548.08	2.1	38.32	100	
NL-39 (Silver hydroxylated ligands)	556.04	1	18	100	
HA241 (Silver amino acid based ligand)	923.07	5.5	59.58	100	
HA266 (Silver hydroxylated ligands)	726.15	9.3	124.6	100	

Table 7.1 (continued): Metal N-Heterocyclic compound structures, stock solution concentrations.

Compound name (description)	Molecular Weight	Weight (mg)	Volume (µl)	Concentration (mM)	Structure
HA229 (copper xanthine derivative)	439.98	3.5	79.55	100	
HA230 (copper xanthine derivative)	473.96	6.1	128.7	100	
HA269 (Ruthenium xanthine derivative)	514.05	2.1	40.85	100	
HA270 (Ruthenium xanthine derivative)	556.10	2	35.97	100	
HA271 (Ruthenium xanthine derivative)	590.08	2	33.89	100	
MD-9 (Silver, clotrimazole based ligands)	467.04	9.7	207.69	100	
HB-34 (Silver clotrimazole based ligands)	501	8.7	173.65	100	
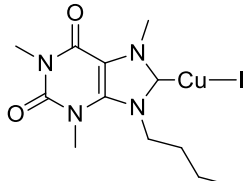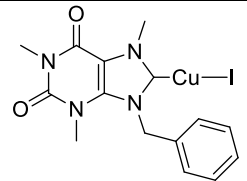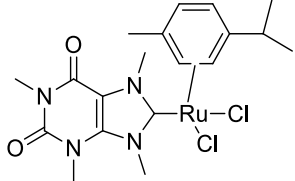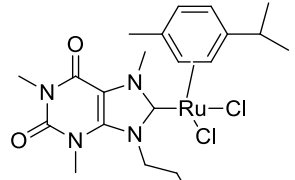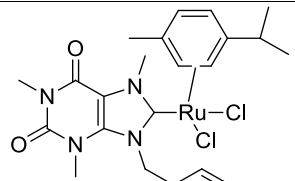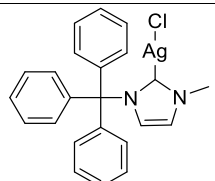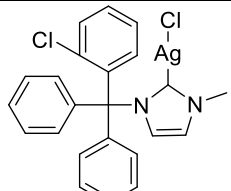
Table 7.1 (continued): Metal N-Heterocyclic compound structures, stock solution concentrations.

Compound name (description)	Molecular Weight	Weight (mg)	Volume (µl)	Concentration (mM)	Structure
HB-38 (Silver clotrimazole based ligands)	527.02	10.5	199.23	100	
MD-44 (Silver clotrimazole based ligands)	493.06	6.4	129.80	100	
HA197 (Silver clotrimazole based ligands)	788.76	6.2	78.60	100	
HA201 (Silver clotrimazole based ligands)	732.16	7.7	105.17	100	
HB-39 (Silver clotrimazole based ligands)	577.04	5	86.64	100	
HA200 (Silver clotrimazole based ligands)	782.18	5	63.92	100	
HA202 (Silver clotrimazole based ligands)	642.09	1.1	17.13	100	
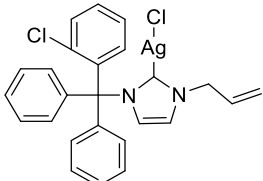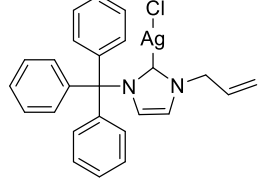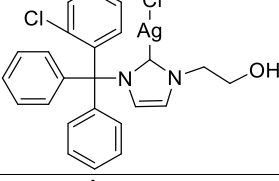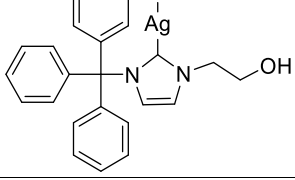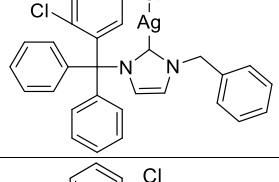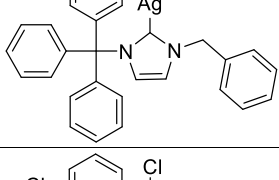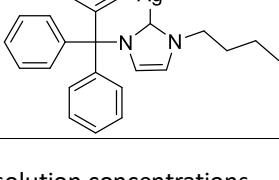
Table 7.1 (continued): Metal N-Heterocyclic compound structures, stock solution concentrations.

Compound name (description)	Molecular Weight	Weight (mg)	Volume (µl)	Concentration (mM)	Structure
HB-16 (Silver clotrimazole based ligands)	643.99	7.5	118.11	100	
HA327 (Silver amino acid based ligands)	778.2	1.2	15.42	100	
HA333 (Silver amino acid based ligands)	514.0	4.1	79.7	100	
HB-13 (Silver clotrimazole based ligands)	621.94	2.5	40	100	
HB-18 (Silver clotrimazole based hydroxylated ligands)	913.04	10.9	119.38	100	
HA341 (Silver clotrimazole based ligands)	788.76	2	25.34	100	
HA345 (Silver clotrimazole based ligands)	732.16	2.3	31.41	100	
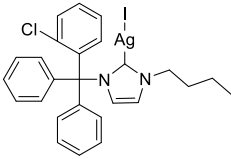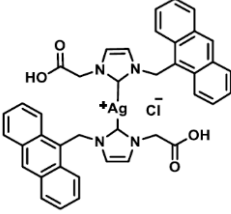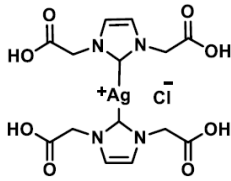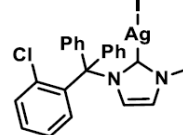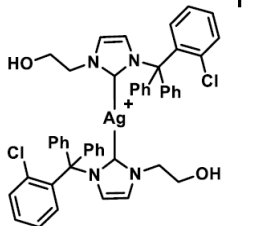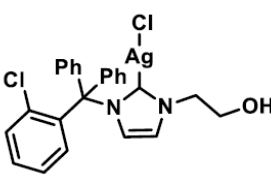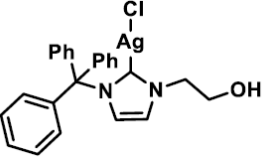
Table 7.1 (continued): Metal N-Heterocyclic compound structures, stock solution concentrations.

7.2.2 - Chemo-Sensitivity Testing, Analysis of Cell Viability and Cell Cycle Parameters

The response of cell lines following continuous 96-hour exposures to test compounds under aerobic conditions and as a drug-polymer system was determined using the MTT assay, details of which have been described elsewhere in this thesis (see 2.5 for aerobic MTT assay and section 7.2.3 for further description of drug-polymer systems). Analysis of cell viability and induction of apoptosis was determined using the NC3000 cytometer, details of which have been described elsewhere (see 2.6). For these experiments, drug exposure concentrations ranged from 2.5µM to 10µM; duration of drug exposures was set at 96 hours to replicate the conditions of the MTT assays.

7.3 - Results

7.3.1 - Chemosensitivity Studies in Aerobic Conditions

Initially all the compounds provided were tested on the Panc10.05 cells with the most potent compounds (with IC_{50} values below 10µM) tested further on ARPE-19 cells. A broad spectrum of activity was obtained ranging from inactive at the highest dose tested (IC_{50}> 100µM; HA151 for example) to potent activity (IC_{50} = 1.25 ± 0.50µM; HA197). Compounds displaying desirable potency and selectivity in the first round of testing were also further investigated on two additional cancerous cell lines MIA-PaCa$_2$ and BE. The only exceptions to this were HA341/345 which were submitted by the Willans group later together with a request to test primarily on the MIA-PaCa$_2$ cell line

to serve as a direct comparison to their corresponding one ligand complex (HB18) which was more potent in the MIA-PaCa$_2$ cell line the Panc10.05 cell line. The full set of chemosensitivity data is displayed in table 7.3 with the response of selected compounds presented in figure 7.2 alongside the results for the platinum based compounds. The selectivity index data for selected test compounds and platinates is presented in figure 7.3.

Compound	IC$_{50}$ µM (SD)			
	Panc10.05	MIA-PA-CA2	BE	ARPE-19
Ag8	11.33±0.4	4.09±0.36	5.85±1.59	36.7± 6.36
HA150	30.57±13.2	-	-	>100
HA151	>100	-	-	-
HA163	24.0±3.43	-	-	-
HA197	1.25±0.50	3.30±1.22	5.75±4.57	21.86±4.41
HA200	9.59±1.23	-	-	-
HA201	5.27±1.66	5.86±1.31	6.13±2.96	27.99±4.19
HA202	10.14±4.61	-	-	16.28±3.15
HA221	14.35±3.73	-	-	-

Table 7.2: Response of pancreatic adenocarcinoma cell lines Panc10.05 and MIA-PaCa$_2$, colorectal carcinoma cell line BE and non-cancerous retinal epithelial cell line ARPE-19, following continuous 96-hour exposure to novel metal NHC complexes in aerobic conditions. The results presented are the mean IC$_{50}$ values ± standard deviations for three independent experiments n=3 (each individual experiment replicated twice). The most promising compounds in terms of potency are highlighted in red. The ">" symbol represents the highest dose tested *in vitro*.

Compound	IC$_{50}$ μM (SD)			
	Panc10.05	MIA-PA-CA2	BE	ARPE-19
HA222	21.06±1.20	-	-	-
HA223	9.17±2.27	-	-	-
HA225	17.05±6.71	-	-	-
HA229	>100	-	-	-
HA236	12.27±3.20	-	-	>100
HA240	7.51±0.34	4.85±2.56	5.4±3.56	19.01±5.12
HA241	10.44±1.86	-	-	-
HA266	8.27±2.06	6.15±3.57	12.0±3.63	13.65±2.91
HA269	93.66±5.06	-	-	-
HA270	>100	-	-	-
HA271	>100	-	-	-
HA327	26.34±11.47	-	-	68.7±7.16
HA230	66.93±12.90	-	-	-
HA333	>100	-	-	>100

Table 7.2 (continued): Response of pancreatic adenocarcinoma cell lines Panc10.05 and MIA-PaCa$_2$, colorectal carcinoma cell line BE and non-cancerous retinal epithelial cell line ARPE-19, following continuous 96-hour exposure to novel metal NHC complexes in aerobic conditions. The results presented are the mean IC$_{50}$ values ± standard deviations for three independent experiments n=3 (each individual experiment replicated twice). The most promising compounds in terms of potency are highlighted in red. The ">" symbol represents the highest dose tested *in vitro*.

Compound	IC$_{50}$ μM (SD)			
	Panc10.05	MIA-PA-CA2	BE	ARPE-19
HA341	-	3.29±0.93	-	90.75±12.67
HA345	-	2.73±0.34	-	92.99±7.45
HB-13	10.04±6.79	5.72±2.30	3.31±1.16	24.21±2.60
HB-16	3.85±1.95	4.55±3.87	3.59±0.93	8.67±1.48
HB-18	13.28±8.16	6.89±2.07	1.99±0.31	15.82±2.93
HB-34	7.10±3.67	11.72±1.56	18.04±4.41	>50
HB-38	9.38±5.63	6.32±4.8	6.73±1.07	11.49±2.96
HB-39	5.75±1.41	7.0±1.61	8.44±1.25	10.25±0.76
MD-9	16.1±0.89	-	-	26.65±7.78
MD-44	16.06±1.96	-	-	27.47±7.52
MD-46	16.80±1.85	-	-	13.77±6.54
NL-17	14.74±3.44	-	-	-
NL-21	16.99±4.07	-	-	-
NL-26	2.95±0.47	5.68±1.80	6.97±2.64	21.44±2.92

Table 7.2 (continued): Response of pancreatic adenocarcinoma cell lines Panc10.05 and MIA-PaCa$_2$, colorectal carcinoma cell line BE and non-cancerous retinal epithelial cell line ARPE-19, following continuous 96-hour exposure to novel metal NHC complexes in aerobic conditions. The results presented are the mean IC$_{50}$ values ± standard deviations for three independent experiments n=3 (each individual experiment replicated twice). The most promising compounds in terms of potency are highlighted in red. The ">" symbol represents the highest dose tested *in vitro*.

	IC$_{50}$ µM (SD)			
Compound	Panc10.05	MIA-PA-CA2	BE	ARPE-19
NL-37	15.77±1.03	-	-	-
NL-39	33.18±3.49	-	-	-
Cisplatin	1.71 ± 0.41	3.62 ± 0.74	0.66 ± 0.33	6.41 ± 0.95
Carboplatin	10.45 ± 3.15	35.59 ± 7.91	32.72 ± 4.64	77.73 ± 10.52
Oxaliplatin	7.54 ± 3.85	6.44 ± 1.05	8.56 ± 0.48	3.12 ± 0.28

Table 7.2 (continued): Response of pancreatic adenocarcinoma cell lines Panc10.05 and MIA-PaCa$_2$, colorectal carcinoma cell line BE and non-cancerous retinal epithelial cell line ARPE-19, following continuous 96-hour exposure to novel metal NHC complexes in aerobic conditions. The results presented are the mean IC$_{50}$ values ± standard deviations for three independent experiments n=3 (each individual experiment replicated twice). The most promising compounds in terms of potency are highlighted in red. The ">" symbol represents the highest dose tested *in vitro*.

7.3.2 - Comparison of "hit" Novel Metal NHC Complexes to Platinum Compounds

The seven "hit" compounds chosen based on their potency and selectivity index are displayed in figures 7.2 and 7.3 respectively. Overall the "hit" compounds show either improved or comparable potency compared to oxaliplatin and carboplatin on Panc10.05, MIAPaCa$_2$ and BE cell lines. Of the cancer cell lines tested, cisplatin is the most active platinum agent making it the gold standard to which compare our novel compounds. With regards to the test compounds, only HA197 was more active against Panc10.05 and MIA-PaCa$_2$ cell lines compared to cisplatin. The activity of all the

selected compounds were nevertheless comparable to the level of activity obtained

for carboplatin and oxaliplatin (figure 7.2. The selectivity index of the test compounds

generally demonstrated significant selectivity for cancer cells compared to ARPE-19

cells with SI values ranging from 0.77 to 17.49 (figure 7.3)) with only a handful of

compounds failing to produce a statistically significant reduction in potential toxicity in

the non-cancerous cell lines opposed to the cancerous cell lines (figure 7.3). Of

particular note, the largest selectivity index was 17.49 for HA197 against the

pancreatic adenocarcinoma cell line Panc10.05 and this was significantly greater than

the highest SI obtained by cisplatin (SI = 3.75), oxalipatin (SI = 7.44) and carboplatin (SI

= 0.41).
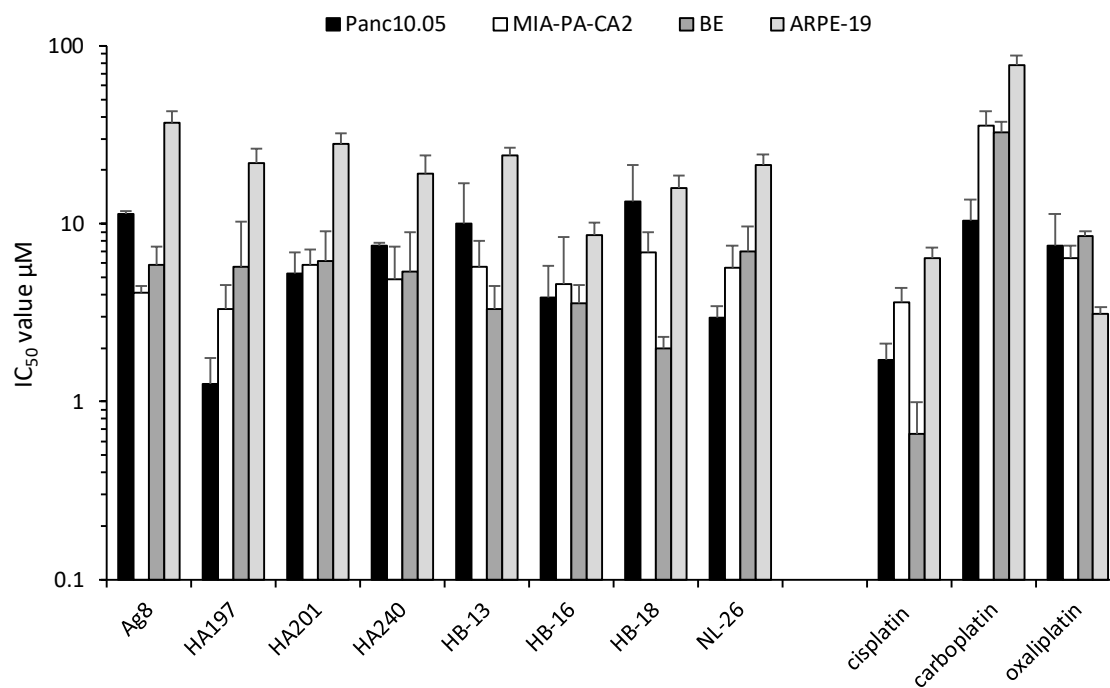
Figure 7.2: Comparison of the potency of novel metal NHC complexes to cisplatin, carboplatin and oxaliplatin on Panc10.05, MIAPaCa$_2$, BE and ARPE-19 cell lines. The values presented are the mean IC$_{50}$ values ± standard deviation of three independent experiments n=3 (each individual experiment replicated twice).
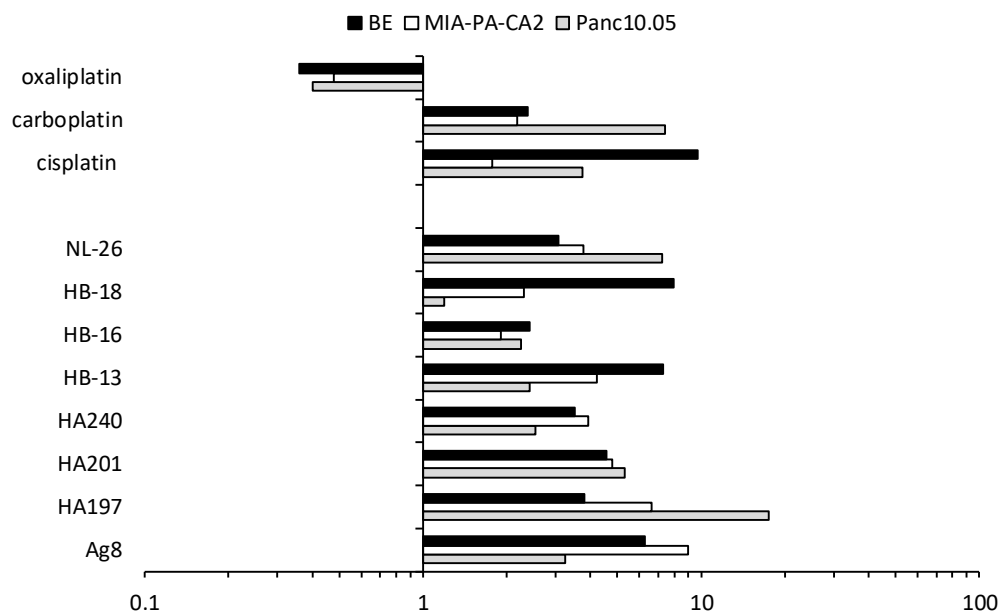
Compound	MIA-PaCa$_2$	p-value	BE	p-value	Panc10.05	p-value
Ag8	8.97	0.012	6.27	0.0081	3.24	0.018
HA197	6.62	0.026	3.8	0.090	17.49	0.013
HA201	4.78	0.018	4.57	0.030	5.31	0.0081
HA240	3.92	0.035	3.52	0.0049	2.53	0.055
HB-13	4.23	0.018	7.31	0.0054	2.41	0.043
HB-16	1.91	0.098	2.42	0.021	2.25	0.047
HB-18	2.3	0.032	7.95	0.018	1.19	0.53
Nl-26	3.77	0.011	3.08	0.0016	7.27	0.010
Cisplatin	1.77	0.10	9.71	0.0043	3.75	0.025
Carboplatin	2.18	0.031	2.38	0.029	7.44	0.0089
Oxaliplatin	0.48	0.020	0.36	0.0064	0.41	0.047

Figure 7.3: Comparison of the selectivity of novel metal NHC compounds cells to cisplatin, carboplatin and oxaliplatin. The selectivity index is defined as the mean IC$_{50}$ for non-cancerous cells divided by the IC$_{50}$ of cancer cells. Values greater than 1 indicate that compounds have selectivity for cancer cells as opposed to non-cancer cells. As the mean IC$_{50}$ values are used to calculate selectivity indices, no error bars are included on the graphs. Ag8 a previous compound synthesised by the Charlotte Willans has also been used as a "yardstick" due to a wealth of previous research surrounding the complex. Statistical analysis was performed using a student's t-test where values <0.05 indicates a statistically significant difference between IC$_{50}$ values in cancerous and none cancerous cell lines.

7.3.3 - Cell Viability and Apoptosis Induction Investigations

Based on their potency and selectivity profile, seven "hit" compounds were selected for further investigation. The results of cell viability and induction of apoptosis using the NC3000 are presented in figures 7.4 to Y. In all cases, cells were treated with increasing concentrations of compound and their viability along with any cell cycle disruption was determined using the viability and cell cycle assays using the same data analysis outlined in section 3.3.5. The results for each of the compounds selected are described in the various sub-sections below.

7.3.3.1 - HA197

The effect of HA197 on the cell number and viability of MIA PaCa$_2$ is shown in figure 7.4. Following a continuous 96-hour exposure to HA197, a dose dependent reduction in cell number and percentage viability was obtained. The IC$_{50}$ obtained using the NC3000 (IC$_{50}$ = 3µM) was comparable to that obtained using the MTT assay described above (IC$_{50}$ = 3.30 $\pm$ 1.22µM). These results are also illustrated visually in figure 7.5 and they confirm that cell viability decreases in a dose dependent manner. The results of apoptosis induction in MIA PaCa$_2$ cells following continuous exposure to HA197 are presented in figure 7.6. These results indicate that HA197 induces apoptosis and it does so in a dose dependent manner (figure 7.6).
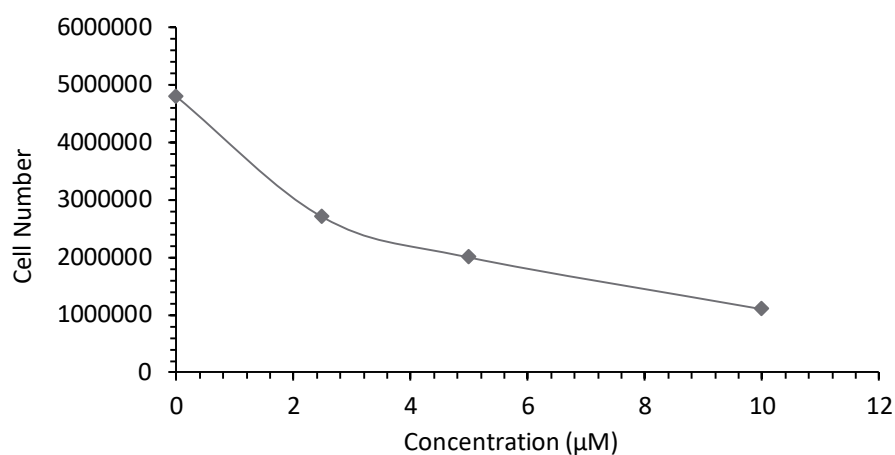
	Control	2.5µM	5µM	10µM
Total cells in sample	4.8×10^6	2.7×10^6	2.0×10^6	1.1×10^6
Percentage cell viability	98.1	91.7	93.3	87.5

Figure 7.4: Effect of increasing doses of HA197 on the cell number of pancreatic adenocarcinoma cell line MIA-PaCa$_2$ after 96-hour exposure. "0" denotes the control sample with concentrations of 2.5µM, 5µM and 10µM being tested. Cell viability is expressed as a percentage based on acridine Orange staining the entire population and DAPI which stains non-viable cells (n=1).
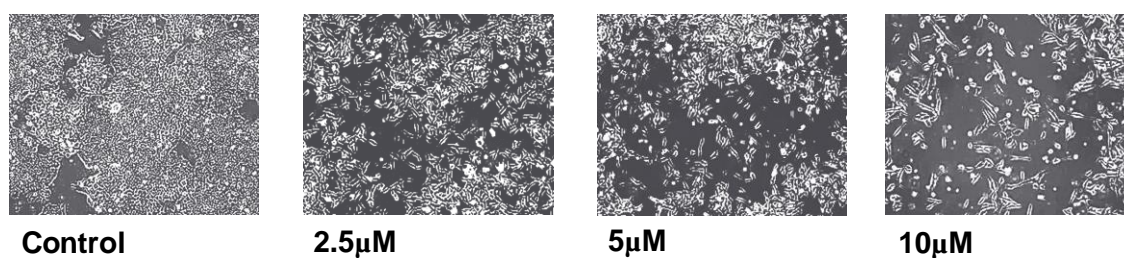
Figure 7.5: Microscope images of MIA-PaCa$_2$ cell line following 96-hour exposures to increasing doses of HA197.
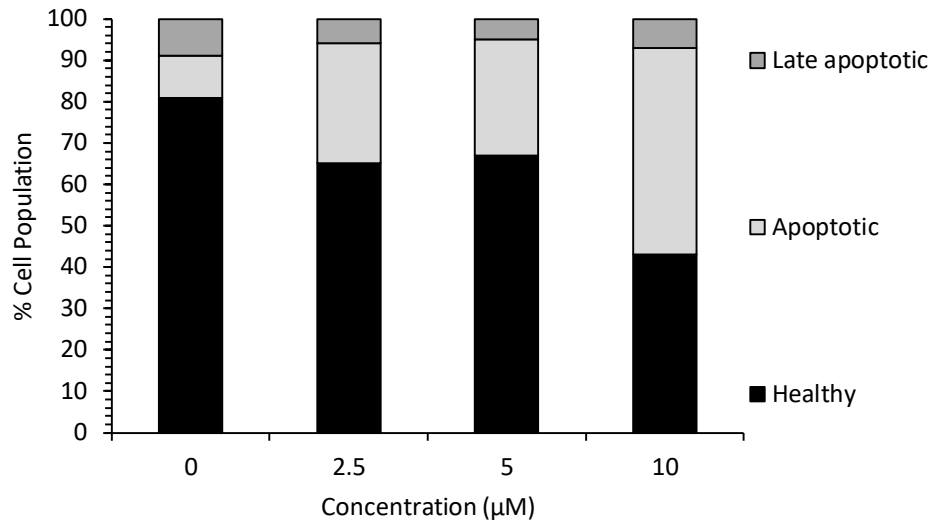
	Percentage of cell population			
Cell state	Control	2.5μM	5μM	10μM
Healthy	81	65	67	43
Apoptotic	10	29	28	50
Late apoptotic	9	6	5	7

Figure 7.6: Mitochondrial potential assay identifying induction of apoptosis in the pancreatic adenocarcinoma cell line MIA-PaCa$_2$ after 96-hour exposure to HA197. The exposure concentrations ranged from 2.5μM - 10μM with "0" denoting the control sample (n=1).

7.3.3.2 - HA201

The effect of HA201 on the cell number and viability of MIA PaCa$_2$ is shown in figure 7.7. Following a continuous 96-hour exposure to HA201, a dose dependent reduction in cell number and percentage viability was obtained. The IC$_{50}$ obtained using the NC3000 (IC$_{50}$ = <2.5µM) was much less than the results obtained using the MTT assay described above (IC$_{50}$ = 5.86 ± 1.31µM). Visually however, the images obtained at 2.5µM (figure 7.8) suggest that a considerable number of cells are present within the cultures. The reason for this discrepancy is unknown. The results of apoptosis induction in MIA PaCa$_2$ cells following continuous exposure to HA201 are presented in figure 7.9. These results along with visual morphological changes (figure 7.8) could indicate that HA201 induces apoptosis and it does so in a dose dependent manner (figure 7.9).
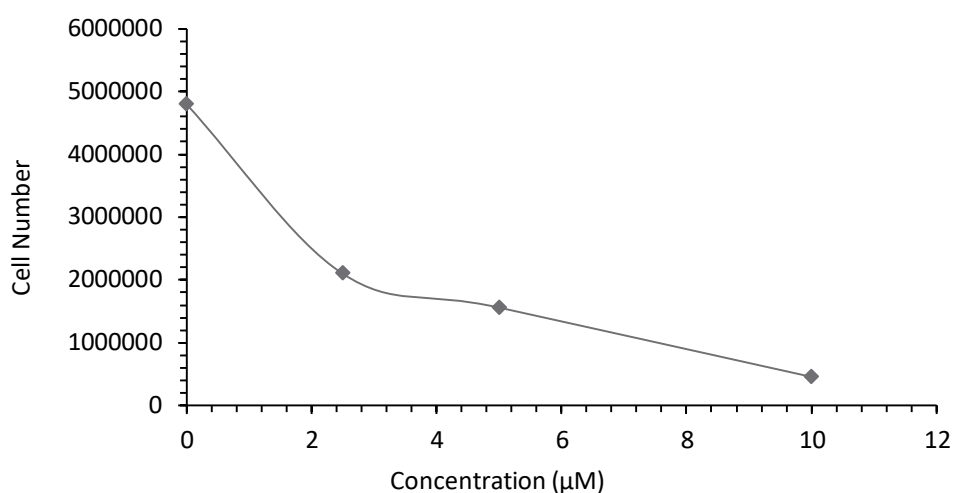
	Control	2.5μM	5μM	10μM
Total cells in sample	4.8×10^6	2.1×10^6	1.56×10^6	4.56×10^5
Percentage cell viability	98.1	88.9	85.5	64.5

Figure 7.7: Effect of increasing doses of HA201 on the cell number of pancreatic adenocarcinoma cell line MIA-PaCa$_2$ after 96-hour exposure. "0" denotes the control sample with concentrations of 2.5μM, 5μM and 10μM being tested. Cell viability is expressed as a percentage based on acridine Orange staining the entire population and DAPI which stains non-viable cells (n=1).
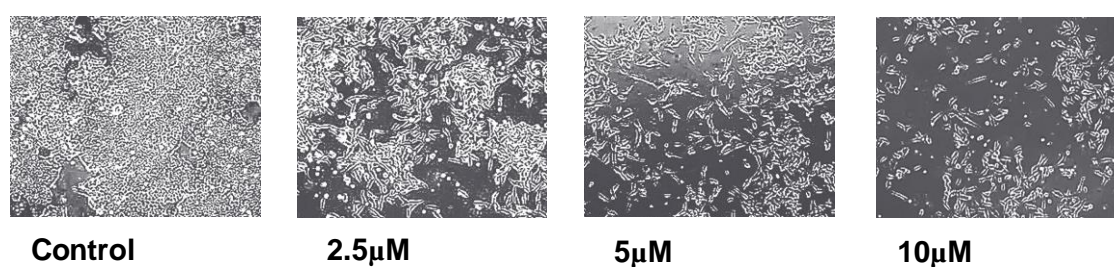
Figure 7.8: Microscope images of MIA-PaCa$_2$ cell line following 96-hour exposures to increasing doses of HA201.
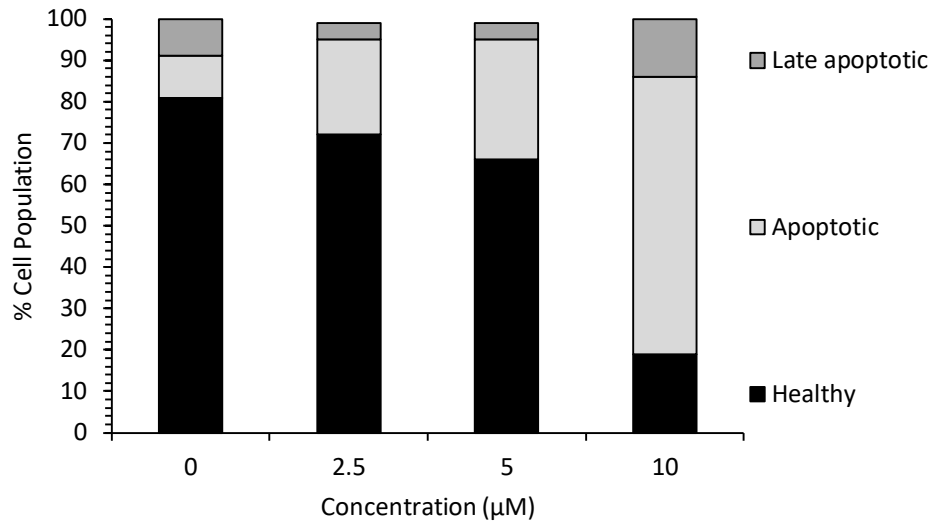
	Percentage of cell population			
Cell state	Control	2.5µM	5µM	10µM
Healthy	81	72	66	19
Apoptotic	10	23	29	67
Late apoptotic	9	4	4	14

Figure 7.9: Mitochondrial potential assay identifying induction of apoptosis in the pancreatic

adenocarcinoma cell line MIA-PaCa$_2$ after 96-hour exposure to HA201. The exposure concentrations

ranged from 2.5µM - 10µM with "0" denoting the control sample (n=1).

7.3.3.3 - HA240

The effect of HA240 on the cell number and viability of MIA PaCa$_2$ is shown in figure 7.10. Following a continuous 96-hour exposure to HA201, a dose dependent reduction in cell number and percentage viability was obtained. The IC_{50} obtained using the NC3000 (IC_{50} = 5µM approximately) was similar to the results obtained using the MTT assay described above (IC_{50} = 4.85 $\pm$ 2.56µM). Visually, these results are confirmed under the microscope (figure 7.11) where cell number is vastly reduced and cells appear to be floating opposed to functional and attached. The results of apoptosis induction in MIA PaCa$_2$ cells following continuous exposure to HA240 are presented in figure 7.12. These results are therefore indicative toward HA240 inducing apoptosis and in a dose dependent manner (figure 7.12).
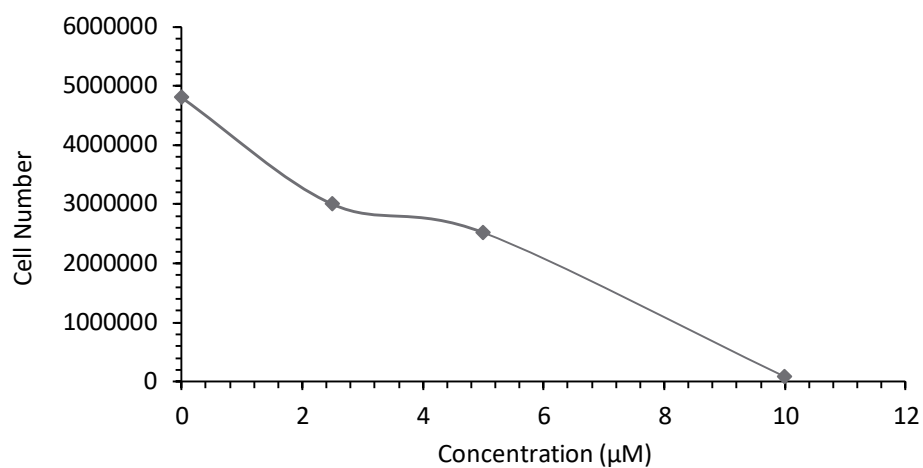
	Control	2.5µM	5µM	10µM
Total cells in sample	4.8×10^6	3×10^6	2.52×10^6	8.48×10^4
Percentage cell viability	98.1	82.4	85.1	69.9

Figure 7.10: Effect of increasing doses of HA240 on the cell number of pancreatic adenocarcinoma cell line MIA-PaCa$_2$ after 96-hour exposure. "0" denotes the control sample with concentrations of 2.5µM, 5µM and 10µM being tested. Cell viability is expressed as a percentage based on acridine Orange staining the entire population and DAPI which stains non-viable cells (n=1).
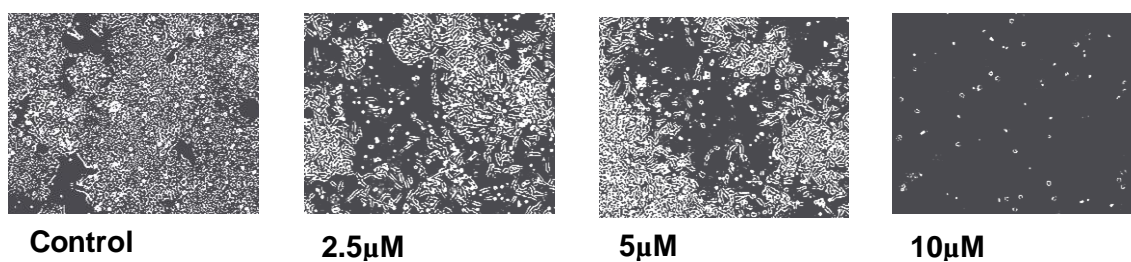
Figure 7.11: Microscope images of MIA-PaCa$_2$ cell line following 96-hour exposures to increasing doses of HA240.
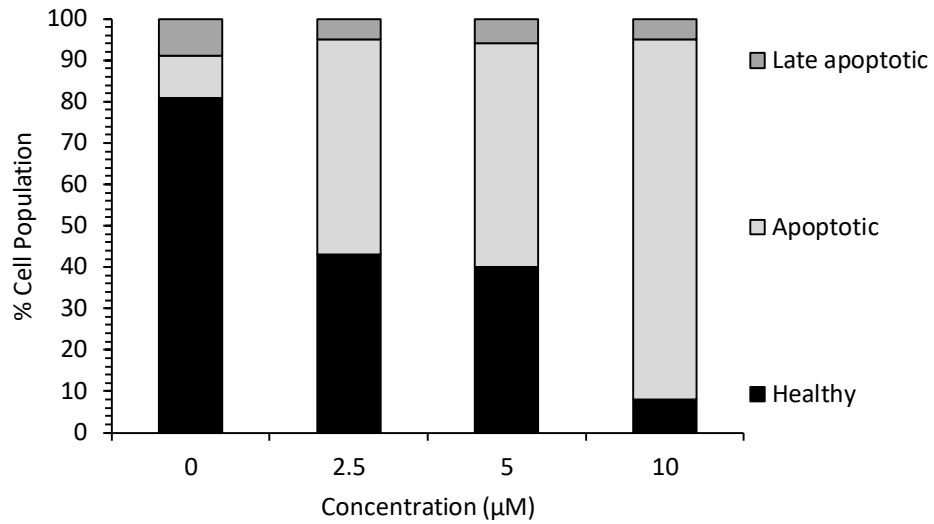
	Percentage of cell population			
Cell state	**Control**	**2.5μM**	**5μM**	**10μM**
Healthy	81	43	40	8
Apoptotic	10	52	54	87
Late apoptotic	9	5	6	5

Figure 7.12: Mitochondrial potential assay identifying induction of apoptosis in the pancreatic adenocarcinoma cell line MIA-PaCa$_2$ after 96-hour exposure to HA240. The exposure concentrations ranged from 2.5μM - 10μM with "0" denoting the control sample (n=1).

7.3.3.4 - HB13

The effect of HB13 on the cell number and viability of MIA PaCa$_2$ is shown in figure 7.13. Following a continuous 96-hour exposure to HB13, a dose dependent reduction in cell number and percentage viability was obtained. The IC$_{50}$ obtained using the NC3000 (IC$_{50}$ = 5μM approximately) was similar to the results obtained using the MTT assay described above (IC$_{50}$ = 5.72 $\pm$ 2.30μM). Visually, these results are confirmed under the microscope with vastly reduced cell number and dramatic alteration in cellular morphology where cells appear almost elongated and less clonogenic (figure 7.14). The results of apoptosis induction in MIA PaCa$_2$ cells following continuous exposure to HB13 are presented in figure 7.15. These results therefore suggest that HB13 induces apoptosis and it does so in a dose dependent manner (figure 7.15).
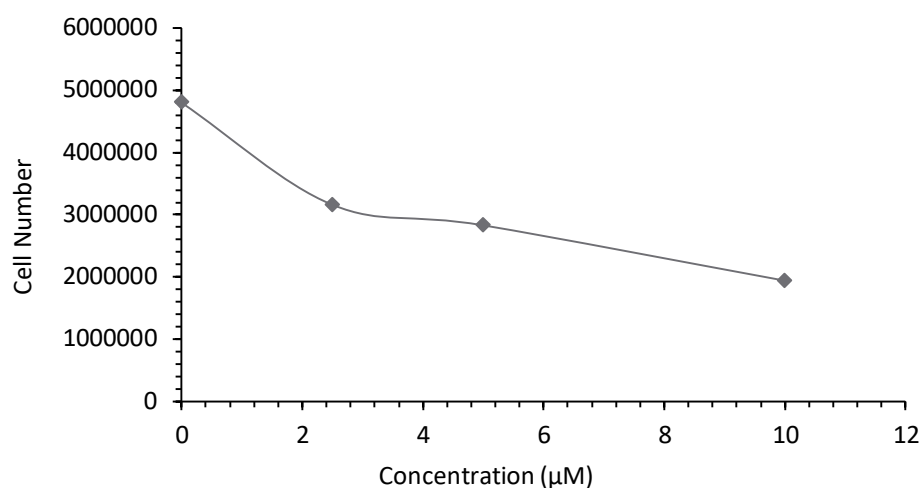
	Control	2.5µM	5µM	10µM
Total cells in sample	4.8×10^6	3.16×10^6	2.83×10^6	1.94×10^6
Percentage cell viability	98.1	80.1	88.9	84.3

Figure 7.13: Effect of increasing doses of HB13 on the cell number of pancreatic adenocarcinoma cell line MIA-PaCa$_2$ after 96-hour exposure. "0" denotes the control sample with concentrations of 2.5µM, 5µM and 10µM being tested. Cell viability is expressed as a percentage based on acridine Orange staining the entire population and DAPI which stains non-viable cells (n=1).

| Control | 2.5µM | 5µM | 10µM |
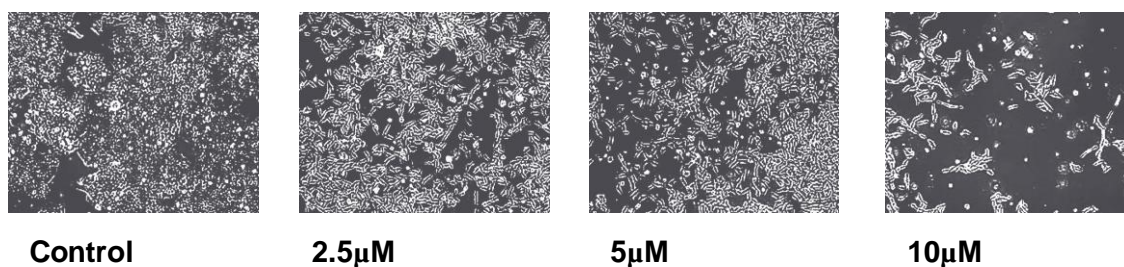
Figure 7.14: Microscope images of MIA-PaCa$_2$ cell line following 96-hour exposures to increasing doses of HB13.
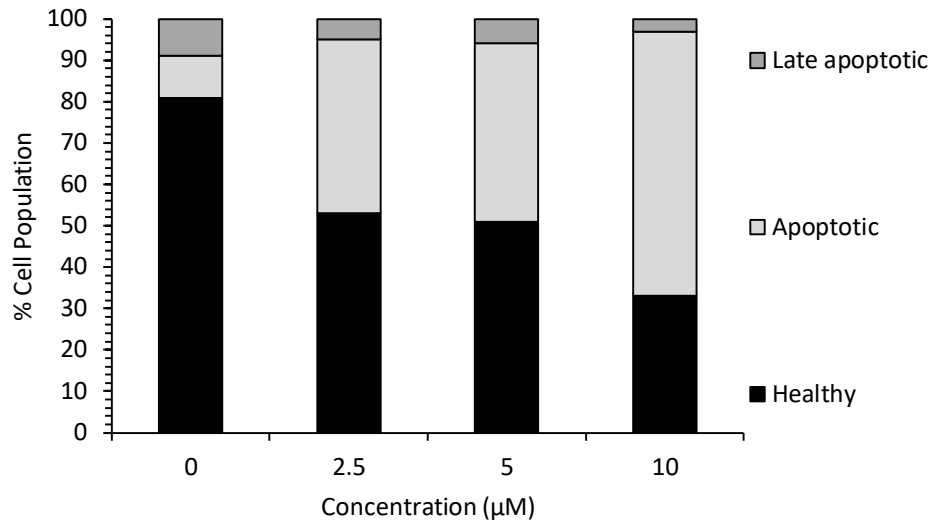
	Percentage of cell population			
Cell state	Control	2.5μM	5μM	10μM
Healthy	81	53	51	33
Apoptotic	10	42	43	64
Late apoptotic	9	5	6	3

Figure 7.15: Mitochondrial potential assay identifying induction of apoptosis in the pancreatic

adenocarcinoma cell line MIA-PaCa$_2$ after 96-hour exposure to HB13. The exposure concentrations

ranged from 2.5μM - 10μM with "0" denoting the control sample (n=1).

7.3.3.5 - HB16

The effect of HB16 on the cell number and viability of MIA-PaCa$_2$ is shown in figure 7.16. Following a continuous 96-hour exposure to HB16, a dose dependent reduction in cell number and percentage viability was obtained. The IC$_{50}$ obtained using the NC3000 (IC$_{50}$ = > 2.5μM approximately) was similar to the results obtained using the MTT assay described above (IC$_{50}$ = 4.55 ± 3.87μM). Visually, these results are confirmed under the microscope with a visual reduction in cell number and interesting alteration in cell morphology where cells appear detached from the flask surface (figure 7.17). The results of apoptosis induction in MIA-PaCa$_2$ cells following continuous exposure to HB16 are presented in figure 7.18. These results clearly demonstrate that HB16 induces apoptosis and it does so in a dose dependent manner (figure 7.18).
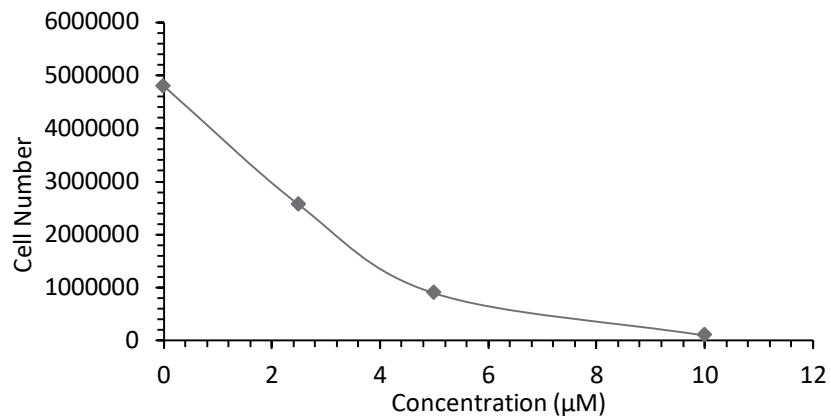
	Control	2.5µM	5µM	10µM
Total cells in sample	4.8×10^6	2.56×10^6	8.94×10^5	9.64×10^4
Percentage cell viability	98.1	94.0	94.7	88.0

Figure 7.16: Effect of increasing doses of HB16 on the cell number of pancreatic adenocarcinoma cell line MIA-PaCa$_2$ after 96-hour exposure. "0" denotes the control sample with concentrations of 2.5µM, 5µM and 10µM being tested. Cell viability is expressed as a percentage based on acridine Orange staining the entire population and DAPI which stains non-viable cells (n=1).
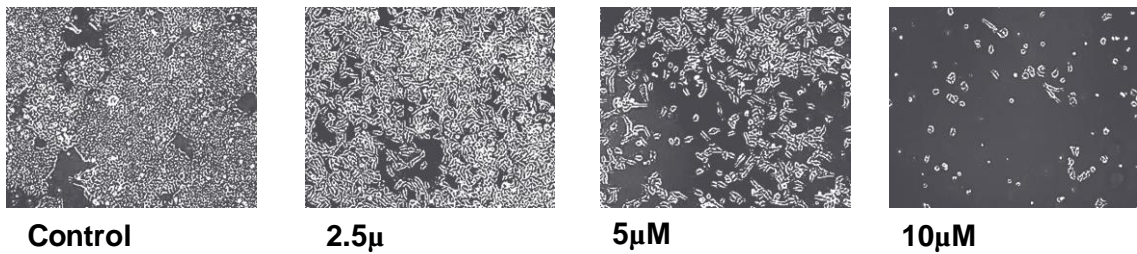
Figure 7.17: Microscope images of MIA-PaCa$_2$ cell line following 96-hour exposures to increasing doses of HB16.
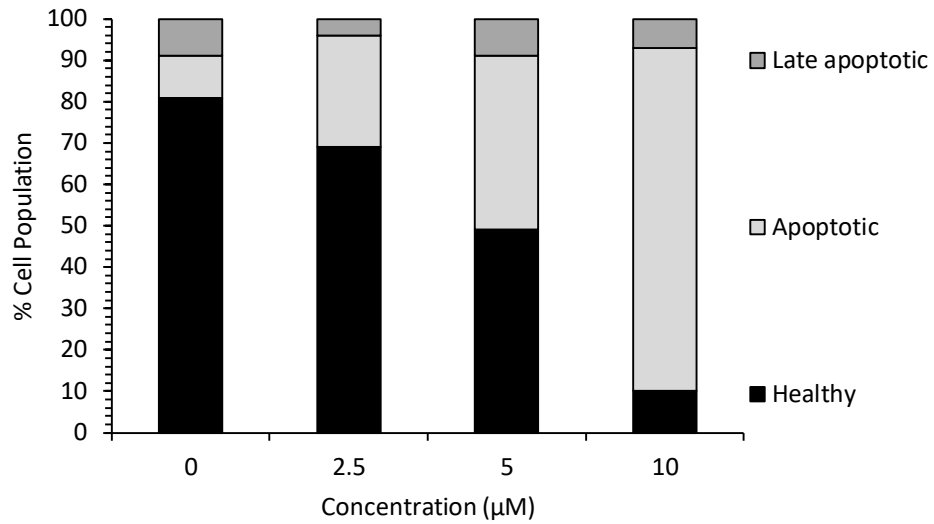
	Percentage of cell population			
Cell state	Control	2.5μM	5μM	10μM
Healthy	81	69	49	10
Apoptotic	10	27	42	83
Late apoptotic	9	4	9	7

Figure 7.18: Mitochondrial potential assay identifying induction of apoptosis in the pancreatic adenocarcinoma cell line MIA-PaCa$_2$ after 96-hour exposure to HB16. The exposure concentrations ranged from 2.5μM - 10μM with "0" denoting the control sample (n=1).

7.3.3.6 - HB18

The effect of HB18 on the cell number and viability of MIA PaCa$_2$ is shown in figure 7.19. Following a continuous 96-hour exposure to HB18, a dose dependent reduction in cell number and percentage viability was obtained. The IC$_{50}$ obtained using the NC3000 (IC$_{50}$ = > 2.5µM approximately) was similar to the results obtained using the MTT assay described above (IC$_{50}$ = 6.89 $\pm$ 2.07µM). Visually, these results are confirmed under the microscope where cell number is greatly reduced and cell seem more dispersed with altered morphology (figure 7.20). The results of apoptosis induction in MIA-PaCa$_2$ cells following continuous exposure to HB18 are presented in figure 7.21. These results clearly demonstrate that HB18 induces apoptosis and it does so in a dose dependent manner (figure 7.21).
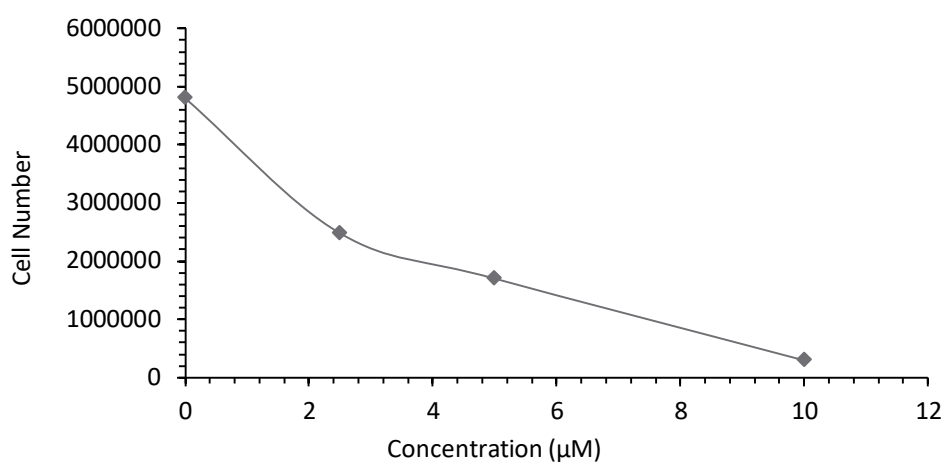
	Control	2.5μM	5μM	10μM
Total cells in sample	4.8×10^6	2.48×10^6	1.70×10^6	2.94×10^5
Percentage cell viability	98.1	82.6	77.5	65.3

Figure 7.19: Effect of increasing doses of HB18 on the cell number of pancreatic adenocarcinoma cell line MIA-PaCa$_2$ after 96-hour exposure. "0" denotes the control sample with concentrations of 2.5μM, 5μM and 10μM being tested. Cell viability is expressed as a percentage based on acridine Orange staining the entire population and DAPI which stains non-viable cells (n=1).
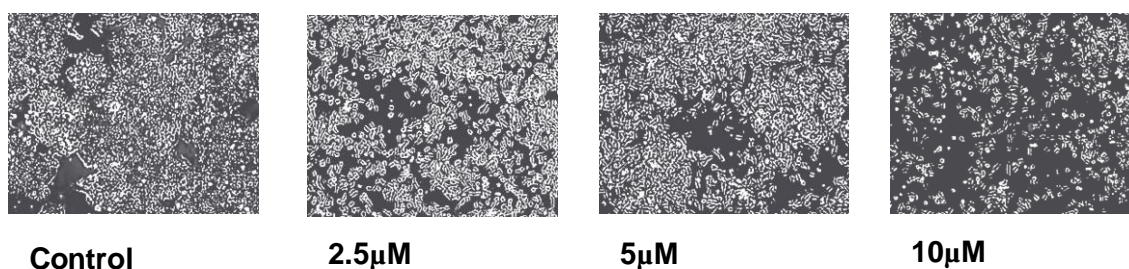
Figure 7.20: Microscope images of MIA-PaCa$_2$ cell line following 96-hour exposures to increasing doses of HB18.
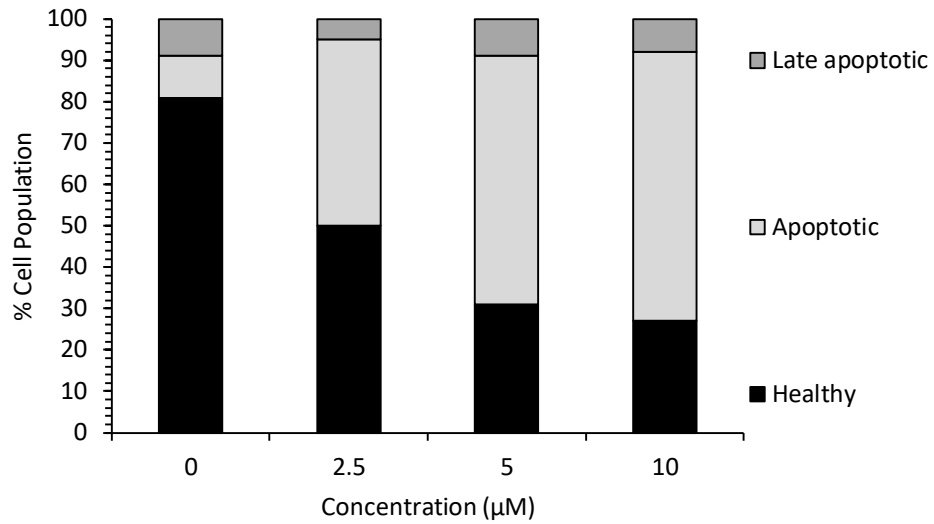
	Percentage of cell population			
Cell state	**Control**	**2.5µM**	**5µM**	**10µM**
Healthy	81	50	31	27
Apoptotic	10	45	60	65
Late apoptotic	9	5	9	8

Figure 7.21: Mitochondrial potential assay identifying induction of apoptosis in the pancreatic adenocarcinoma cell line MIA-PaCa$_2$ after 96-hour exposure to HB18**.** The exposure concentrations ranged from 2.5µM - 1µM with "0" denoting the control sample (n=1).

7.3.3.7 - NL26

The effect of NL26 on the cell number and viability of MIA-PaCa$_2$ is shown in figure 7.22. Following a continuous 96-hour exposure to NL26, a dose dependent reduction in cell number and percentage viability was obtained. The IC$_{50}$ obtained using the NC3000 (IC$_{50}$ = > 10µM approximately) was much lower than the results obtained using the MTT assay described above (IC$_{50}$ = 5.68 $\pm$ 1.80µM). Visually, cells appear to be viable at 5 µM and even at 10µM, a significant number of viable cells are present, the cells do however alter in morphology and appear as individual finely dispersed cells which look to have detached from the cell culture flasks (figure 7.23). The reasons for the discrepancy between the MTT assay and the NC3000 data are not known. The results of apoptosis induction in MIA-PaCa$_2$ cells following continuous exposure to NL26 are presented in figure 7.24. These results clearly demonstrate that NL26 induces apoptosis and it does so in a dose dependent manner (figure 7.24).
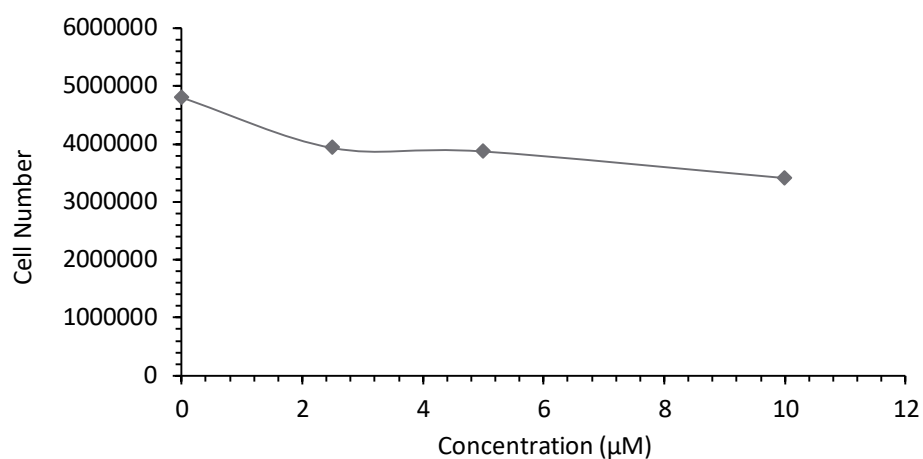
	Control	2.5μM	5μM	10μM
Total cells in sample	4.8×10^6	3.93×10^6	3.87×10^6	3.41×10^6
Percentage cell viability	98.1	67.8	66.0	56.0

Figure 7.22: Effect of increasing doses of NL26 on the cell number of pancreatic adenocarcinoma cell line MIA-PaCa$_2$ after 96-hour exposure. "0" denotes the control sample with concentrations of 2.5μM, 5μM and 10μM being tested. Cell viability is expressed as a percentage based on acridine Orange staining the entire population and DAPI which stains non-viable cells (n=1).

Control   **2.5μM**   **5μM**   **10μM**
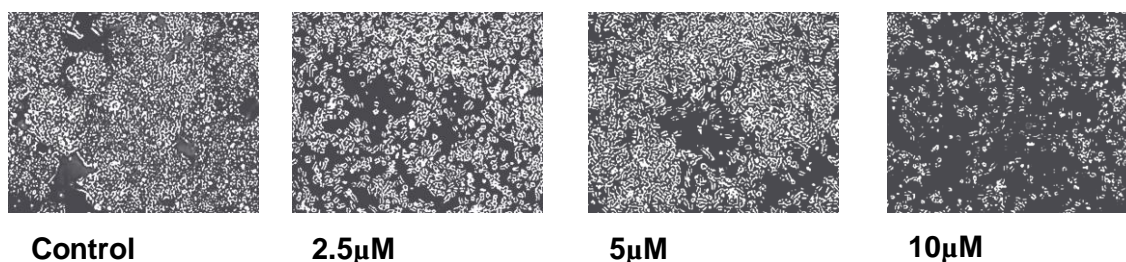
Figure 7.23: Microscope images of MIA-PaCa$_2$ cell line following 96-hour exposures to increasing doses of NL26.
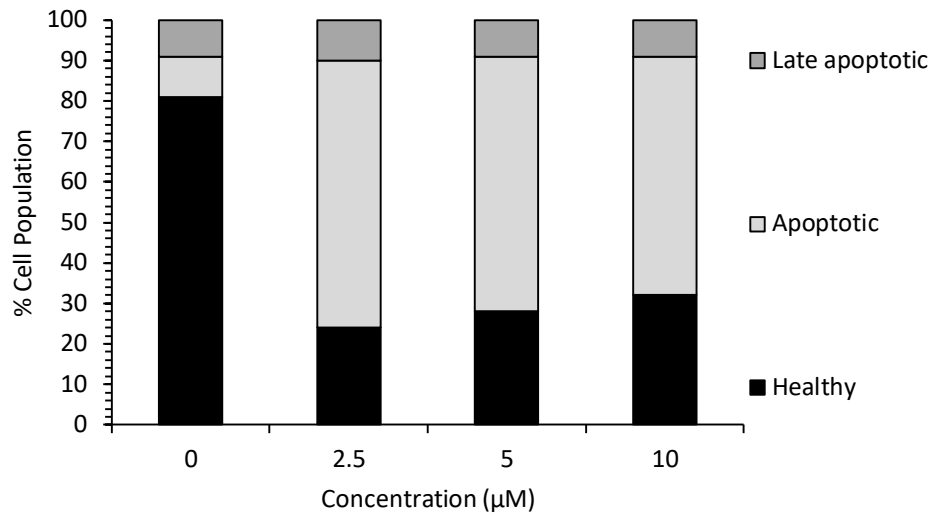
	Percentage of cell population			
Cell state	**Control**	**2.5µM**	**5µM**	**10µM**
Healthy	81	24	28	32
Apoptotic	10	66	63	59
Late apoptotic	9	10	9	9

Figure 7.24: Mitochondrial potential assay identifying induction of apoptosis in the pancreatic

adenocarcinoma cell line MIA-PaCa$_2$ after 96-hour exposure to NL26. The exposure concentrations

ranged from 2.5µM - 10µM with "0" denoting the control sample (n=1).

7.4 - Discussion

The results of this study have identified a number of metal NHC complexes as illustrated in table 7.3. Seven 'hit' compounds were identified based upon equivalent or increased potency and selectivity index compared to the platinates. All the lead compounds are silver NHCs with the copper and ruthenium complexes displaying poor activity towards the Panc10.05 cell line with IC_{50} values of above 51µM (table 7.3). Therefore, despite the promising mechanistic selectivity of ruthenium and its ability to act as a pro-drug, the compounds synthesised exerted poor activity on cancer cells. This could be due to its in ability to enter the cell and become active in the oxidising environment of the cancer cell or it could simply be that it's anti-proliferative effect is poor (structural issue).

Copper NHC complexes in this study failed to display adequate chemotoxicity with the most potent complex being HA230 (IC_{50} = 66.93 ± 12.90µM against the Panc10.05 cell line). Although these compounds demonstrate a poor cytotoxic profile, previous studies have shown that alternative copper NHC complexes do possess a strong cytotoxic profile with its mechanism of action being attributed to substantial DNA damage as a result of ROS production (Oehninger et al., 2013), (Gautier & Cisnetti, 2012). This therefore suggests copper NHC complexes do have appeal as novel therapeutic agents but in regard to the complexes investigated in this study, their poor activity means that they are not worth pursuing further.

From the hit silver NHCs identified as potential lead compounds, five out of the seven compounds are silver(I)-N-heterocyclic carbene complexes derived from clotrimazole. These are compounds HB-13, HB-18, HA-197, HA-201 and HB-16. From the IC_{50} values alone it is apparent the use of clotrimazole derivatives as a precursor for silver-NHCs improves their cytotoxic activity with HA197 displaying IC_{50} values comparable to that of cisplatin in both the Panc10.05 and MIA-PaCa$_2$ cell lines (figure 7.2). To further understand the nature of silver-clotrimazole NHC complexes as novel cytotoxic agents, a number of clotrimazole derivatives were tested using a unique sensing device which has been developed by Coldrick, Steenson, Millner, Davies, and Nelson (2009). The device mimics the cell membrane and it consists of dioleoyl phosphatidyl choline (DOPC) monolayers on which all five of the silver clotrimazole derivatives were tested at the University of Leeds by our collaborative group. The DOPC monolayer is positioned on a micro fabricated Pt/Hg electrode, which measures and displays two peaks of current corresponding to the entry of electrolytes into the cell membrane layer and the reorganisation of the layer in initiation of pore formation (Coldrick et al., 2009; Mohamadi, Tate, Vakurov, & Nelson, 2014; Nelson & Nolan, 2013).

The resulting images produced by the chemical department at Leeds University (figure 12.3 in the appendix) demonstrate the compounds ability to interact with the cell membrane and this broadly correlates with the chemosensitivity results obtained

in this study. Interaction with the membrane is denoted by the deviation of the red line signal away from the undisturbed DOPC signal (grey line).

As with the chemo-sensitivity assays, clotrimazole compounds HA197 and HB-18 display a larger interaction with the cell membrane. The resulting data displayed in 12.3 suggest they possess a mechanism of improved cell entry and potentially increase irreversible cell membrane damage as the signal does not return to its baseline. To investigate the role of the clotrimazole precursor the imidazolium salts plus ligands with no silver ion were also tested, which resulted in an initial interruption (indicating cell membrane diffusion) the disruption was completely reversed, and the signal returned to baseline (figure 12.3). This indicates it is the silver entity initiating the irreversible damage observed by the original compounds. Cisplatin was also investigated as a negative control (figure 12.3), which as expected showed no membrane disruption as cisplatin is widely known to enter the cell *via* copper influx transporters and not *via* passive diffusion (Holzer, Manorek, & Howell, 2006). These assays although completed externally validate the screening methodology we have adopted by further confirming the exclusion of inactive compounds and selection of active lead compounds.

It is unclear how clotrimazole exerts its anti-cancer effects either directly or whether it possibly enhances the activity of silver itself. The majority of mechanistic data currently available are focused on its anti-bacterial and anti-fungal activities but little is known about its activity on cancer cells. This makes any mechanistic

investigation surrounding these complexes novel and potentially of high impact in the field of chemotherapeutic organometallic complexes. The most active and selective compound HA197 is believed to be so due to its intermediate lipophilicity owed to it having both hydrophilic and lipophilic properties. Its hydrophilic properties owed to hydroxylether group increasing the compounds solubility improving its transfer through the bloodstream. Its lipophilic properties owed to its triphenyl group typical of clotrimazole compounds, improves the compounds ability to pass through the cell membrane.

To gain more insight into the mechanistic profile of these novel lead compounds, a mitochondrial potential assay was completed to investigate if these compounds induce cancer cell death *via* apoptosis. All the "hit" compounds tested result in dose dependent reductions in cell number and increased rates of apoptotic induction. Each compound displays varying degrees of dose dependent cell death with HA240 (figure 7.10) and HB16 (7.16) resulting in the greatest reduction in cell number and largest percentage of cells undergoing apoptosis at concentrations of 10μM. Although these compounds do not display the lowest IC_{50} values in the previous chemo-sensitivity assays on the MIA-PaCa$_2$ cell line, the viability and mitochondrial potential assays suggest these compounds have a greater attainable response than compounds such as HA197 which demonstrates a lower IC_{50} value. Further studies are however required to (i) evaluate shorter drug exposure conditions (ii) confirm the induction of apoptosis using other assays such as Annexin V and (iii) conduct similar experiments on ARPE-19

cells to determine if the induction of apoptosis is cancer specific. In addition to further mechanistic investigations it is imperative to mention our appreciation of conducting additional experiments in order to further support the data already generated. In light of this priority investigation will consist of rerunning experiments already conducted in order to produce mean values ruling out experimental bias or random error.

Alongside generating more robust and informative mechanistic data undertaking more informative chemo-sensitivity investigations would shed light on the toxicity profile of the compounds in regards to if they induce a cytostatic or cytotoxic response in the cancerous cell lines. This can be managed *via* MTT assays establishing the absorbance of the cell seeding densities on the day of treatment in order to determine if the reduction in cell number is due to cell death or cytostatic action. This in conjunction with the optimisation and implementation of clonogenic assays will give a greater insight into the nature of chemosensitivity of the cell lines toward these novel complexes.

7.5 - Conclusion

In conclusion, the results of this study have identified seven novel metal NHC compounds that are as potent as the platinates (particularly cisplatin). Silver based NHC compounds were found to be the most active metal complexes with clotrimazole derivatives being the most active. Initial mechanistic studies were performed in the form of mitochondrial potential assays and viability cell count assays. Although it showed a number of compounds induced apoptosis, the assay has limitations. The main being that a reduction in the mitochondrial potential of a cell is not specific to apoptosis and can be induced *via* other external stresses and therefore an additional apoptotic assay is required to further validate the results obtained. Several of the compounds not only rival the platinum agents in regard to the chemo-sensitivity and selectivity data but the indication of alternative mechanistic pathways *via* cell membrane DOPC investigations suggest an application for these complexes in platinum resistant tumours. In the context of the overall objectives of the thesis, the phenotypic screen based on potency alone compared to platinates identified seven compounds of interest. With regards to the selectivity index *in vitro*, only one compound (HA197) showed greater selectivity than all the platinates tested. This demonstrates that the selectivity index together with potency data has greater discrimination than potency alone and is capable of identifying promising hit compounds.

Chapter 8 - Half Sandwich Metal Complexes as Anti-Cancer Therapies

8.1 - Introduction

Due to their versatility, half sandwich organometallic complexes have been extensively researched during the past few decades. They have had wide spread application and have been especially prominent in the field of catalysis (Gras et al., 2010). The piano stool, pseudo-tetrahedral complex displayed in figure 8.1 offers great flexibility, with the piano seat arene moiety protecting the oxidation state of the central metal ion by occupying 3 coordinating sites. The L ligand controls the reactivity of the complex while the chelating ligand when dissociated reveals the biomolecule targeting active site. The substitution of either arene, chelating ligand or leaving group therefore strongly influences the biological activity of these complexes (Adhikari et al., 2016). Our collaboration with North Eastern Hill, India focused on the investigation of half sandwich complexes with varying ligands, counter ions, leaving groups and central metal ions. Iridium and ruthenium have been discussed in more detail in chapter 5 and their activity is investigated in this chapter as part of a half sandwich system.

Rhodium a group 9 transition metal, like cobalt and iridium, long thought to be inert, has recently sparked interest as part of a half sandwich system with its lability thought to be responsible for observed anti-cancer activity. This is thought to induce cytostatic activity, cellular uptake and DNA binding *via* intercalation (Ma et al., 2016).

This chapter explores the use of various ligands and metal centres in order to manipulate the half sandwich structures and synthesise complexes with both high potency and selectivity towards cancerous cells. One of the ligands investigated in this chapter are chain diazine Schiff base ligands linked by a single N-N bond, which offer flexibility and a variety of coordination complexes. Another ligand in the half sandwich system is the oxime ligand and these have been shown to induce pronounced cytotoxicity and antimicrobial activity with the potency of some complexes exceeding that of cisplatin (Gerasimchuk, Gamian, Glover, & Szponar, 2010; Gerasimchuk et al., 2007).The appeal of the oxime ligands is thought to be their ability to form an ambidentate ligand coordinating with the metal ion thereby stabilising and protecting its oxidation state and reducing premature degradation (Adhikari et al., 2016). Like oxime ligands, pyrimidine ligands are intermediates for a number of biologically active complexes, with metal oxime complexes being poorly understood in comparison to pyrimidine which is a core structure in a large number of biologically important complexes. Pyrimidine ligands are not only present in both DNA and RNA but are the building blocks of a number of antibacterial, anti-HIV, anti-convulsant and ant-hypertensive agents they also already hold a role in cancer chemotherapy in the form of 5-fluorouracil (Dudhe, Sharma, Verma, & Chaudhary, 2011).
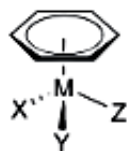
Figure 8.1: Classic half sandwich "piano stool" adapted from Gasser et al. (2010)

Over the past few years Dr Mohan Rao and his research group have synthesised many half sandwich Ru (II), Ir (III) and Rh (III) complexes with azine, oxime and pyrimidine ligands. These compounds were not designed to target specific biochemical pathways and therefore the initial aim of this study was to conduct a phenotype based approach using potency and selectivity for cancer cells as the primary endpoint for selecting lead compounds for subsequent evaluation.

8.2 - Methods

8.2.1 - Preparation of Drug Stock Solution
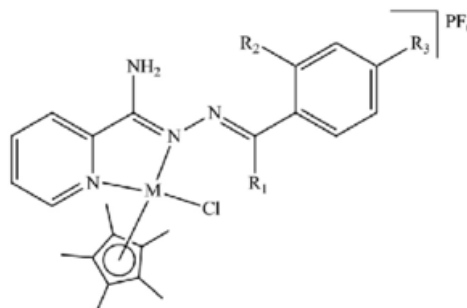
Compound name (Metal)	MW	Weight (mg)	Diluent	Volume (µl)	Concentration (mM)	Ligands
KMR-SA03 (Rh)	688.84	2.5	DMSO	36.29	100	R_1=H, R_2=OH, R_3=OCH$_3$
KMR-SA04 (Ir)	778.15	3.2	DMSO	41.12	100	R_1=H, R_2=OH, R_3=OCH$_3$
KMR-SA05 (Rh)	658.81	2	DMSO	30.36	100	R_1=H, R_2=OH, R_3=H
KMR-SA06 (Ir)	748.12	5.4	DMSO	72.18	100	R_1=H, R_2=OH, R_3=H
KMR-SA07 (Rh)	672.84	2.8	DMSO	41.61	100	R_1= CH$_3$, R_2=OH, R_3=H
KMR-SA08 (Ir)	762.15	3.6	DMSO	47.23	100	R_1= CH$_3$, R_2=OH, R_3=H
KMR-SA09 (Rh)	642.81	4.2	DMSO	65.34	100	R_1= CH$_3$, R_2=H, R_3=H
KMR-SA10 (Ir)	732.12	2.7	DMSO	36.88	100	R_1= CH$_3$, R_2=H, R_3=H

Table 8.1: Concentration of drug solutions and structure of novel iridium and rhodium half sandwich compounds containing azine Schiff base ligands.
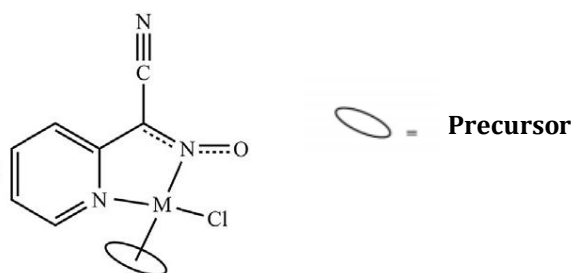
Precursor

Compound name (Metal)	MW	Weight (mg)	Diluent	Volume (µl)	Concentration (mM)	Precursor
KMR-SA01 (Ru)	416.87	10.5	DMSO	252	100	
KMR-SA02 (Rh)	417.88	10.7	DMSO	256	100	
KMR-SA11 (Ir)	509.02	3.52	DMSO	69.2	100	

Table 8.2: Concentration of drug solutions and structure of novel ruthenium, iridium and rhodium neutral half sandwich complexes with 2-pyridyl cyanoxime ligands.
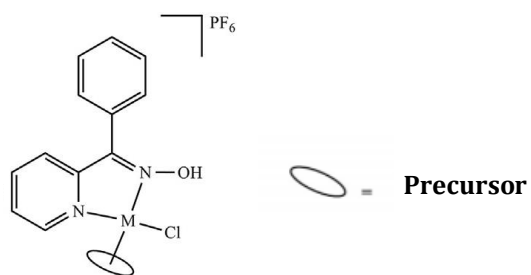
Precursor

Compound name (<u>M</u>etal)	MW	Weight (mg)	Diluent	Volume (μl)	Concentration (mM)	Precursor
KMR-SA12 (Ru)	613.93	4.25	DMSO	69.2	100	
KMR-SA13 (Rh)	616.77	3.23	DMSO	52.4	100	
KMR-SA14 (Ir)	706.08	1.70	DMSO	24	100	

Table 8.3: Concentration of drug solutions and structure of novel ruthenium, iridium and rhodium cationic half sandwich complexes with 2- pyridyl phenyloxime ligands.
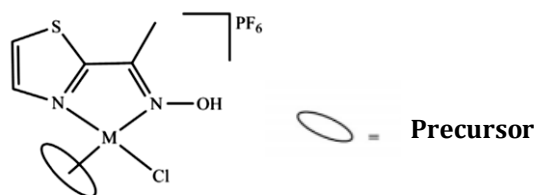
Compound name (Metal)	MW	Weight (mg)	Diluent	Volume (μl)	Concentration (mM)	Precursor
KMR-SA15 (Ru)	557.88	8.96	DMSO	160.6	100	
KMR-SA16 (Rh)	559.73	6.46	DMSO	115.4	100	
KMR-SA17 (Ir)	650.04	6.40	DMSO	98.5	100	

Table 8.4: Concentration of drug solutions and structure of novel ruthenium, iridium and rhodium cationic half sandwich complexes with 2-thiazolyl methyloxime ligands.
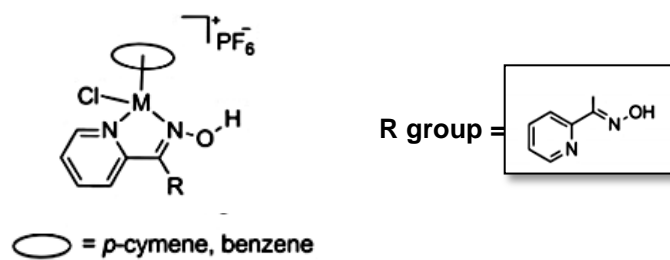
= p-cymene, benzene

Compound name (M=Ru)	MW	Weight (mg)	Diluent	Volume (μl)	Concentration (mM)	Precursor
KMR-NR 1	495.75	4.6	DMSO	92.79	100	benzene
KMR-NR 3	551.86	6.9	DMSO	125.09	100	p-cymene

Table 8.5: Concentration of drug solutions and structure of novel ruthenium half sandwich complexes with ketoxime ligands.
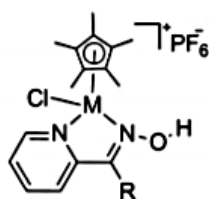
Compound name (Metal)	MW	Weight (mg)	Diluent	Volume (µl)	Concentration (mM)	R group
KMR-NR 2 (Ir)	629.99	9.2	DMSO	146.03	100	
KMR-NR 4 (Rh)	540.68	5.5	DMSO	101.72	100	
KMR-NR 5 (Rh)	572.72	7.1	DMSO	123.97	100	
KMR-NR 7 (Rh)	1001.87	2.8	DMSO	27.95	100	
KMR-NR 8 (Ir)	1180.45	7.9	DMSO	66.92	100	

Table 8.6: Concentration of drug solutions and structure of novel rhodium and iridium CP*half sandwich complexes with aldoxime, ketoxime, amioloxime ligands.
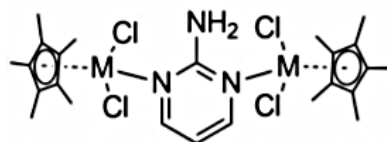
Compound name	MW	Weight (mg)	Diluent	Volume (µl)	Concentration (mM)	Metal
KMR-SA 9	713.17	6.2	DMSO	86.94	100	Rh
KMR-SA 10	891.75	8.9	DMSO	99.80	100	Ir

Table 8.7: Concentration of drug solutions and structure of novel binuclear rhodium and iridium half sandwich complexes with aminopyrimidine ligands.
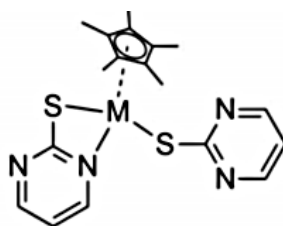
Compound name	MW	Weight (mg)	Diluent	Volume (µl)	Concentration (mM)	Metal
KMR-SA 13	460.42	11.1	DMSO	241.08	100	Rh
KMR-SA 14	549.71	9.4	DMSO	170.10	100	Ir

Table 8.8: Concentration of drug solutions and structure of novel mononuclear rhodium and iridium half sandwich complexes with 2-mercaptopyrimidine ligands.
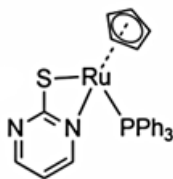
Compound name	MW	Weight (mg)	Diluent	Volume (μl)	Concentration (mM)	Metal
KMR-NR 11	539.57	10.7	DMSO	198.31	100	Ru

Table 8.9: Concentration of drug solutions and structure of novel mononuclear ruthenium half sandwich complex with 2-mercaptopyrimidine ligand.

Once dissolved the compounds were aliquoted into single-use batches to prevent freeze thawing, each aliquot was given a 3-month expiry.

8.2.2 - Chemo-Sensitivity, Viability and Mitochondrial Potential Assays

The response of cell lines following continuous 96-hour exposures to test compounds under aerobic and hypoxic conditions was determined using the MTT assay, details of which have been described elsewhere in this thesis (see 2.5). Analysis of cell viability and cell cycle parameters was determined using the NC3000 cytometer, details of which have been described elsewhere (see 2.6). For these experiments, drug exposure concentrations ranged from 5μM to 20μM; duration of drug exposures was set at 96 hours to replicate the conditions used in the MTT assays.

8.3 - Results

8.3.1 - Response of MIA-PaCa$_2$, HT-29 and ARPE-19 Cells to Test Compounds Under Aerobic Conditions

Compound	IC$_{50}$ value (µM) ± SD		
	MIA-PaCa$_2$	HT-29	ARPE-19
KMR-SA 3 (Rh)	93.68±8.94	56.95±11.76	85.31±14.86
KMR-SA 4 (Ir)	98.50±2.28	89.42±18.33	93.45±11.34
KMR-SA 5 (Rh)	>100	82.32±15.55	83.03±14.76
KMR-SA 6 (Ir)	98.39±2.89	96.93±5.31	>100
KMR-SA 7 (Rh)	95.26±6.70	46.17±12.78	97.39±4.53
KMR-SA 8 (Ir)	>100	83.74±28.17	>100
KMR-SA 9 (Rh)	>100	93.16±11.84	>100
KMR-SA 10 (Ir)	>100	88.09±20.63	>100
Cisplatin	3.62±0.38	0.25±0.11	6.41±0.95

Table 8.10: Response of pancreatic carcinoma cell line MIA-PaCa$_2$, colorectal adenocarcinoma cell line HT-29 and the non-cancerous retinal epithelial cell line ARPE-19 following continuous 96-hour exposure to novel iridium and rhodium half sandwich compounds containing azine Schiff base ligands. The results presented are the mean IC$_{50}$ values ± standard deviations for three independent experiments n=3 (each individual experiment replicated twice). The ">" symbol represents the highest dose tested *in vitro*.

	IC$_{50}$ value (µM) ± SD			
Complex (metal)	Be	HT-29	MIA-Pa-Ca$_2$	ARPE-19
KMR-SA 1 (Ru)	>100	>100	>100	>100
KMR-SA 2 (Rh)	23.74±4.25	22.25±5.29	9.16±2.89	24.95±8.36
KMR-SA 11 (Ir)	-	5.82±2.41	2.87±0.26	8.12±2.30
KMR-SA 12 (Ru)	-	68.83±27.0	26.42±0.67	71.63±8.10
KMR-SA 13 (Rh)	-	42.32±10.69	67.18±3.16	70.53±8.73
KMR-SA 14 (Ir)	-	7.92±1.00	8.35±0.29	17.92±7.76
KMR-SA 15 (Ru)	-	12.56±4.45	8.28±0.42	18.95±1.51
KMR-SA 16 (Rh)	-	>100	>100	>100
KMR-SA 17 (Ir)	-	10.54±4.73	9.65±1.68	11.50±2.12
KMR-NR 1 (Ru)	>100	>100	-	-
KMR-NR 2 (Ir)	6.32±0.06	10.00±2.77	5.46±3.41	12.76±5.4
KMR-NR 3 (Ru)	6.91±0.50	13.24±6.47	5.31±1.95	28.92±6.05
KMR-NR 4 (Rh)	>100	>100	-	-
KMR-NR 5 (Rh)	>100	>100	-	-
KMR-NR 7 (Rh)	>100	>100	-	-
KMR-NR 8 (Ir)	>100	>100	-	-
Cisplatin	0.66±0.33	0.25±0.11	3.62±0.38	6.41±0.95

Table 8.11: Response of pancreatic carcinoma cell line MIA-PaCa$_2$, colorectal adenocarcinoma cell line HT-29 and the non-cancerous retinal epithelial cell line ARPE-19 following continuous 96-hour exposure to novel half sandwich ruthenium, iridium and rhodium compounds with oxime and oximato ligands. The results presented are the mean IC$_{50}$ values ± standard deviations for three independent experiments n=3 (each individual experiment replicated twice). The most promising results in terms of potency are highlighted in red. The ">" symbol represents the highest dose tested *in vitro*.

	IC$_{50}$ value (μM) $\pm$ SD			
Complex	Be	HT-29	MIA-Pa-Ca$_2$	ARPE-19
KMR-NR 9	>100	>100	>100	>100
KMR-NR 10	23.13$\pm$3.83	>100	>100	>100
KMR-NR 11	>100	>100	-	-
KMR-NR 12	>100	>100	-	-
KMR-NR 13	14.25$\pm$2.14	24.32$\pm$2.80	20.43$\pm$4.59	47.22$\pm$4.88
KMR-NR 14	42.09$\pm$8.68	57.46$\pm$2.97	19.86$\pm$4.58	69.25$\pm$1.75
Cisplatin	0.66$\pm$0.33	0.25$\pm$0.11	3.62$\pm$0.38	6.41$\pm$0.95

Table 8.12: Response of pancreatic carcinoma cell line MIA-PaCa$_2$, colorectal adenocarcinoma cell line HT-29 and the non-cancerous retinal epithelial cell line ARPE-19 following continuous 96-hour exposure to novel half sandwich complexes with pyridine derivative ligands. The results presented are the mean IC$_{50}$ values $\pm$ standard deviations for three independent experiments n=3 (each individual experiment replicated twice). The ">" symbol represents the highest dose tested *in vitro*.

8.3.2 - Comparison of "hit" Novel Metal NHC Complexes to Platinum Compounds

The four "hit" compounds chosen based on their potency and selectivity index are displayed in figures 8.2 and 8.3 respectively. In the cancer cell lines tested, cisplatin presented as the most active platinum agent toward the pancreatic adenocarcinoma MIA-PaCa$_2$ cell line and the only agent with complete colorectal adenocarcinoma HT-29 data making it the gold standard to which compare our novel compounds. Overall the "hit" compounds show either improved or comparable potency compared to cisplatin on the MIAPaCa$_2$ cell line with KMR-SA 11 demonstrating improved potency (2.87 $\pm$ 0.26μM). On the HT-29 cell line however cisplatin displays far superior potency than any of the hit compounds tested. The selectivity index of the test compounds generally demonstrated intermediate selectivity for cancer cells compared to ARPE-19 cells with SI values up to 5.45 displayed by KMR-NR 3 on MIA-PaCa$_2$ cells (figure 8.3) which was

the only novel compounds to display a statistically significant reduction in toxicity toward the none cancerous cell line opposed to the cancerous lines. Of particular note, all the novel complexes displayed superior selectivity toward the MIA-PaCa$_2$ cell line (Cisplatin = 1.71) yet cisplatin was over 10-fold more selective than the most selective novel compounds on HT-29 cells (Cisplatin =25.64).
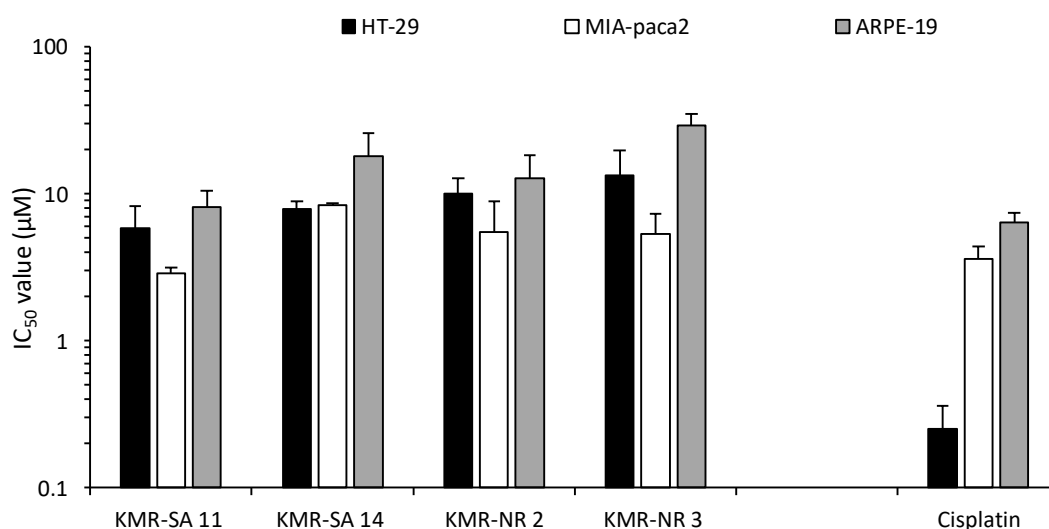
Figure 8.2: Comparison of the potency of lead novel half sandwich ruthenium and iridium compounds with oxime and oximato ligands to cisplatin on MIA-PaCa$_2$, HT-29 and ARPE-19 cells. The values presented are the mean IC$_{50}$ values ± standard deviation of three independent experiments n=3 (each individual experiment replicated twice).
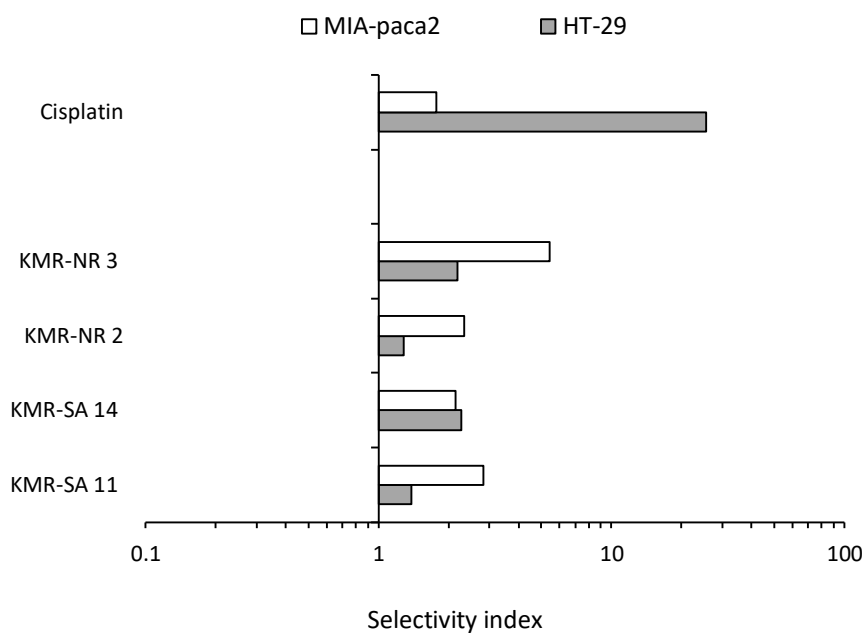
Compound	MIA-PaCa$_2$	*p*-value	HT-29	*p*-value
KMR-NR 2	2.34	0.19	1.28	0.46
KNR-NR 3	5.45	0.010	2.18	0.063
KMR-SA 11	2.83	0.054	1.39	0.41
KMR-SA 14	2.15	0.17	2.26	0.16
Cisplatin	1.77	0.10	25.64	0.0028

Figure 8.3: Comparison of the selectivity of novel half sandwich ruthenium and iridium compounds with oxime and oximato ligands to cisplatin on cancerous cell lines MIA-PaCa$_2$ and HT-29 in comparison to non-cancerous cell line ARPE-19**.** The selectivity index is defined as the mean IC$_{50}$ for non-cancerous cells divided by the IC$_{50}$ of cancer cells. Values greater than 1 indicate that compounds have selectivity for cancer cells as opposed to non-cancer cells. As the mean IC$_{50}$ values are used to calculate selectivity indices, no error bars are included on the graphs. Statistical analysis was performed using a student's t-test where values <0.05 indicates a statistically significant difference between IC$_{50}$ values in cancerous and none cancerous cell lines.

8.3.3 - Cell Viability and Apoptosis Induction Investigations

Based on their potency and selectivity profile, four "hit" compounds were selected for further investigation. The results of cell viability and induction of apoptosis using the NC3000 are presented in figures 8.4 to 8.15. In all cases, cells were treated with increasing concentrations of compound and their viability along with any cell cycle disruption was determined using the viability and mitochondrial potential assays using the same data analysis outlined in sections 3.3.5.1 and 3.3.5.3. The results for each of the compounds selected are described in the various sub-sections below.

8.3.3.1 - KMR-SA 11

The effect of KMR-SA 11 on the cell number and viability of MIA-PaCa$_2$ is shown in figure 8.4. Following a continuous 96-hour exposure to KMR-SA 11, a dose dependent reduction in cell number and percentage viability was obtained. The IC$_{50}$ obtained using the NC3000 (IC$_{50}$ = 10µM approximately) was significantly higher than that obtained using the MTT assay described above (IC$_{50}$ = 2.87 $\pm$ 0.26µM) yet the cell response at 10µM and above are dramatic. These results are also illustrated visually in figure 8.5 and they confirm that cell viability decreases in a dose dependent manner with dramatic changes to cell morphology with increasing drug concentration. The results of apoptosis induction in MIA-PaCa$_2$ cells following continuous exposure to KMR-SA 11 are presented in figure 8.6. These results clearly demonstrate that KMR-SA 11 induces apoptosis and it does so in a dose dependent manner (figure 8.6).
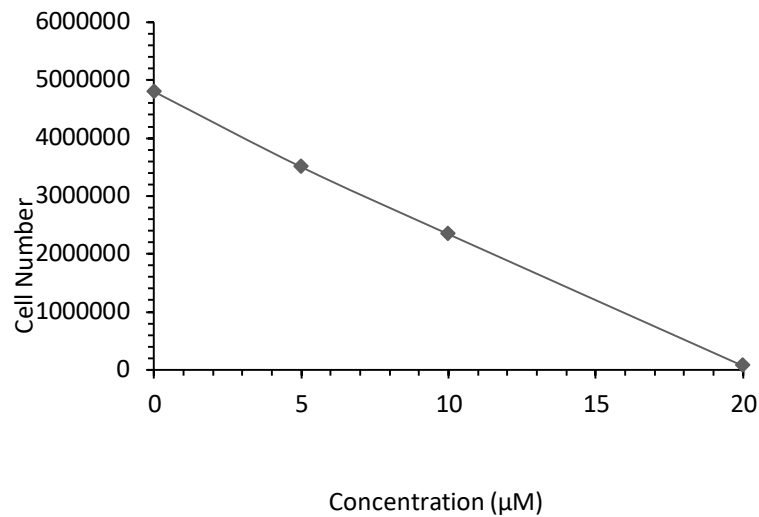
	Control	5µM	10µM	20µM
Total cells in sample	4.8×10^6	3.5×10^6	2.34×10^6	6.72×10^4
Percentage cell viability	98.1	91.5	94.9	61.7

Figure 8.4: Effect of increasing doses of KMR-SA 11 on the cell number of pancreatic adenocarcinoma cell line MIA-PaCa$_2$ after 96-hour exposure. "0" denotes the control sample with concentrations of 5µM, 10µM and 20µM being tested. Cell viability is expressed as a percentage based on acridine Orange staining the entire population and DAPI which stains non-viable cells (n=1).
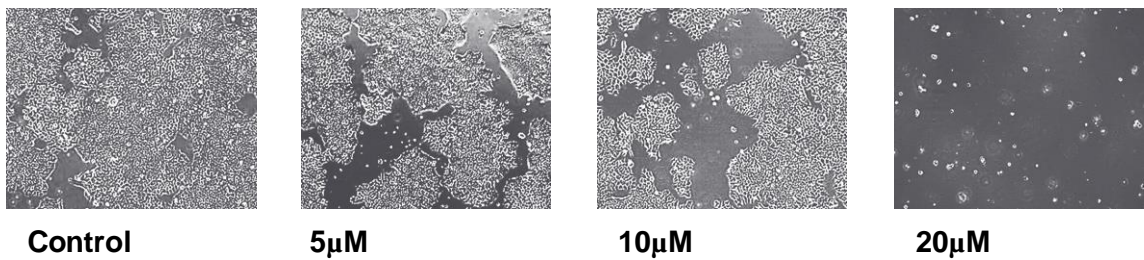
Figure 8.5: Microscope images of pancreatic adenocarcinoma cell line MIA-PaCa$_2$ cell line exposed to increasing doses of KMR-SA 11 over a 96-hour exposure time.
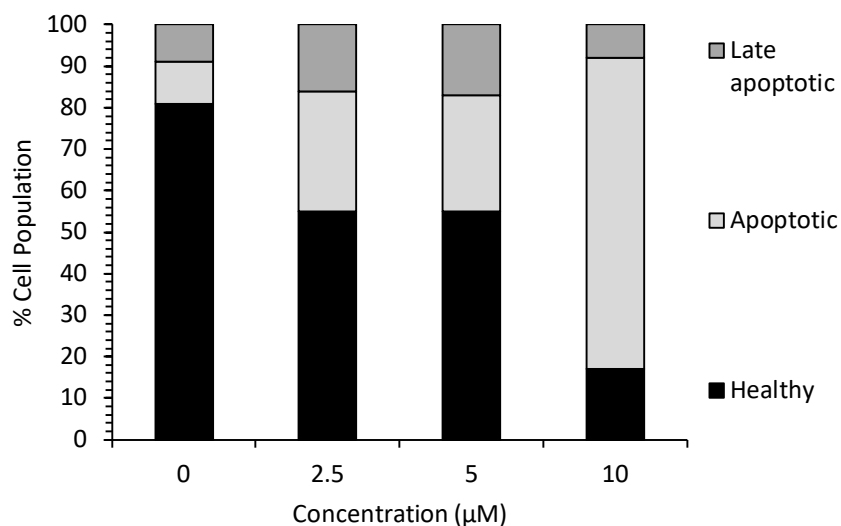
Cell state	Percentage of cell population			
	Control	5µM	10µM	20µM
Healthy	81	55	55	17
Apoptotic	10	29	28	75
Late apoptotic	9	16	17	8

Figure 8.6: Mitochondrial potential assay identifying induction of apoptosis in the pancreatic

adenocarcinoma cell line MIA-PaCa$_2$ after 96-hour exposure to KMR SA-11. The exposure concentrations

ranged from 5µM - 20µM with "0" denoting the control sample (n=1).

8.3.3.2 - KMR-SA 14

The effect of KMR-SA 14 on the cell number and viability of MIA-PaCa$_2$ is shown in figure 8.7. Following a continuous 96-hour exposure to KMR-SA 14, a dose dependent reduction in cell number and percentage viability was obtained. The IC$_{50}$ obtained using the NC3000 (IC$_{50}$ = between 5μM and 10μM) was comparable to that obtained using the MTT assay described above (IC$_{50}$ = 8.35 $\pm$ 0.29μM). These results are also illustrated visually in figure 8.8 and they confirm that cell viability decreases in a dose dependent manner again displaying morphological changes in the cells with increasing drug concentration with remaining cells appearing detached and potentially undergoing apoptosis. The results of apoptosis induction in MIA-PaCa$_2$ cells following continuous exposure to KMR-SA 14 are presented in figure 8.9. These results clearly demonstrate that KMR-SA 14 induces apoptosis and it does so in a dose dependent manner (figure 8.9).
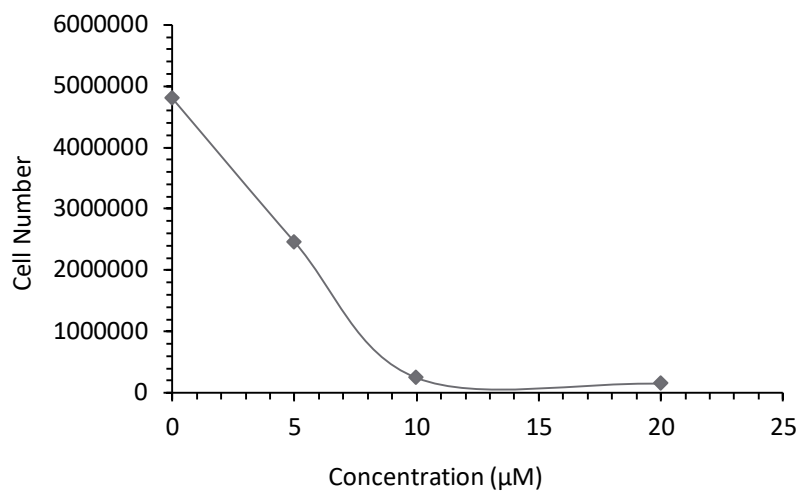
	Control	5μM	10μM	20μM
Total cells in sample	4.8×10^{6}	2.46×10^{6}	2.45×10^{5}	1.5×10^{5}
Percentage cell viability	98.1	79.0	69.2	71.3

Figure 8.7: Effect of increasing doses of KMR-SA 14 on the cell number of pancreatic adenocarcinoma cell line MIA-PaCa$_2$ after 96-hour exposure. "0" denotes the control sample with concentrations of 5μM, 10μM and 20μM being tested. Cell viability is expressed as a percentage based on acridine Orange staining the entire population and DAPI which stains non-viable cells (n=1).

Control   **5μM**   **10μM**   **20μM**
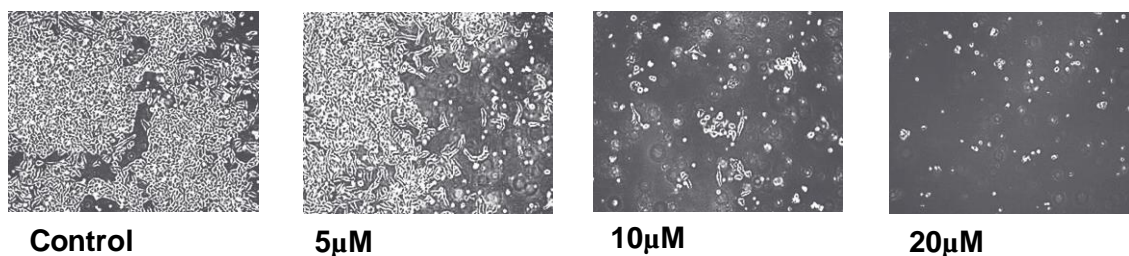
Figure 8.8: Microscope images of pancreatic adenocarcinoma cell line MIA-PaCa$_2$ cell line exposed to increasing doses of KMR-SA 14 over a 96-hour exposure time.
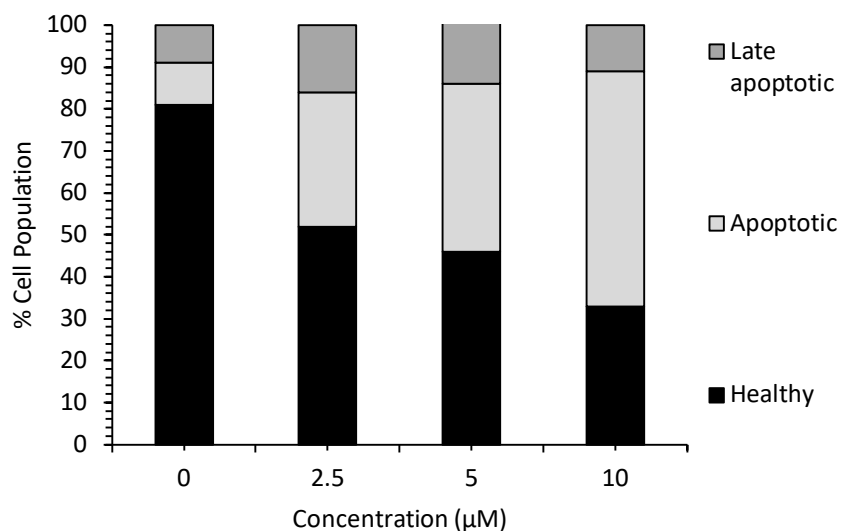
	Percentage of cell population			
Cell state	**Control**	**5μM**	**10μM**	**20μM**
Healthy	81	52	46	33
Apoptotic	10	32	40	56
Late apoptotic	9	16	15	11

Figure 8.9: Mitochondrial potential assay identifying induction of apoptosis in the pancreatic adenocarcinoma cell line MIA-PaCa2 after 96-hour exposure to KMR SA-14. The exposure concentrations ranged from 5μM - 20μM with "0" denoting the control sample (n=1).

8.3.3.3 - KMR-NR 2

The effect of KMR-NR 2 on the cell number and viability of MIA-PaCa$_2$ is shown in figure 8.10. Following a continuous 96-hour exposure to KMR-SR 2, a dose dependent reduction in cell number and percentage viability was obtained. The IC_{50} obtained using the NC3000 (IC_{50} = between 5µM and 10µM) was comparable to that obtained using the MTT assay described above (IC_{50} = 5.46 $\pm$ 3.41µM). These results are also illustrated visually in figure 8.11 and they confirm that cell viability decreases and alterations to cell morphology occur in a dose dependent manner. The results of apoptosis induction in MIA-PaCa$_2$ cells following continuous exposure to KMR-SR 2 are presented in figure 8.12. These results therefore suggest that KMR-SR 2 induces apoptosis and it does so in a dose dependent manner (figure 8.12).
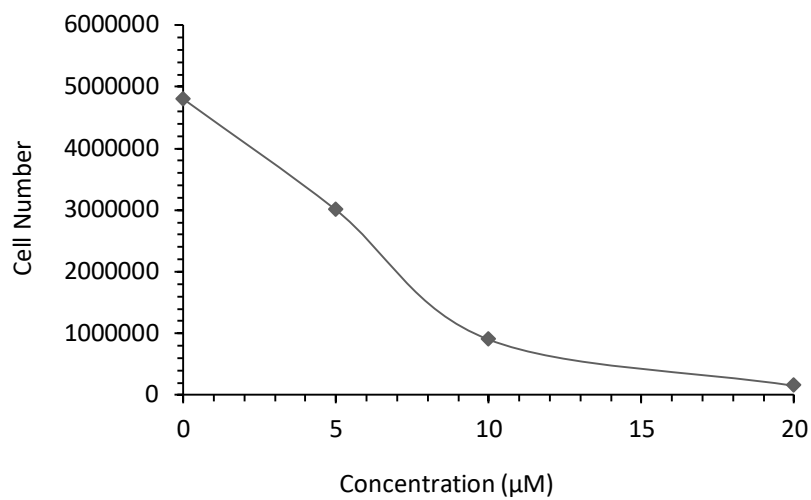
	Control	5µM	10µM	20µM
Total cells in sample	4.8×10^6	3×10^6	9×10^5	1.5×10^5
Percentage cell viability	98.1	76.5	81.8	72.5

Figure 8.10: Effect of increasing doses of KMR-NR 2 on the cell number of pancreatic adenocarcinoma cell line MIA-PaCa$_2$ after 96-hour exposure. "0" denotes the control sample with concentrations of 5µM, 10µM and 20µM being tested. Cell viability is expressed as a percentage based on acridine Orange staining the entire population and DAPI which stains non-viable cells (n=1).

Control   **5µM**   **10µM**   **20µM**
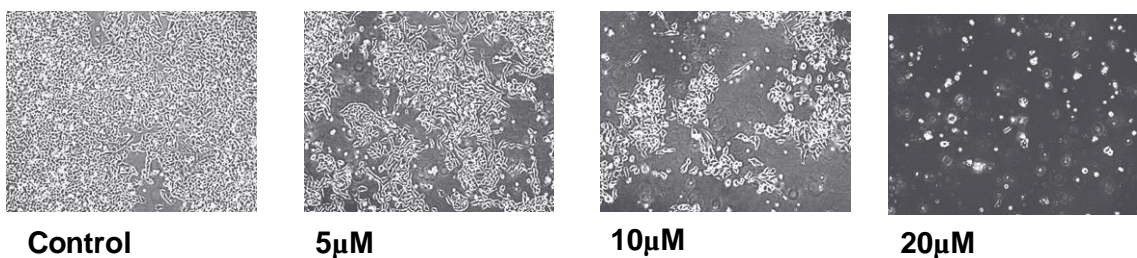
Figure 8.11: Microscope images of pancreatic adenocarcinoma cell line MIA-PaCa$_2$ cell line exposed to increasing doses of KMR-NR 2 over a 96-hour exposure time.
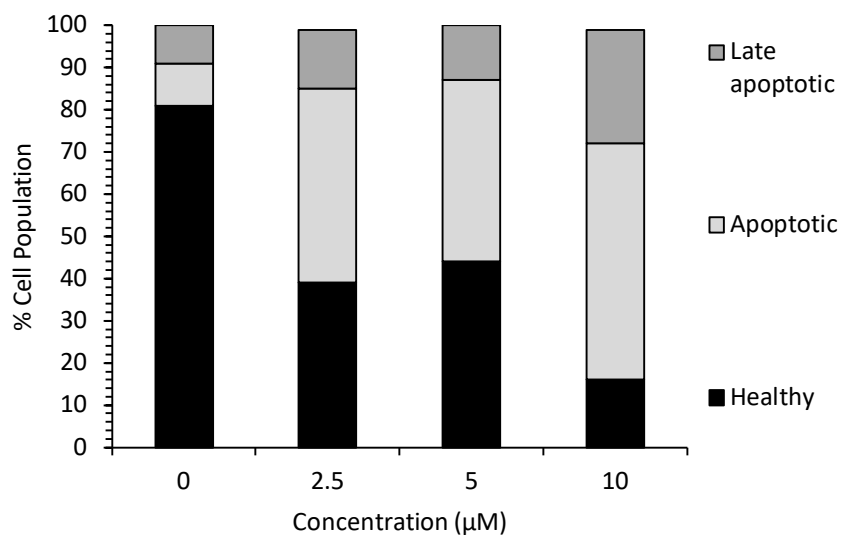
	Percentage of cell population			
Cell state	**Control**	**5µM**	**10µM**	**20µM**
Healthy	81	39	44	16
Apoptotic	10	46	43	56
Late apoptotic	9	14	13	27

Figure 8.12: Mitochondrial potential assay identifying induction of apoptosis in the pancreatic adenocarcinoma cell line MIA-PaCa$_2$ after 96-hour exposure to KMR –NR 2. The exposure concentrations ranged from 5µM - 20µM with "0" denoting the control sample (n=1).

8.3.3.4 - KMR-SR 3

The effect of KMR-NR 3 on the cell number and viability of MIA-PaCa$_2$ is shown in figure 8.13. Following a continuous 96-hour exposure to KMR-NR 3, a dose dependent reduction in cell number and percentage viability was obtained. The IC$_{50}$ obtained using the NC3000 (IC$_{50}$ = >10µM) was higher to that obtained using the MTT assay described above (IC$_{50}$ = 5.31 $\pm$ 1.95µM). These results are also illustrated visually in figure 8.14 and they confirm that cell viability decreases in a dose dependent manner, which like the MTT assays sees a cell response from 5µM.   Figure   8.14   also demonstrates that the novel compound KMR-SR 3 induces morphological changes in the MIA-PaCa$_2$ cell line with very little in the form of functional living cells remaining at higher concentrations. The results of apoptosis induction in MIA-PaCa$_2$ cells following continuous exposure to KMR-SR 3 are presented in figure 8.15. These results are indicative that KMR-SR 3 induces apoptosis and it does so in a dose dependent manner (figure 8.15).
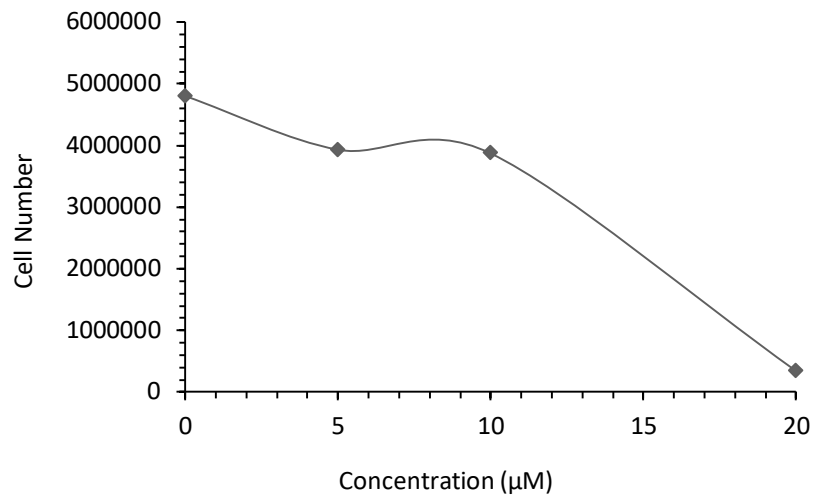
	Control	5μM	10μM	20μM
Total cells in sample	4.8×10^6	3.93×10^6	3.87×10^6	3.41×10^5
Percentage cell viability	98.1	67.8	66.0	56.0

Figure 8.13: Effect of increasing doses of KMR-NR 3 on the cell number of pancreatic adenocarcinoma cell line MIA-PaCa$_2$ after 96-hour exposure. "0" denotes the control sample with concentrations of 5μM, 10μM and 20μM being tested. Cell viability is expressed as a percentage based on acridine Orange staining the entire population and DAPI which stains non-viable cells (n=1).
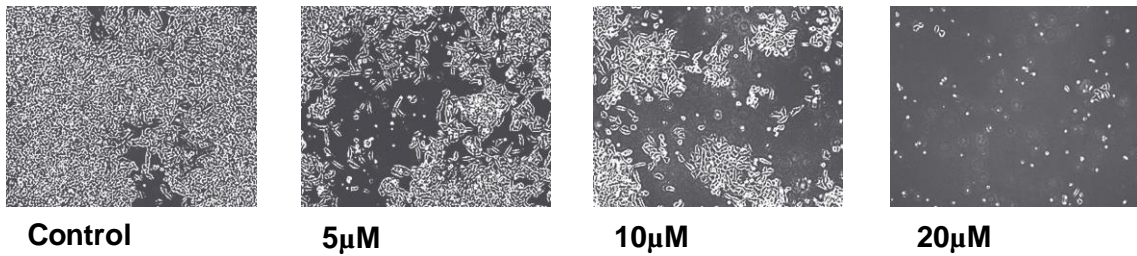
Figure 8.14: Microscope images of pancreatic adenocarcinoma cell line MIA-PaCa$_2$ cell line exposed to increasing doses of KMR-NR 3 over a 96-hour exposure time.
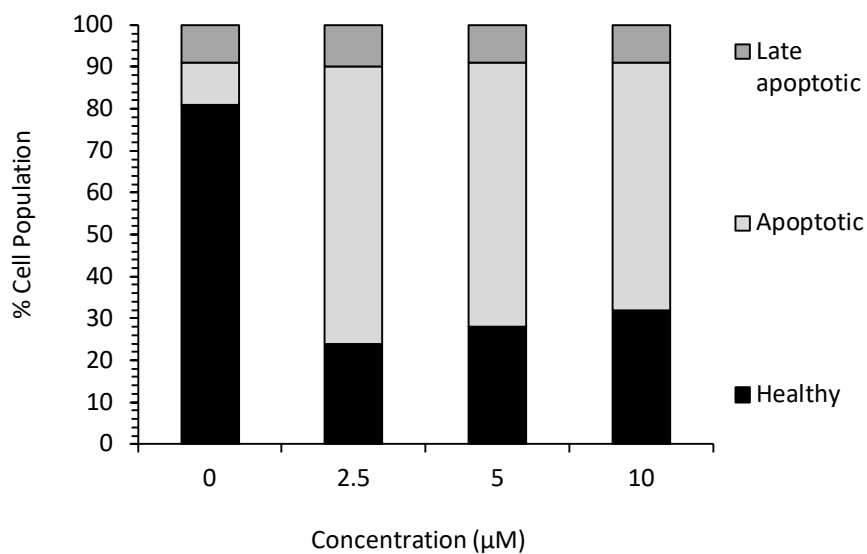
		Percentage of cell population		
Cell state	**Control**	**5µM**	**10µM**	**20µM**
Healthy	81	24	28	32
Apoptotic	10	66	63	59
Late apoptotic	9	10	9	9

Figure 8.15: Mitochondrial potential assay identifying induction of apoptosis in the pancreatic

adenocarcinoma cell line MIA-PaCa$_2$ after 96-hour exposure to KMR –NR 3. The exposure concentrations

ranged from 5µM - 20µM with "0" denoting the control sample (n=1).

8.4 - Discussion

A number of varying ruthenium, iridium and rhodium half sandwich complexes were investigated with novel ruthenium and iridium oxime and oximato ligand compounds being the most promising (table 8.11). These "hit" compounds were identified based upon equivalent or increased potency and selectivity in comparison to cisplatin the platinate gold standard. Despite the novel potential of rhodium as an alternative to existing platinum and ruthenium metallodrugs (Leung, Zhong, Chan, & Ma, 2013) in this investigation the rhodium complexes synthesised fail to exert sufficient cytotoxic activity.

From the four lead compounds selected in this investigation KMR-SA 11 is the most potent displaying superior potency to cisplatin on the pancreatic adenocarcinoma cell line MIA-PaCa$_2$ (IC$_{50}$=2.87 ± 0.26µM table 8.2) with the potency of the other three lead compounds displaying IC$_{50}$ values of between 5µM and 8µM (cisplatin=3.62 ± 0.74µM). Although the potency of the majority of these compounds is less than that of cisplatin the selectivity profile of these novel compounds is very promising with all the compounds displaying superior selectivity to cisplatin on the pancreatic adenocarcinoma cancer cell line MIA-PaCa$_2$ relative to the non-cancerous retinal epithelial cell line ARPE-19 (table 8.3). KMR-NR 2 displays the highest selectivity index at 5.45 the compound is 3-fold more selective than the gold standard cisplatin (SI=1.77) on this particular cell line. The extreme potency and selectivity displayed by cisplatin on the HT-29 colorectal adenocarcinoma cell line does result in neither of the

novel compounds displaying comparable potency or selectivity in this particular cell line. Another observation throughout the exposure of the cancerous cell lines to the lead novel compounds is that the morphology of cells is dramatically altered with increasing concentration. Observations from the microscope images show cells become more circular, appearing less functional (floating opposed to attached) and unable to form colonies as they become dispersed.

As discussed in chapter 7 additional investigations such as alternative apoptotic assays will give greater insight and further prove/disprove the initiation of apoptosis following exposure to the novel compounds. Greater clarification of the activity of the compounds to determine whether the compounds are cytotoxic or cytostatic will also increase our understanding of the mechanistic profile of these compounds. Alongside additional assays reruns of assays already completed will allow for more robust data, as previously discussed running an assay once does not allow for potential error.

8.5 - Conclusion

In conclusion, the results of this study have identified four novel ruthenium and iridium oxime and oximato ligand compounds that are as potent as cisplatin in the pancreatic adenocarcinoma cell line MIA-PaCa$_2$. Ruthenium and iridium based compounds were found to be the most active metal complexes and rhodium being the most inactive. Initial mechanistic studies were performed in the form of mitochondrial potential assays and viability cell count assays. Although it showed all the compounds resulted in dose dependent apoptosis, the assay has limitations. The main being that a reduction in the mitochondrial potential of a cell is not specific to apoptosis and can be induced *via* other external stresses and therefore an additional apoptotic assay is required to further validate the results obtained. These investigations would also benefit from further studies to (i) evaluate shorter drug exposure conditions (ii) confirm the induction of apoptosis using other assays such as Annexin V and (iii) conduct similar

In the context of the overall objectives of the thesis, the phenotypic screen based on potency alone compared to platinates identified four compounds of interest from thirty-one previously unscreened compounds. With regards to the selectivity index *in vitro*, all four of the four identified lead compounds showed greater selectivity than cisplatin with one of the compounds KMR-SA 11 also displaying superior potency to cisplatin on the MIA-PaCa$_2$ cell lines.

Chapter 9 - Evaluation of Metallohelices as Anti-Cancer Therapies

9.1 - Introduction

In the field of anti-cancer drug development, there are certain rules or guidelines that steer the development of novel compounds (Lipinski, Lombardo, Dominy, & Feeney, 2001). These are called the Lipinski rules and for a molecule to be active following oral administration, specific conditions should be met; (i) the total number of oxygen-hydrogen and nitrogen-hydrogen bonds (collectively called hydrogen bond donors) should be no more than 5 (ii) Hydrogen bond acceptors (all nitrogen or oxygen atoms) should number no more than 10 (iii) the molecular mass should be less than 500 Daltons (iv) the log P value (octanol/water partition coefficient) should not be greater than 5. In this chapter, the evaluation of a series of large molecular weight metallohelices are described, none of which comply the Lipinski these rules described.

There are many exceptions to the Lipinski rules and the work described in this chapter exemplifies this. The molecules examined are a series of metallohelicies developed by Professor Peter Scott at the University of Warwick. They were initially developed not only because of their interesting chemistry but also because their helical shape and structure suggested that they may act as pepdidomimetics. There is considerable interest in the development of peptides and peptidomimetics as direct acting anti-cancer drugs and as immunomodulatory agents (Junaid et al., 2015). One of the major limitations of peptide based drugs is their pharmacological instability in

biological systems and peptidomimetics are widely viewed as an important way forward to tackling this problem (Cunningham, Qvit, & Mochly-Rosen, 2017). This was the primary reason for selecting these compounds for evaluation in this thesis. It is important to stress that the compounds tested were not developed to target a specific pathway and therefore a phenotype based approach was the strategy adopted.

Metallohelices are assemblies of rigid organic ligands around a metal ion core, resembling α-helices in terms of their diameter and charge (shown in figure 9.1) (Kaner & Scott, 2015; Lehn et al., 1987). These are complex, large molecular weight compounds and in order to be potential anti-cancer drugs, a number of issues should be addressed. These include optical purity, stability, solubility, availability on a practical scale and synthetic diversity. Therefore the key has been to develop simple self-assembling, optically pure, monometallic complexes utilising amino acids as the source of chirality and not rigid ligands (Howson et al., 2009). This was achieved by preparing thermodynamically stable, single enantiomers of monometallic units connected together by organic linkers resulting in self-assembling, water stable, helicate-like compounds with high stereo-chemical purity. These compounds are referred to as flexicates, with one such being an iron (II) "flexicate" system exhibiting promising antimicrobial activity (Howson et al., 2012). The general structures of these compounds together with specific examples of ligands and compounds is presented in figure 9.2. The compounds described in this chapter exhibit structural diversity and the details will be described in each sub-section. The overall aim of the studies conducted

here was to assess (i) potency and (ii) selectivity against cancer and non-cancer cells *in vitro* with the aim of selecting potential lead compounds for mechanistic studies. Selected compounds were also evaluated *in vivo* against human tumour xenografts and this work was conducted under the direction of Dr Steve Shnyder at the University of Bradford. These results are reported here to illustrate the effectiveness of the screening procedures and acknowledgment to those who performed the studies is given at the appropriate place.
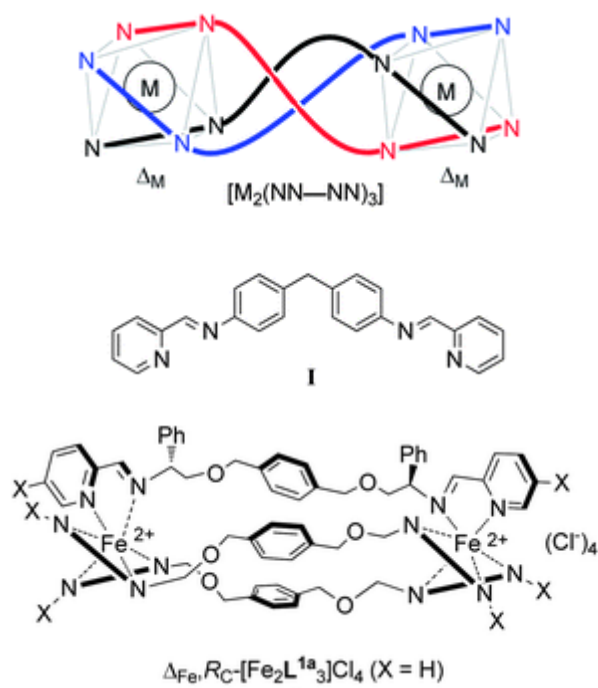
Figure 9.1: Chemical structures of metallohelicates. Schematic representation (upper) of one enantiomer, which comprises of three relatively rigid ditopic ligands, in this example the N-N system (middle), wrapped in a helical array around two metal ions. Taken from(Brabec et al., 2013). The compound in the lower panel represents the full helicate structure of one of the complexes under investigation in this thesis.

9.2 - Methods

9.2.1 - Chemosensitivity Studies

The response of tumour and non-cancer cell lines to the novel metallohelices were determined using the MTT assays as described in sections 2.5.3. As with previous chapters the aim of the initial chemosensitivity was to identify "hit" compounds with regards to (i) potency and (ii) selectivity. The potency of the compounds was tested on colonic adenocarcinoma HCT116 p53+/+ cell lines and the relative selectivity measured by testing the said compounds on the retinal epithelial non-cancerous cell line ARPE-19. As with previous MTT investigations, the results represent the mean ± standard deviation of three independent experiments. The selectivity index is defined as the mean IC_{50} of non-cancer cells divided by the IC_{50} for tumour cells; values >1 indicate selectivity for tumour cells *in vitro*.

9.2.1.1 - Chemical Structures and Preparation of Drug Stock Solution

A series of compounds were obtained from Professor Peter Scott's research group and these were organised into Classes 1 and 3 each with class 1 compounds split into 2 sets (1a and 1b) and class 3 split into five subsets sets based on structural criteria. The chemical structures and preparation of stock solutions are presented below. A number of compounds were initially dissolved in methanol and in these cases, the final concentration of methanol in all cell culture experiments was 0.1% (v/v) which is not toxic to cells.

Class 1a
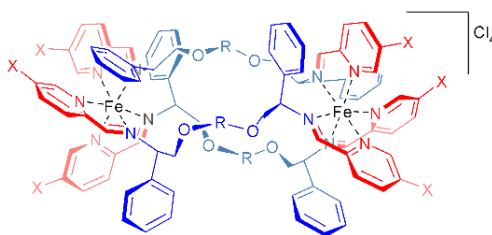
Compound	Compound type	Fe	Diluent	MW	Weight (mg)	Volume (µl)	Concentration (mM)
AKK015	(m)Xylene-H	Λ	Methanol	1911.54	3.55	18.57	100
AKK022	(m)Xylene-H	Δ	Methanol	1911.54	4.80	25.11	100
SEH531	(P)Xylene-H	Λ	Methanol	2043.7	3.14	15.36	100
SEH532	(P)Xylene-H	Δ	Methanol	2043.7	7.08	34.64	100
DHS41	DBFuran-H	Λ	Methanol	2187.82	1.96	8.95	100
DHS42	DBFuran-H	Δ	Methanol	2187.82	4.79	21.89	100
DHS74	Biphen-H	Λ	Methanol	2145.87	1.92	8.95	100
DHS115	Biphen-H	Δ	Methanol	2145.87	3.15	14.68	100
DHS101	PhSPh-H	Λ	Methanol	2242.05	1.83	8.17	100
DHS103	PhSPh-H	Δ	Methanol	2242.05	6.20	27.65	100
DHS124	PhOPh-H	Λ	Methanol	2193.86	3.25	14.81	100
DHS105	PhOPh-H	Δ	Methanol	2193.86	2.62	11.94	100
DHS128	PhCH2Ph-H	Δ	Methanol	2187.95	3.64	16.64	100
DHS130	PhCH2Ph-H	Λ	Methanol	2187.95	4.43	20.25	100
DHS132	Bibenzyl-H	Δ	Methanol	2230.03	2.39	10.72	100
DHS134	Bibenzyl-H	Λ	Methanol	2230.03	4.14	18.56	100
KLB016	(m)Xylene-OProp	Λ	Methanol	2386	3.91	16.39	100
KLB007	(m)Xylene-OProp	Δ	Methanol	2386	2.44	10.23	100

Table 9.1: Class 1a flexicate metallohelix complexes structure and stock solution preparation.

Class 1b
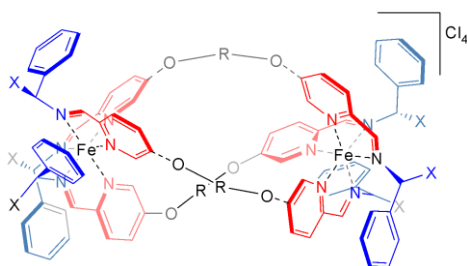
Compound	Compound type	Fe	Diluent	MW	Weight (mg)	Volume (µl)	Concentration (mM)
RAK373	F-ALKE-H	Δ	Methanol	1767.37	3.45	19.52	100
HS183	F-HS-Alkyne	Λ	Methanol	2340.71	4.48	19.14	100
HS186	F-HS-Alkyne	Δ	Methanol	2322.70	6.63	28.54	100

Table9.2: Class 1b flexicate metallohelix complexes structure and stock solution preparation.
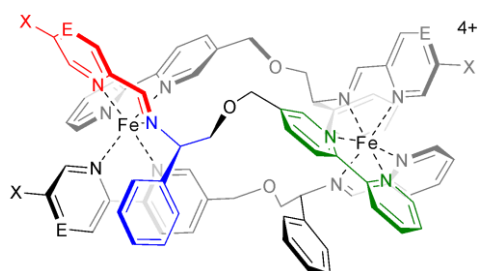
Class 3a

T-ADF-H
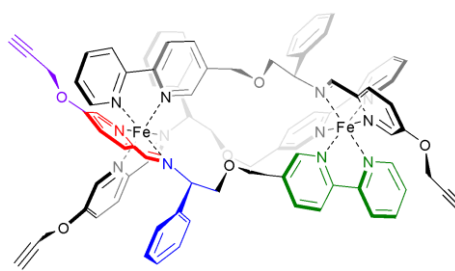
T-HS-ALKYNE

Compound	Compound type	Fe	Diluent	MW	Weight (mg)	Volume (ml)	Concentration (μM)
ADF495	T-ADF-H	Δ	Medium	1599.05	4.38	27.39	100
HS138	T-HS-Alkyne	Λ	Medium	1920.46	1.70	8.85	100
HS139	T-HS-Alkyne	Δ	Medium	1920.46	7.01	36.50	100

Table 9.3: Class 3a triplex metallohelixes complex structure and stock solution preparation.

Class 3a click

Table 9.4: Class 3a triplex metallohelix complexes with sugar and arene clicked R groups structure and stock solution preparation. Representative of R groups Glucose **(A)** and benzyl **(B)** displayed above.
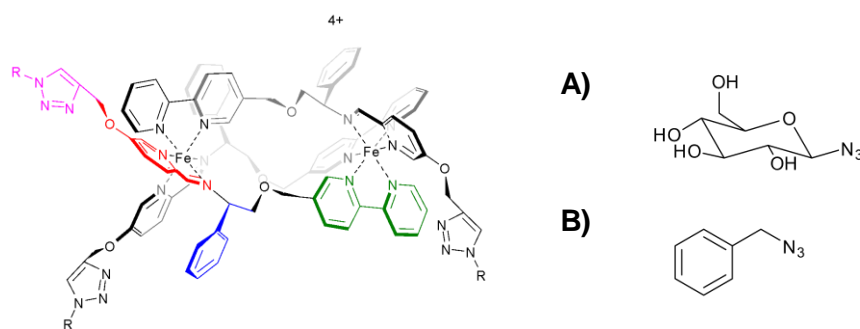
Compound	Compound type	Fe	Diluent	MW	Weight (mg)	Volume	Concentration
HS130	T-HS-FluorBenzene	Λ	Methanol	2355.66	3.86	16.4µl	100Mm
HS103	T-HS-FluorBenzene	Δ	Methanol	2391.68	9.52	39.8µl	100Mm
HS093	T-HS-Methoxybenzene	Λ	Methanol	2463.76	12.55	50.9µl	100Mm
HS085	T-HS-Methoxybenzene	Δ	Methanol	2481.77	1.88	7.6µl	100Mm
HS094	T-HS-benzonitrile	Λ	Methanol	2430.7	3.93	16.2µl	100Mm
HS095	T-HS-benzonitrile	Δ	Methanol	2376.67	4.10	17.3µl	100Mm
HS100	T-HS-Benzoic acid	Λ	Methanol	2415.65	3.15	13.0µl	100Mm
HS104	T-HS-Benzoic acid	Δ	Methanol	2433.66	5.98	24.6µl	100Mm
HS089	T-HS-peracetylated-Glucose	Λ	Methanol	3165.92	7.75	24.5µl	100Mm
HS090	T-HS-peracetylated-Glucose	Δ	Methanol	3183.93	2.50	7.9µl	100Mm
HS120	T-HS-Glucose	Λ	Medium	2517.7	1.20	4.8ml	100µM
HS121	T-HS-Glucose	Δ	Medium	2553.73	1.65	6.5ml	100µM
HS136	T-HS-Deoxy-glucose	Λ	Medium	2463.67	1.33	5.4ml	100µM
HS137	T-HS-Deoxy-glucose	Δ	Medium	2463.67	1.30	5.3ml	100µM
HS111	T-HS-peracetylated-Galactose	Λ	Methanol	3147.91	11.01	35µl	100Mm
HS112	T-HS-peracetylated-Galactose	Δ	Methanol	3183.93	6.68	21µl	100Mm
HS118	T-HS-Galactose	Λ	Medium	2589.75	3.07	11.9ml	100µM
HS119	T-HS-Galactose	Δ	Medium	2553.73	1.49	5.8ml	100µM

Compound	Compound type	Fe	Diluent	MW	Weight (mg)	Volume	Concentration
HS097	T-HS-Aceylgalactosamine	Λ	Medium	2676.81	3.02	11.3ml	100μM
HS098	T-HS-Aceylgalactosamine	Δ	Medium	2640.78	1.25	4.7ml	100μM
HS131	T-HS-peracetylated-Mannose	Λ	Methanol	3057.85	4.01	13.1μl	100Mm
HS132	T-HS-peracetylated-Mannose	Δ	Methanol	3057.85	6.84	22.4μl	100Mm
HS134	T-HS-Mannose	Λ	Medium	2481.68	4.03	16.2ml	100μM
HS135	T-HS-Mannose	Δ	Medium	2463.67	1.25	5.1ml	100Mm
HS141	T-HS-Benzyl	Λ	Methanol	2337.71	7.05	30.16μl	100Mm
HS142	T-HS-Benzyl	Δ	Methanol	2391.74	2.71	11.3μl	100Mm
HS145	T-HS-Aceylglucosamine	Δ	Medium	2640.78	1.45	5.5μl	100mM
HS146	T-HS-Aceylglucosamine	Λ	Medium	2658.79	1.15	4.3μl	100mM

Table 9.4 (continued): Class 3a triplex metallohelix complexes with sugar and arene clicked R groups structure and stock solution preparation. Representative of R groups Glucose **(A)** and benzyl **(B)** displayed above.

Class 3a Partially Clicked Alkynes
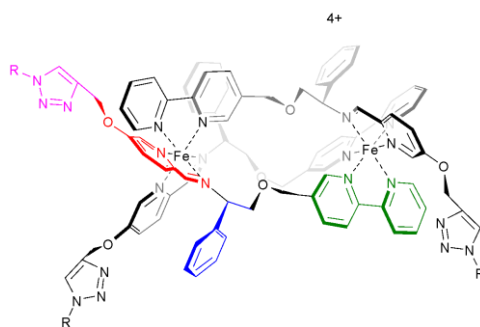
Compound	Compound type	Fe	Diluent	MW	Weight (mg)	Volume	Concentration
HS252	Partially clicked arenes based on HS142	Λ	Methanol	2154.74	2.60	12.07μl	100mM
HS253	Partially clicked arenes based on HS142	Δ	Methanol	2154.74	5.18	24.04μl	100mM
HS255	Partially clicked sugars based on HS121	Λ	Medium	2165.71	10.20	47.10ml	100μM
HS256	Partially clicked sugars based on HS121	Δ	Medium	2165.71	2.09	9.65ml	100μM

Table 9.5: Class 3a triplex metallohelix complexes with partially clicked alkyne R groups structure and
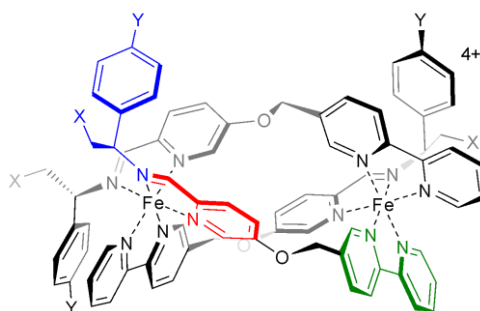
stock solution preparation

Class 3b

Compound	Compound type	Fe	Diluent	MW	Weight (mg)	Volume (ml)	Concentration (µM)
RAK435	T-RAK-ALKY	Λ	Medium	1599.05	1.92	12.01	100
RAK434	T-RAK-ALKY	Δ	Medium	1599.05	4.79	29.96	100

Table 9.6: Class 3b triplex metallohelix complexes structure and stock solution preparation.

Class 3C
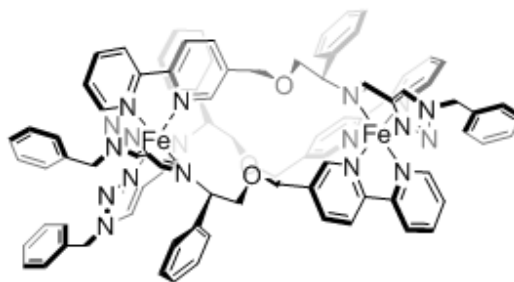
Compound	Compound type	Fe	Diluent	MW	Weight (mg)	Volume	Concentration
HS220	T-HS-Benzyl-triazol-aldehyde	Λ	Medium	1926.54	3.24	16.82ml	100µM
HS224	T-HS-Benzyl-triazol-aldehyde	Δ	Medium	1926.54	3.8	19.72ml	100µM
HS232	T-HS-Benzonitrile-triazol-aldehyde	Λ	Medium	1965.51	6.34	32.26ml	100µM
HS233	T-HS-Benzonitrile-triazol-aldehyde	Δ	Medium	1947.50	5.10	26.19ml	100µM
HS238	T-HS-methoxybenzyl-triazol-aldehyde	Λ	Medium	2016.58	4.34	21.52ml	100µM
HS239	T-HS-methoxybenzyl-triazol-aldehyde	Δ	Medium	2016.58	3.44	17.06ml	100µM
HS240	T-HS-fluorobenzyl-triazol-aldehyde	Λ	Medium	1962.50	3.60	18.34ml	100µM
HS241	T-HS-fluorobenzyl-triazol-aldehyde	Δ	Medium	1962.50	4.79	24.41ml	100µM
HS244	T-HS-benzoic acid-triazol-aldehyde	Λ	Methanol	2076.52	3.33	16.04µl	100mM
HS245	T-HS-benzoic acid-triazol-aldehyde	Δ	Methanol	2094.53	2.78	13.27µl	100mM

Table 9.7: Class 3c triplex metallohelix complexes structure and stock solution preparation. Class 3b with triazole aldehyde in the place of pyridine.

9.2.2 - Analysis of Cell Viability, Apoptotic Induction and Cell Cycle Parameters

Cell lines were exposed to "hit" compounds for 2, 8 and 24 hours and analysis of cell viability, induction of apoptosis and effects on cell cycle parameters were determined using the NC3000 cytometer, details of which have been described elsewhere (see 2.6 seeded as per 2.6.2). For these experiments, drug exposure concentrations were dependent upon the dose response curve of the complexes on both HCT116 and ARPE-19 cell lines; a single concentration which exert maximal toxic effect on the cancerous cell line but did not prove toxic to non-cancerous cells were chosen for each 'hit' compound.

9.2.3 - Drug Localisation Assay

HCT116 p53$^{+/+}$ and ARPE-19 cells were seeded at 10,000 cells per well into each of the eight chambers of The Falcon™ Chambered Cell Culture Slides (Cat# 10162861). These were then incubated for 24 hours (37°C 5% CO_2). After 24 hours, the cells were exposed to 10µM and 100µM concentrations of compounds containing alkyne groups suitable for click conjugation reactions (compounds summarised in table 9.5). Corresponding control wells were also treated with media alone or media plus 0.1% methanol dependent on the diluent used to dissolve the compound To conduct the click reaction, the following reagents were prepared:

1. **Click IT reaction buffer (10 x Tris-buffered saline):** 4ml Tris 10x buffer and 36ml of ultra-pure distilled water which can be stored at 2-6°C for up to 6 months.

2. **Alexa Fluor 555 Azide:** 200µl of high quality cell culture grade methanol was added to 0.5mg MW powder to give a final concentration of 5µM). This can be stored at -20°C for up to 12 months.

3. **Click IT reaction additive (sodium ascorbate):** A 100mM solution of sodium ascorbate in ultra-pure water was freshly prepared on the day of the experiment and protected from light as it is prone oxidisation (presenting as a light brown liquid).

After 1-hour drug exposure, the medium was carefully removed, and cells were carefully washed with PBS and fixed with 4% paraformaldehyde in PBS for 15 minutes. The paraformaldehyde was removed, and cells given one wash in PBS. The cells were then permeabilised with 0.1% Triton-X100 in PBS for 5mins and washed once again in PBS. To block any unspecific binding, the cells were then washed in 2% BSA in PBS and 500µl of freshly prepared Click-IT reaction cocktail was then added to each well. The Click-IT cocktail consisted of; 3.82ml reaction buffer **(1)**, 100µl (2.5mM) reaction additive **(3)**, 6.8µl 555 Alexafluor azide and 80µl $CoSO_4$ 100mM aqueous solution. The chamber with the Click-IT cocktail are then incubated at room temperature in the absence of light for 30 mins. After 30 minutes the cocktail was removed and DAPI (1µM) in PBS was added for a further 5 minutes at room temperature and protected from light. After 5 minutes the cells were then washed with 2% BSA in PBS followed by a further wash in PBS to reduce the BSA causing smear marks on images. Immediately after washing, the slides are then mounted with Mounting Medium and coverslips

carefully placed on the slides using tweezers to avoid causing air bubbles. The samples were processed on the Leica SP5 X laser scanning confocal microscope located at The University of Warwick, where the drug localisation investigations were completed.

Compound	MW	Diluent	Classification
HS138	2340.71	Medium	Class 1b alkynes based on RAK373
HS139	2322.70	Medium	
HS183	1920.46	Medium	Class 3a alkynes based ADF495
HS186	1920.46	Medium	
HS255	2165.71	Medium	Partially clicked sugars based on HS121
HS256	2165.71	Medium	
HS252	2154.74	Methanol	Partially clicked arenes based on HS142
HS253	2154.74	Methanol	
RAK434	1599.05	Medium	Class 3b alkyne
RAK435	1599.05	Medium	
KLB007	2386.00	Methanol	Class 1a alkyne based on AKK022
KLB013	2386.00	Methanol	

Table 9.8: Alkyne click compounds used for drug localisation investigation. These compounds were used due to their available "click" alkyne ligands to which Alexa Fluor 555 attaches. Concentrations used were either 100µM or 10µM as specified in the results section.

9.2.4 - Autophagy Inhibition *Via* the Use of 3-Methyladenine (3-MA)

Because a small number of compounds (ADF495, RAK373, HS220 and HS121) induced clearly visible vacuole formation in the cytoplasm, their ability to induce autophagy was investigated. These compounds were tested in the absence and presence of 3 methyladenine (3-MA) which is an autophagy inhibitor. If autophagy is being induced by these compounds leading to cell death, the addition of 3-MA should reduce the sensitivity of cells to test compounds *in vitro*. 96 well plates were seeded as per optimum density from the seeding density assay (2.5.2), plated as per section 2.5.3 and left overnight in the incubator at 37°C 5% CO_2 for cells to adhere to the plates.

After 24 hours the medium is removed, washed with PBS and replaced with fresh 3-MA (5mM) supplemented media containing drug solutions covering a range of concentration. Control lanes were also treated with 3-MA (5mM). Following a 96-hour drug exposure under aerobic conditions, cell survival was determined using the MTT assay as described above. Each experiment was repeated in triplicate and the results presented are the mean ± standard deviation n=3 (each individual experiment replicated twice).

9.3 - Results

9.3.1 - Chemo-Sensitivity Assays

68 compounds were initially synthesised and evaluated. The results in terms of their potency and *in vitro* selectivity index are presented below. Out of the 68 compounds tested, only 5 failed to show potency below 10µM. These compounds are therefore potent cytotoxic agents with IC_{50} values that are comparable to the platinates. In many cases, sub-micromolar IC_{50} values were obtained which represents a significant increase in potency relative to cisplatin, oxaliplatin and carboplatin in particular. Selection of compounds for further analysis based on potency criteria alone would have led to a large number of compounds being identified as potential 'hit' compounds. From the 68 compounds, several compounds from each class were selected based on potency and their *in vitro* selectivity index. A total of 11 'hit' compounds were identified, all of which underwent further investigation. Description

of said "hit" compounds and their selection are described in more detail in the corresponding sections.

9.3.1.1 - Chemosensitivity Studies: Class 1a Compounds

Within this class of compounds, there are a number of very potent compounds displaying IC_{50} values in the nM range. The most active compound was DHS74 with an IC_{50} of 40 nM (figure 9.2). All compounds tested had IC_{50} values under 10µM deeming them all potent against the colonic adenocarcinoma HCT116 $p53^{+/+}$ cell line. In contrast, the response of ARPE-19 cells was much less with IC_{50} values ranging from 23.10µM (KLB016) to 170 nM (DHS74). These results demonstrate that several compounds have a good selectivity index *in vitro* which exceeds that of cisplatin and this will be described in more detail once the chemosensitivity data for all the compounds tested has been reported.
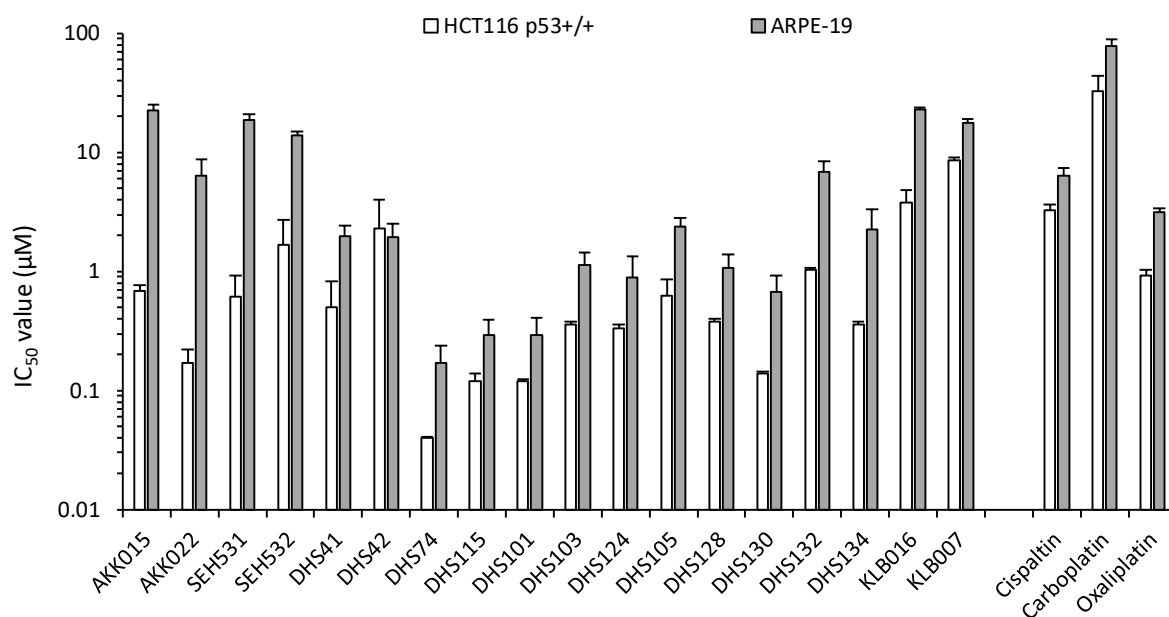
	IC$_{50}$ value (µM) ± SD	
Compound	HCT116 p53$^{+/+}$	ARPE-19
AKK015	0.69 ± 0.08	22.44 ± 2.56
AKK022	0.17 ± 0.05	6.39 ± 2.36
SEH531	0.61 ± 0.31	18.69 ± 2.09
SEH532	1.66 ± 1.05	13.90 ± 1.14
DHS41	0.50 ± 0.32	1.98 ± 0.45
DHS42	2.31 ± 1.71	1.94 ± 0.56
DHS74	0.04 ± 0.001	0.17 ± 0.07
DHS115	0.12 ± 0.02	0.29 ± 0.10
DHS101	0.12 ± 0.005	0.29 ± 0.12
DHS103	0.36 ± 0.02	1.14 ± 0.31
DHS124	0.33 ± 0.03	0.89 ± 0.46
DHS105	0.63 ± 0.23	2.37 ± 0.46

Figure 9.2: Response of HCT116 p53+/+ and ARPE-19 cells following continuous 96-hour exposure to novel Class 1a flexicate metallohelix complexes under aerobic conditions. The results are presented in both graphical and tabular forms and in both cases, the mean IC$_{50}$ values ± standard deviations for three independent experiments are presented n=3 (each individual experiment replicated twice).

	IC$_{50}$ value (µM) ± SD	
DHS128	0.38 ± 0.02	1.07 ± 0.32
DHS130	0.14 ± 0.004	0.67 ± 0.25
DHS132	1.03 ± 0.04	6.84 ± 1.57
DHS134	0.36 ± 0.02	2.26 ± 1.07
KLB016	3.78 ± 1.07	23.10 ±0.72
KLB007	8.61 ± 0.38	17.59 ±1.55
Cisplatin	3.26 ± 0.38	6.41 ± 0.95
Carboplatin	32.37 ± 11.14	77.73 ± 10.52
Oxaliplatin	0.93 ± 0.11	3.12 ± 0.28

Figure 9.2 (continued): Response of HCT116 p53+/+ and ARPE-19 cells following continuous 96-hour exposure to novel Class 1a flexicate metallohelix complexes under aerobic conditions. The results are presented in both graphical and tabular forms and in both cases, the mean IC$_{50}$ values ± standard deviations for three independent experiments are presented n=3 (each individual experiment replicated twice).

9.3.1.2 - Chemosensitivity Studies: Class 1b Compounds.

This class as with class 1a comprises of 3 potent candidates but with a clear lead compound (RAK373) which is at least 5 times more potent than HS183 and HS186. The sensitivity of ARPE-19 cells is also significantly less than HCT116 cells, particularly so in the case of RAK373 where a very high selectivity index exists (described in greater detail later in this chapter).
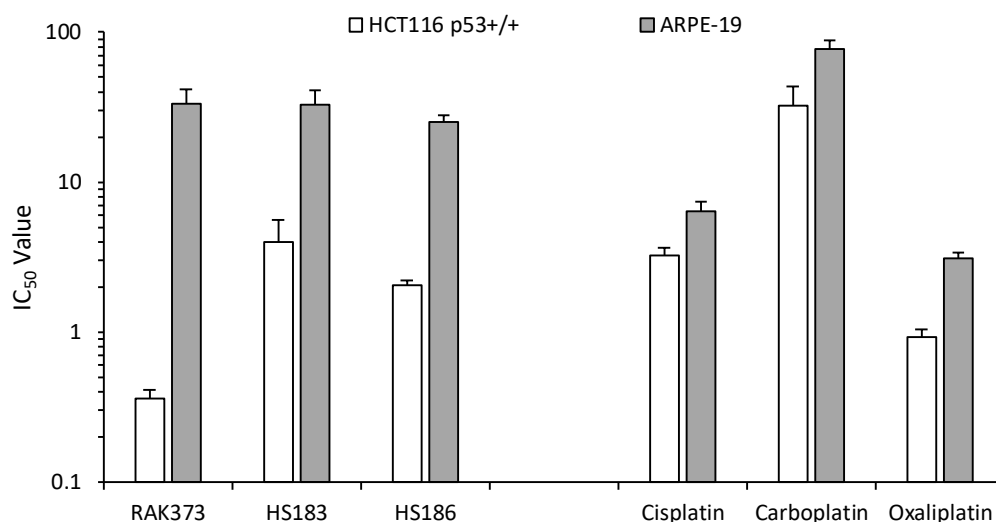
	IC$_{50}$ value (µM) ± SD	
Compound	HCT116 p53$^{+/+}$	ARPE-19
RAK373	0.36 ± 0.05	33.42 ± 8.25
HS183	3.96 ± 1.60	32.62 ± 8.49
HS186	2.06 ± 0.15	25.32 ± 2.52
Cisplatin	3.26 ± 0.38	6.41 ± 0.95
Carboplatin	32.37 ± 11.14	77.73 ± 10.52
Oxaliplatin	0.93 ± 0.11	3.12 ± 0.28

Figure 9.3: Response HCT116 p53+/+ and ARPE-1 cells following continuous 96-hour exposure to novel Class 1b flexicate metallohelix complexes in aerobic conditions. The results presented are the mean IC$_{50}$ values ± standard deviations for three independent experiments n=3 (each individual experiment replicated twice).

9.3.1.3 - Chemosensitivity Studies: Class 3a Compounds

Of the three compounds in this class, HS138 proved to exhibit comparatively low potency with an IC$_{50}$ against HCT116 cells of 19.35 ± 1.55µM. ADF495 and HS139 were active with IC$_{50}$ values below 10µM and both compounds showed reduced potency against ARPE-19 cells indicating a degree of selectivity for HCT116 cells.
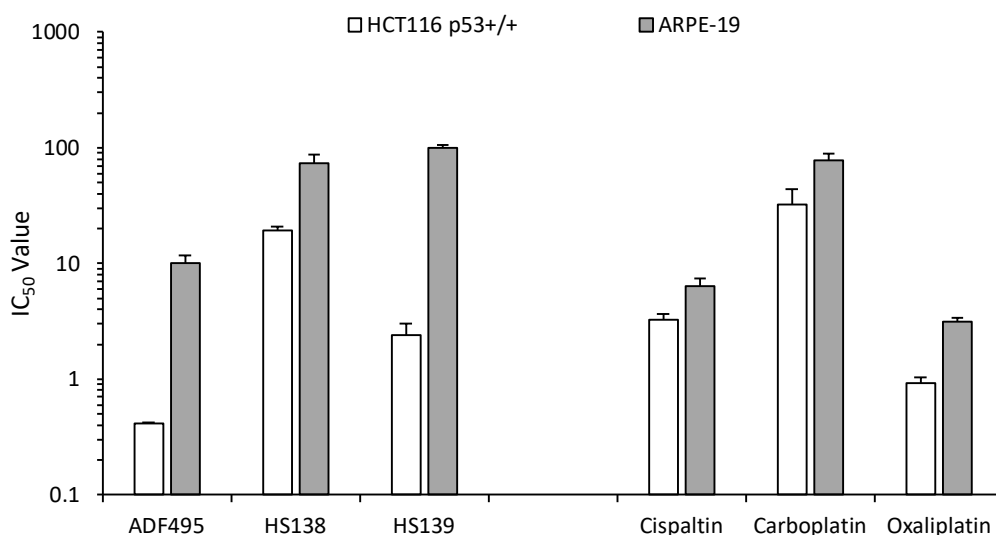
	IC$_{50}$ value (µM) ± SD	
Compound	HCT116 p53$^{+/+}$	ARPE-19
ADF495	0.41 ± 0.01	10.0 ± 1.77
HS138	19.35 ± 1.55	73.81 ± 13.05
HS139	2.41 ± 0.60	100.44 ± 4.67
Cisplatin	3.26 ± 0.38	6.41 ± 0.95
Carboplatin	32.37 ± 11.14	77.73 ± 10.52
Oxaliplatin	0.93 ± 0.11	3.12 ± 0.28

Figure 9.4: Response of HCT116 p53$^{+/+}$ and ARPE-19 cells following continuous 96-hour exposure to novel Class 3a triplex metallohelix complexes in aerobic conditions. The results presented are the mean IC$_{50}$ values ± standard deviations for three independent experiments n=3 (each individual experiment replicated twice).

9.3.1.4 - Chemosensitivity Studies: Class 3a Click Compounds

This class is not only of interest due to the nature of the compounds which are tethered to various ligands including various sugar tethered complexes, but it also offers a large number of potent compounds. Out of the 28 investigated, only 4 compounds have IC_{50} values above 10µM and these, with the exception for HS098, can be excluded based on their potency alone. The rationale of not initially excluding HS098 is due to the importance of its structure and very low potency against ARPE-19. In discussion with Professor Peter Scott's group in Warwick University, the sugar tethered complexes were considered priority compounds and HS098 was not rejected after the initial round of testing. In cases where IC_{50} values of > 100µM were recorded in the first round of testing against ARPE19 cells, concentrations of compound were increased in order to obtain an IC_{50} value and therefore obtain an accurate selectivity index *in vitro*.
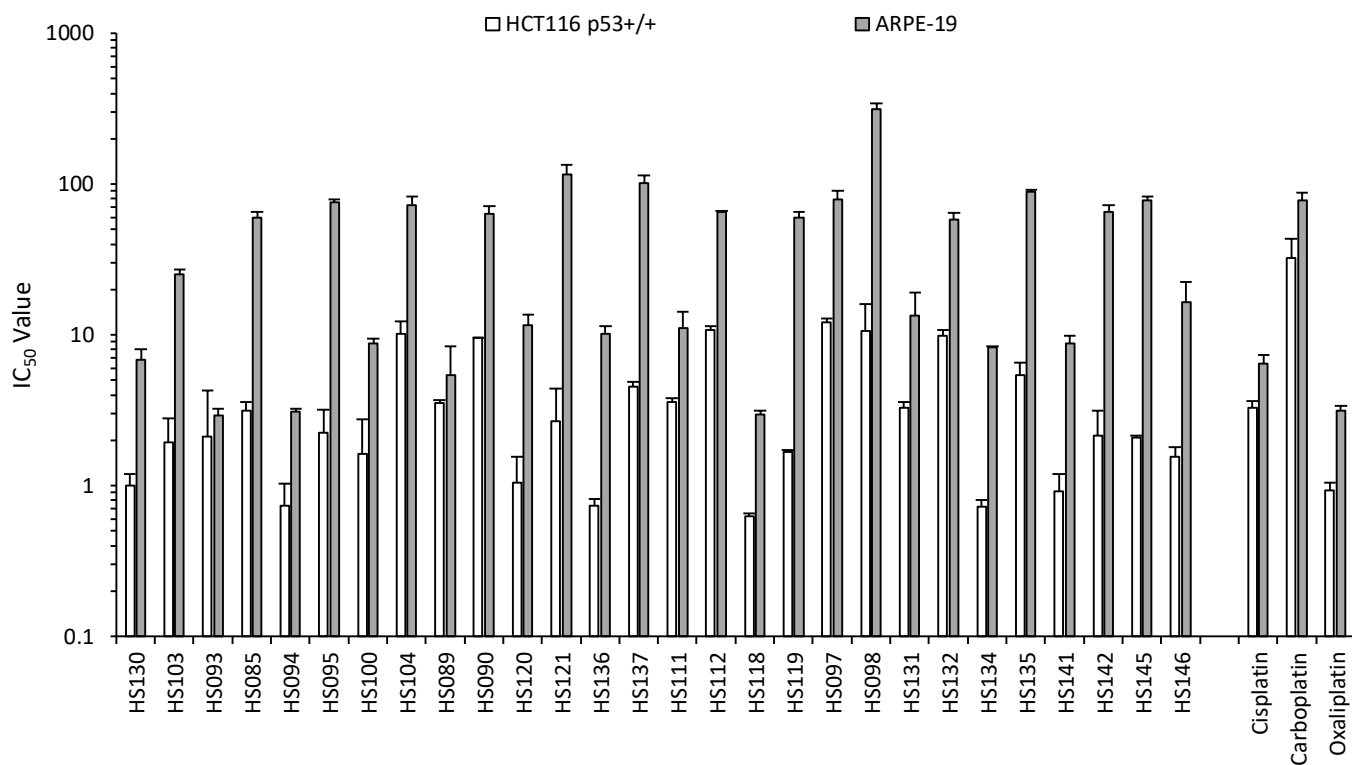
	IC$_{50}$ value (µM) ± SD	
Compound	**HCT116 p53$^{+/+}$**	**ARPE-19**
HS130	1.00 ± 0.19	6.88 ± 1.2
HS103	1.94 ± 0.84	25.37 ± 1.94
HS093	2.12 ± 2.17	2.94 ± 0.31
HS085	3.13 ± 0.47	59.60 ± 5.60
HS094	0.73 ± 0.30	3.08 ± 0.15
HS095	2.25 ± 0.96	76.14 ± 3.66
HS100	1.63 ± 1.13	8.75 ± 0.63
HS104	10.15 ± 2.12	72.23 ± 10.52
HS089	3.53 ± 0.18	5.44 ± 3.01
HS090	9.52 ± 0.10	63.17 ± 8.08
HS120	1.05 ± 0.51	11.64 ± 1.98

Figure 9.5: Response of HCT116 p53$^{+/+}$ and ARPE-19, following continuous 96-hour exposure to novel

Class 3a sugar and arene clicked triplex metallohelix complexes. The results presented are the mean IC$_{50}$

values ± standard deviations for three independent experiments n=3 (each individual experiment

replicated twice).

	IC$_{50}$ value (µM) ± SD	
Compound	HCT116 p53$^{+/+}$	ARPE-19
HS121	2.69 ± 1.71	115.55 ± 19.28
HS136	0.74 ± 0.08	10.18 ± 1.21
HS137	4.54 ± 0.31	101.12 ± 12.91
HS111	3.6 ± 0.23	11.04 ± 3.25
HS112	10.7 ± 0.74	65.45 ± 1.44
HS118	0.63 ± 0.02	2.96 ± 0.19
HS119	1.68 ± 0.04	59.68 ± 5.44
HS097	12.16 ± 0.74	79.64 ± 10.67
HS098	10.62 ± 5.42	315.35 ± 29.78
HS131	3.28 ± 0.28	13.35 ± 5.85
HS132	9.93 ± 0.92	57.9 ± 6.31
HS134	0.72 ± 0.08	8.22 ± 0.19
HS135	5.42 ± 1.16	89.31 ± 2.43
HS141	0.91 ± 0.28	8.82 ± 1.04
HS142	2.16 ± 0.97	65.58 ± 6.82
HS145	2.08 ± 0.08	77.73 ± 5.28
HS146	1.56 ± 0.23	16.56 ± 5.76
Cisplatin	3.26 ± 0.38	6.41 ± 0.95
Carboplatin	32.37 ± 11.14	77.73 ± 10.52
Oxaliplatin	0.93 ± 0.11	3.12 ± 0.28

Figure 9.5 (continued): Response of HCT116 p53$^{+/+}$ and ARPE-19, following continuous 96-hour exposure to novel Class 3a sugar and arene clicked triplex metallohelix complexes. The results presented are the mean IC$_{50}$ values ± standard deviations for three independent experiments n=3 (each individual experiment replicated twice).

9.3.1.5 - Chemosensitivity Studies: Class 3a Partially Clicked Alkyne Compounds

These compounds were initially synthesised for the use in the drug localisation assay (section 6.2.3) as they have an alkyne click to which the fluorescent dye attaches to. They do however display favourable potency.

	IC$_{50}$ value (µM) ± SD	
Compound	HCT116 p53$^{+/+}$	ARPE-19
HS252	2.51 ± 0.29	11.42 ± 4.51
HS253	2.29 ± 0.68	11.82 ± 3.93
HS255	1.56 ± 0.91	9.22 ± 3.26
HS256	1.22 ± 0.94	9.12 ± 1.19
Cisplatin	3.26 ± 0.38	6.41 ± 0.95
Carboplatin	32.37 ± 11.14	77.73 ± 10.52
Oxaliplatin	0.93 ± 0.11	3.12 ± 0.28

Figure 9.6: Response of HCT116 p53+/+ and ARPE-19 cells following continuous 96-hour exposure to novel Class 3a partially alkyne clicked triplex metallohelix complexes in aerobic conditions. The results presented are the mean IC$_{50}$ values ± standard deviations for three independent experiments n=3 (each individual experiment replicated twice).

9.3.1.6 - Chemosensitivity Studies: Class 3b Partially Clicked Alkyne Compounds

This group has less potent compounds than the previous groups with one compound (RAK434) displaying an IC_{50} value above 10µM. The values on the cancerous and non-cancerous cell lines are also very close demonstrating that the selectivity of these compounds is poor.
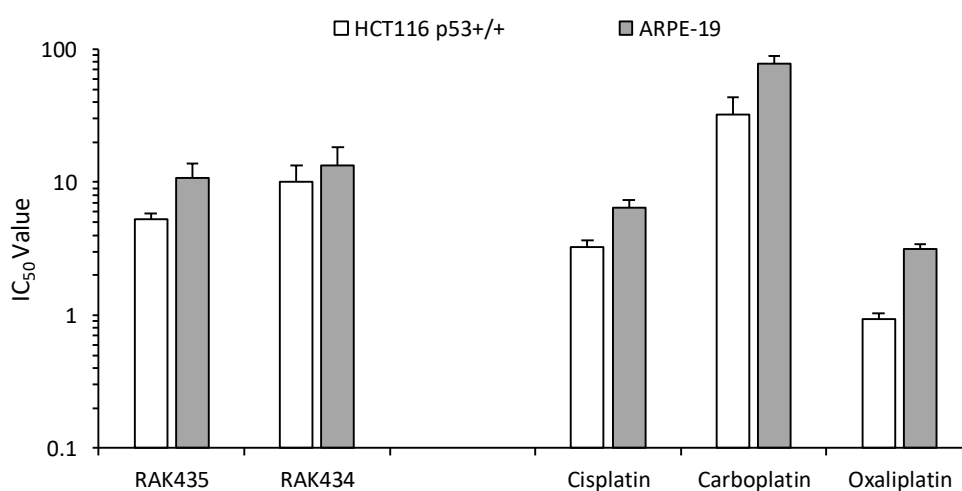
Compound	IC$_{50}$ value (µM) ± SD	
	HCT116 p53$^{+/+}$	ARPE-19
RAK435	5.28 ± 0.49	10.75 ± 3.14
RAK434	10.02 ± 3.32	13.35 ± 4.95
Cisplatin	3.26 ± 0.38	6.41 ± 0.95
Carboplatin	32.37 ± 11.14	77.73 ± 10.52
Oxaliplatin	0.93 ± 0.11	3.12 ± 0.28

Figure 9.7: Response of HCT116 p53$^{+/+}$ and ARPE-19 cells following continuous 96-hour exposure to novel Class 3b triplex metallohelix complexes in aerobic conditions. The results presented are the mean IC_{50} values ± standard deviations for three independent experiments n=3 (each individual experiment replicated twice).

9.3.1.7 - Chemosensitivity Studies: Class 3C Compounds

This class hosts extremely potent compounds against HCT116 p53$^{+/+}$ cells with only one compound displaying an IC$_{50}$ value above 0.5μM (HS245). In general, potency against ARPE19 cells was less with IC$_{50}$ values generally being in the μM range.

	IC$_{50}$ value (μM) ± SD	
Compound	**HCT116 p53$^{+/+}$**	**ARPE-19**
HS220	0.19 ± 0.01	0.97 ± 0.25
HS224	0.32 ± 0.14	6.31 ± 0.78
HS232	0.20 ± 0.02	1.83 ± 0.80
HS233	0.35 ± 0.20	9.88 ± 3.82
HS238	0.20 ± 0.01	2.22 ± 0.58
HS239	0.23 ± 0.02	7.97 ± 1.18
HS240	0.20 ± 0.01	1.92 ± 0.43
HS241	0.41 ± 0.30	6.89 ± 1.94
HS244	0.30 ± 0.10	0.72 ± 0.11
HS245	1.72 ± 0.07	3.05 ± 1.29
Cisplatin	3.26 ± 0.38	6.41 ± 0.95
Carboplatin	32.37 ± 11.14	77.73 ± 10.52
Oxaliplatin	0.93 ± 0.11	3.12 ± 0.28

Figure 9.8: Response of HCT116 p53$^{+/+}$ and ARPE-19 cells following continuous 96-hour exposure to novel Class 3c triplex metallohelix complexes in aerobic conditions. The results presented are the mean IC$_{50}$ values ± standard deviations for three independent experiments n=3 (each individual experiment replicated twice).

9.3.1.8 - Selectivity Indices *In Vitro:* Class 1a Compounds

Using the IC_{50} values presented above, the selectivity index for all the class 1a compounds tested was determined. Of all the compounds tested, only one compound (DHS42) displays a selectivity index below 1 highlighting how selective these compounds are. AKK022 displays the greatest selectivity and potency of these compounds and is over four times more potent than AKK015 an SEH531.
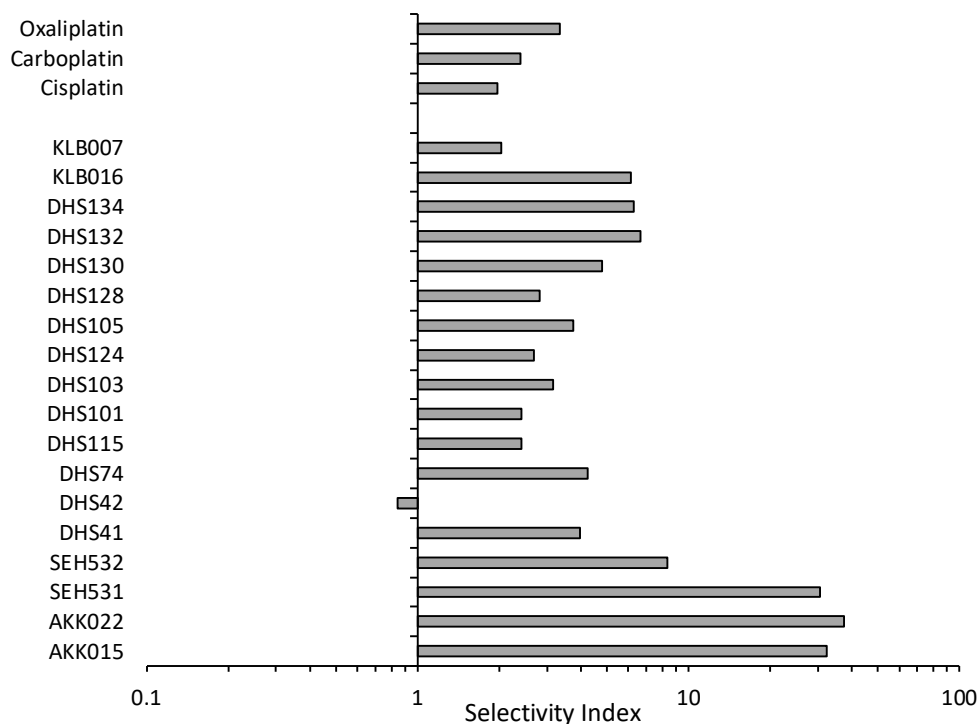
Compound	Selectivity Index
AKK015	32.52
AKK022	37.59
SEH531	30.64
SEH532	8.37
DHS41	3.96
DHS42	0.84
DHS74	4.25
DHS115	2.42
DHS101	2.42
DHS103	3.17
DHS124	2.70
DHS105	3.76

Figure 9.9: Selectivity of novel Class 1a flexicate metallohelix complexes. The selectivity index is defined as the mean IC_{50} ARPE-19 cells divided by the IC_{50} for HCT116 p53$^{+/+}$ cells. Values greater than 1 indicate that compounds have selectivity for cancer cells as opposed to non-cancer cells. As the mean IC_{50} values are used to calculate selectivity indices, no error bars are included on the graphs. This legend applies to all the figures reporting selectivity indices below.

Compound	Selectivity Index
DHS128	2.82
DHS130	4.79
DHS132	6.64
DHS134	6.28
KLB016	6.11
KLB007	2.04
Cisplatin	1.97
Carboplatin	2.40
Oxaliplatin	3.35

Figure 9.9 (continued): Selectivity of novel Class 1a flexicate metallohelix complexes. The selectivity index is defined as the mean IC_{50} ARPE-19 cells divided by the IC_{50} for HCT116 p53$^{+/+}$ cells. Values greater than 1 indicate that compounds have selectivity for cancer cells as opposed to non-cancer cells. As the mean IC_{50} values are used to calculate selectivity indices, no error bars are included on the graphs. This legend applies to all the figures reporting selectivity indices below.

9.3.1.9 - Selectivity Indices *In Vitro*: Class 1b

As with the potency profile RAK373 is far superior and displays the highest selectivity index of all the compounds of 92.83.
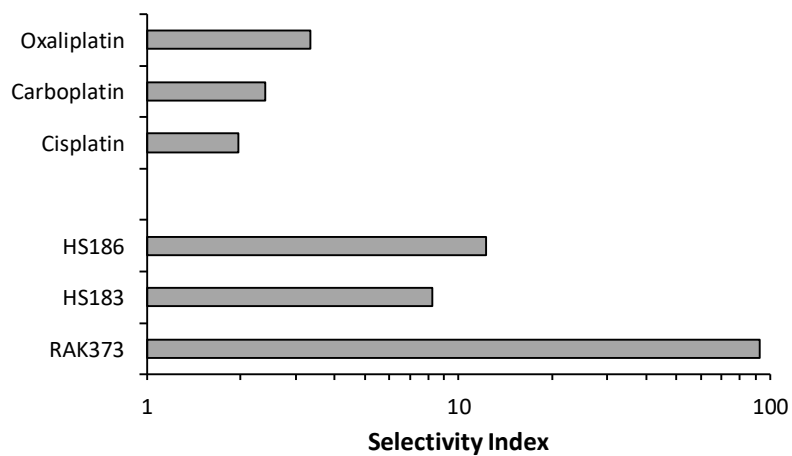
Compound	Selectivity Index
HS186	92.83
HS183	8.24
RAK373	12.29
Cisplatin	1.97
Carboplatin	2.40
Oxaliplatin	3.35

Figure 9.10: Selectivity of novel Class 1b flexicate metallohelix complexes.

9.3.1.10 - Selectivity Indices *In Vitro:* Class 3a

ADF495 and HS139 display superior selectivity and their role as unclicked 3a compounds can give real insight to the effects of tethering the complexes.
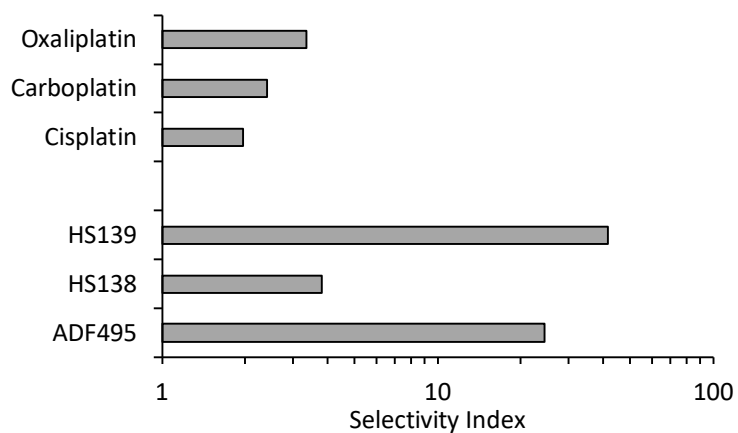
Compound	Selectivity Index
HS139	41.68
HS138	3.81
ADF495	24.39
Cisplatin	1.97
Carboplatin	2.40
Oxaliplatin	3.35

Figure 9.11: Selectivity of novel Class 3a triplex metallohelix complexes.

9.3.1.11 - Selectivity Indices *In Vitro*: Class 3a Click

This class of compounds displayed mixed selectivity profiles with HS145, HS142, HS098, HS119, HS121 and HS095 displaying the highest selectivity values.
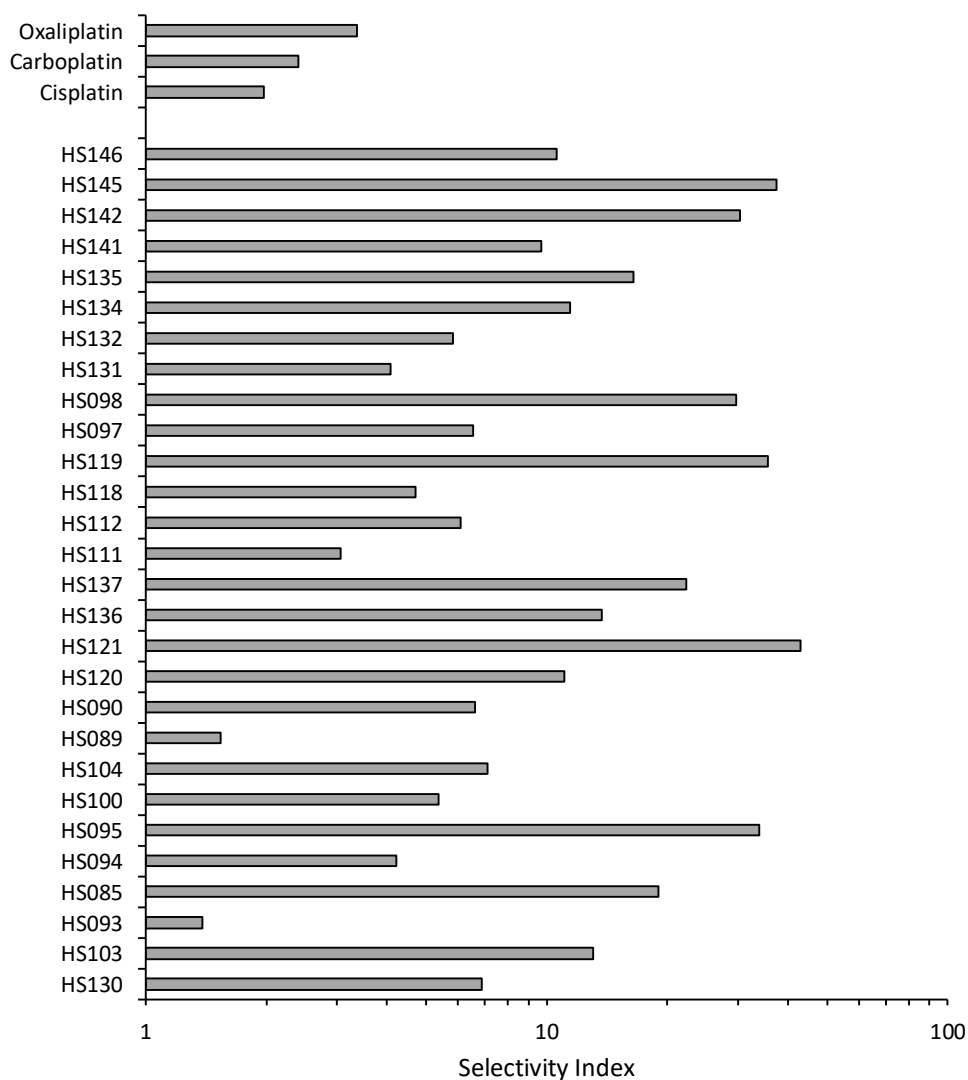
Figure 9.12: Selectivity of novel Class 3a sugar and arene clicked triplex metallohelix complexes.

Compound	Selectivity Index
HS103	6.88
HS093	13.08
HS085	1.39
HS094	19.04
HS095	4.22
HS100	33.84
HS104	5.37
HS089	7.12
HS090	1.54
HS120	6.64
HS121	11.09
HS136	42.96
HS137	13.76
HS111	22.27
HS112	3.07
HS118	6.12
HS119	4.70
HS097	35.52
HS098	6.55
HS131	29.69
HS132	4.07
HS134	5.83
HS135	11.42
HS141	16.48
HS142	9.69
HS145	30.36
HS146	37.37
Cisplatin	1.97
Carboplatin	2.40
Oxaliplatin	3.35

Figure 9.12 (continued): Selectivity of novel Class 3a sugar and arene clicked triplex metallohelix complexes.

9.3.1.12 - Selectivity Indices *In Vitro*: Class 3a Partially Clicked Alkynes

These compounds were synthesized as alkyne click compounds for drug localization assays, they show selectivity index values of between 4-8, which in comparison to other leads fairs poorly.
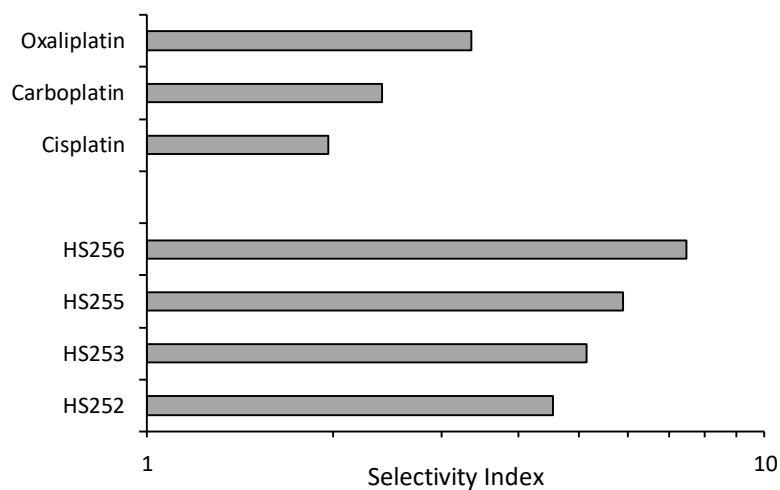
Compound	Selectivity Index
HS256	7.48
HS255	5.91
HS253	5.16
HS252	4.55
Cisplatin	1.97
Carboplatin	2.40
Oxaliplatin	3.35

Figure 9.13: Selectivity of novel Class 3a partially alkyne clicked triplex metallohelix complexes.

9.3.1.13 - Selectivity Indices *In Vitro*: Class 3b

This class of compounds displays low selectivity and potency and are therefore undesirable complexes for further chemo-toxicity investigation.
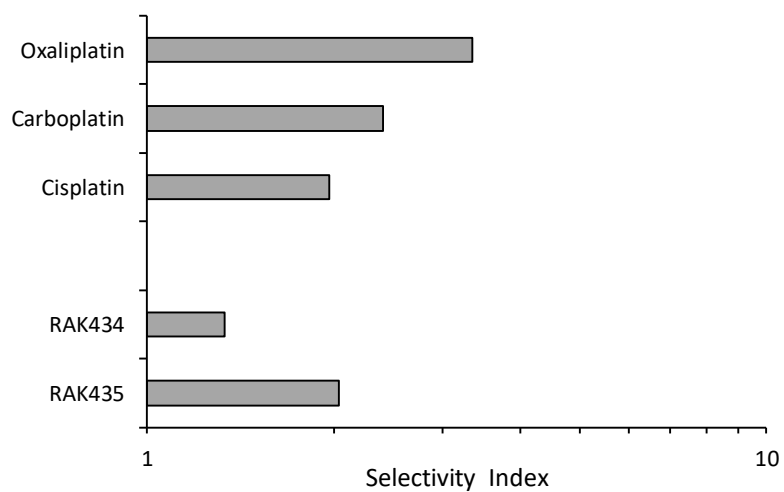
Compound	Selectivity Index
RAK434	1.33
RAK435	2.04
Cisplatin	1.97
Carboplatin	2.40
Oxaliplatin	3.35

Figure 9.14: Selectivity of novel Class 3b triplex metallohelix complexes.

9.3.1.14 - Selectivity Indices *In Vitro*: Class 3c

This class of compounds shows a varied selectivity with HS239 displaying the highest selectivity.
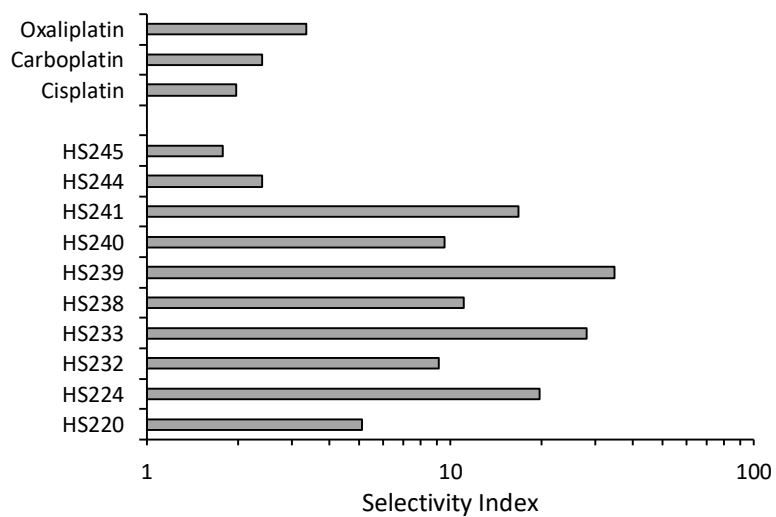
Compound	Selectivity Index
HS220	5.11
HS224	19.72
HS232	9.15
HS233	28.23
HS238	11.1
HS239	34.65
HS240	9.6
HS241	16.80
HS244	2.4
HS245	1.77
Cisplatin	1.97
Carboplatin	2.40
Oxaliplatin	3.35

Figure 9.15: Selectivity of novel Class 3c triplex metallohelix complexes.

9.3.2 - Comparison of "hit" Novel Metal NHC Complexes to Platinum Standard Complex

9.3.2.1 - Chemosensitivity Data *In Vitro*: Comparison to Platinates

The IC_{50} values of the selected leads are displayed in figure 9.16 with the IC_{50} values of the platinum standards as a comparative platform. All the "hit" compounds display greater potency than carboplatin and only two compounds HS098 and HS135 displaying reduced potency compared to cisplatin. Oxaliplatin is considered a highly potent standard yet four of the eleven "hit compounds" display greater potency.
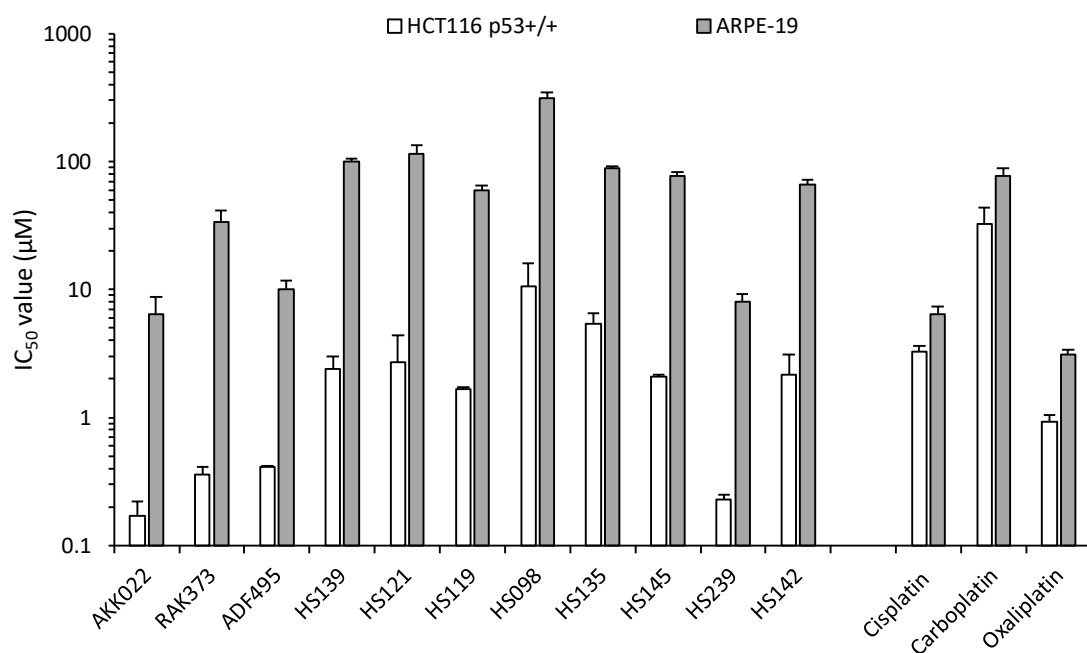
Figure 9.16: Comparison of the potency of novel metallohelix complexes to cisplatin, carboplatin and oxaliplatin in cancerous HCT116 p53^{+/+} and non-cancerous ARPE-19 cell lines. The values presented are the mean IC_{50} values ± standard deviation of three independent experiments n=3 (each individual experiment replicated twice).

9.3.2.2 - Selectivity Indices *In Vitro*: Comparison to Platinates
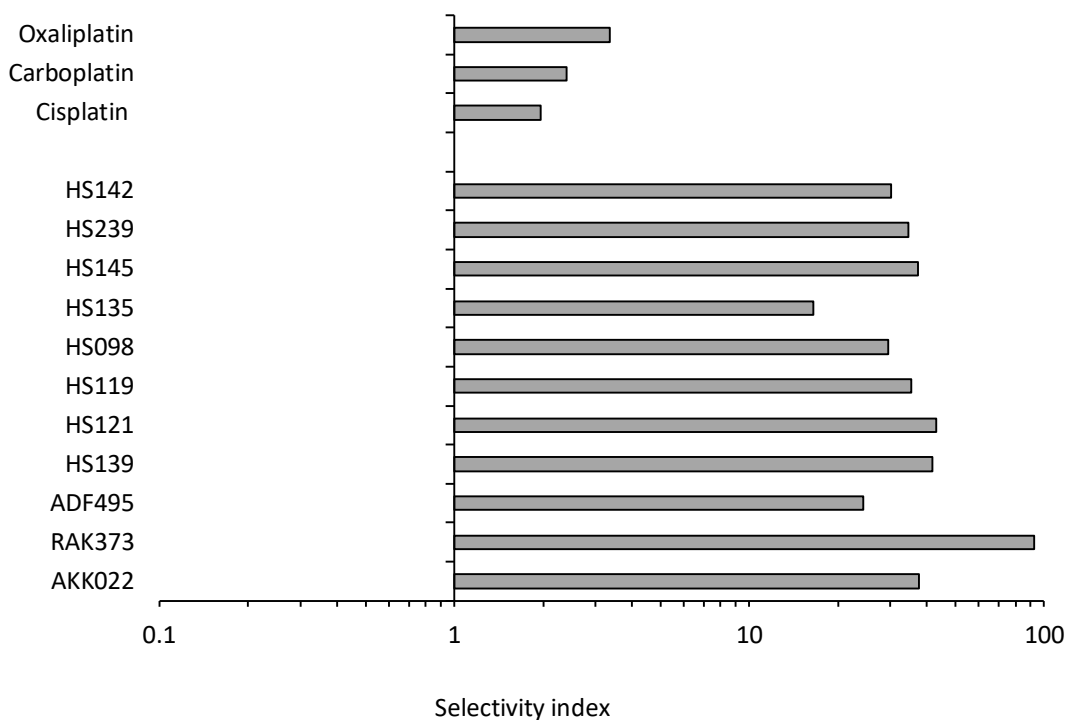
Figure 9.17: Comparison of the selectivity of novel metal NHC compounds cells to cisplatin, carboplatin and oxaliplatin. The selectivity index is defined as the mean IC_{50} for ARPE-19 cells divided by the IC_{50} of HCT116 p53$^{+/+}$. Values greater than 1 indicate that compounds have selectivity for cancer cells as opposed to non-cancer cells. As the mean IC_{50} values are used to calculate selectivity indices, no error bars are included on the graphs.

9.3.3 - Response of HCT116 Cells to Cisplatin, Carboplatin and Oxaliplatin: P53 Dependency

The HCT116 p53$^{+/+}$ and HCT116 p53$^{-/-}$ cells are isogenic colorectal carcinoma cells that differ only with regards to their p53 status. The relationship between p53 status and the response of cells to the "hit" metallohelix complexes is presented in table 9.9 and illustrated graphically in figure 9.18. With all the lead compounds the loss of p53 causes a significant reduction in potency with the exception of HS142 which is equitoxic to both cell lines. The degree of resistance to test compounds in the HCT116 p53$^{-/-}$ cell line is greater than that observed with the platinum compounds.

	IC$_{50}$ (μM)		
Compound	HCT116 p53$^{+/+}$	HCT116 p53$^{-/-}$	p-value
ADF495	0.41 ± 0.01	4.7 ± 0.43	0.42
HS121	2.69 ± 1.71	11.46 ± 2.15	0.0083
HS139	2.41 ± 0.6	3.36 ± 0.15	0.12
HS119	1.68 ± 0.04	7.25 ± 0.57	0.0033
HS135	5.42 ± 1.16	26.89 ± 4.82	0.014
HS098	10.62 ± 5.42	>100	0.00030
HS145	2.08 ± 0.08	29.99 ± 4.88	0.010
RAK373	0.36 ± 0.05	12.74 ± 3.32	0.089
HS142	2.16 ± 0.97	3.31 ± 0.28	0.0082
HS239	0.23 ± 0.02	1.46 ± 0.56	0.069
AKK022	0.17 ± 0.05	2.07 ± 0.17	0.30
Cisplatin	3.26 ± 0.38	7.52 ± 0.65	0.0035
Carboplatin	32.37 ± 11.14	35.7 ± 9.06	0.25
Oxaliplatin	0.93 ± 0.11	6.44 ± 1.05	0.086

Table 9.9: Comparison of IC$_{50}$ values ± SD of "hit" metallohelix and platinate compounds towards p53$^{+/+}$ and p53$^{-/-}$ isogenic clones of HCT116 human colorectal epithelial cancer cells. Data generated by triplicated MTT assays completed on consecutive days n=3 (each individual experiment replicated twice). Statistical analysis was performed using a student's t-test where values <0.05 indicates a statistically significant difference between IC$_{50}$ values HCT116 p53$^{+/+}$ and HCT116 p53$^{-/-}$ cell lines.
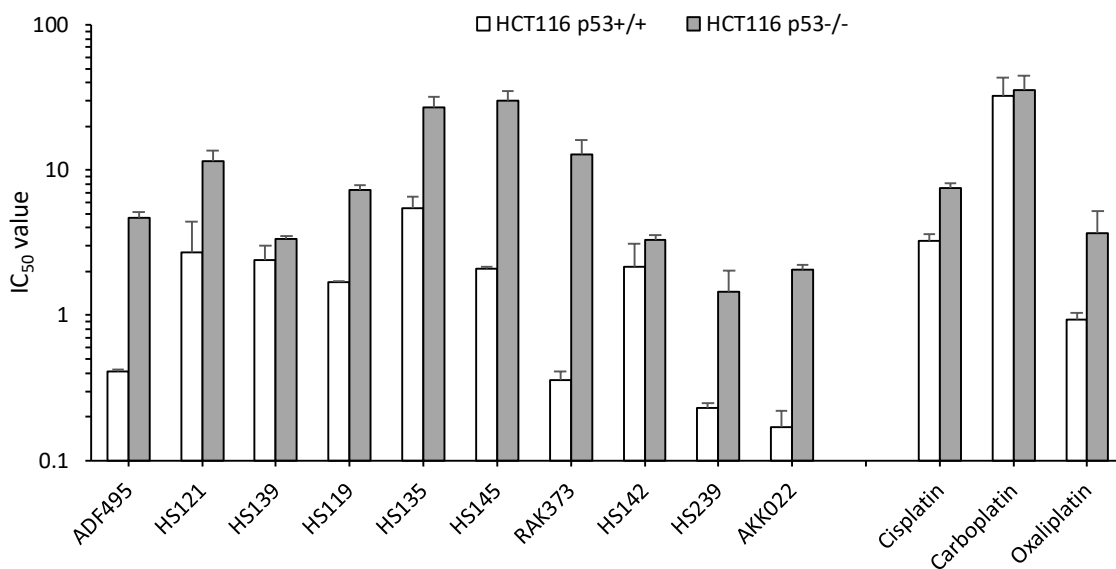
Figure 9.18: Comparison of IC$_{50}$ values ± SD of "hit" metallohelix compounds and platinum compounds towards p53$^{+/+}$ and p53$^{-/-}$ isogenic clones of HCT116 cancer cells. Data generated by triplicated MTT assays completed on consecutive days n=3 (each individual experiment replicated twice). The data for HS098 is not included in this figure with the IC$_{50}$ on the HCT116 p53$^{-/-}$ cell line being over the maximum concentration tested (100μM).

9.3.4 - Response of Cancer Cells Following Continuous Exposure to Novel Metallohelices Under Pseudo-Hypoxic Conditions

The response of HCT116 p53$^{+/+}$ cells to potent and selective sugar tethered triplex metallohelix complexes under aerobic and pseudo-hypoxic conditions is presented in figures 9.18 - 9.25. HS139 which is the parent compound to HS121 minus the glucose tether acts as a comparison to the sugar tethered compounds to investigate if the addition of various sugars effects the chemosensitivity of compounds under varying conditions. These pseudo-hypoxic investigations are the beginning of investigations into the role of the sugar moiety in these potent and selective compounds. The results demonstrate that pseudo-hypoxic conditions result in increased resistance to the metallohelix compounds. The non-sugar tethered complexes HS139 is less active under pseudo-hypoxic conditions but it display a lesser shift in potency compared to the sugar tethered complexes.

	IC$_{50}$ (µM)		
Compound	HCT116 p53$^{+/+}$ Aerobic	HCT116 p53$^{+/+}$ Pseudo-hypoxic	p-value
HS139	2.41 ± 0.6	87.99 ± 16.16	0.011
HS121	2.69 ± 1.71	53.15 ± 7.09	0.013
HS119	1.68 ± 0.04	58.34 ± 15.14	0.023
HS135	5.42 ± 1.16	58.44 ± 14.44	0.024
HS098	10.62 ± 5.42	>100	0.00025
HS145	2.08 ± 0.08	56.28 ± 12.45	0.017
HS142	2.16 ± 0.97	21.59 ± 2.32	0.0052
Cisplatin	3.26 ± 0.38	6.83 ± 2.12	0.095
Carboplatin	32.37 ± 11.14	>100	0.0089
Oxaliplatin	0.93 ± 0.11	1.53 ± 0.52	0.14

Table 9.18b: Comparison of IC$_{50}$ values ± SD of "hit" metallohelix and platinate compounds towards p53$^{+/+}$ human colorectal epithelial cancer cells in aerobic and pseudo-hypoxic condtions. Data generated by triplicated MTT assays completed on consecutive days n=3 (each individual experiment replicated twice). Statistical analysis was performed using a student's t-test where values <0.05 indicates a statistically significant difference between IC$_{50}$ values HCT116 p53$^{+/+}$ in aerobic and pseudo-hypoxic conditions.
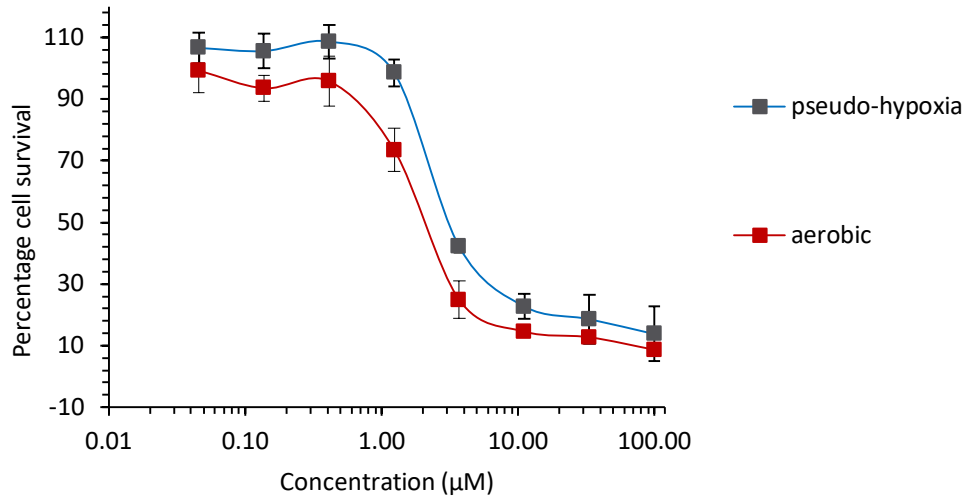
Figure 9.19: Dose response curves of HS139 class 3a triplex towards HCT116^{+/+} cell lines in both pseudo-hypoxic and aerobic conditions. Data from three independent MTT assays and are represented by the mean ± SE n=3 (each individual experiment replicated twice). The percentage cell survival values are expressed as a percentage of viable cells compared with untreated controls.
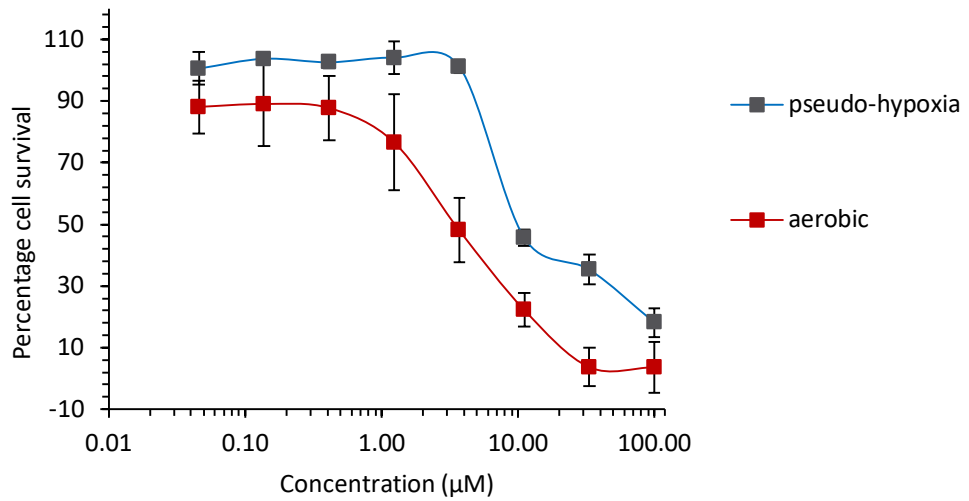
Figure 9.20: Dose response curves of HS121 class 3a glucose click triplex towards HCT116+/+ cell lines in both pseudo-hypoxic and aerobic conditions. Data from three independent MTT assays and are represented by the mean ± SE n=3 (each individual experiment replicated twice). The percentage cell survival values are expressed as a percentage of viable cells compared with untreated controls.
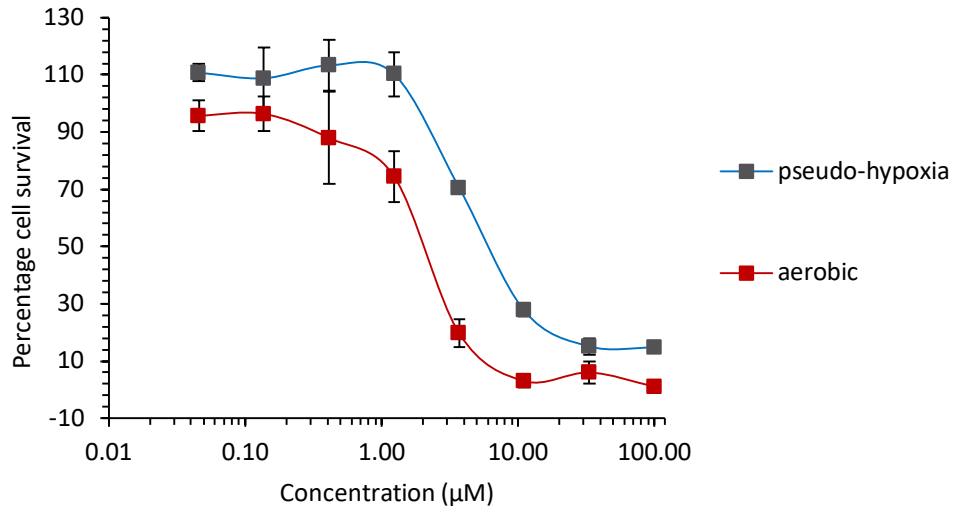
Figure 9.21: Dose response curves of HS119 class 3a galactose click triplex towards HCT116$^{+/+}$ cell lines in both pseudo-hypoxic and aerobic conditions. Data from three independent MTT assays and are represented by the mean ± SE n=3 (each individual experiment replicated twice). The percentage cell survival values are expressed as a percentage of viable cells compared with untreated controls.
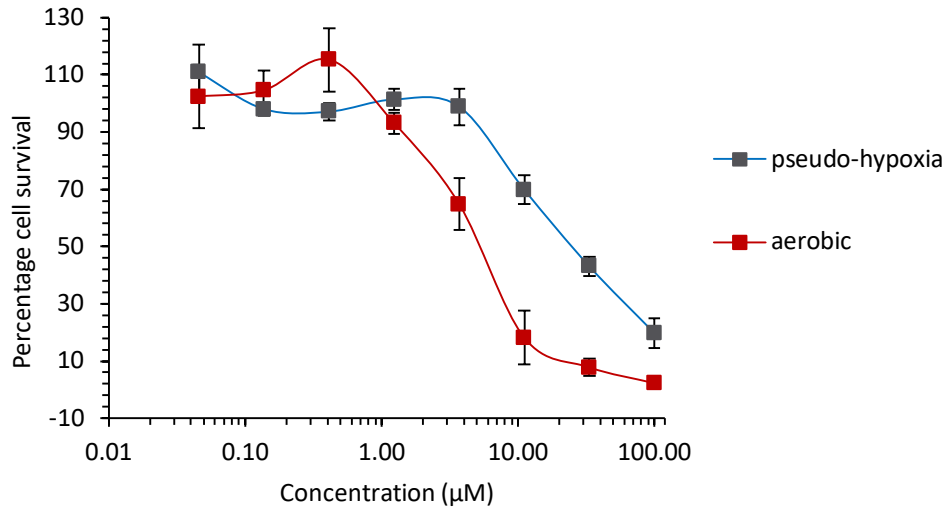
Figure 9.22: Dose response curves of HS135 class 3a mannose click triplex towards HCT116$^{+/+}$ cell lines in both pseudo-hypoxic and aerobic conditions. Data from three independent MTT assays and are represented by the mean ± SE n=3 (each individual experiment replicated twice). The percentage cell survival values are expressed as a percentage of viable cells compared with untreated controls.
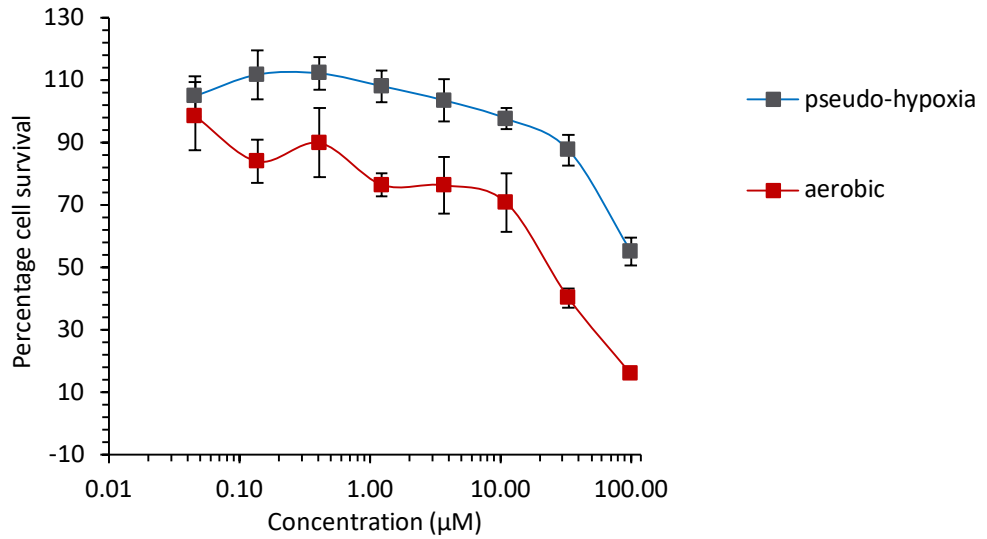
Figure 9.23: Dose response curves of HS098 class 3a acetyl-galactosamine click triplex towards

HCT116$^{+/+}$ cell lines in both pseudo-hypoxic and aerobic conditions. Data from three independent MTT

assays and are represented by the mean ± SE n=3 (each individual experiment replicated twice). The

percentage cell survival values are expressed as a percentage of viable cells compared with untreated

controls.
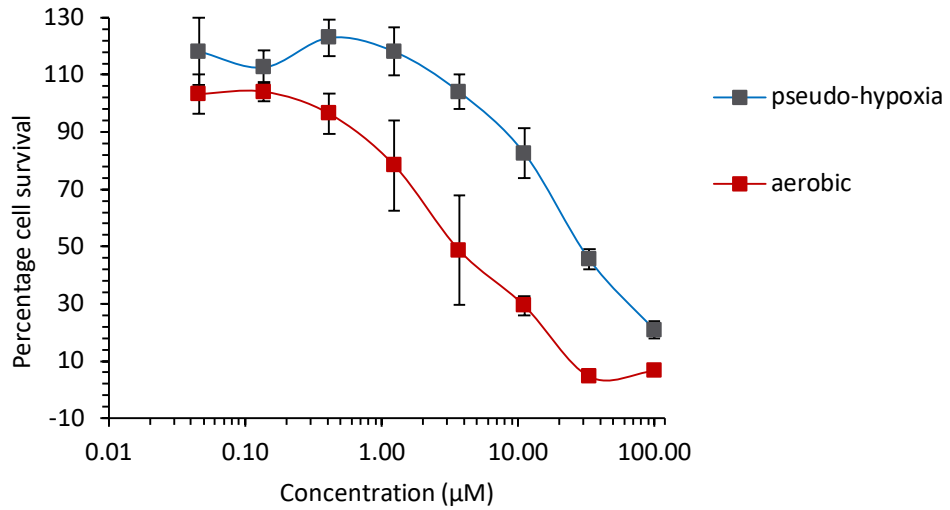
Figure 9.24: Dose response curves of HS145 class 3a acetyl-glucosamine click triplex towards HCT116^{+/+}

cell lines in both pseudo-hypoxic and aerobic conditions. Data from three independent MTT assays and

are represented by the mean ± SE n=3 (each individual experiment replicated twice). The percentage

cell survival values are expressed as a percentage of viable cells compared with untreated controls.
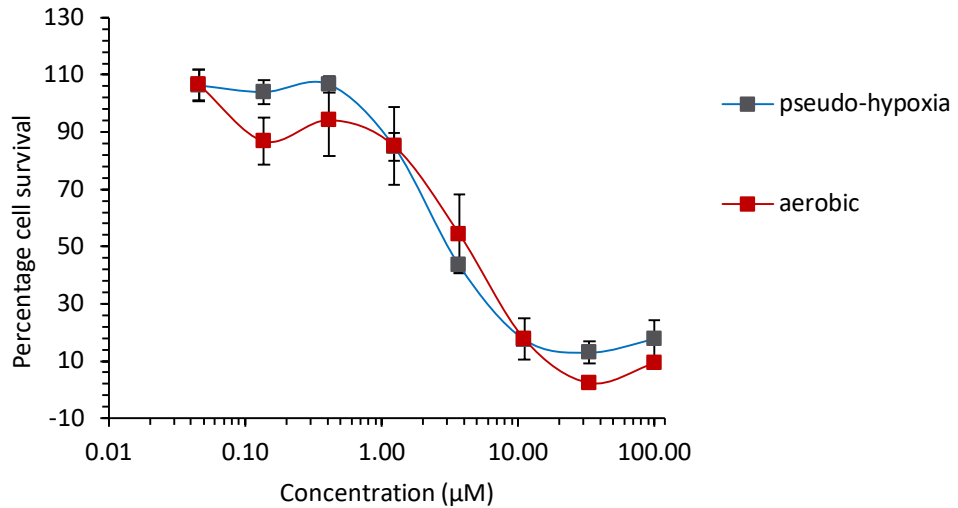
Figure 9.25: Dose response curves of HS142 class 3a benzyl click triplex towards HCT116^{+/+} cell lines in both pseudo-hypoxic and aerobic conditions. Data from three independent MTT assays and are represented by the mean ± SE n=3 (each individual experiment replicated twice). The percentage cell survival values are expressed as a percentage of viable cells compared with untreated controls.

9.3.5 - Analysis of Induced Apoptosis, Reduction in Cell Viability and Cell Cycle Arrest

To gain further insight into the mechanism in which these novel "hit" compounds exert their activity, their effect on (i) cell viability, (ii) the induction of apoptosis and (iii) cell cycle parameters was investigated using the NC3000 cytometer. Description of the assays and the interpretation of the resulting data is explained in chapter 3. The measurements were taken after 24-hour exposures which was informed by previous cisplatin investigations deeming this an appropriate time interval to a) have optimal cell numbers for the experimental procedures b) measure initiation of apoptosis (if present) and c) observe cell cycle disruption (if initiated). The working concentrations

for the novel "hit" compounds were determined from the dose response curve for both HCT116 p53$^{+/+}$ and ARPE-19. The concentration at which maximal effect on HCT116 p53$^{+/+}$ cells but had minimal effect on ARPE-19 cells was determined and identified as the working concentration (figure 9.26, summary of all concentrations displayed in table 9.10). A number of these working concentrations were similar to the compounds IC$_{50}$ value but some compounds such as HS119 display a marked difference in drug response therefore higher concentrations were selected. Throughout this section, the compounds are split by their diluent as some were dissolved in methanol and in medium resulting in the requirement of separate control samples.
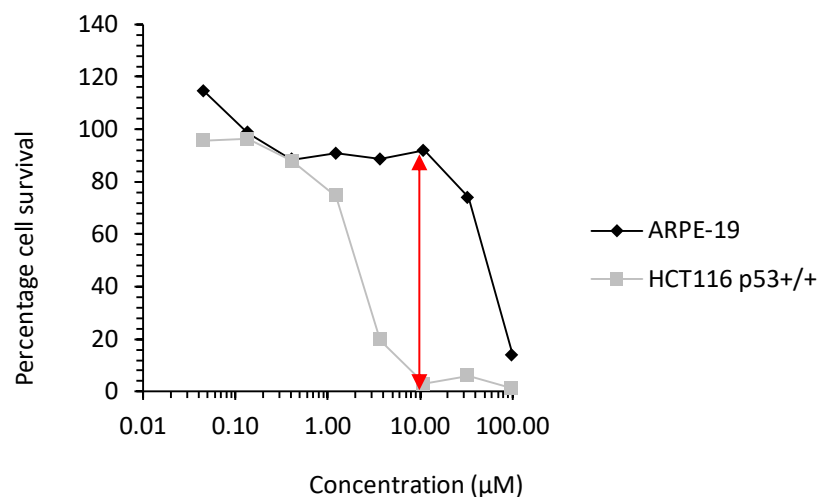
Figure 9.26: Drug response of both HCT116 p53$^{+/+}$ cells ARPE-19 cells to HS119. The optimum working concentration selected for NC3000 investigations is illustrated by the arrows which show the dose where major cell kill occurs in HCT116 cells, but minimal effects are present in the ARPE-19 cells.

Compound	HCT116 p53$^{+/+}$ IC$_{50}$ (µM)	Working concentration (µM)
ADF495	0.41 ± 0.01	0.4
HS121	2.69 ± 1.71	3
HS139	2.41 ± 0.6	20
HS119	1.68 ± 0.04	10
HS135	5.42 ± 1.16	20
HS098	10.62 ± 5.42	11
HS145	2.08 ± 0.08	20
RAK373	0.36 ± 0.05	0.4
HS142	2.16 ± 0.97	10
HS239	0.23 ± 0.02	0.3
AKK022	0.17 ± 0.05	0.4

Table 9.10: Working concentrations identified for each "hit" compound based on dose response curves as explained in figure 9.26.

9.3.5.1 - Viability Assay and Microscope Images

The effect of 24-hour drug exposure with the selected "hit" compounds was investigated using a viability assay which not only provides an accurate cell count but also measures the viability of the cell population measured. This was completed on both HCT116 p53$^{+/+}$ cells and ARPE-19 cells. The cell viability (tables 9.11, 9.13, 9.12 and 9.14 respectively) overall remains consistent and does not drop below 80% viability. Relatively small variations on cell number were observed across the panel of compounds tested with the largest reduction in cell number being seen in HS119 treated cultures (figures 9.27 and 9.28). Figures 9.29 and 9.30 demonstrate the visual effects of the novel compounds after 24-hour exposure. The main observations being the presence of potential autophagic vacuoles in HCT116 p53$^{+/+}$ samples treated with

ADF495, HS139 and AKK022. Furthermore, cells treated with HS098 had a very different morphology compared to controls (figure 9.29).

Sample	Total cells in sample	Percentage cell viability
Control	3.80×10^6	89.3
HS139	2.48×10^6	90.6
ADF495	3.64×10^6	87.3
HS121	3.12×10^6	88.5
HS119	1.56×10^6	80.8
HS135	1.89×10^6	88.1
HS098	2.96×10^6	87.7
HS145	3.04×10^6	87.6
HS239	2.27×10^6	90.6

Table 9.11: Viability assay data of water soluble metallohelices on HCT116 p53$^{+/+}$ cells after 24 hours exposure. The viability is presented as a percentage and an accurate cell count calculated based on the entire population which is stained with Acridine Orange and non-viable cells stained by 4',6-diamidino-2-phenylindole (DAPI) (n=1).

Sample	Total cells in sample	Percentage cell viability
Control	1.31×10^6	94.0
HS139	6.2×10^5	94.8
ADF495	1.08×10^6	93.9
HS121	1.19×10^6	95.5
HS119	5.02×10^5	92.2
HS135	9.84×10^5	94.2
HS098	1.11×10^6	95.4
HS145	1.15×10^6	95.9
HS239	1.22×10^6	92.2

Table 9.12: Viability assay data of water soluble metallohelices on non-cancerous ARPE-19 cells after 24 hours exposure. The viability is presented as a percentage and an accurate cell count calculated based on the entire population which is stained with Acridine Orange and non-viable cells stained by 4',6-diamidino-2-phenylindole (DAPI) (n=1).
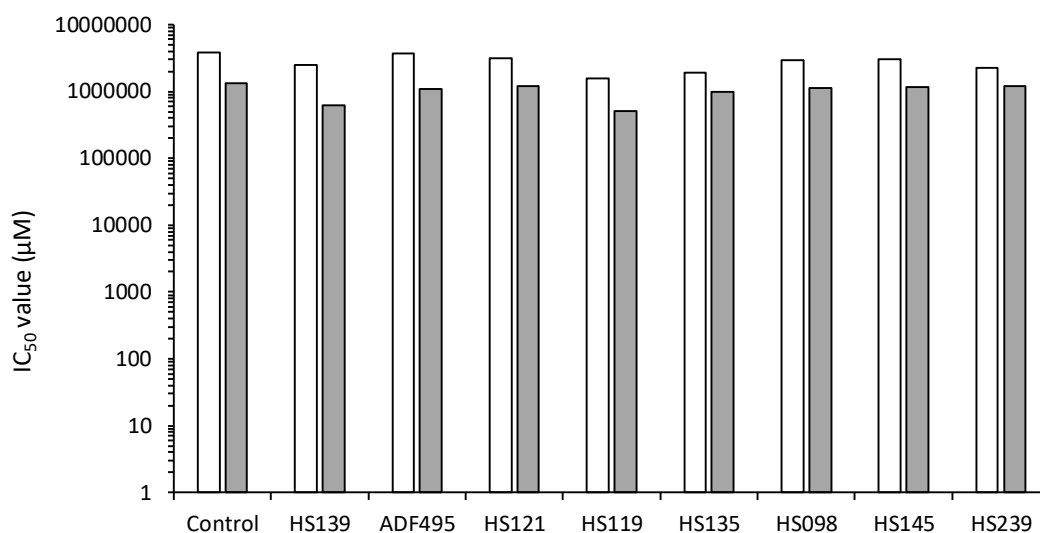
Figure 9.27: The influence of water soluble metallohelices on the cell number of both cancerous HCT116 p53+/+ cells and non-cancerous ARPE-19 cells after 24-hour exposure (n=1).

	Control	RAK373	HS142	AK022
Total cells in sample	5.12×10^6	4.14×10^6	2.52×10^6	4.96×10^6
Percentage cell viability	72.7	89.5	90.5	88.4

Table 9.13: Viability assay data of methanol soluble metallohelices on HCT116 p53$^{+/+}$ cells after 24 hours exposure. The viability is presented as a percentage and an accurate cell count calculated based on the entire population which is stained with Acridine Orange and non-viable cells stained by 4',6-diamidino-2-phenylindole (DAPI) (n=1).

	Control	RAK373	HS142	AK022
Total cells in sample	1.47×10^6	1.22×10^6	1.17×10^6	1.45×10^6
Percentage cell viability	92.8	93.4	93.1	91.5

Table 9.14: Viability assay data of methanol soluble metallohelices on non-cancerous ARPE-19 cells after 24 hours exposure. The viability is presented as a percentage and an accurate cell count calculated based on the entire population which is stained with Acridine Orange and non-viable cells stained by 4',6-diamidino-2-phenylindole (DAPI) (n=1).
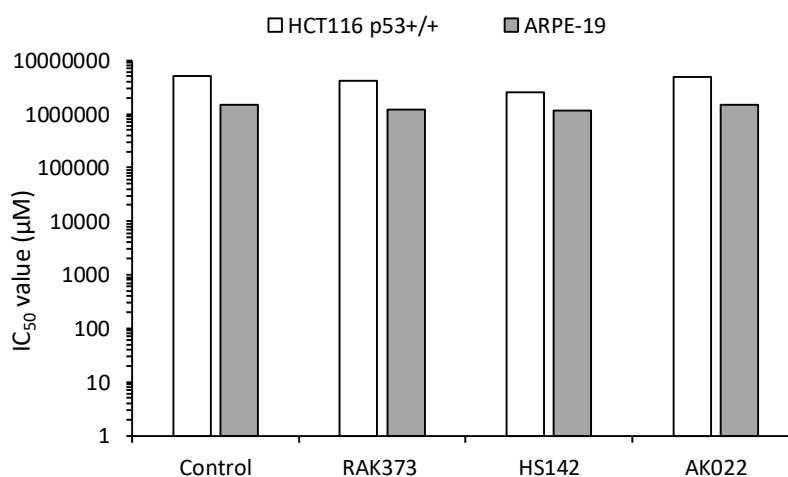
Figure 9.28: The influence of methanol soluble metallohelices on the cell number of both HCT116 p53^{+/+} cells and ARPE-19 cells after 24-hour exposure (n=1).
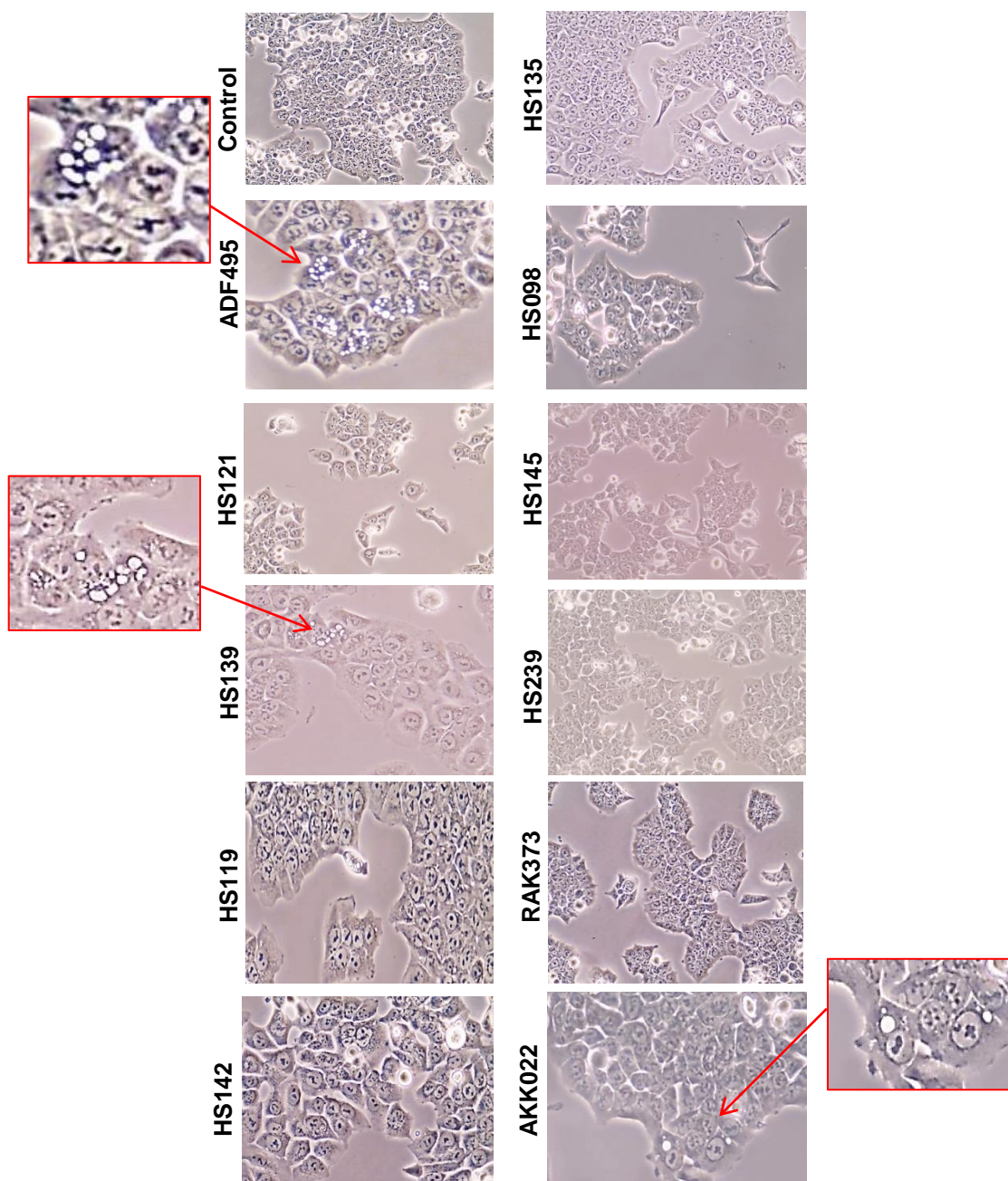
Figure 9.29: Microscope images of colorectal adenocarcinoma HCT116 p53$^{+/+}$ cells after 24-hour exposure to a number of novel metallohelix compounds.
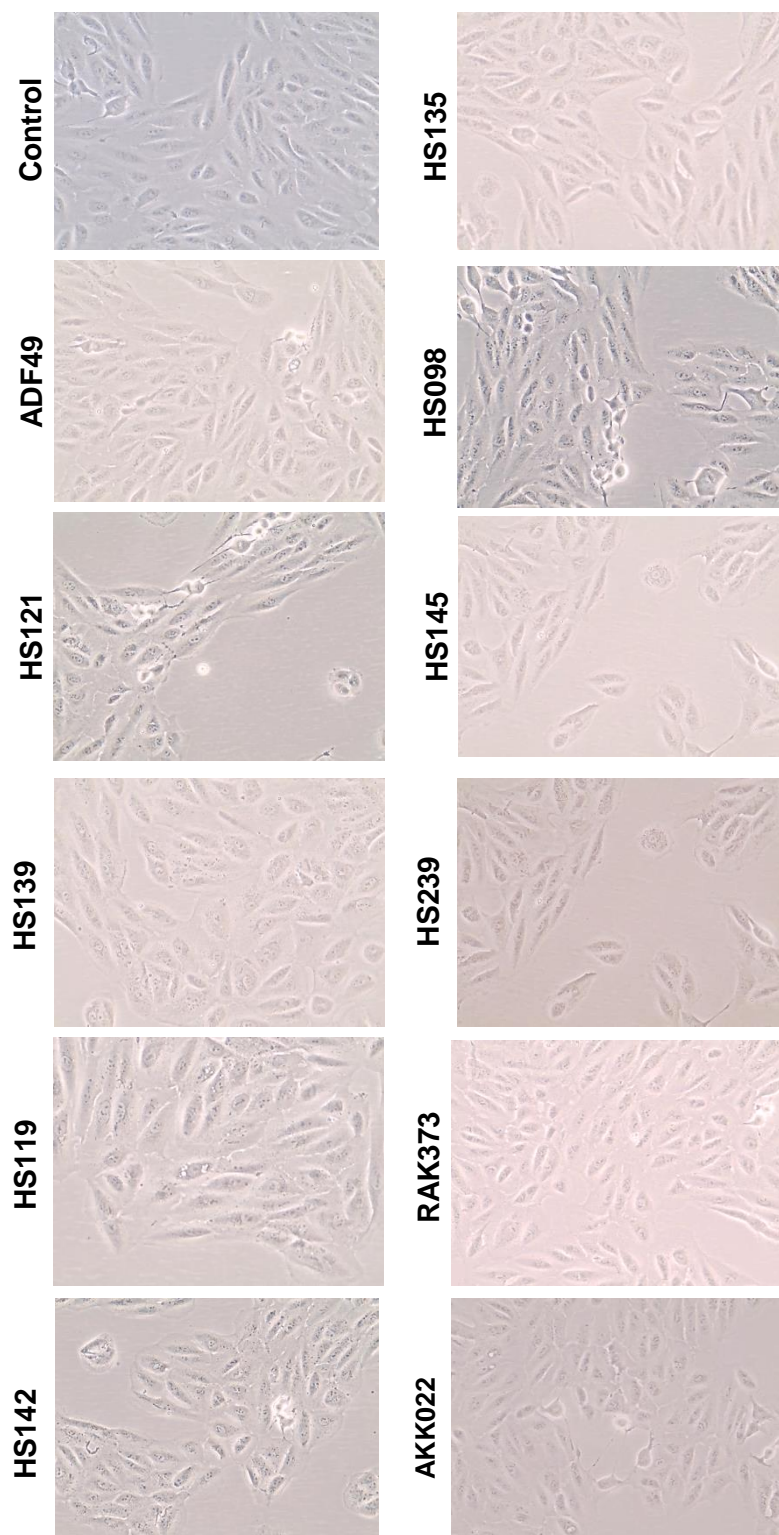
Figure 9.30: Microscope images of colorectal adenocarcinoma non-cancerous retinal epithelial ARPE-19 cells after 24-hour exposure to a number of novel metallohelix compounds.

9.3.5.2 - Annexin V Assay

As previously discussed in section 2.6.5 this assay detects the induction of apoptosis via the expression of annexin V an apoptotic marker protein. Displayed in figures 9.31 – 9.38 it can be observed there is no significant induction of apoptosis in either HCT116 p53$^{+/+}$ and ARPE-19 cells across the panel of compounds tested. There is a slight increase in the non-viable cells for compounds
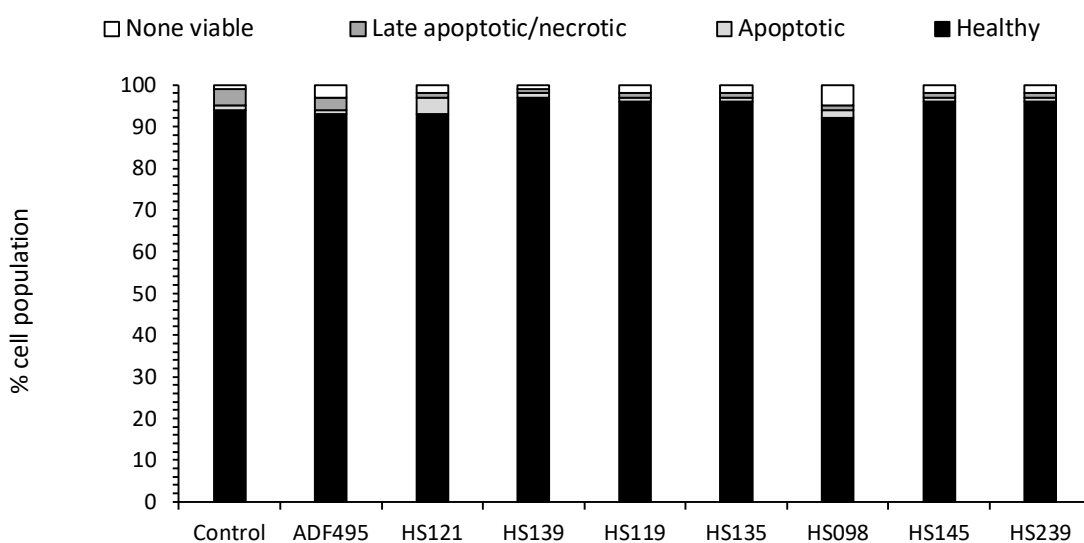
	Control	ADF 495	HS 121	HS 139	HS 119	HS 135	HS 098	HS 145	HS 239
Healthy	94	93	93	97	96	96	92	96	96
Apoptotic	1	1	4	1	1	1	2	1	1
Late apoptotic/ Necrotic	4	3	1	1	1	1	1	1	1
None viable	1	3	2	1	2	2	5	2	2

Figure 9.31: Summary of annexin V assay on HCT116 p53$^{+/+}$ cells after exposure to media soluble metallohelix compounds after 24-hour exposure (n=1).
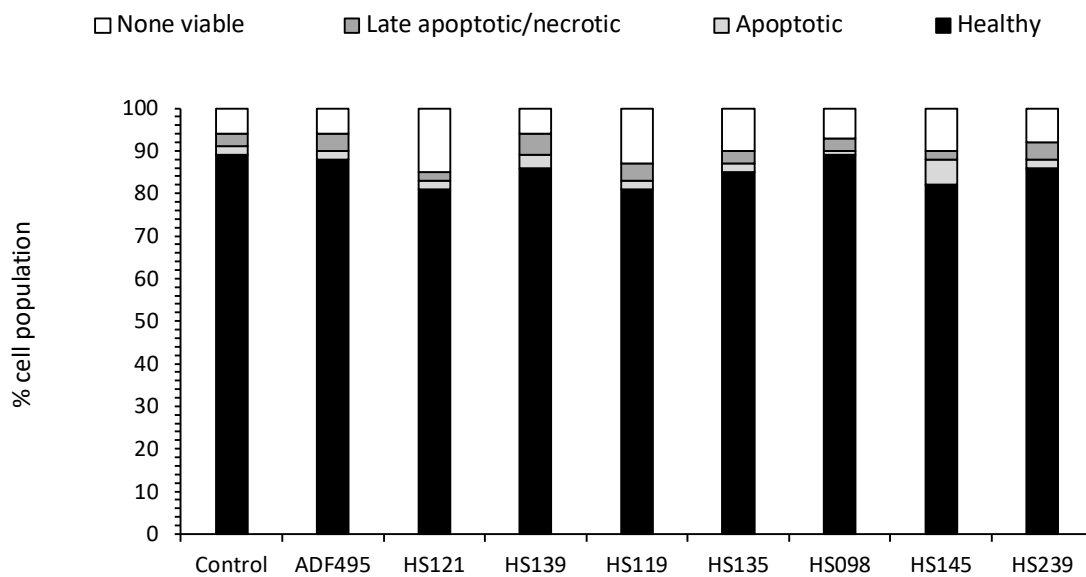
	Control	ADF 495	HS 121	HS 139	HS 119	HS 135	HS 098	HS 145	HS 239
Healthy	89	88	81	86	81	85	89	82	86
Apoptotic	2	2	2	3	2	2	1	6	2
Late apoptotic/ necrotic	3	4	2	5	4	3	3	2	4
None viable	6	6	15	6	13	10	7	10	8

Figure 9.32: Summary of annexin V assay on non-cancerous ARPE-19 cells after exposure to media soluble metallohelix compounds after 24-hour exposure (n=1).
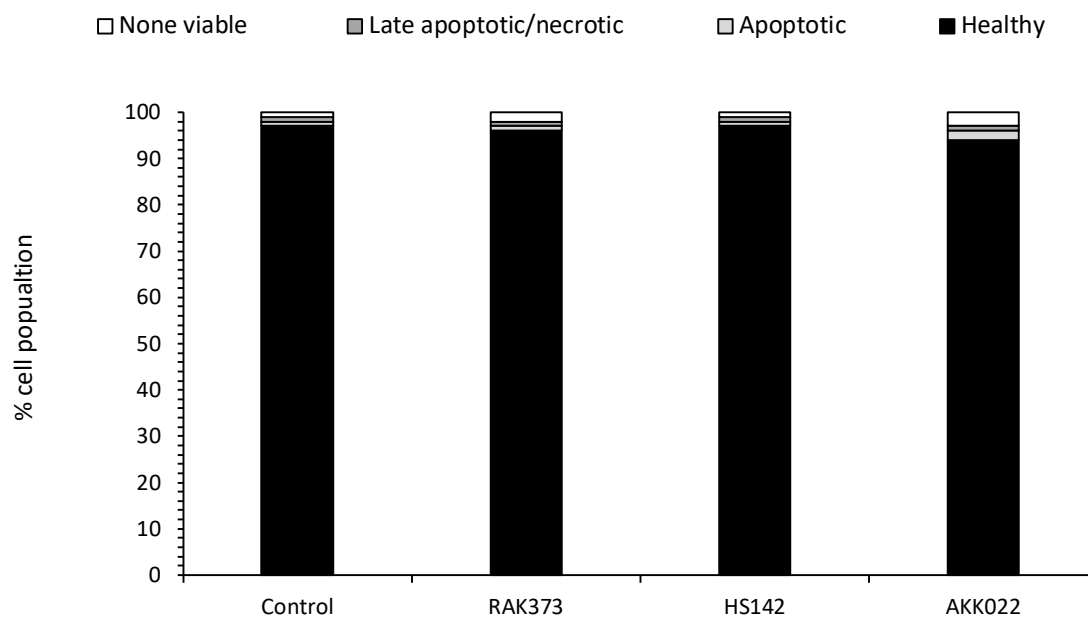
	Control	RAK373	HS142	AKK022
Healthy	97	96	97	94
Apoptotic	1	1	1	2
Late apoptotic/ necrotic	1	1	1	1
None viable	1	2	1	3

Figure 9.33: Summary of annexin V assay on HCT116 p53$^{+/+}$ cells after exposure to Methanol soluble metallohelix compounds after 24-hour exposure (n=1).
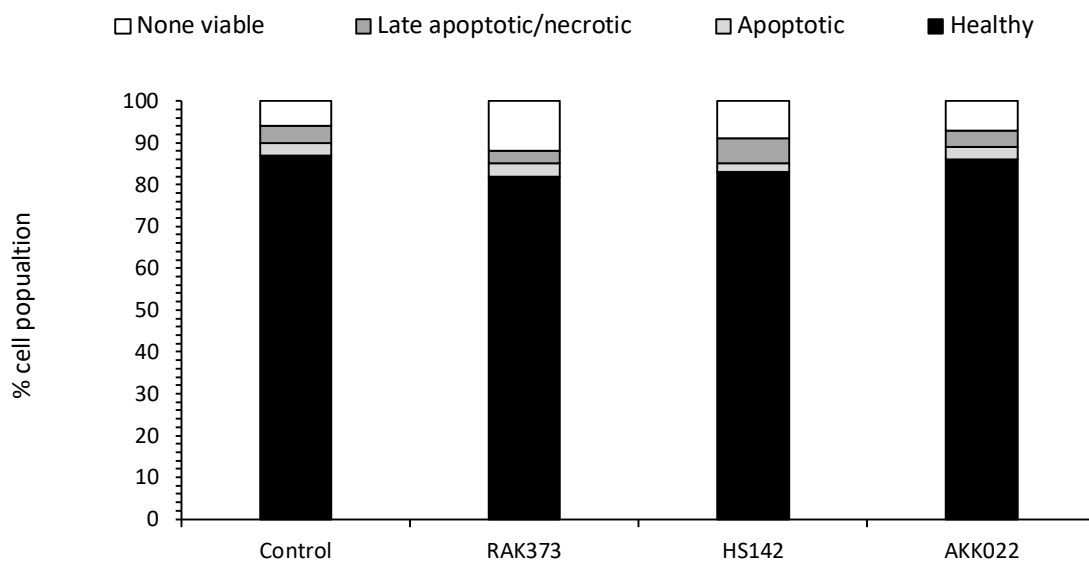
	Control	RAK373	HS142	AKK022
Healthy	87	82	83	86
Apoptotic	3	3	2	3
Late apoptotic/ necrotic	4	3	6	4
None viable	6	12	9	7

Figure 9.34: Summary of annexin V assay on non-cancerous r ARPE-19 cells after exposure to Methanol soluble metallohelix compounds after 24-hour exposure (n=1).

9.3.5.3 - Mitochondrial Potential Assay

The use of an additional apoptotic assay is always recommended due to the lack of specificity of most apoptotic assays to apoptosis alone. The loss of mitochondrial membrane potential is known to precede apoptosis and will further validate the previous apoptotic investigations. Overall the healthy portion of the cells remains consisted with only slight increases in apoptotic and necrotic cell populations observed.
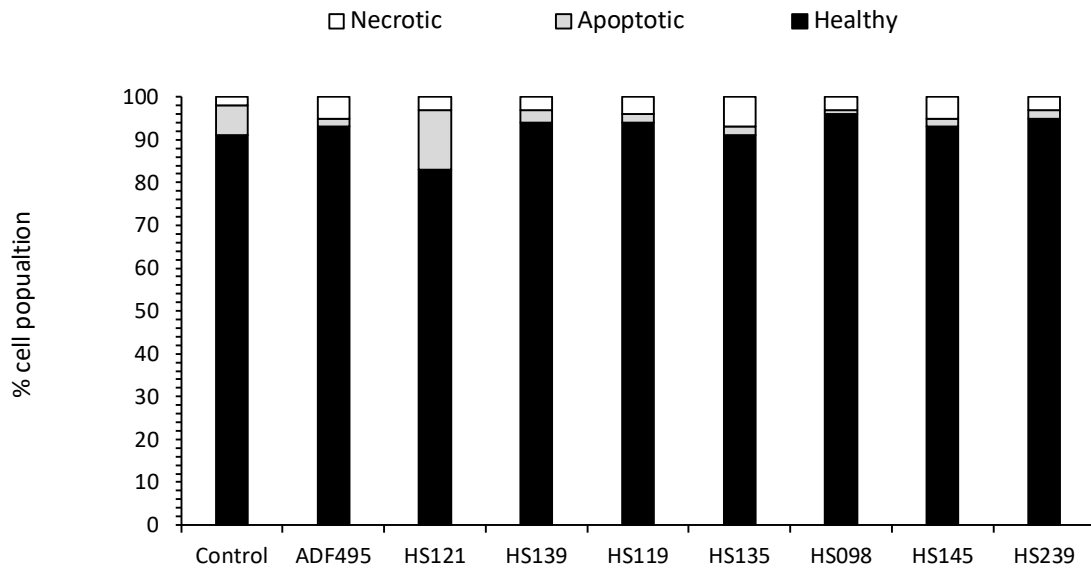
	Control	ADF 495	HS 121	HS 139	HS 119	HS 135	HS 098	HS 145	HS 239
Healthy	91	93	83	94	94	91	96	93	95
Apoptotic	7	2	14	3	2	2	1	2	2
Necrotic	2	5	3	3	4	7	3	5	3

Figure 9.35: measurement of mitochondrial potential on HCT116 p53$^{+/+}$ cells following 24-hour exposure to water soluble novel metallohelices to investigate the presence of apoptotic induction (n=1).
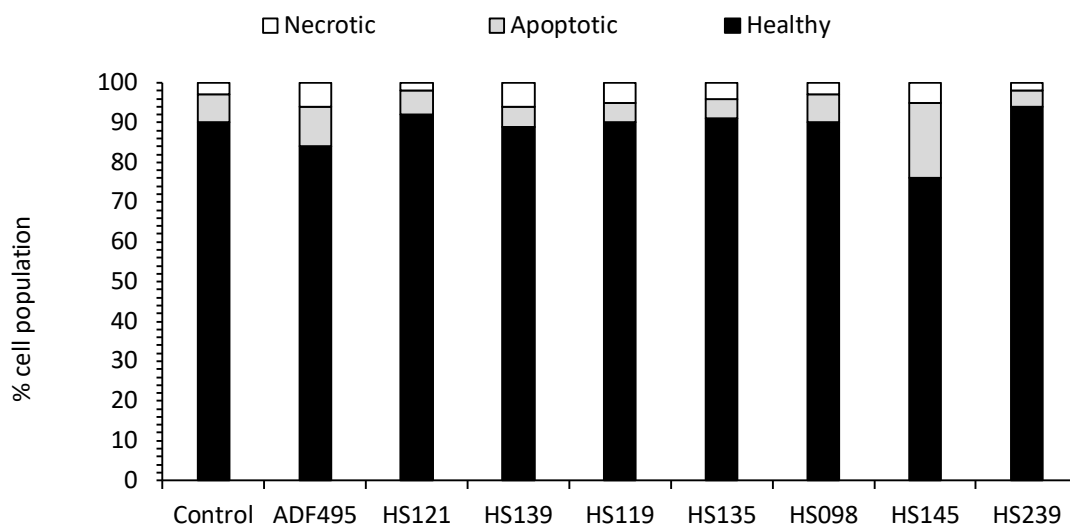
	Control	ADF 495	HS 121	HS 139	HS 119	HS 135	HS 098	HS 145	HS 239
Healthy	90	84	92	89	90	91	90	76	94
Apoptotic	7	10	6	5	5	5	7	19	4
Necrotic	3	6	2	6	5	4	3	5	2

Figure 9.36: Measurement of mitochondrial potential on non-cancerous retinal epithelial ARPE-19 cells following 24-hour exposure to water soluble novel metallohelices to investigate the presence of apoptotic induction (n=1).
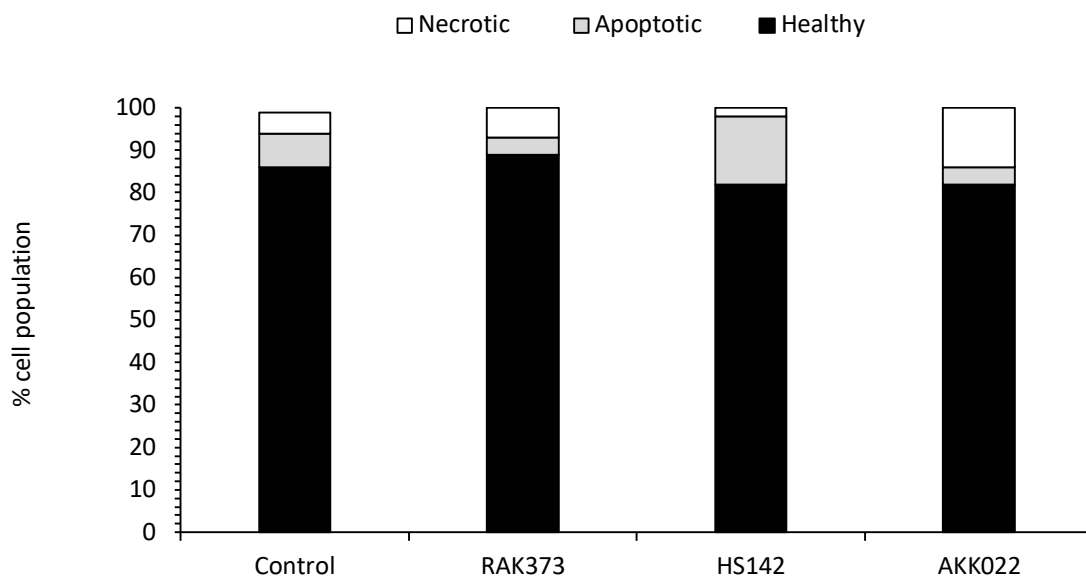
	Control	RAK373	HS142	AKK022
Healthy	86	89	82	82
Apoptotic	8	4	16	4
Necrotic	5	7	2	14

Figure 9.37: measurement of mitochondrial potential on HCT116 p53$^{+/+}$ cells following 24-hour exposure to Methanol soluble novel metallohelices to investigate the presence of apoptotic induction (n=1).
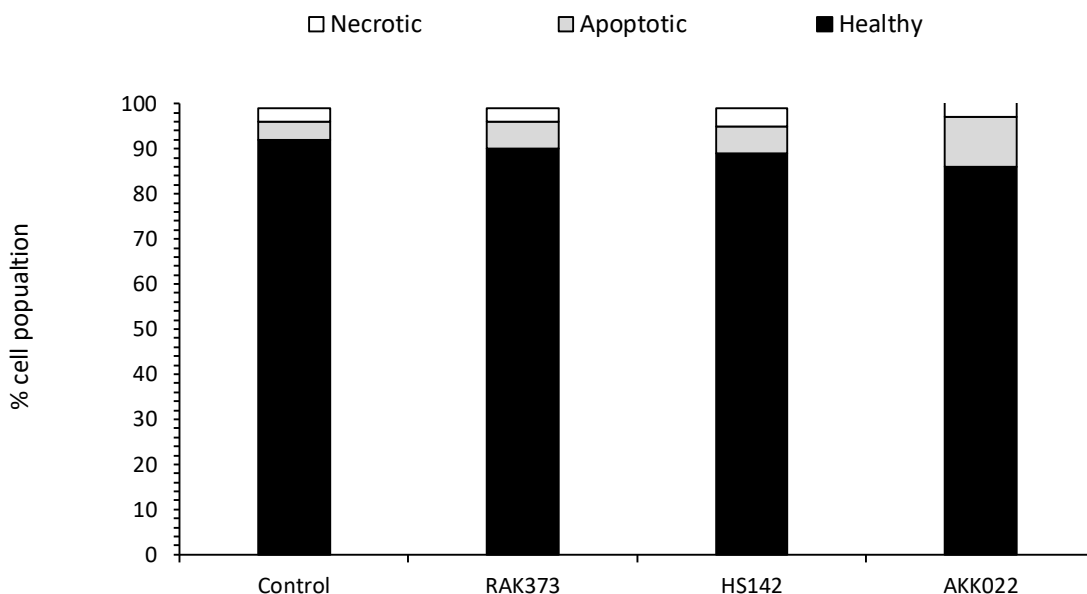
	Control	RAK373	Control	AKK022
Healthy	92	90	89	86
Apoptotic	4	6	6	11
Necrotic	3	3	4	4

Figure 9.38: measurement of mitochondrial potential on non-cancerous ARPE-19 cells following 24-hour exposure to water soluble novel metallohelices to investigate the presence of apoptotic induction (n=1).

9.3.5.4 - Cell Cycle Assay

To investigate if these novel metallohelices induce a cell cycle arrest, cells were treated with test compound (at previously determined working concentrations, table 9.10) for 24 hours and the cell cycle was performed as described in section 2.6.6. The cell cycle assay was completed by quantifying DNA, allowing identification of specific cell cycle phases. Overall slight variations are observed across the compounds with the only marked differences seen with HS135 which increases the cell population within

the S phase on HCT116 p53$^{+/+}$ cells but not in ARPE-19 cells. HS139 also causes a small increase in the S phase in the ARPE-19 but not the HCT116 p53$^{+/+}$ cells.
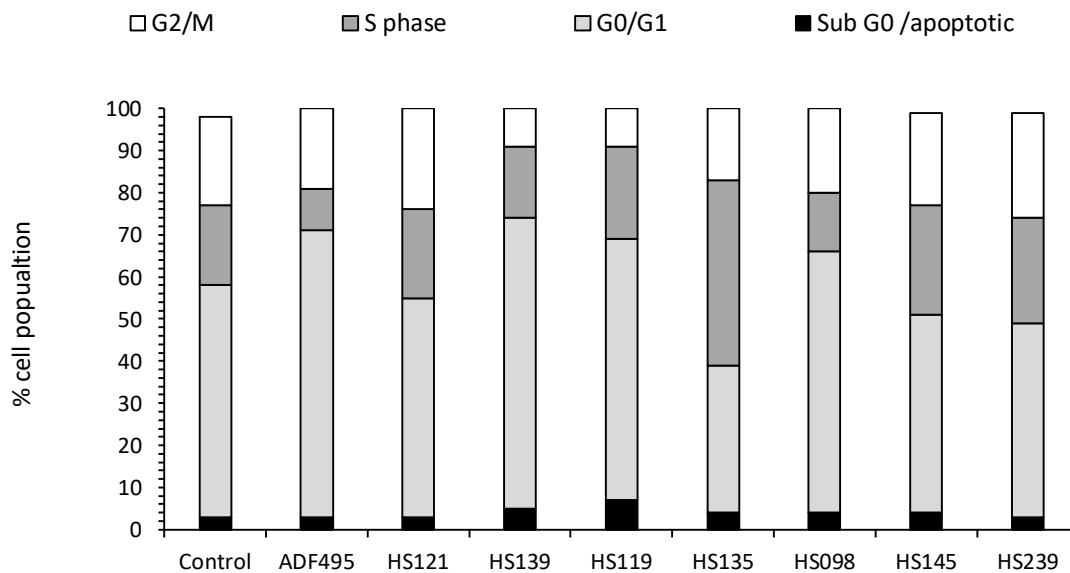
	Control	ADF 495	HS 121	HS 139	HS 119	HS 135	HS 098	HS 145	HS 239
Sub G_0/apoptotic	3	3	3	5	7	4	4	4	3
G_0/G_1	55	68	52	69	62	35	62	47	46
S phase	19	10	21	17	22	44	14	26	25

Figure 9.39: Effects of exposure to novel water soluble metallohelices on HCT116 p53$^{+/+}$ cell cycle distribution after 24-hour exposure. Determination of cell cycle phase based on DNA intensity of DAPI stained cells (n=1).
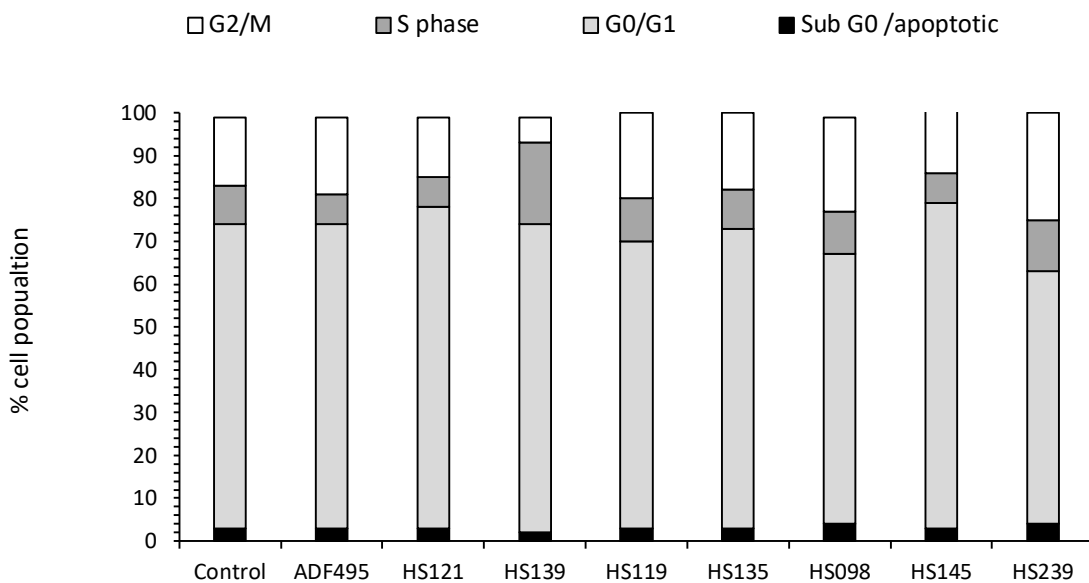
	Control	ADF 495	HS 121	HS 139	HS 119	HS 135	HS 098	HS 145	HS 239
Sub G_0/apoptotic	3	3	3	2	3	3	4	3	4
G_0/G_1	71	71	75	72	67	70	63	76	59
S phase	9	7	7	19	10	9	10	7	12
G_2/M	16	18	14	6	20	18	22	15	25

Figure 9.40: Effects of exposure to novel water soluble metallohelices on non-cancerous ARPE-19 cell cycle distribution after 24-hour exposure. Determination of cell cycle phase based on DNA intensity of DAPI stained cells (n=1).
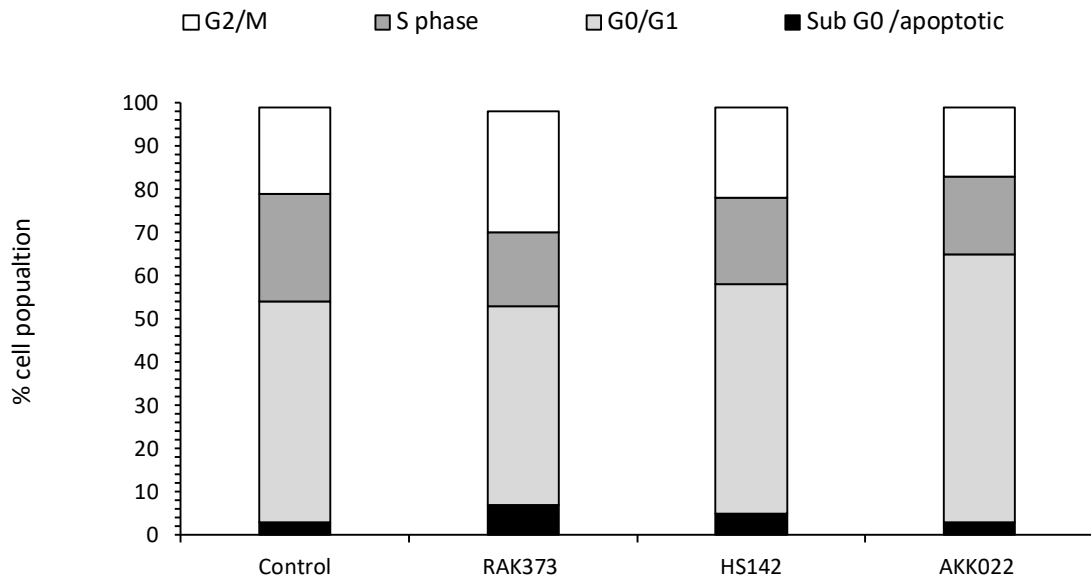
	Control	RAK373	HS142	AKK022
Sub G$_0$/apoptotic	3	7	5	3
G$_0$/G$_1$	51	46	53	62
S phase	25	17	20	18
G$_2$/M	20	28	21	16

Figure 9.41: Effects of exposure to novel methanol soluble metallohelices on HCT116 p53+/+ cell cycle distribution after 24-hour exposure. Determination of cell cycle phase based on DNA intensity of DAPI stained cells (n=1).
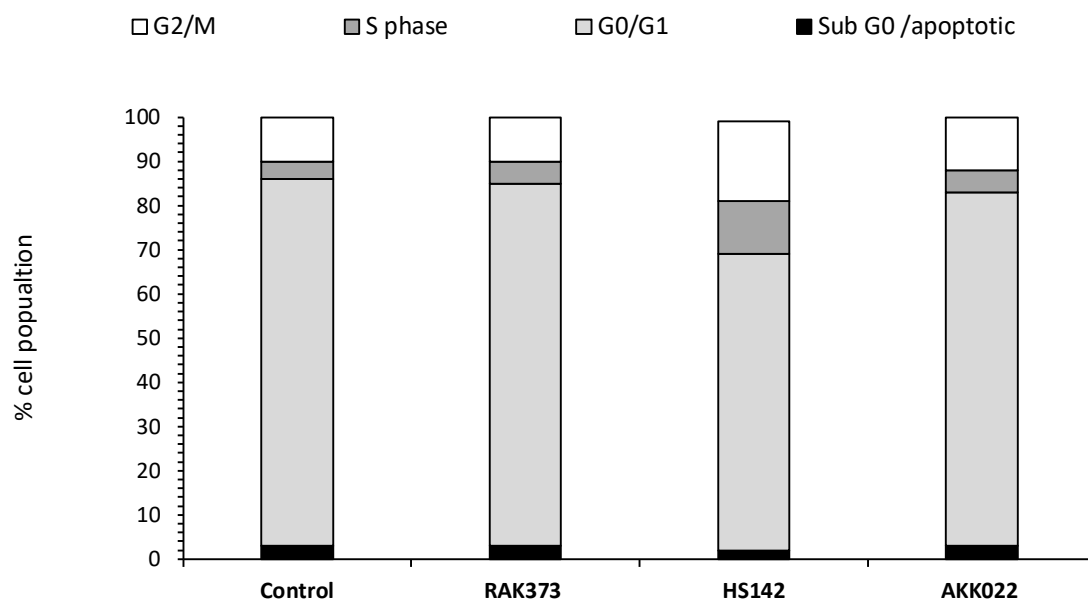
	Control	RAK373	HS142	AKK022
Sub G_0/apoptotic	3	3	2	3
G_0/G_1	83	82	67	80
S phase	4	5	12	5
G_2/M	10	10	18	12

Figure 9.42: Effects of exposure to novel methanol soluble metallohelices on non-cancerous retinal epithelial ARPE-19 cell cycle distribution after 24-hour exposure. Determination of cell cycle phase based on DNA intensity of DAPI stained cells (n=1).

9.3.6 - Autophagy Inhibition *Via* the Use of 3-Methyladenine (3-MA)

From visual observations (figure 9.29) made mainly during NC3000 cytometer studies, potential autophagic vacuoles were seen thereby prompting studies to investigate the potential role of autophagy in the cytotoxic activity exerted by the compounds. Selected compounds were tested in the presence an absence of the

autophagy inhibitor 3-MA to determine if IC_{50} values are reduced. The results in figure 9.43 demonstrate that potency is reduced in the presence of 3-MA suggesting that autophagy plays a role in the mechanism of action of these compounds.
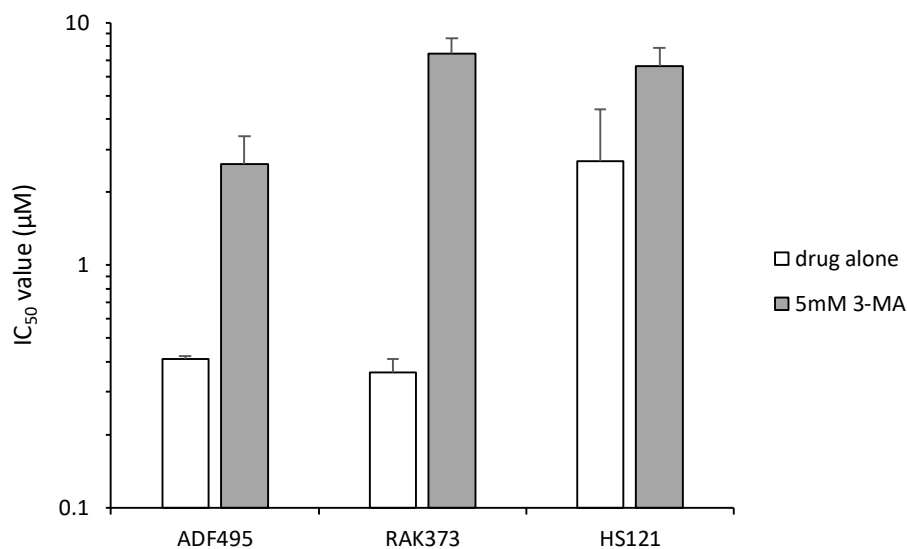
	Average IC_{50} (µM) ± SD		
Compound	Drug alone	+3-MA 5mM	Fold reduction
ADF495	0.41±0.01	2.61±0.8	6-fold
RAK373	0.36±0.05	7.46±1.11	20-fold
HS121	2.69±1.71	6.61±1.28	2.4-fold

Figure 9.43: Comparison of IC_{50} values ± SD of "hit" metallohelix compounds towards HCT116 p53+/+ ± 3-MA. Data generated by triplicated MTT assays completed on consecutive days n=3 (each individual experiment replicated twice).

9.3.7 - Drug Localisation Determination by Confocal Laser Microscopy

To gain insight into the mechanism of these novel compounds a number of compounds which possess an alkyne click region were tagged with a complimentary fluorescent dye (Alexafluor 555) which helps visualise where the compounds localise in

the cells. Specific localisation within organelles would help guide future studies designed to explore mechanism(s) of action. To validate the assay and to discount any unspecific binding, control samples were processed for both the media soluble and methanol soluble compounds (displayed in 9.3.7.1). Only the DAPI stained nucleus are present with no visible red light which attach to the drug.

A sample of the confocal images are displayed in figures 9.44 to 9.48 which clearly demonstrate that the compounds are able to enter the cell within a one-hour drug exposure. The compounds do not seem to localise into specific sites within the cell but appear to be present throughout the cytoplasm and the nucleus. There are variations to this general statement and these are described in each specific case presented below.

9.3.7.1 - Control

Cells were stained with DAPI (blue) and Alexafluor 555 (red) and only the nuclei of cells appear blue with no red staining apparent. This is the same for both media and methanol controls.

A) Media alone
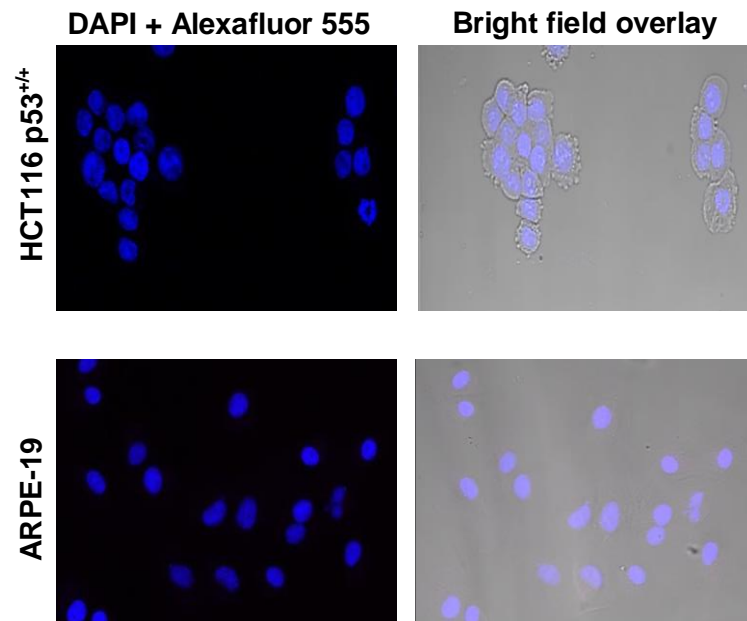
B) 0.1% (v/v) methanol
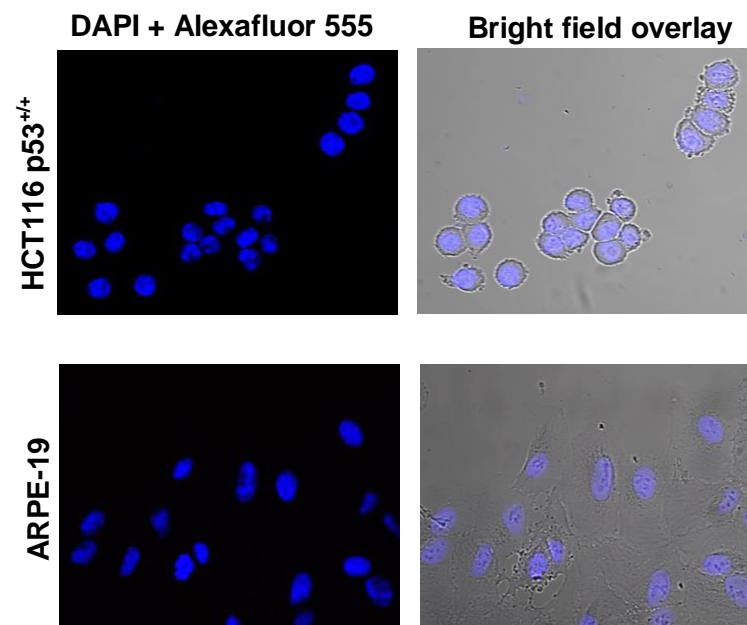
Figure 9.44: Untreated media and methanol control HCT116 p53$^{+/+}$ and ARPE-19 cells stained with 4',6-

Diamidino-2-Phenylindole, Dihydrochloride (DAPI) and Alexafluor reactive dye.

9.3.7.2 - HS138

In general terms, positive staining is observed in both the nucleus and cytoplasm of cells indicating that HS138 is able to penetrate into cells. There does not appear to be a significant difference in the staining pattern between HCT116 and ARPE-19 cells although there is some evidence of punctate staining in ARPE-19 cells suggesting some localisation to regions of unknown identity.
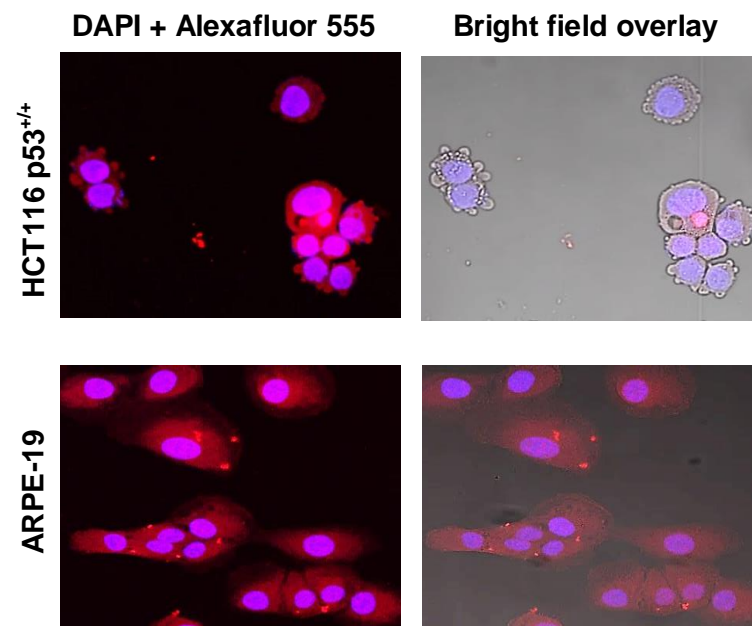
Figure 9.45: Confocal scanning microscope images of HCT116 p53$^{+/+}$ and ARPE-19 cells treated with 100µm HS138 for 1 hour. Samples stained with 4',6-Diamidino-2-Phenylindole, Dihydrochloride (DAPI) staining the nucleus blue and Alexafluor reactive dye (red).

9.3.7.3 - RAK434

Strong positive staining is observed in both the cytoplasm of cells but less staining in the nucleus. These results demonstrate that RAK434 is able to penetrate into cells. There does not appear to be a significant difference in the staining pattern between HCT116 and ARPE-19 cells. There is however clear evidence of the formation of vacuoles in the cytoplasm of both cells following treatment with RAK434.
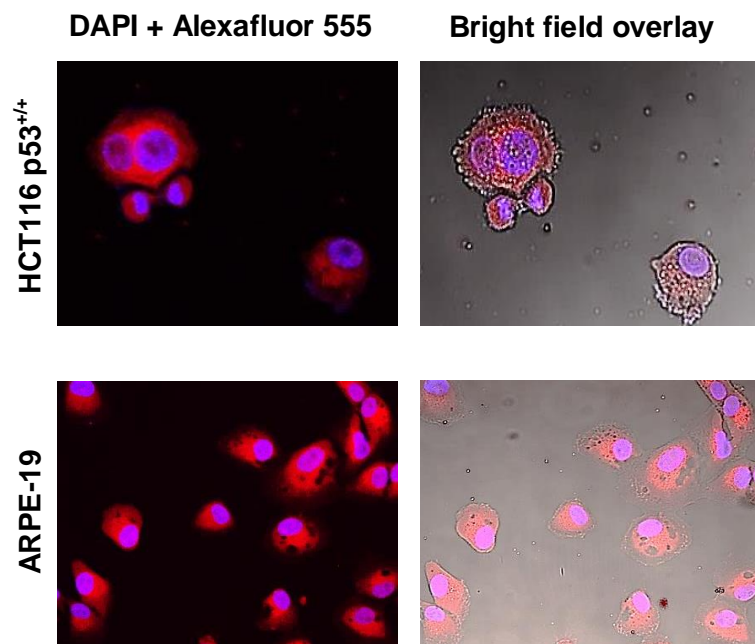
Figure 9.46: Confocal scanning microscope images of HCT116 p53$^{+/+}$ and ARPE-19 cells treated with 100µM RAK434 for 1 hour. Samples stained with 4',6-Diamidino-2-Phenylindole, Dihydrochloride (DAPI) staining the nucleus blue and Alexafluor reactive dye (red).

9.3.7.4 - HS255

Positive staining is observed in both the nucleus and cytoplasm of cells indicating that HS255 is able to penetrate into cells. The intensity of red staining in ARPE-19 cells is less than that in HCT116 p53$^{+/+}$ cells suggesting that selective uptake may be occurring.
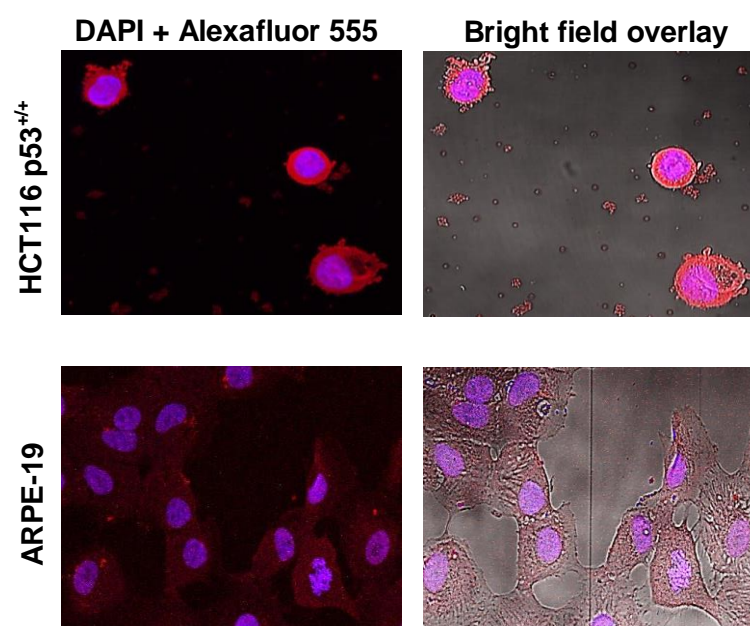
Figure 9.47: Confocal scanning microscope images of HCT116 p53$^{+/+}$ and ARPE-19 cells treated with 100µM HS255 for 1 hour. Samples stained with 4',6-Diamidino-2-Phenylindole, Dihydrochloride (DAPI) staining the nucleus blue and Alexafluor reactive dye (red).

9.3.7.5 - HS252

In general, positive staining is observed in both the nucleus and cytoplasm of cells indicating that HS138 is able to penetrate into cells. There does not appear to be a significant difference in the staining pattern between HCT116 p53$^{+/+}$ and ARPE-19 cells.
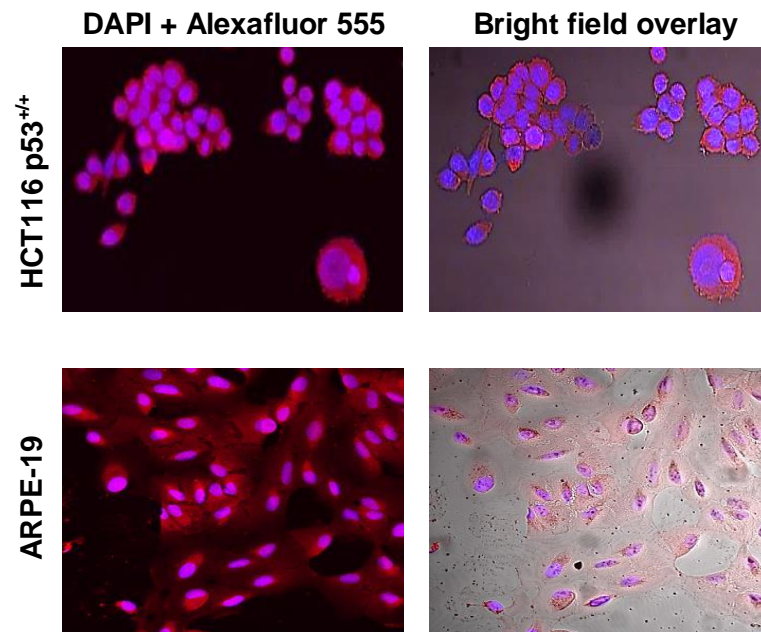
Figure 9.48: Confocal scanning microscope images of HCT116 p53+/+ and ARPE-19 cells treated with 100μM HS252 for 1 hour. Samples stained with 4',6-Diamidino-2-Phenylindole, Dihydrochloride (DAPI) staining the nucleus blue and Alexafluor reactive dye (red).

9.3.8 - *In Vivo* Investigation of "hit" Compounds

Based on their potency and selectivity *in vitro*, ADF495, HS121 and RAK373 were selected for evaluation against human tumour xenografts *in vivo*. These studies were conducted by Dr. Steve Shnyder at the University of Bradford and are reported here to demonstrate that the compounds emerging from the phenotypic screen have activity against tumours *in vivo*. Initial studies focused on establishing the dose that can be safely administered to animals and the results are presented in figure 12.3 in the appendix. All compounds were administered intravenously and acute (behavioral changes, obvious signs of distress etc. immediately after administration) and chronic (weight loss over several days) toxicities were determined. The maximum doses that could be administered to non-tumour bearing animals were 0.3 mg/Kg, 1.75 mg/Kg and 2.75 mg/Kg for ADF495, HS121 and RAK373 mg/Kg respectively. Whilst this is less than the maximum tolerated doses for cisplatin (6 mg/Kg), the test compounds did not cause any loss of weight whereas cisplatin caused a small drop in body weight which reached a maximum at 2 days after drug administration before recovering.

The response of HCT116 p53$^{-/-}$ human tumour xenografts to test compounds and cisplatin administered intravenously on day 0 of the experiment are presented in figure 12.4 in the appendix. The mean relative tumour volumes (RTV) were recorded and the growth delay (time taken for the tumours to reach RTV2 in treated compared to control populations) determined. As illustrated in figure 12.4, cisplatin and the test compounds induce a modest but statistically significant growth delay with RAK373 being as active as cisplatin in this experimental model. These results demonstrate that compounds selected for *in vivo* evaluation using the criteria of potency and selectivity have activity *in vivo* at a level that is comparable to cisplatin but at doses that cause less toxicity to animals in terms of body weight loss.

9.4 - Discussion

9.4.1 Chemosensitivity Investigations

From this investigation, it is very clear these compounds are very promising candidates for further investigation demonstrating superior potency and selectivity *in vitro* compared to the platinum standards cisplatin, carboplatin and oxaliplatin. One of the hit compounds identified (RAK373) not only displays significant potency toward the colonic adenocarcinoma HCT116 p53$^{+/+}$ cell line (IC$_{50}$ values for RAK373 were 0.36±0.05µM compared to oxaliplatin which was 0.93±0.11µM) but the compound also demonstrates a selectivity index of 93. This is nearly 28 times more selective than the most selective platinum based drug (oxaliplatin) under comparative experimental conditions. This finding alone demonstrates the potential of this class of compound albeit at a very early stage in the drug discovery process. The initial part of this discussion focuses on specific compounds that emerge from the screen before moving on to discuss the mechanistic studies conducted aimed at characterising certain pharmacological properties of selected compounds.

The class 1a flexicate complexes coded AKK/SHE in figure 77 have been evaluated by our group before with regards to potency only (Brabec et al., 2013) whereas the compounds coded DHS have not been evaluated previously. After initial chemosensitivity testing and comparison to previous hit compounds in this class, whilst the DHS compounds were very potent compounds, they were generally poor in

terms of their low selectivity indices. Only one compound (AKK022) was selected based on its potency (0.17±0.05µM) and selectivity (37.6).

The novel class 3a flexicates coded HS showed high activity in the HCT116 p53^{+/+} with ADF495 demonstrating an IC_{50} value of 0.41±0.01µM and a selectivity of 24.4. HS139 although displaying a poorer degree of potency (2.41±0.6µM) its selectivity index is one of the highest (41.7). Class 3a click flexicates were the most promising class resulting in seven "hit" compounds selected based heavily on their selectivity index. The majority of these compounds displayed good potency and if this was the only criteria used to select compounds for further evaluation, the majority of these compounds would have been selected. The use of the *in vitro* selectivity index significantly reduced the number of 'hit' compounds and is therefore more discriminatory than just potency alone. Pharmacologically, these compounds were of significant interest as the tethered sugar could offer increased potency and selectivity to cancer cells that are metabolically reprogrammed to favour aerobic glycolysis over oxidative phosphorylation. On the whole, all of the class 3a click compounds fail to exert the same potent cytotoxic potency as ADF495 but selectivity indexes are improved suggesting that the attachment of various sugars to the molecule improves the selectivity index considerably. This is further exemplified by the addition of glucose to "sugar naked" compounds HS255 and HS256 to give the glucose 3a click compound HS121. HS255 and HS256 display potent cytotoxic potential (1.56±0.91µM and 1.22±0.94µM respectively), which is reduced with the addition of glucose

(HS121=2.69±1.71µM). Although the potency is reduced as observed with ADF495 (parent 3a compound) the result of adding a glucose alone increases the selectivity of HS255 and HS255 (SI=5.91 and 7.48 respectively) up to 7 fold (HS121, SI = 42.95).

To gain further insight into the role of sugars on these molecules, the hypoxia-mimetic cobalt chloride which stabilises the HIF-1α protein and promotes HIF1 transcriptional activity against important metabolic processes such as glucose uptake (Pourpirali et al., 2015). HIF1 is known to up-regulate glucose transporters and it was proposed that if sugar clicked compounds were interacting with glucose transporters, enhanced activity of click 3a sugar compounds may be observed in the presence of cobalt chloride. As illustrated in figures 9.19-9.25, the response of HCT116 p53$^{+/+}$ cells to class 3a sugar click compounds decreases significantly in all cases. The reasons for this observation are not known but it is possible that by up-regulating glucose transporters, more free glucose is being taken and this is out competing and nullifying the effects of class 3a sugar click compounds on biochemical pathways such as glycolysis. Further studies are required to verify this hypothesis, but the results clearly demonstrate that conditioning of cells with cobalt chloride significantly decreases the activity of these compounds.

To investigate the potential role of these "hit" compounds in more chemo-resistant cell lines the potency of the 11 lead compounds were tested on the HCT116 p53$^{-/-}$ cell line which is typically more resistant to the platinates than the HCT116 p53$^{+/+}$ isogenic clone (table 9.9 and figure 9.18). Although the potency is decreased with the reduction

of p53 expression, the IC_{50} values of AKK022, HS239, HS142, HS119 and HS139 show superior potency toward HCT116 p53$^{-/-}$ cells compared to all three platinate compounds (table 9.9 and figure 9.18) which suggests these compounds could be successful chemotherapuetic agents in more p53 deficient cell lines.

9.4.2 - Investigation of Cell Viability, Induction of Apoptosis and Disruption of Cell Cycle Parameter Via NC3000 Cytometry

On selection of lead compounds, initial mechanistic studies using the NC3000 were conducted following a 24-hour drug exposure to test compounds. These conditions were based on the results obtained with platinates which demonstrated that major effects on cell viability, apoptosis and cell cycle occurred within this time scale (section 3.3.5). Two apoptosis induction assays were completed but unlike with the positive control (cisplatin), no substantial induction of apoptosis was observed (sections 9.3.5.2 – 9.3.5.3). There was a slight increase in apoptotic cell population after exposure to HS121 (figures 9.31, 9.32, 9.35 and 9.36) but overall, it can be concluded that these compounds are not inducing apoptotic cell death. Cell cycle analysis on the lead compounds also failed to demonstrate any significant effects post drug exposure (section 9.3.5.4). Some effect on the cell cycle by HS135 was observed with an increase in S phase population of over 20% suggesting it could possibly be causing an S phase arrest. Overall however, the analysis of cell cycle disruption does not offer any significant clues as to the compounds mechanism of action. Finally, viability assays were completed to not only measure cell number in each sample but to demonstrate

the effects of the novel flexicates on cell viability. The viability of the cell population remains consistent for both HCT116 p53$^{+/+}$ and ARPE-19 cell lines with cell number reducing slightly after 24-hour exposure. This is a counter intuitive observation as the compounds clearly have cytotoxic activity as demonstrated by the MTT assay but it could be explained on the basis that cell death could have occurred rapidly (within the 24 hour drug exposure period) and those cells that remained would appear viable. Further studies are required to refine these experimental procedures to address this possible explanation but for now, the results of the viability experiments need to be interpreted with caution. As discussed in chapter 7 one single experiment is not robust enough and does not remove any potential bias or error it is therefore paramount these assays are also rerun to produce mean data. In addition to rerunning assays new assays will need to be developed to firstly confirm the potential absence of apoptosis *via* additional apoptosis assays such a caspase assays.

In conclusion, the results from NC3000 investigations suggest the compounds do not induce apoptosis and therefore cell death is induced *via* alternative mechanisms. Further investigation to determine the mechanism of cell death are required and this includes the induction of autophagy described below.

9.4.3 - Drug Localisation Assay

These compounds exert dramatic cytotoxic effects on both isogenic clones HCT116 cells whilst demonstrating a high selectivity in comparison to non-cancerous ARPE-19 cell lines. To try and identify possible reasons for this selectivity, cell localisation

studies to determine key differences in the cellular distribution of drugs between cancer and non-cancer cell lines may provide clues as to potential mechanism(s) of action. The inclusion of alkyne groups on molecules provides the opportunity to attach fluorophores post drug exposure using click chemistry reactions. This allows the drug to distribute naturally in cells and following fixation, the presence of the drug can be detected by the addition of a fluorophore. The results of these studies demonstrate a number of things, the most obvious being that these large molecular weight compounds are able to rapidly penetrate and distribute throughout the cell. This is not a trivial observation in view of their molecular weight and demonstrates that they can penetrate and cross several barriers including the plasma and other membranous systems in the cell (e.g. nuclear membrane). With regards to localisation within the cell, it is apparent that the drugs distribute to both the cytoplasm and the nucleus and in many cases, there is little difference in staining between the nucleus and the cytoplasm. Metallohelicates have been shown to bind to DNA previously (Brabec et al., 2013) and therefore their effects could be mediated through DNA damage although the lack of induction of apoptosis in this study suggests otherwise. Furthermore, no major differences in drug distribution between HCT116p53$^{+/+}$ cells and ARPE19 cells were observed and the same applies to the lack of specific loci or fluorescent 'hot spots' in cells. There were some exceptions to this (HS225 and HS138 for example) but overall, distribution of drug within the cell was largely uninformative in the current experimental design. It is possible that any specific localisation is masked by too much 'unbound' drug within the cell and if this is the case, removing the drug after a one-

hour exposure and incubating cells in drug free media for defined periods of time to allow any unbound drug to efflux may reveal the location of bound drug. Further studies are therefore required before any firm conclusions can be made.

9.4.4 - Autophagic Induction of Complexes

Visual observations made during and following drug exposure (figure 9.44) demonstrate the appearance of vacuoles within the cytoplasm of cells. In the absence of apoptosis induction, this suggested that cells may be undergoing autophagic cell death and this possibility was explored further in this study. The results demonstrate that the addition of the autophagy inhibitor 3-MA significantly reduced the cytotoxic potency of compounds tested (figure 9.43). This suggests that the compounds are inducing autophagy and further studies are required to confirm this potential mechanism of action. Autophagy defined as a self-degradative process is important for balancing energy levels in specific developmental stages and in response to external stress factors. In addition to ensuring adequate energy levels for basal cell function autophagy plays a housekeeping role in degrading "faulty" cellular components such as misfolded, aggregated proteins, damaged organelles and internal pathogens. Autophagy is therefore primarily a survival mechanism sustaining cell survival yet if executed until completion is a means of achieving cell death (Glick, Barth, & Macleod, 2010; Jin & White, 2007). Autophagy is a complex process which can be viewed as a cell death or a survival pathway (Kondo, Kanzawa, Sawaya, & Kondo, 2005) but in this

case, the results suggest that the compounds are inducing autophagy leading to cell death.

The use of additional autophagy inhibitors such as bafilomycin A1 and western blot analysis to detect autophagic markers would further support this hypothesis but due to time constraints, these studies were not conducted in this thesis.

9.4.5 - *In Vivo* Anti-Tumour Activity of Selected Compounds

Studies conducted by the University of Bradford demonstrated that the most promising "hit" compounds (RAK373, ADF495, HS121) have anti-tumour activity *in vivo*. These studies were completed alongside a control and a cisplatin treated positive control (figures 12.3 and 12.4 in the appendix). The parameters measured were the mean relative tumour volume, growth delay and percentage body weight loss which is an indicator of host health post administration. The cell line investigated were HCT116 p53$^{-/-}$ for which only ADF495 was more potent but the selectivity indexes (especially in HS121) combined with competitive potency made this tumour model a good choice. The data generated are very promising and it demonstrates that anti-tumour activity that is comparable to cisplatin occurs and furthermore, this level of activity occurs at doses of compounds that do not induce significant weight loss (unlike cisplatin).

9.5 - Conclusion

In the context of the main question being addressed in this thesis, these results demonstrate that the use of a phenotypic approach to drug evaluation based upon potency and selectivity combined with the use of clinically approved platinates to

serve as a 'yardstick' to measure the relative merits of test compounds has identified novel compounds that have anti-cancer activity *in vivo*. This approach led to the selection of 3 compounds out of a total of 68 compounds with potent cytotoxic activity *in vitro*, the majority of which were more potent than the platinates. If potency alone was used to select compounds, this would not have been sufficiently discriminatory to select limited number of compounds for further development. This demonstrates that the screen has increased discriminatory powers to enable the rationale selection of compounds for further studies including mechanistic and *in vivo* studies. No screening process is ever going to be 100% efficient and both false positive and false negative predictions will occur, but this approach represents a potential way forward for rationalising the selection of compounds based upon a phenotypic approach to drug discovery.

Chapter 10 - General Conclusion

In the field of anti-cancer drug discovery, a number of preclinical strategies are employed to identify potential therapeutic agents. These can be broadly segregated into two main areas; target orientated drug discovery and random or phenotypic based drug discovery (Moffat, Rudolph, & Bailey, 2014). Target based drug discovery is based on the premise that understanding the biology of cancer will lead to the development of drugs that target key pathways and considerable investment in this area has been made. Whilst a number of novel therapeutic agents have been developed, it is now recognized that the investment made has not been reciprocated in the discovery of new molecular entities. Random screening or phenotype based drug discovery programs have the potential to discover new chemical entities and it is estimated that 33% of new small molecule molecular entities discovered between 1998 and 2008 emerged from phenotypic based drug discovery programs whereas only 17% came from target based discovery (Swinney & Anthony, 2011). It is therefore clear to see why a renaissance in phenotypic drug discovery is occurring.

The process of phenotype based drug discovery is a difficult and time consuming one with high rates of attrition. Large scale operations such as the NCI60 screen have successfully identified novel therapeutic agents but the process is expensive and time consuming. These screens rely heavily on characterising the response of cancer cells to novel compounds and they do not take into account the response of normal or non-cancer cell lines. In this thesis, a phenotype based screen has been employed to

evaluate a range of different organometallic complexes with the aim of selecting compounds based upon (i) potency (ii) an *in vitro* selectivity index and (iii) comparable or improved performance in these screens compared to three clinically used anti-cancer drugs. Over the course of this research, compounds from 6 different collaborative groups were entered into the screen. A total of 210 useable compounds were evaluated with many more discounted due to solubility issues. Of these 210 compounds 24 were deemed comparable with 5 determined "hit" compounds based on their meeting the 3 phenotypic profiles outlined above. If the compounds were selected based on potency alone, a total of 91 compounds would have been selected making evaluation unmanageable in subsequent mechanistic studies. The incorporation of an *in vitro* selectivity index into the decision-making process makes this a more discriminatory tool and provides a good rationale for taking compounds forward to *in vivo* testing. It should be stressed that no selectivity index determined *in vitro* is going to faithfully translate into a good selectivity index *in vivo* but by comparing the selectivity indices of test compounds to clinically approved drugs in the same experimental system, taking compounds forward for further evaluation can be done with greater confidence.

In this thesis, a wide range of selectivity indices were obtained with several compounds showing values below 1. The majority of compounds had selectivity indices which were broadly comparable to the platinates but the most promising results were obtained with the series of metallohelicate compounds obtained from the University

of Warwick. In this case, several compounds with selectivity indices much higher than the platinates were discovered and all of these were novel chemical entities that did not fit the convention with respect to Lipinski rules. Three compounds were taken forward for *in vivo* testing and whilst the results were not dramatic, growth delays were observed, and these were comparable to those obtained with cisplatin in the same xenograft model. Anti-tumour activity *in vivo* was observed at doses that did not induce any weight loss or any other signs of toxicity. With regards to the mechanisms of action of these lead compounds, studies demonstrated that cell death was not by the induction of apoptosis but preliminary data suggest that these compounds work by inducing autophagy. Further studies are required to confirm this but due to time constraints, these studies were not performed in this thesis.

In conclusion, this study has developed a robust and reliable phenotype based screen where the inclusion of an *in vitro* selectivity index into the decision-making process provides greater discriminatory powers to select novel compounds for further testing. Of all the compounds evaluated, the large molecular weight metallohelicates developed by Prof Peter Scott and his team are the most interesting with *in vitro* selectivity indices that were significantly higher than clinically used platinum based anti-cancer drugs. The inclusion of an *in vitro* selectivity index into phenotype based drug discovery programs has not been done before (to the best of our knowledge) and this thesis provides evidence to support the development of this concept further.

Chapter 11 - References

ACS, A. c. s. (2016, February 2016). American Cancer Society: Cancer Facts and Figures 2016. Retrieved from http://www.cancer.org/acs/groups/content/@research/documents/document/acspc-047079.pdf

Adhikari, S., Palepu, N. R., Sutradhar, D., Shepherd, S. L., Phillips, R. M., Kaminsky, W., . . . Kollipara, M. R. (2016). Neutral and cationic half-sandwich arene ruthenium, Cp*Rh and Cp*Ir oximato and oxime complexes: Synthesis, structural, DFT and biological studies. *Journal of Organometallic Chemistry*. doi:http://dx.doi.org/10.1016/j.jorganchem.2016.08.004

Ai, Z., Lu, Y., Qiu, S., & Fan, Z. (2016). Overcoming cisplatin resistance of ovarian cancer cells by targeting HIF-1-regulated cancer metabolism. *Cancer Letters, 373*(1), 36-44.

Airley, R. (2009). *Cancer chemotherapy: basic science to the clinic*: John Wiley & Sons.

Al-Dimassi, S., Abou-Antoun, T., & El-Sibai, M. (2014). Cancer cell resistance mechanisms: a mini review. *Clinical and Translational Oncology, 16*(6), 511-516.

Alberts, B. (2002). *Molecular biology of the cell* (Vol. 4th). New York: Garland Science.

Ali, R., Mirza, Z., Ashraf, G. M., Kamal, M. A., Ansari, S. A., Damanhouri, G. A., . . . Sheikh, I. A. (2012). New anticancer agents: recent developments in tumor therapy. *Anticancer research, 32*(7), 2999-3005.

Allardyce, C. S., & Dyson, P. J. (2001). Ruthenium in medicine: current clinical uses and future prospects. *Platinum Metals Review, 45*(2), 62-69.

Allison, S. J., Sadiq, M., Baronou, E., Cooper, P. A., Dunnill, C., Georgopoulos, N. T., . . . Stratford, I. J. (2017). Preclinical anti-cancer activity and multiple mechanisms of action of a cationic silver complex bearing N-heterocyclic carbene ligands. *Cancer Letters*.

Amin, A., & Buratovich, M. A. (2009). New Platinum and Ruthenium complexes-the latest class of potential chemotherapeutic drugs-A review of recent developments in the field. *Mini reviews in medicinal chemistry, 9*(13), 1489-1503.

Antonarakis, E. S., & Emadi, A. (2010). Ruthenium-based chemotherapeutics: are they ready for prime time? *Cancer chemotherapy and pharmacology, 66*(1), 1-9.

Aparicio, L. A., Blanco, M., Castosa, R., Concha, A., Valladares, M., Calvo, L., & Figueroa, A. (2015). Clinical implications of epithelial cell plasticity in cancer progression. *Cancer Lett*. doi:10.1016/j.canlet.2015.06.007

Bailón-Moscoso, N., Romero-Benavides, J. C., & Ostrosky-Wegman, P. (2014). Development of anticancer drugs based on the hallmarks of tumor cells. *Tumor Biology, 35*(5), 3981-3995.

Baitalik, S., & Adhikary, B. (1997). Heterochelates of ruthenium (II): electrochemistry, absorption spectra, and luminescence properties. *Polyhedron, 16*(23), 4073-4080.

Baran, N., & Konopleva, M. (2017). Molecular Pathways: Hypoxia-activated prodrugs in cancer therapy. *Clinical Cancer Research*.

Bergamo, A., Gagliardi, R., Scarcia, V., Furlani, A., Alessio, E., Mestroni, G., & Sava, G. (1999). In vitro cell cycle arrest, in vivo action on solid metastasizing tumors, and host toxicity of the antimetastatic drug NAMI-A and cisplatin. *Journal of Pharmacology and Experimental Therapeutics, 289*(1), 559-564.

Bergamo, A., Riedel, T., Dyson, P. J., & Sava, G. (2015). Preclinical combination therapy of the investigational drug NAMI-A+ with doxorubicin for mammary cancer. *Investigational New Drugs, 33*(1), 53-63.

Berndtsson, M., Hägg, M., Panaretakis, T., Havelka, A. M., Shoshan, M. C., & Linder, S. (2007). Acute apoptosis by cisplatin requires induction of reactive oxygen species but is not associated with damage to nuclear DNA. *International journal of cancer, 120*(1), 175-180.

Bhosle, J., & Hall, G. (2009). Principles of cancer treatment by chemotherapy. *Surgery (Oxford), 27*(4), 173-177.

Boran, A. D., & Iyengar, R. (2010). Systems approaches to polypharmacology and drug discovery. *Current opinion in drug discovery & development, 13*(3), 297.

Bourzac, K. (2014). Biology: Three known unknowns. *Nature, 509*(7502), S69-S71. doi:10.1038/509S69a

Brabec, V., Howson, S. E., Kaner, R. A., Lord, R. M., Malina, J., Phillips, R. M., . . . Scott, P. (2013). Metallohelices with activity against cisplatin-resistant cancer cells; does the mechanism involve DNA binding? *Chemical Science, 4*(12), 4407-4416.

Bragado, P., Armesilla, A., Silva, A., & Porras, A. (2007). Apoptosis by cisplatin requires p53 mediated p38α MAPK activation through ROS generation. *Apoptosis, 12*(9), 1733-1742. doi:10.1007/s10495-007-0082-8

Bruijnincx, P. C., & Sadler, P. J. (2008). New trends for metal complexes with anticancer activity. *Current opinion in chemical biology, 12*(2), 197-206.

Bryant, H. E., Schultz, N., Thomas, H. D., Parker, K. M., Flower, D., Lopez, E., . . . Helleday, T. (2005). Specific killing of BRCA2-deficient tumours with inhibitors of poly (ADP-ribose) polymerase. *Nature, 434*(7035), 913.

Büchel, G. E., Kossatz, S., Sadique, A., Rapta, P., Zalibera, M., Bucinsky, L., . . . Reiner, T. (2017). cis-Tetrachlorido-bis (indazole) osmium (IV) and its osmium (III) analogues: paving the way towards the cis-isomer of the ruthenium anticancer drugs KP1019 and/or NKP1339. *Dalton Transactions.*

Cepeda, V., Fuertes, M. A., Castilla, J., Alonso, C., Quevedo, C., & Pérez, J. M. (2007). Biochemical mechanisms of cisplatin cytotoxicity. *Anti-Cancer Agents in Medicinal Chemistry (Formerly Current Medicinal Chemistry-Anti-Cancer Agents), 7*(1), 3-18.

Cersosimo, R. J. (2005). Oxaliplatin-associated neuropathy: a review. *Annals of Pharmacotherapy, 39*(1), 128-135.

Chakravarty, J., & Bhattacharya, S. (1996). Ruthenium phenolates. Synthesis, characterization and electron-transfer properties of some salicylaldiminato and 2-(arylazo)phenolato complexes of ruthenium. *Polyhedron, 15*(7), 1047-1055. doi:http://dx.doi.org/10.1016/0277-5387(95)00362-2

Coldrick, Z., Steenson, P., Millner, P., Davies, M., & Nelson, A. (2009). Phospholipid monolayer coated microfabricated electrodes to model the interaction of molecules with biomembranes. *Electrochimica Acta, 54*(22), 4954-4962.

Conconi, A. (2013). Cisplatin (Cis-diaminedichloroplatinum).   Retrieved from http://www.conconilab.ca/projects/

Conroy, T., Desseigne, F., Ychou, M., Bouché, O., Guimbaud, R., Bécouarn, Y., . . . de la Fouchardière, C. (2011). FOLFIRINOX versus gemcitabine for metastatic pancreatic cancer. *New England Journal of Medicine, 364*(19), 1817-1825.

Cunningham, A. D., Qvit, N., & Mochly-Rosen, D. (2017). Peptides and peptidomimetics as regulators of protein–protein interactions. *Current opinion in structural biology, 44*, 59-66.

de Souza, I. C. A., Faro, L. V., Pinheiro, C. B., Gonzaga, D. T. G., da Silva, F. d. C., Ferreira, V. F., . . . Lanznaster, M. (2016). Investigation of cobalt (III)-triazole systems as prototypes for hypoxia-activated drug delivery. *Dalton Transactions, 45*(35), 13671-13674.

Drews, J. (2000). Drug discovery: a historical perspective. *Science, 287*(5460), 1960-1964.

Drummond, J. T., Anthoney, A., Brown, R., & Modrich, P. (1996). Cisplatin and adriamycin resistance are associated with MutLα and mismatch repair deficiency in an ovarian tumor cell line. *Journal of Biological Chemistry, 271*(33), 19645-19648.

Dudhe, R., Sharma, P. K., Verma, P., & Chaudhary, A. (2011). Pyrimidine as anticancer agent: a review. *J. Adv. Sci. Res, 2*(3), 10-17.

ElShamy, W. M., & Duhé, R. J. (2013). Overview: cellular plasticity, cancer stem cells and metastasis. *Cancer Letters, 341*(1), 2-8.

Elshebeiny, M., & Almorsy, W. (2016). Gemcitabine–oxaliplatin (GEMOX) for epithelial ovarian cancer patients resistant to platinum-based chemotherapy. *Journal of the Egyptian National Cancer Institute, 28*(3), 183-189.

Elvers, B., Hawkins, S., & Schultz, G. (1992). Ullmans encyclopedia of chemical technology: New York: VCH Publishing.

Farmer, H., McCabe, N., Lord, C. J., Tutt, A. N., Johnson, D. A., Richardson, T. B., . . . Knights, C. (2005). Targeting the DNA repair defect in BRCA mutant cells as a therapeutic strategy. *Nature, 434*(7035), 917.

Frühauf, S., & Zeller, W. (1991). New platinum, titanium, and ruthenium complexes with different patterns of DNA damage in rat ovarian tumor cells. *Cancer Research, 51*(11), 2943-2948.

Galanski, M., Jakupec, M. A., & Keppler, B. K. (2005). Update of the preclinical situation of anticancer platinum complexes: novel design strategies and innovative analytical approaches. *Current medicinal chemistry, 12*(18), 2075-2094.

Galluzzi, L., Senovilla, L., Vitale, I., Michels, J., Martins, I., Kepp, O., . . . Kroemer, G. (2012). Molecular mechanisms of cisplatin resistance. *Oncogene, 31*(15), 1869-1883.

Garcia, M., Jemal, A., Ward, E., Center, M., Hao, Y., Siegel, R., & Thun, M. (2007). Global cancer facts & figures 2007. *Atlanta, GA: American cancer society, 1*(3), 52.

Gasser, G., Ott, I., & Metzler-Nolte, N. (2010). Organometallic anticancer compounds. *Journal of medicinal chemistry, 54*(1), 3-25.

Gautier, A., & Cisnetti, F. (2012). Advances in metal-carbene complexes as potent anti-cancer agents. *Metallomics : integrated biometal science, 4*(1), 23-32. doi:10.1039/c1mt00123j

Geldmacher, Y., Oleszak, M., & Sheldrick, W. S. (2012). Rhodium (III) and iridium (III) complexes as anticancer agents. *Inorganica Chimica Acta, 393*, 84-102.

Gerasimchuk, N., Gamian, A., Glover, G., & Szponar, B. (2010). Light insensitive silver (I) cyanoximates as antimicrobial agents for indwelling medical devices. *Inorganic chemistry, 49*(21), 9863-9874.

Gerasimchuk, N., Maher, T., Durham, P., Domasevitch, K. V., Wilking, J., & Mokhir, A. (2007). Tin (IV) cyanoximates: synthesis, characterization, and cytotoxicity. *Inorganic chemistry, 46*(18), 7268-7284.

Giaccone, G. (2000). Clinical perspectives on platinum resistance. *Drugs, 59*(4), 9-17.

Glick, D., Barth, S., & Macleod, K. F. (2010). Autophagy: cellular and molecular mechanisms. *The Journal of pathology, 221*(1), 3-12.

Goodman, L. S., Wintrobe, M. M., Dameshek, W., Goodman, M. J., Gilman, A., & McLennan, M. T. (1946). Nitrogen mustard therapy: Use of methyl-bis (beta-chloroethyl) amine hydrochloride and tris (beta-chloroethyl) amine hydrochloride for Hodgkin's disease, lymphosarcoma, leukemia and certain allied and miscellaneous disorders. *Journal of the American Medical Association, 132*(3), 126-132.

Gottesman, M. M., Fojo, T., & Bates, S. E. (2002). Multidrug resistance in cancer: role of ATP–dependent transporters. *Nature Reviews Cancer, 2*(1), 48-58.

Gras, M., Therrien, B., Süss-Fink, G., Casini, A., Edafe, F., & Dyson, P. J. (2010). Anticancer activity of new organo-ruthenium, rhodium and iridium complexes containing the 2-(pyridine-2-yl) thiazole N, N-chelating ligand. *Journal of Organometallic Chemistry, 695*(8), 1119-1125.

Gravitz, L. (2014). Therapy: This time it's personal. *Nature, 509*(7502), S52-S54. doi:10.1038/509S52a

Greaves, M., & Maley, C. C. (2012). Clonal evolution in cancer. *Nature, 481*(7381), 306-313.

Gujral, T. S., Peshkin, L., & Kirschner, M. W. (2014). Exploiting polypharmacology for drug target deconvolution. *Proceedings of the National Academy of Sciences, 111*(13), 5048-5053.

Hall, M. D., Telma, K. A., Chang, K.-E., Lee, T. D., Madigan, J. P., Lloyd, J. R., . . . Gottesman, M. M. (2014). Say no to DMSO: dimethylsulfoxide inactivates cisplatin, carboplatin, and other platinum complexes. *Cancer Research, 74*(14), 3913-3922.

Hanahan, D., & Weinberg, R. A. (2000). The Hallmarks of Cancer. *Cell, 100*(1), 57-70. doi:http://dx.doi.org/10.1016/S0092-8674(00)81683-9

Hanahan, D., & Weinberg, Robert A. (2011). Hallmarks of Cancer: The Next Generation. *Cell, 144*(5), 646-674. doi:http://dx.doi.org/10.1016/j.cell.2011.02.013

Hartwell, L. H., & Kastan, M. B. (1994). Cell cycle control and cancer. *Science, 266*(5192), 1821.

Heffern, M. C., Yamamoto, N., Holbrook, R. J., Eckermann, A. L., & Meade, T. J. (2013). Cobalt derivatives as promising therapeutic agents. *Current opinion in chemical biology, 17*(2), 189-196. doi:http://dx.doi.org/10.1016/j.cbpa.2012.11.019

Herrmann, W. A. (2002). N-Heterocyclic Carbenes: A New Concept in Organometallic Catalysis. *Angewandte Chemie International Edition, 41*(8), 1290-1309.

Hollstein, M., Hergenhahn, M., Yang, Q., Bartsch, H., Wang, Z.-Q., & Hainaut, P. (1999). New approaches to understanding p53 gene tumor mutation spectra. *Mutation Research/Fundamental and Molecular Mechanisms of Mutagenesis, 431*(2), 199-209.

Holzer, A. K., Manorek, G. H., & Howell, S. B. (2006). Contribution of the major copper influx transporter CTR1 to the cellular accumulation of cisplatin, carboplatin, and oxaliplatin. *Molecular pharmacology, 70*(4), 1390-1394.

Hopkins, A. L. (2008). Network pharmacology: the next paradigm in drug discovery. *Nat Chem Biol, 4*(11), 682-690.

Howson, S. E., Allan, L. E., Chmel, N. P., Clarkson, G. J., van Gorkum, R., & Scott, P. (2009). Self-assembling optically pure Fe (A–B) 3 chelates. *Chemical Communications*(13), 1727-1729.

Howson, S. E., Bolhuis, A., Brabec, V., Clarkson, G. J., Malina, J., Rodger, A., & Scott, P. (2012). Optically pure, water-stable metallo-helical 'flexicate' assemblies with antibiotic activity. *Nature chemistry, 4*(1), 31-36.

Iglehart, J. D., & Silver, D. P. (2009). Synthetic lethality--a new direction in cancer-drug development. *New England Journal of Medicine, 361*(2), 189.

Igney, F. H., & Krammer, P. H. (2002). Death and anti-death: tumour resistance to apoptosis. *Nature reviews. Cancer, 2*(4), 277.

Jin, S., & White, E. (2007). Role of autophagy in cancer: management of metabolic stress. *Autophagy, 3*(1), 28-31.

Johnson, N. A., Southerland, M. R., & Youngs, W. J. (2017). Recent Developments in the Medicinal Applications of Silver-NHC Complexes and Imidazolium Salts. *Molecules, 22*(8), 1263.

Junaid, A., Deb, P. K., Ooi, H., El-Rabie, D., Shuaib, F. O., & Rajasingam, R. (2015). Design, Synthesis and Pharmacological Properties of Peptidomimetics. *Asian Journal of Chemistry, 27*(9), 3137.

Kaner, R. A., & Scott, P. (2015). Metallohelices: potential mimetics of α-helical peptides in cancer treatment? *Future medicinal chemistry, 7*(1), 1-4.

Karnthaler-Benbakka, C., Groza, D., Kryeziu, K., Pichler, V., Roller, A., Berger, W., . . . Kowol, C. R. (2014). Tumor-Targeting of EGFR Inhibitors by Hypoxia-Mediated Activation. *Angewandte Chemie International Edition, 53*(47), 12930-12935.

Kelland, L. R. (2000). Preclinical perspectives on platinum resistance. *Drugs, 59*(4), 1-8.

Kelland, L. R. (2007). The resurgence of platinum-based cancer chemotherapy. *Nature reviews. Cancer, 7*(8), 573.

Kerbel, R., Kobayashi, H., & Graham, C. H. (1994). Intrinsic or acquired drug resistance and metastasis: are they linked phenotypes? *Journal of cellular biochemistry, 56*(1), 37-47.

Kondo, Y., Kanzawa, T., Sawaya, R., & Kondo, S. (2005). The role of autophagy in cancer development and response to therapy. *Nature Reviews Cancer, 5*(9), 726-734.

Kostova, I. (2006). Platinum complexes as anticancer agents. *Recent patents on anti-cancer drug discovery, 1*(1), 1-22.

Lee, J., & Bogyo, M. (2013). Target deconvolution techniques in modern phenotypic profiling. *Current opinion in chemical biology, 17*(1), 118-126.

Lehn, J.-M., Rigault, A., Siegel, J., Harrowfield, J., Chevrier, B., & Moras, D. (1987). Spontaneous assembly of double-stranded helicates from oligobipyridine ligands and copper (I) cations: structure of an inorganic double helix. *Proceedings of the National Academy of Sciences, 84*(9), 2565-2569.

Leijen, S., Burgers, S. A., Baas, P., Pluim, D., Tibben, M., van Werkhoven, E., . . . Schellens, J. H. (2015). Phase I/II study with ruthenium compound NAMI-A and gemcitabine in patients with non-small cell lung cancer after first line therapy. *Investigational New Drugs, 33*(1), 201-214.

Leung, C.-H., Zhong, H.-J., Chan, D. S.-H., & Ma, D.-L. (2013). Bioactive iridium and rhodium complexes as therapeutic agents. *Coordination Chemistry Reviews, 257*(11), 1764-1776.

Lipinski, C. A., Lombardo, F., Dominy, B. W., & Feeney, P. J. (2001). Experimental and computational approaches to estimate solubility and permeability in drug discovery and development settings1. *Advanced drug delivery reviews, 46*(1-3), 3-26.

Liu, W., & Gust, R. (2013). Metal N-heterocyclic carbene complexes as potential antitumor metallodrugs. *Chemical Society Reviews, 42*(2), 755-773.

Loehrer, P. J., & Einhorn, L. H. (1984). Cisplatin. *Annals of Internal Medicine, 100*(5), 704-713. doi:10.7326/0003-4819-100-5-704

Lord, C. J., Tutt, A. N., & Ashworth, A. (2015). Synthetic lethality and cancer therapy: lessons learned from the development of PARP inhibitors. *Annual review of medicine, 66*, 455-470.

Lord, R. M., Hebden, A. J., Pask, C. M., Henderson, I. R., Allison, S. J., Shepherd, S. L., . . . McGowan, P. C. (2015). Hypoxia-Sensitive Metal beta-Ketoiminato Complexes Showing Induced Single-Strand DNA Breaks and Cancer Cell Death by Apoptosis. *J Med Chem, 58*(12), 4940-4953. doi:10.1021/acs.jmedchem.5b00455

Lucas, S. J., Lord, R. M., Wilson, R. L., Phillips, R. M., Sridharan, V., & McGowan, P. C. (2012). Synthesis of iridium and ruthenium complexes with (N, N),(N, O) and (O, O) coordinating bidentate ligands as potential anti-cancer agents. *Dalton Transactions, 41*(45), 13800-13802.

Luqmani, Y. (2005). Mechanisms of drug resistance in cancer chemotherapy. *Medical Principles and Practice, 14*(Suppl. 1), 35-48.

Ly, J. D., Grubb, D. R., & Lawen, A. (2003). The mitochondrial membrane potential (Δψm) in apoptosis; an update. *Apoptosis, 8*(2), 115-128. doi:10.1023/a:1022945107762

Ma, D.-L., Wang, M., Mao, Z., Yang, C., Ng, C.-T., & Leung, C.-H. (2016). Rhodium complexes as therapeutic agents. *Dalton Transactions, 45*(7), 2762-2771.

Meacham, C. E., & Morrison, S. J. (2013). Tumour heterogeneity and cancer cell plasticity. *Nature, 501*(7467), 328-337. doi:10.1038/nature12624

Mercs, L., & Albrecht, M. (2010). Beyond catalysis: N-heterocyclic carbene complexes as components for medicinal, luminescent, and functional materials applications. *Chemical Society Reviews, 39*(6), 1903-1912.

Mestres, J., Gregori-Puigjané, E., Valverde, S., & Solé, R. V. (2009). The topology of drug–target interaction networks: implicit dependence on drug properties and target families. *Molecular BioSystems, 5*(9), 1051-1057.

Misset, J. L., Bleiberg, H., Sutherland, W., Bekradda, M., & Cvitkovic, E. (2000). Oxaliplatin clinical activity: a review. *Critical reviews in oncology/hematology, 35*(2), 75-93.

Moffat, J. G., Rudolph, J., & Bailey, D. (2014). Phenotypic screening in cancer drug discovery [mdash] past, present and future. *Nature reviews Drug discovery, 13*(8), 588-602.

Mohamadi, S., Tate, D. J., Vakurov, A., & Nelson, A. (2014). Electrochemical screening of biomembrane-active compounds in water. *Analytica chimica acta, 813*, 83-89.

Mohamed, H. A., Lake, B. R., Laing, T., Phillips, R. M., & Willans, C. E. (2015). Synthesis and anticancer activity of silver(I)-N-heterocyclic carbene complexes derived from the natural xanthine products caffeine, theophylline and theobromine. *Dalton Trans, 44*(16), 7563-7569. doi:10.1039/c4dt03679d

Munteanu, C. R., & Suntharalingam, K. (2015). Advances in cobalt complexes as anticancer agents. *Dalton Transactions, 44*(31), 13796-13808.

Narang, A., & Desai, D. (2009). Anticancer Drug Development. In Y. Lu & R. I. Mahato (Eds.), *Pharmaceutical Perspectives of Cancer Therapeutics* (pp. 49-92): Springer US.

NCI, N. C. I. (2016). SEER Stat Fact Sheets: Pancreas Cancer.   Retrieved from http://seer.cancer.gov/statfacts/html/pancreas.html

Nelson, D. J., & Nolan, S. P. (2013). Quantifying and understanding the electronic properties of N-heterocyclic carbenes. *Chemical Society Reviews, 42*(16), 6723-6753.

Nobel, P., & Farmacológico, D. Origins of chemotherapy.

Oehninger, L., Rubbiani, R., & Ott, I. (2013). N-Heterocyclic carbene metal complexes in medicinal chemistry. *Dalton Trans, 42*(1), 3269-3284. doi:10.1039/c2dt32617e

Paolini, G. V., Shapland, R. H., van Hoorn, W. P., Mason, J. S., & Hopkins, A. L. (2006). Global mapping of pharmacological space. *Nature biotechnology, 24*(7), 805-815.

Park, D.-G. (2014). Antichemosensitizing effect of resveratrol in cotreatment with oxaliplatin in HCT116 colon cancer cell. *Annals of surgical treatment and research, 86*(2), 68-75.

Peltomäki, P. (2001). Deficient DNA mismatch repair: a common etiologic factor for colon cancer. *Human Molecular Genetics, 10*(7), 735-740. doi:10.1093/hmg/10.7.735

Phillips, R. M. (2016). Targeting the hypoxic fraction of tumours using hypoxia-activated prodrugs. *Cancer chemotherapy and pharmacology, 77*(3), 441-457.

Piccart, M., Lamb, H., & Vermorken, J. B. (2001). Current and future potential roles of the platinum drugs in the treatment of ovarian cancer. *Annals of oncology, 12*(9), 1195-1203.

Piskunova, T., Iurova, M., Zabezhinskiĭ, M., & Anisimov, V. (2007). Poly (ADP-ribosa) polymerase--the relationships with life span and carcinogenesis. *Advances in gerontology= Uspekhi gerontologii, 20*(2), 82.

Plenderleith, I. H. (1990). Treating the treatment: toxicity of cancer chemotherapy. *Can Fam Physician, 36*, 1827-1830.

Pluim, D., van Waardenburg, R. A., Beijnen, J., & Schellens, J. (2004). Cytotoxicity of the organic ruthenium anticancer drug Nami-A is correlated with DNA binding in four different human tumor cell lines. *Cancer chemotherapy and pharmacology, 54*(1), 71-78. doi:10.1007/s00280-004-0773-6

Pourpirali, S., Valacca, C., Merlo, P., Rizza, S., D'Amico, S., & Cecconi, F. (2015). Prolonged pseudohypoxia Targets Ambra1 mRNA to P-bodies for translational repression. *PloS one, 10*(6), e0129750.

Pray, L. (2008). Gleevec: The breakthrough in cancer treatment. *Nature Education, 1*(1), 37.

Press, P. (2017). *Martindale The complete Drug Reference* (39th ed.). London: Phamraceutical Press.

Puckett, C. A., Ernst, R. J., & Barton, J. K. (2010). Exploring the cellular accumulation of metal complexes. *Dalton Transactions, 39*(5), 1159-1170.

Raymond, E., Chaney, S. G., Taamma, A., & Cvitkovic, E. (1998). Oxaliplatin: A review of preclinical and clinical studies. *Annals of Oncology, 9*(10), 1053-1071.

Sadler, P. J., & Peacock, A. F. (2008). Medicinal organometallic chemistry: designing metal arene complexes as anticancer agents. *Chemistry–An Asian Journal, 3*(11), 1890-1899.

Sawyers, C. (2004). Targeted cancer therapy. *Nature, 432*(7015), 294-297.

Sclafani, F., Cunningham, D., Okines, A., Ratnayake, G., & Chau, I. (2017). Chemotherapy for Advanced Pancreatic Cancer. *Pancreatic Cancer*, 1-48.

Sellers, W. R., & Fisher, D. E. (1999). Apoptosis and cancer drug targeting. *Journal of Clinical Investigation, 104*(12), 1655.

Semenza, G. L. (2003). Targeting HIF-1 for cancer therapy. *Nature Reviews Cancer, 3*(10), 721-732.

Sigel, A., Sigel, H., & Sigel, R. K. (2013). *Interrelations between essential metal ions and human diseases*: Springer.

Stein, S. M., Tiersten, A., Hochster, H. S., Blank, S. V., Pothuri, B., Curtin, J., . . . Joseph, B. (2013). A Phase II Study of Oxaliplatin Combined with Continuous Infusion Topotecan for Patients with Previously Treated Ovarian Cancer. *International journal of gynecological cancer: official journal of the International Gynecological Cancer Society, 23*(9).

Sweetman, S. C. (2009). *Martindale: the complete drug reference*: Pharmaceutical press.

Swinney, D. C., & Anthony, J. (2011). How were new medicines discovered? *Nature reviews Drug discovery, 10*(7), 507-519.

Teicher, B. A. (1994). Hypoxia and drug resistance. *Cancer and Metastasis Reviews, 13*(2), 139-168.

Turner, N. C., & Reis-Filho, J. S. (2012). Genetic heterogeneity and cancer drug resistance. *The lancet oncology, 13*(4), e178-e185.

Unruh, A., Ressel, A., Mohamed, H. G., Johnson, R. S., Nadrowitz, R., Richter, E., . . . Wenger, R. H. (2000). The hypoxia-inducible factor-1[alpha] is a negative factor for tumor therapy. *Oncogene, 22*(21), 3213-3220.

Vacca, A., Bruno, M., Boccarelli, A., Coluccia, M., Ribatti, D., Bergamo, A., . . . Sava, G. (2002). Inhibition of endothelial cell functions and of angiogenesis by the metastasis inhibitor NAMI-A. *British journal of cancer, 86*(6), 993-998.

Vaisman, A., Varchenko, M., Umar, A., Kunkel, T. A., Risinger, J. I., Barrett, J. C., . . . Chaney, S. G. (1998). The role of hMLH1, hMSH3, and hMSH6 defects in cisplatin and oxaliplatin resistance: correlation with replicative bypass of platinum-DNA adducts. *Cancer Research, 58*(16), 3579-3585.

Wagers, P. O., Shelton, K. L., Panzner, M. J., Tessier, C. A., & Youngs, W. J. (2014). Synthesis and Medicinal Properties of Silver–NHC Complexes and Imidazolium Salts. *N-Heterocyclic Carbenes: Effective Tools for Organometallic Synthesis*, 151-172.

Weiss, R. B., & Christian, M. C. (1993). New Cisplatin Analogues in Development. *Drugs, 46*(3), 360-377. doi:10.2165/00003495-199346030-00003

Wheate, N. J., Walker, S., Craig, G. E., & Oun, R. (2010). The status of platinum anticancer drugs in the clinic and in clinical trials. *Dalton Transactions, 39*(35), 8113-8127.

WHO, T. W. H. O. (2015). Statistics at a Glance: The Burden of Cancer in the United States. Retrieved from http://www.cancer.gov/about-cancer/what-is-cancer/statistics

Wilson, T. R., Longley, D. B., & Johnston, P. G. (2006). Chemoresistance in solid tumours. *Annals of Oncology : Official Journal of the European Society for Medical Oncology / ESMO, 17 Suppl 10*(Supplement 10), x315-x324. doi:10.1093/annonc/mdl280

Yamamoto, H., & Okamoto, H. (1980). Protection by picolinamide, a novel inhibitor of poly (ADP-ribose) synthetase, against both streptozotocin-induced depression of proinsulin synthesis and reduction of NAD content in pancreatic islets. *Biochemical and biophysical research communications, 95*(1), 474-481.

Zaffaroni, N., Silvestrini, R., Orlandi, L., Bearzatto, A., Gornati, D., & Villa, R. (1998). Induction of apoptosis by taxol and cisplatin and effect on cell cycle-related proteins in cisplatin-sensitive and-resistant human ovarian cells. *British journal of cancer, 77*(9), 1378.

Zheng, W., Thorne, N., & McKew, J. C. (2013). Phenotypic screens as a renewed approach for drug discovery. *Drug discovery today, 18*(21), 1067-1073.

Zorzet, S., Bergamo, A., Cocchietto, M., Sorc, A., Gava, B., Alessio, E., . . . Sava, G. (2000). Lack of in vitro cytotoxicity, associated to increased G2-M cell fraction and inhibition of matrigel invasion, may predict in vivo-selective antimetastasis activity of ruthenium complexes. *Journal of Pharmacology and Experimental Therapeutics, 295*(3), 927-933.

Chapter 12 - Appendix

12. 1 – Ruthenium and iridium Compounds as Anti-Cancer Agents

	IC$_{50}$ value (µM) ± SD (selectivity index)			
	HT-29	**MCF-7**	**A2780**	**A2780cis**
Cisplatin	0.25 ± 0.11	1.09 ± 0.08	0.94 ± 0.04	10.50 ± 0.20
1	3.50 ± 0.30	1.90 ± 0.10	2.60 ± 0.08	3.13 ± 0.09
7	6.10 ± 0.30	3.55 ± 0.09	2.5 ± 0.2	3.69 ± 0.09
8	10.30 ± 0.6	6.20 ± 0.20	2.3 ± 0.2	7.00 ± 0.04
9	11.80 ± 0.80	-	-	-
11	10.21 ± 0.09	2.9 0 ± 0.10	2.87 ± 0.05	9.1 ± 0.1
12	22.00 ± 2.00	13.00 ± 0.20	-	-
13	6.30 ± 0.30	7.20 ± 0.20	1.90 ± 0.10	3.80 ± 0.09
14	53.00 ± 1.00	-	56.00 ± 2.00	-
15	18.00 ± 2.00	18.40 ± 0.80	19.40 ± 0.80	24.30 ± 0.50
18	93.00 ± 7.00	51.00 ± 4.00	35.00 ± 1.00	51.00 ± 1.00

Table 12.1: Response of colonic adneocarcinoma HT2-29, metastatic epithelial mammary gland, parent ovarian carcinoma A2780 and cisplatin resistant form A2780cis cell lines continuous 96-hour exposure to novel RML Ruthenium and Iridium β-ketoiminate based compounds. The results presented are the mean IC$_{50}$ values ± standard deviations for three independent experiments. The ">" symbol represents the highest dose tested *in vitro*. Data collected by Rhianne Lord et al. externally.

12. 2 - N-Heterocyclic Compounds as Anti-Cancer Agents
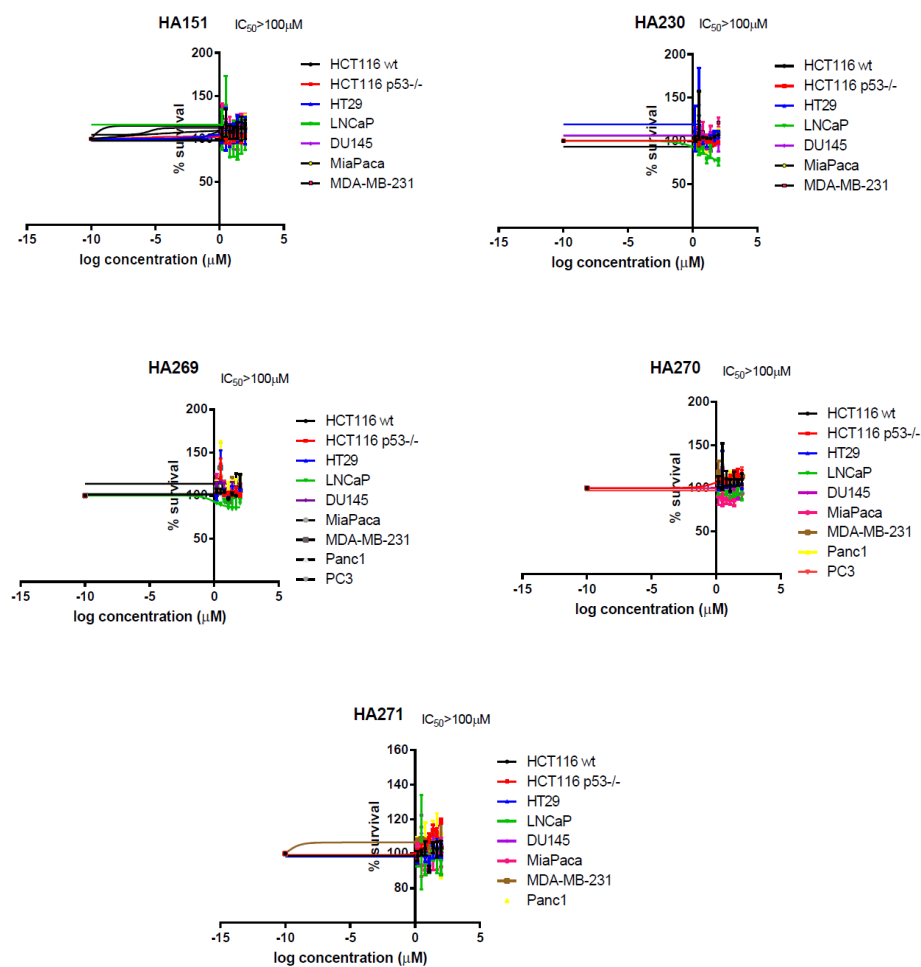
Figure 12.2: SRB analysis of five novel Silver-NHC complexes synthesised by Charlotte Wilans' research groups (chapter 7).
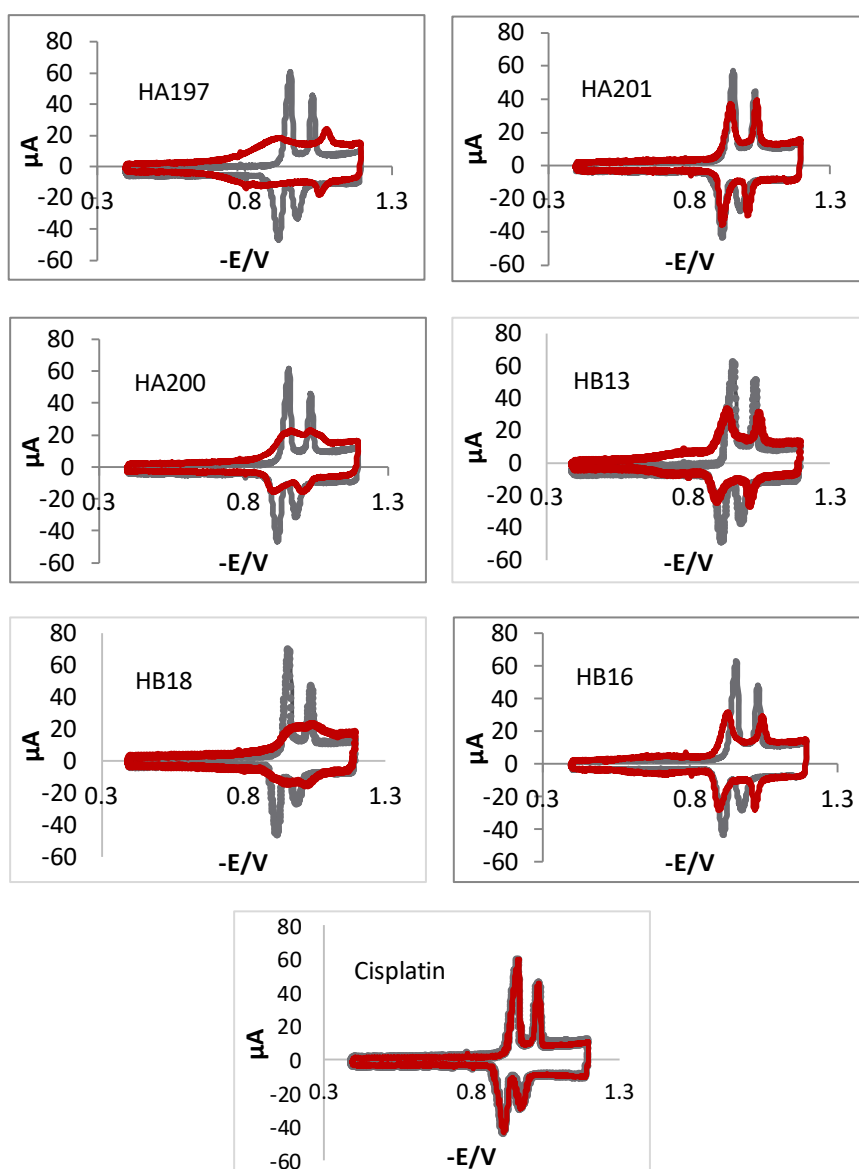
Figure 12.3: RCVs recorded at 40 V s^{-1} of a DOPC coated Pt/Hg electrode (grey), overlaid with either one of six silver(I)-NHC complexes at 50µM or 2mM of cisplatin (red). Synthesised by Charlotte Wilans' research groups (chapter 7).

12. 3 - Metallohelices as Anti-Cancer Agents
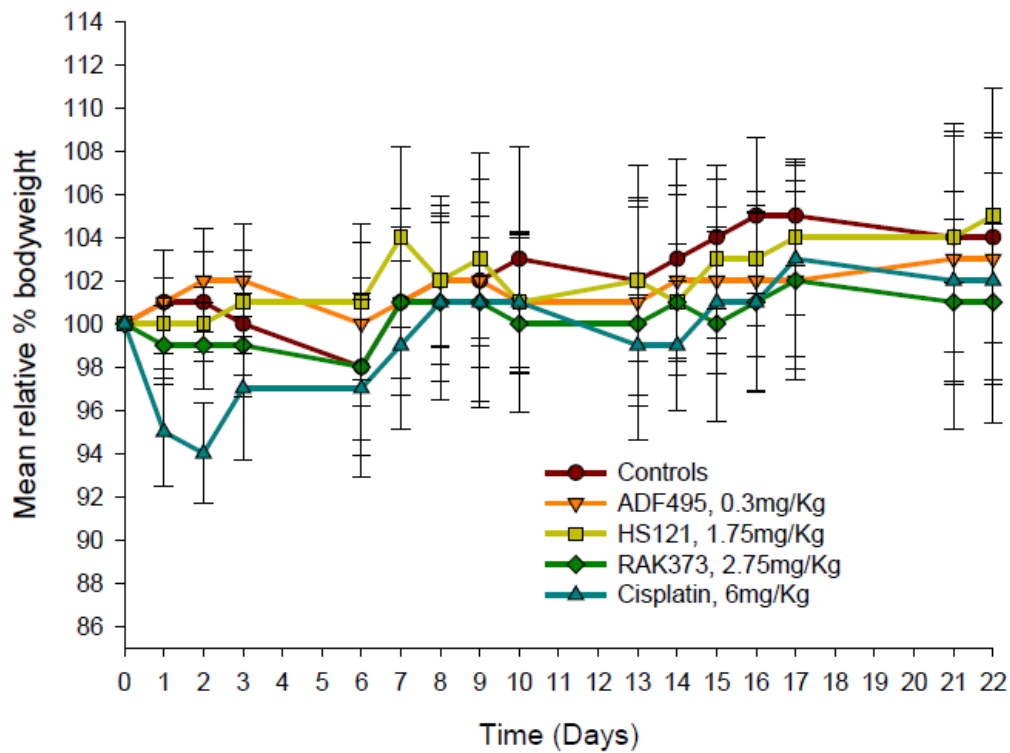
Figure 12.4: Body weight of non-tumour bearing animals treated with ADF495, HS121, RAK373 and cisplatin, all of which were administered intravenously at the doses indicated (single injection given at day 0). Group sizes for each experiment were 3 animals and the results presented represent the mean weight ± the standard deviation for 3 animals (chapter 9).
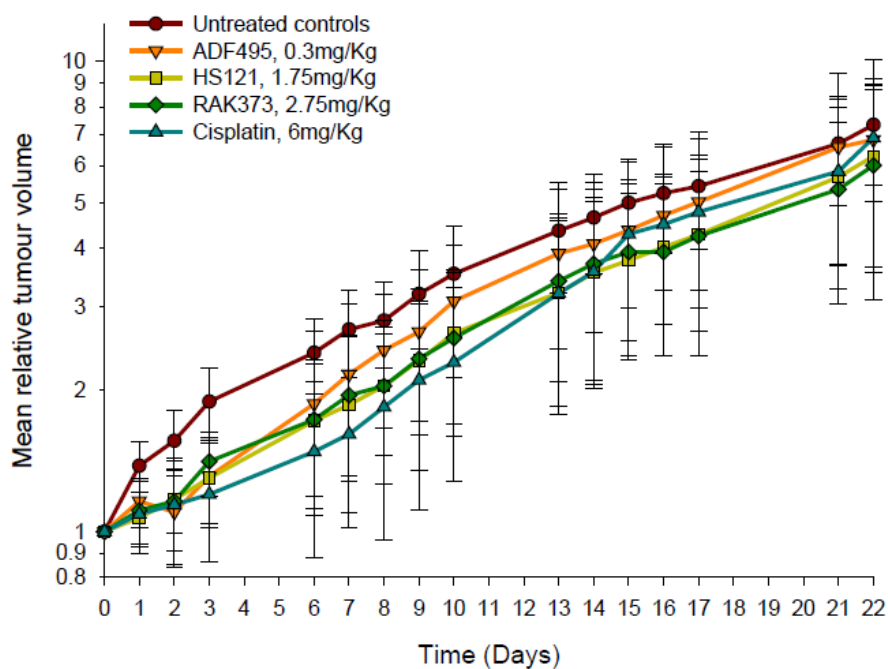
Group number	Median time RTV2 (days)	Growth delay	Significance	Maximum % weight loss
Control	4.2	-	-	2.0 (day 6)
ADF495	6.8	2.6	P<0.05	0
HS121	8.5	4.3	P<0.01	0
RAK373	9.0	4.8	P<0.01	2.0 (day 6)
Cisplatin	8.9	4.7	P<0.01	6.0 (day 2)

Figure 12.5: Anti-tumour activity data of three "hit" novel metallohelices and cisplatin against HCT116 p53$^{-/-}$ tumours *in vivo*. Related to chapter 9.